CRANFIELD UNIVERSITY

P A SMITH

INVESTIGATION INTO FUSION BOUNDARY CARBON DIFFUSION IN ½Cr½Mo¼V WELDMENTS

SCHOOL OF INDUSTRIAL AND MANUFACTURING SCIENCE

MASTER OF SCIENCE

CRANFIELD UNIVERSITY

SCHOOL OF INDUSTRIAL AND MANUFACTURING SCIENCE

MSc THESIS

Academic Year 1994-5

P A SMITH

INVESTIGATION INTO FUSION BOUNDARY CARBON DIFFUSION IN ½Cr½Mo¼V WELDMENTS

Supervisor: J Spurrier

September 1994

This thesis is submitted in partial fulfilment of the requirements for the degree of Master of Science

ABSTRACT

The steam lines in the majority of power stations operating in the UK were fabricated from ½Cr½Mo¼V steam pipe material joined using 2CrMo weld metal. Throughout the life of these systems, which operate typically at 565°C and 165bar, weldment cracking problems have been encountered. Many of these problems are well understood and are managed effectively. In recent years a creep cracking mechanism in the heat affected zone adjacent to the fusion boundary has been identified, referred to as Type IIIa cracking.

This project has identified significant carbon migration across the fusion boundary of these weldments, from the lower alloyed ½Cr½Mo¼V to the more highly alloyed 2CrMo weld metal. Carbon diffusion has been identified as occurring during the welding cycle, however the majority of carbon diffusion occurs during post weld heat treatment and particularly during service exposure.

Carbon migration results in marked reduction in carbon content in the heat affected zone adjacent to the fusion boundary with a corresponding band of enhanced carbon content in the weld metal adjacent to the fusion boundary. The width of these areas increase with time at temperature.

Micro hardness measurements have confirmed a reduction in the hardness of the heat affected zone region as a result of carbon diffusion. Hardness measurements have also pointed to a step change in hardness across the fusion boundary. This may result in a corresponding step change in creep properties. It is suggested that this mismatch in creep properties, coupled with a predominantly fine grained microstructure at the fusion boundary, can result in the fusion boundary heat affected zone region being the weakest region of the weldment.

CONTENTS

FIGURES

4.0 **RESULTS**

ABBREVIATIONS

2CrMo	2¼Cr1Mo
9Cr	9Cr1Mo
AGED	PWHT and Artificially Aged
AW	As Welded
CGB	Coarse Grained Bainite
CMV	½Cr½Mo¼V
HAZ	Heat Affected Zone
MMA	Manual Metal Arc
NRA	Nuclear Reaction Analysis
PIXE	Particle Induced X-ray Analysis
PWHT	Post Weld Heat Treated or Treatment
RS	Refined Structure

ACKNOWLEDGMENTS

I would like to express my gratitude to my supervisor, Dr J Spurrier, and to J Norish of Cranfield University for their guidance during the preparation of this thesis.

My thanks also go to C King of National Power for agreeing to sponsor me for this MSc course.

For many valuable technical discussions and encouragement I am particularly grateful to Dr S Brett of National Power. I would also like to thank other National Power colleagues C Johnston for his assistance in the practical work and P Earl and M Askins for their advice and assistance in completing the thesis.

I would also like to thank MUREX UK for supplying some of the electrodes used in this project.

Finally, and most importantly I thank my wife, Christine, for her unfailing support and my children James, Helen and Catherine for their patience.

1.0 INTRODUCTION

The aim of this project is to investigate the phenomenon of carbon diffusion in ½Cr½Mo¼V (CMV) weldments. The project investigates the level of fusion boundary carbon diffusion occurring as a result of welding, post weld heat treatment and extended thermal cycles in weldments made with a range of ferritic welding consumables.

The main steam and hot reheat pipework in the majority of conventional power generation plant operating in this country was fabricated from CMV material using 2¼Cr1Mo (2CrMo) weld metal. The steam pipework has typically operated for periods in excess of 100,000 hours at high pressures and temperatures of around 165bar and 565°C. In recent years some weld failures have been attributed to creep cracks in the parent material adjacent to the fusion boundary. It is considered that carbon diffusion to the weld metal may have played a significant role in the loss of creep properties of this area of the weldment.

Work has been carried out looking into the effect of carbon diffusion on the properties of transition joints. However, the majority of this work has studied its effect on the properties of austenitic/ferritic welded joints. A lesser amount of work has been concerned with its effect on dissimilar ferritic joints and little work has focused on the relative levels of carbon diffusion occurring as a result of the weldment thermal cycles seen during fabrication and service.

2.0 **LITERATURE SURVEY**

2.1 THE SERVICE PERFORMANCE OF CMV MATERIAL

The majority of power generation plant constructed in the UK in the 1960s and early 1970s used the low alloy ferritic steel ½Cr½Mo¼V (CMV) for main steam and hot reheat pipework systems. The sections of pipe are joined using 2¼Cr1Mo (2CrMo) weld metal, deposited primarily using the manual metal arc (MMA) process. These systems typically operate at temperatures of 565°C and at pressures of 165bar and 40bar respectively. The integrity of these systems is conditional upon the design criteria ensuring that they do not fail within their original design life.

2.1.1 Design Considerations

The design code used for pipework systems in steam generating plant in the UK is BS809[1]. The design codes take account of the operating temperature, pressure and the creep properties of the material being considered. From the codes, the mean diameter hoop stress is given by equation (1), and the axial stress by equation (2).

$$Hoop\ Stress = \frac{PD_m}{2t} \quad \ldots\ldots\ldots\ldots\ (1)$$

$$Axial\ Stress = \frac{PD_m}{4t} \quad \ldots\ldots\ldots\ldots\ (2)$$

Where P is the pressure, D_m the mean diameter and t the wall thickness. It can be seen from these equations that the hoop pressure stress is twice the axial pressure stress. The design stress is therefore based on the calculated hoop stress. From the codes the end of life failure for the pipe material would therefore be expected to be an axial split driven by the hoop stress.

Much of the steam generating plant has now operated for periods in excess of 100,000hrs. In this time the CMV pipe material has essentially operated trouble free, showing that the codes are conservative. However, service experience with the weldments has differed markedly from the pipework. Cracking in the weldments has occurred early in the operation of new plant, midway through plant design

life and when the plant has reached and exceeded its plant life. The weldment has invariably proved to be the weakest link in the pipework. The design codes assume the properties of the weldment at least match those of the parent material, but experience has shown this not to be the case.

As a consequence of this shortfall in the properties of the weldments, the companies involved in the operation of the steam generating plant have been forced to spend large sums of money on inspections, system appraisals and weld repairs to manage the problem and to ensure the continued safe operation and reliability of the plant. Over the past twenty five years extensive generic research work has also been carried out to support these management activities. Many of the cracking problems are now well understood, some have been overcome and to an extent others can be predicted.

Brief details are given below of plant experience, concentrating on the most significant cracking mechanisms encountered during the service life of these pipework systems.

2.1.2 Plant Experience

From initial fabrication to approximately 20,000hrs service the most common cracking mechanism encountered was reheat cracking (sometimes known as stress relief cracking)[3]. Early trials showed that when a matching CMV weld consumable was used, both the weld and heat affected zone (HAZ) were susceptible to reheat cracking. However, the 2CrMo weld metal ultimately chosen for these joints was found to be more resistant to reheat cracking because of its lower strength and greater ductility. The use of 2CrMo therefore reduced reheat cracking in the weld metal. Hence the majority of significant early failures occurred circumferentially in the HAZ of the CMV parent material.

As the name implies, reheat cracking occurs during the reheating of a weldment. Cracking can occur either during the post weld stress relief heat treatment or during service at temperatures in the creep range. Circumferential cracking in the HAZ occurs in the coarse grained region adjacent to the fusion boundary. The coarse grained region has low creep ductility in comparison with the surrounding material[2] and hence is not able to accommodate the strains resulting from the relaxation of the residual weld stresses during stress relief and early service. A coarse grained structure, high residual elements, such as phosphorus, sulphur, arsenic, antimony

and tin[3], and vanadium levels[4], were found to increase the propensity to this cracking mechanism.

The cracks arose largely as the result of poor welding and stress relief practice[5][6]. The coarse grained microstructure was the result of high heat input during the welding process. The recommended stress relief temperature at that time was 670°-710°C[7], today the recommended temperature for stress relief is 690-720°C[8]. This change coupled with the fact that the treatment was often badly controlled, meant that the residual stresses were not being removed effectively.

Two mechanisms contribute to the stress relief of welds[9]. The first is the reduction of the yield strength of the material by raising the temperature, which allows the stresses to relax by local yielding. Further relaxation then takes place as a result of creep. It can be seen that the higher the temperature of stress relief the lower the level of stresses that need to be removed by creep. The upper limit on temperature is limited because of the possibility of significant carbide spheroidisation that affects the longer term creep strength of the weldment.

Because reheat cracking occurs early in the life of a weldment, the problem has largely gone away. The use of improved welding techniques, coupled with the improved compositional control of consumables and the improved control of post weld heat treatment activities, means that welds introduced today rarely suffer from reheat cracking problems.

The most commonly seen cracks today are circumferential creep cracks in the intercritically heated region of the HAZ, **Fig 2.1**. These defects have been identified as Type IV cracks, after a German classification of weldment cracking[10], **Fig 2.2**. The defects can initiate after periods of service of less than 50,000hrs, although they are more common from mid-life onwards.

The intercritically heated region of the HAZ has a mixed grain size. The region contains untransformed grains the same size as those in the parent material and refined grains which have transformed as part of the weld heating cycle. The poor creep strength of this region has been attributed to the short heating transient associated with the welding cycle resulting in a small grain size, limited carbide precipitation and limited carbon diffusion to bainite[11]. The defects initiate as creep cavities which increase in density and then link up to form micro-cracks which in turn link up to form larger cracks. It is only when the larger cracks form, having sizes greater than 2-

3mm, that they can be detected by conventional NDT techniques such as ultrasonics and magnetic particle inspection.

Uniaxial creep tests have shown that in many cases the creep strength of the Type IV region of a weldment is only about 60% that of the parent material[12]. This means that the creep life of the region is likely to be in the order of only 25% of the parent material, **Fig 2.3**. The Type IV region is relatively narrow, normally about 1mm wide. Hence the defects necessarily form circumferentially and as such are being driven by an axial stress. It was seen from design considerations that the hoop stress resulting from internal pressure alone is twice the axial stress. Although the Type IV region is weak relative to the parent material it is considered from the nature of these failures that in a number of cases welds are being subjected to additional axial stresses[13]. The stresses are often difficult to quantify. Nevertheless, inadequate cold pull and pipe support could be contributory factors as can local bending stresses. The majority of Type IV cracking problems have been at terminal welds where these additional axial and bending stresses are likely to be highest as they cannot be accommodated by pipework movement.

More recently a new cracking mechanism has been identified, occurring in the weld HAZ adjacent to the fusion boundary, referred to as Type IIIa cracking. It is in this cracking mechanism that fusion boundary carbon diffusion is considered to be playing a significant role.

2.1.3 TYPE IIIa CRACKING

The name Type IIIa cracking is again based on the German classification system[10], **Fig 2.2**. The 'a' subscript was adopted by the Central Electricity Generating Board (CEGB) to avoid confusion with other fusion boundary HAZ cracking mechanisms such as reheat cracking.

Although cracking occurs in the HAZ adjacent to the fusion boundary as does reheat cracking, the mechanism appears to be more similar to Type IV cracking in that it is associated with a band of creep weak material with a fine grain size. The region in which the cracks form is generally very narrow, three or four grain widths wide, the cavitation density is often relatively low and more variable than in the Type IV region. In welds with a mixed coarse and fine grained microstructure, the defects can often be seen to initiate in the fine grained region and then die out as they enter coarse grained regions.

The level of grain refinement in the HAZ is dictated by the welding sequence and the heat input during welding. Today it is common to try to achieve a refined microstructure in this region to avoid the grain coarsening which had previously contributed to reheat cracking. It is however clear that an almost fully refined heat effected zone has been achieved in a number of original welds. It is in these weldments that recent Type IIIa cracks have been seen, **Fig 2.4.**

It is unclear why this region should be weaker in creep than the Type IV region which will always exist and has been considered to the weakest region of weldment due to the absence or suppression of factors normally associated with creep strength[11]. However, an investigation into a Type IIIa crack[13] identified the region as being denuded in carbon as a result of carbon migration to the Chromium rich 2CrMo weld metal. An identical form of cracking has been reported by another author[15] and attributed to carbon loss. This reduction in carbon content may therefore explain the greater than expected loss of creep strength of this region[11]. This project aims to increase understanding of the cracking by investigating the observed carbon diffusion.

2.2 CARBON DIFFUSION

It is known that carbon diffusion plays a significant role in the long term degradation and failure of transition joints between austenitic and ferritic materials[16]. On the other hand, carbon diffusion between ferritic joints with modest differences in alloy content has not normally been highlighted as degrading the properties of such joints and contributing to their ultimate failure. However recent fusion boundary creep cracking in weldments between CMV weld metal and 2CrMo weld metal operating at 565°C has suggested that carbon diffusion may be playing a significant role in these failures.

The term diffusion in solids is used to describe the movement of atoms or molecules in a medium which is essentially stationary. Fick's second law of diffusion has been shown to predict diffusion between alloyed material and a pure metal[17].

$$\frac{dc}{dt} = -D\frac{d^2C}{dx^2}$$

Where D is the diffusivity of the alloying element which is temperature dependant. **Fig 2.5,** shows concentration profiles predicted from the law with time. Fick's second law is derived by considering random jumps of solute atoms within the material. The above profiles are therefore determined simply because there are more solute atoms to move down the concentration gradient than up it. From Fick's second law the characteristic depth of diffusion can be calculated from $x=(Dt)^{½}$[17]. This approach is used to determine the depth of penetration of carbon in the carburization process.

Fick's law implies that the concentration gradient is the driving force for diffusion, the end point of which should be complete uniformity of composition. However this may not be the case when diffusion in metallic systems is being considered, because the equilibrium state of the alloy is not necessarily that in which the composition is the same everywhere. This has been shown in a classic experiment[18], in which carbon was shown to diffuse from a lower carbon steel to a more highly alloyed higher carbon steel held at 1050°C. It is explained that although the concentration gradient would dictate that carbon moved from the higher carbon to the lower carbon steel, the difference in alloy content creates an activity gradient which counteracts the carbon concentration gradient, causing the carbon to migrate from a lower carbon to a

higher carbon more highly alloyed steel. This phenomenon is often referred to as uphill diffusion.

Sharp changes in carbon concentration at the fusion boundary of low alloy steel weldments has previously been reported[19]. Experiments with a number of alloy combinations in the temperature range 590-700°C showed carbon being denuded on the low alloy side of the fusion boundary and concentrated on the higher alloy side. The majority of the steels used in the investigations were alloyed with Cr and Mo. They report that increasing the alloy content on the higher alloy side of the joint increases the level of carbon diffusion. However they also report that relatively small increases in alloy content on the lower alloy side of the joint significantly reduces the level of carbon diffusion from the low alloy side. Their observations were made using simple metallographic techniques. They also carried out a limited amount of mechanical testing which included short term creep tests. From these tests they concluded that there was no evidence that the weldment properties were degraded as a result of the observed carbon diffusion. The mechanism proposed for carbon diffusion in this study is presented in the discussion.

The effects of normalising and tempering heat treatments on fusion boundary carbon redistribution in steels with relatively small differences in chemical composition have been modelled[20]. The alloy system used in the investigation was between 2CrMo weld metal and CMV parent material. The investigation suggested that carbon segregation observed in weldments subjected to this combination of heat treatments was not primarily due to carbon diffusion during the austenitising heat treatment.

Investigations with the same alloy system in the same normalised and tempered heat treatment condition by other authors[21], also concluded that carbon segregation from parent CMV to 2CrMo weld metal occurs primarily during the stress relief or tempering treatments at 700°C for periods of typically 10h and not during normalisation. Indeed it was also concluded that renormalisation could partially homogenise carbon segregation produced during stress relief.

Neither of these authors specifically considered the effects of service exposure at normal steam temperatures of 565°C for periods of 10^5 hrs on carbon diffusion. Nevertheless it might be considered that tempering at 700°C is merely an acceleration of the processes occurring at lower temperatures. However, it is reported[21] from work on austenitic/ferritic transition joints that the

mechanism of carbon diffusion may change significantly between 700°C and 565°C such that a carbon depleted zone created at 700°C could be reduced in extent by prolonged exposure at 565°C.

Post weld normalising and tempering treatments were normally only applied to thick section cast power plant components because of concerns about reheat cracking discussed in para 2.2. The majority of 2CrMo welds in CMV pipe material operating in this country are only given a post weld stress relief treatment at 690-720°C for a typical period of 3hrs and no normalising treatment. It is in these weldments that recent fusion boundary creep cracking has been observed.

It is not immediately apparent whether the bulk of carbon diffusion occurs during the thermal cycles associated with welding, during stress relief heat treatment or during subsequent service exposure at 565°C.

2.3 CONTROL OF HEAT AFFECTED ZONE MICROSTRUCTURES

This study of fusion boundary carbon diffusion is being carried out to increase understanding of Type IIIa cracking. As described in para. 2.3. Type IIIa cracking is associated with a fine grained fusion boundary HAZ microstructure. It was therefore necessary to produce weld samples for the test programme with a fine grained microstructure adjacent to the fusion boundary.

The grain size of the HAZ adjacent to the fusion boundary in CMV weldments is largely dictated by the weld heating cycle, the effect of alloy content is mentioned later. In single pass welds this grain size can only be controlled by the heat input during welding and the extent to which it can be controlled is necessarily limited by the need to achieve fusion during welding. However in multipass welds it is possible to refine the grain size of one weld pass by a subsequent weld pass.

As far as the author is aware three techniques were developed within the CEGB to control HAZ microstructures. The driving force for their development was the avoidance of reheat cracking, discussed in para 2.2, when repairing CMV weldments that failed early in their service life. These techniques rely on controlling the heat input during welding and adopting particular deposition sequences to produce the desired microstructure.

Two approaches were considered for this investigation, the third was a Tungsten Inert Gas welding technique which was not considered relevant.

a) Two layer refinement technique[22] - As the name implies this technique relies on the coarse grained HAZ of the first layer of weld metal being refined by a second weld layer.

b) Weld bead overlap technique[2] - This technique relies on the coarse grained HAZ region produced by one weld bead being refined by a subsequent weld bead in the same layer.

The two layer refinement technique was developed essentially as a buttering technique and is not very suitable for normal 'V' butt weld preparations used for pipework. However, it would have been possible to use the technique in this investigation as only one weld face was being produced on the test pieces. It was nevertheless considered that the technique would not accurately reproduce the HAZ thermal cycles representative of service welds.

The bead overlap technique is ideal for use with 'V' type weld preparations. It was also considered that it would better reproduce the heating cycles that led to fine grained microstructures in weldments that failed by Type IIIa cracking in service.

A general description of ferritic HAZ microstructures and how the microstructure in the HAZ can be modified is described below.

2.3.1 HAZ Microstructure

In manual metal arc (MMA) welding the arc made between the welding electrode and workpiece melts an area of the base material forming a molten pool. In addition to melting the workpiece the electrode core progressively melts, molten metal being transferred through the arc to the workpiece. As the arc moves on, the molten material cools and freezes to form a weld bead. The effect of the heating and cooling cycles associated with deposition of a weld bead will have a metallurgical effect on the base material around the weld bead. This metallurgically affected area is referred to as the heat affected zone (HAZ). **Fig 2.6**[23] gives a schematic representation of the microstructural features of the HAZ of a plain carbon steel, with reference to the Fe-C equilibrium phase diagram. Although this does not represent the alloy system under consideration, and the microstructural constituents will be different, the HAZ grain size variations will be similar.

2.3.2 HAZ Microstructure of a Single Weld Bead

The microstructure of the HAZ associated with a single weld bead is dependent on the heating rate, cooling rate and time at temperature but within the bounds of normal MMA welding speeds can be considered to be determined predominantly by the peak temperature reached. The temperature profile associated with a long single weld bead can be considered to decay radially away from the fusion boundary.

As shown in **Fig 2.6**, the heat affected zone consists of a number of well defined zones. However for the purpose of this description the grain coarsened and grain refined zones (annuli) only have been considered **Fig 2.7**[2], these annuli in a CMV parent material have been described as follows.

Grain Coarsened Zone (Annulus 1) - Material heated to peak temperatures within the isotherms corresponding to the

melting point (T_m) and the austenite grain coarsening temperature ($T_{max} \approx 1200°C$) is transformed on cooling to a coarse grained bainitic microstructure (CGB) of prior austenite grain size ASTM 2-3. The width of this region in thick section manual metal arc (MMA) welds under typical conditions is about 1mm. The grain coarsened zone corresponds to temperatures at which precipitates such as vanadium, molybdenum and chromium carbides dissolve in the austenite and are therefore no longer able to restrict grain growth by pinning grain boundaries.

Recrystallised Zone (Annulus 2) - Material contained within the isotherms extending from the grain coarsening temperature down to the upper critical temperature (Ac_3 dynamic $\approx 950°C$) transforms on heating to fine grained austenite (ASTM 7-9). This austenite, on cooling, transforms to a refined structure (RS) consisting either of bainite or a mixture of proeutectoid ferrite and bainite depending on the precise local hardenability (i.e. composition) and cooling rate. Irrespective of the detailed microstructure, the effective grain size within this region is similar to that of the pre-existing austenite. The width of this refined annulus is also typically about 1mm in thick section MMA welds.

2.3.3 The Heat Affected Zone of a Multipass Weld

The grain size produced in the HAZ of a multipass weld is developed as a consequence of the thermal cycle associated with the deposition of subsequent weld beads. Simplistically the level of refinement achieved can be considered to be the result of the degree of overlap of the annuli achieved. **Fig 2.8** shows this schematically for a weld deposited with low overlap and hence a low level of refinement.

The refining annulus, annulus 2, of each successive weld bead intersects and effectively refines a proportion of the annulus containing CGB, annulus 1, produced by the preceding bead. The region of refined structure has approximately the same grain size as that produced in annulus 2 of a single weld bead[2].

A typical multipass weld will therefore consist of alternating bands of CGB and RS. It is apparent that the relative proportion of RS is therefore largely determined by the degree of weld bead overlap. However the size of the weld bead, determined by size of welding electrode used, welding conditions and travel speed also has a significant effect.

It has been shown[2] that when using 3.25mm electrodes, and a low angle of attack relative to the weld preparation surface, a high degree of weld bead overlap can be achieved, **Fig 2.9**. This technique with welding speeds between 2.5 and 2.9mm/s produced between 80-90% grain refinement. It was these conditions that were specified for the production of test pieces for this exercise.

2.4 THE HARWELL NUCLEAR MICROPROBE

Nuclear microprobe analysis has been used extensively in materials science studies to study the distribution of light elements such as carbon. It has been chosen in this study as it is considered to have a number of advantages over the use of other techniques such as a scanning electron microscopy.

Nuclear reaction analysis, NRA, is used to study the distribution of carbon in steel specimens. Ions of Deuterium, Deuterons, are accelerated towards the sample or target using a Van de Graaff accelerator. When a Deuteron collides with a carbon nuclei a proton is emitted. This nuclear reaction is characterised by the expression $C^{12}(d,p)C^{13}$,. The emitted protons are measured using a silicon barrier detector to arrive at a quantitative carbon value, J W McMillan[24]. Before testing can commence the equipment is calibrated using samples of known carbon content. The proton energy emitted from the metal surface varies with depth. The equipment is therefore gated so that typically proton emissions from the first 0.2μm of material are not counted. This is one of the advantages of the technique as it discriminates against surface contamination. Proton emissions with an energy corresponding with a maximum depth of material of about 2μm were measured in this investigation.

Another advantage of the technique is that particle induced X-ray emission, PIXE, analysis to give a qualitative chromium level in the sample is carried out simultaneously with the NRA analysis, McMillan[25]. This enables unambiguous identification of the position of fusion boundary to be made which is vital in analysing the results.

A further advantage of the use of NRA analysis in identifying the spatial distribution of light elements is sighted by McMillan, Pummery and Pollard[26]. The sensitivity in nuclear microprobe analysis is enhanced since the signal to noise ratio for the detection of the emitted particles is much higher than for the detection of electron induced X-rays.

As well as these advantages, carbon profiles have previously been produced for some CMV weldments which have failed in service using the nuclear microprobe. It will therefore be possible to compare results from this exercise with previous results.

Carbon and Chromium profiles were produced by scanning across the weld fusion boundary of each of the weldments

under investigation. Each weldment was scanned at three scanning sensitivities giving resolutions of 250μm, 40μm and <5μm. These scans can be considered to be coarse, medium and fine scans.

The purpose of the coarse scan (~5mm about fusion boundary) was to give an overall picture of the level of carbon diffusion occurring. The purpose of the medium scan (~0.5mm about the fusion boundary) was to investigate in more detail the carbon profile close to the fusion boundary. The purpose of the fine scan (~0.125mm about the fusion boundary) was to focus on the levels of carbon in the fine grained parent material immediately adjacent to the fusion boundary. In particular there is considered to be a possibility that a trough in the carbon content occurs immediately adjacent to the fusion boundary which may not have been detected by the coarser scans and could explain the very poor creep properties of this area. As far as the author is aware, this is the first time such a fine scanning sensitivity has been used.

The errors in terms of carbon concentration for each reading are dependant on:

1. The charge deposited, which affects the total number of counts used to generate a particular point in the carbon profile.

2. The carbon concentration in the specimen, its effect is shown below.

The errors are expected to be highest for the fine scanning sensitivity because a smaller charge, 0.25μC, is being deposited. The predicted errors for the fine scanning sensitivity are calculated below[27]

Carbon Concentration	Predicted Error (1σ)
0.030% (wt)	±0.0013% (wt)
0.010% (wt)	±0.0008% (wt)
0.003% (wt)	±0.0004% (wt)
0.001% (wt)	±0.00025% (wt)

Consequently, a measured carbon concentration of 100ppm will be subject to an error of ~8% relative, whereas at a concentration of 10ppm carbon the error will increase to ~25% relative

FIG 2.1

Type IV Cracking

German Classification for Weld Metal Cracking

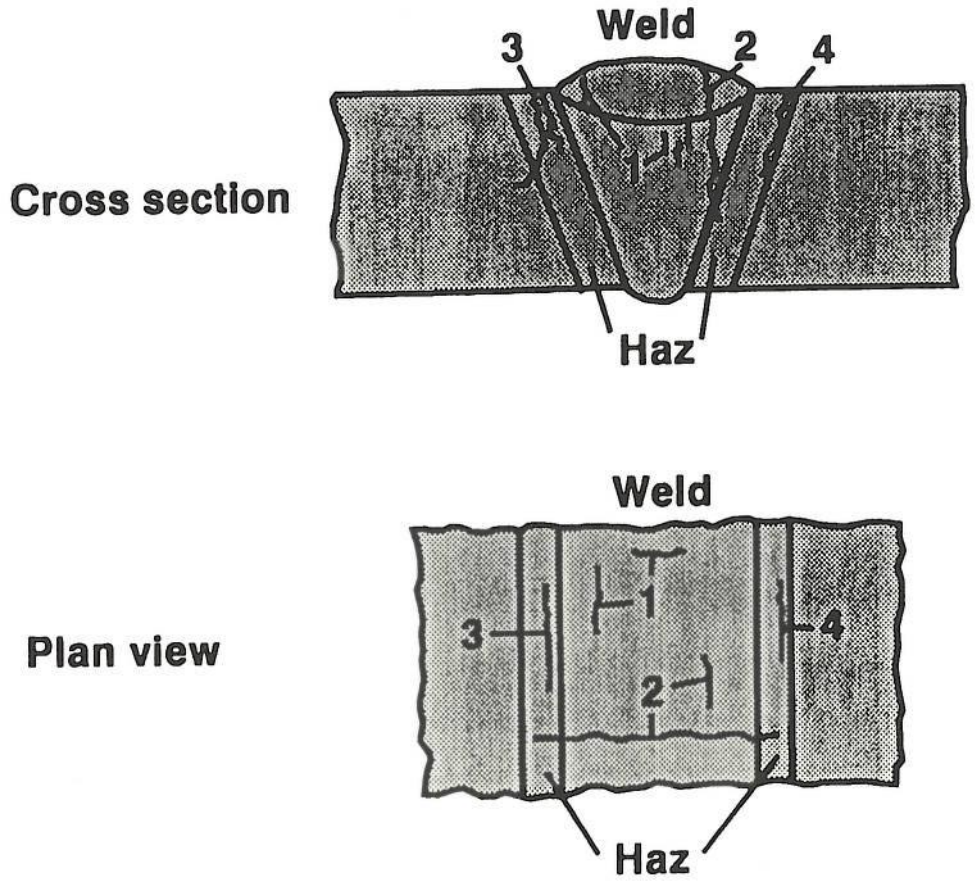

FIG 2.2

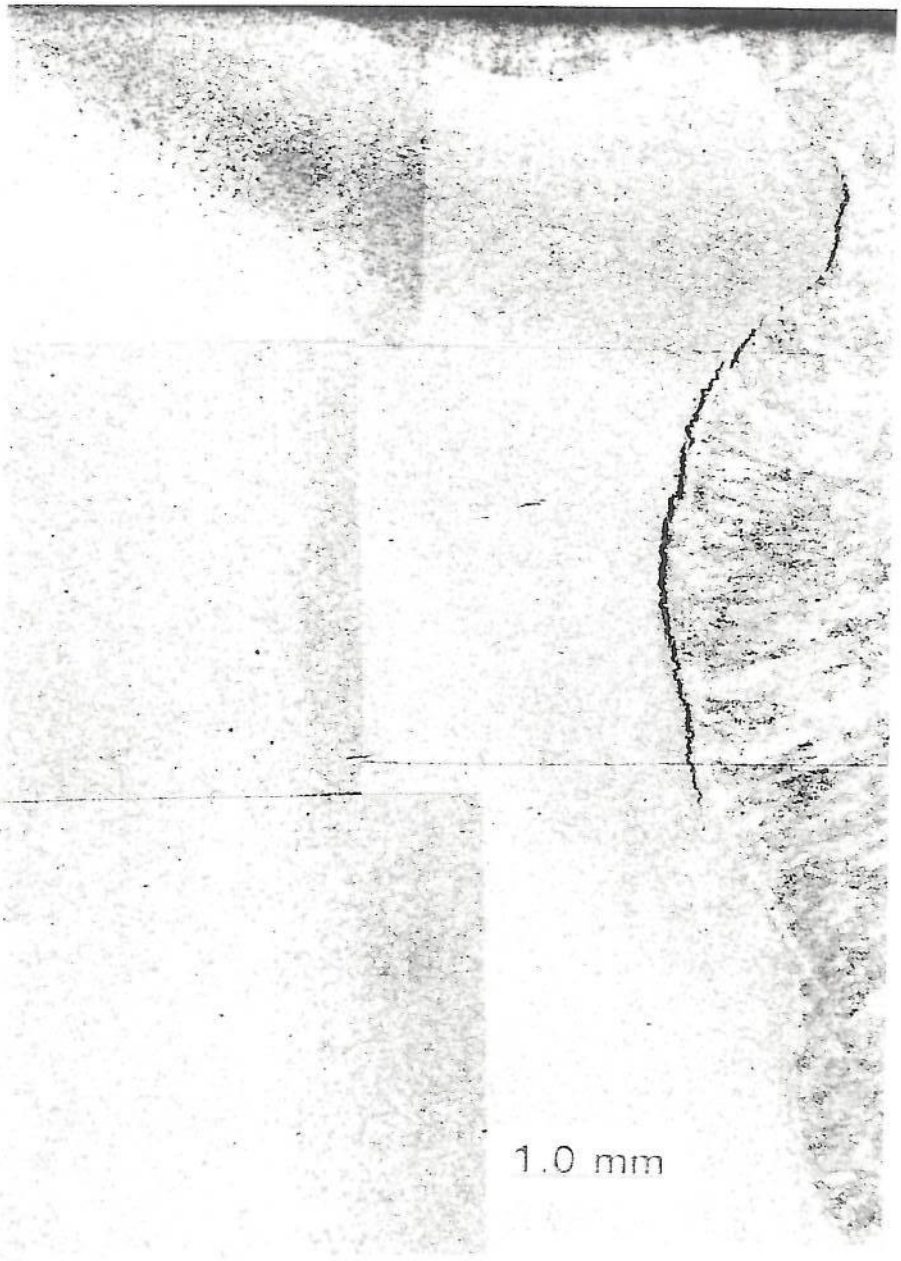

FIG 2.4

Type IIIa Cracking

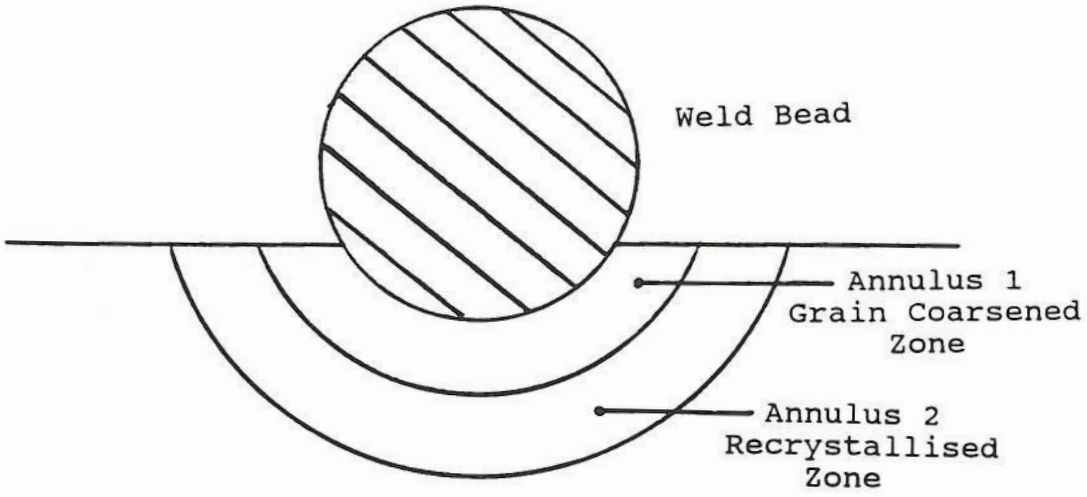

FIG 2.7

Schematic Representation of the Heat Affected Zone associated with a Single Weld Bead

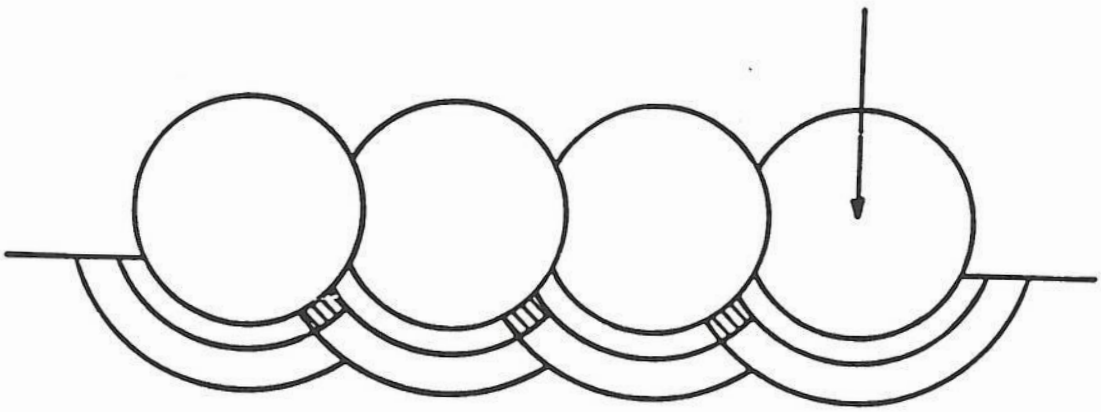

FIG 2.8

Schematic Representation showing Grain Refined Zones (Hatched Areas) formed as a consequence of a Low Level of Overlap between Weld Beads

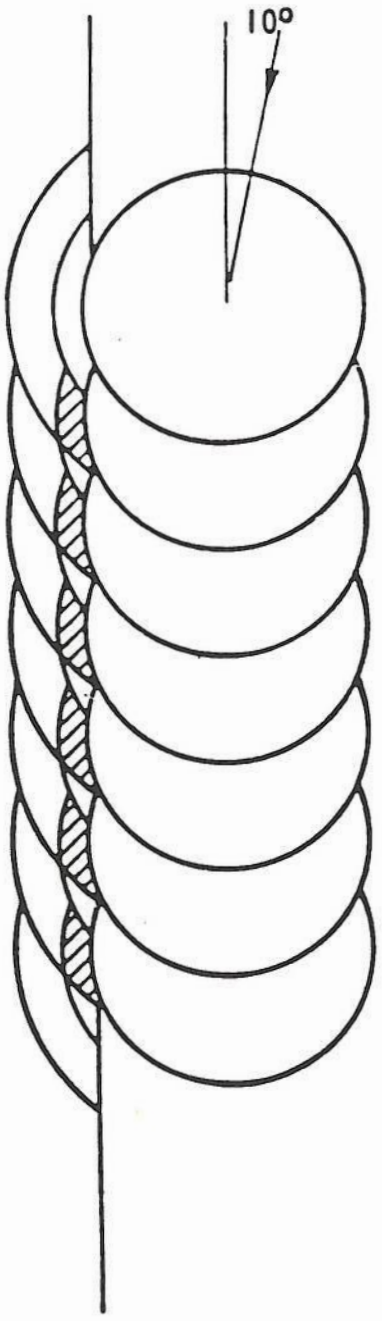

FIG 2.9

Schematic Representation showing Grain Refined Zones (Hatched Areas) formed as a consequence of a High Level of Overlap between Weld Beads

3.0 EXPERIMENTAL PROCEDURE

To investigate the effects of weld metal alloy content on carbon diffusion in CMV material, test pieces were produced with a range of welding consumables of different alloy content. The weld pieces were produced using the controlled deposition technique, described in section 2.3, designed to achieve a predominantly fine grained microstructure in the HAZ adjacent to the fusion boundary.

To investigate the effects on carbon diffusion of different thermal cycles, sections from each weld test piece were;

a) left in the as welded condition

b) post weld heat treated

c) post weld heat treated followed by a further ageing heat treatment designed to simulate service exposure.

3.1 PARENT MATERIAL

The ½Cr½Mo¼V parent material used in this investigation was service exposed main steam pipework material removed from a conventional power station. Type IIIa cracking problems had been associated with this material, and the chemical composition of the material is shown in **Table 3.1**. The dimensions of the material are;

Outside Diameter - 345mm
Wall Thickness - 62mm

For the purposes of the investigation the service exposed material was renormalised and tempered. The treatment given was in accordance the requirements of BS3604 Part 1[28].

3.2 ELECTRODES

To investigate fusion boundary carbon diffusion during the welding, post weld heat treatment and aging heat treatment cycles, four different electrode types were used.

a) Mild Steel - BS639 E51XXB
b) 2Cr1Mo - BS2493 2CrMoB
c) 9Cr1Mo - BS2493 9CrMoB
d) ½Cr½Mo¼V - Based on Suprex F, formerly part of the Murex Hymet range of electrodes.

The ½Cr½Mo¼V Suprex F electrode is no longer in production and was made especially for this project courtesy of MUREX UK. The actual composition of the electrode was just outside the originally specified range in terms of the manganese and vanadium content. However in all other respects the electrodes met the compositional requirements. The composition of all the electrodes used in this investigation are shown in **Table 3.2.**

3.3 TEST PIECE PRODUCTION

The test pieces were prepared with a 10° weld face angle and a flat bottom, **Fig 3.1.** The weld face angle conforms to the requirements of BS2633[9] for the upper part of a double 'V' weld preparation typically used for thick section pipework welds. The flat base included in the preparation was solely for supporting the weld metal during deposition. There was considered no point in producing a full weld sample as the fusion boundary was the area of interest.

The test pieces were held in a welding manipulator during deposition enabling the welder to index them during welding, thus maintaining optimum welding conditions, **Fig 3.2. Fig 3.3** shows the test piece in the manipulator, a piece of mild steel plate has been tacked onto the test piece to further help support the weld material during deposition. Also, Instead of welding onto a test piece that was part of a ring, **FIG 3.1**, a fully circumferential test piece was used, which was then cut to size after welding. The test piece was preheated to a minimum temperature of 250°C throughout the welding process. Preheat was applied electrically using a heating blanket. The temperature was controlled automatically using thermocouples. The interpass temperature was kept below 350°C throughout welding.

Welding was carried out using a technique of high bead overlap, described in section 2.3, to produce a fine grained microstructure in the HAZ adjacent to the fusion boundary. Welding was carried out in a nominally downhand position with the electrode essentially vertical to the weld preparation face, in so doing a high degree of weld bead overlap was maintained.

3.2mm diameter electrodes were used for the first pass and either 3.25 or 4.0mm electrodes for subsequent passes. The welding current was set according to the manufacturers recommendations but was kept at the lower end of the range. A travel speed between 2.5mm/s and 2.9mm/s was

specified for the first two weld passes.

The current, voltage and run out length for each pass were recorded using an OIS weld monitor, **Fig 3.4.** From this information the heat input during each weld run was calculated using the formulae below taken from BS5135[29].

$$\frac{IV}{W}$$

Where I and V are the average recorded current and voltage and W is the welding speed in mm/s for a particular weld run. The weld sequence and run number were also recorded. The welding conditions, heat input and run sequence for each test piece are recorded in **Appendix A.**

3.4 TRIAL WELD

Before producing the test plates for the investigation a trial test weld was produced to give the welder an opportunity to familiarise himself with the electrode characteristics and the required welding conditions. It also gave him an opportunity to become familiar with the indexing of the test plate during welding.

3.5 TEST PIECE SECTIONING AND HEAT TREATMENT

On completion of the test welds, the ends of each of the test plates were discarded as these would have contained the majority of the start stop positions. It was also considered likely that the specified welding conditions may not have been consistently achieved because of the time taken for the arc to stabilise and for the welder to get into his 'rhythm'.

3.5.1 Sectioning

The test plates were cut into three nominally equal pieces. One section from each test weld was left in the as welded condition, the two further test plates were post weld heat treated. One of the post weld heat treated test plates was then given a further heat treatment designed to simulate service exposure of the order of 100,000hrs. The conditions for post weld heat treatment are given in section 3.5.2.

Before proceeding with post weld heat treatment the sections were macro-etched to confirm they were

essentially free of defects and that the desired fusion boundary microstructure had been achieved.

On completion of the heat treatments the top and the bottom 25mm of each sample were discarded and the central section was cut up to produce four samples for carbon diffusion measurements and detailed macroscopic and microscopic examination.

The samples were given abbreviated identifiers, which were;

MS - Mild Steel weld metal
CMV - CMV weld metal
2Cr - 2CrMo weld metal
9Cr - 9Cr weld metal

3.5.2 Post Weld Heat Treatment:

Post weld heat treatment was carried out to the requirements of BS2633[8] in a top hat furnace:

Temperature - 690°C to 720°C
Time - 3hrs
Heating Rate - 100°C/h max. above 400°C
Cooling Rate - 50°C/h max. above 400°C then air cooled

Heat treatment was carried out in an inert atmosphere of argon to minimise surface decarburization. Each of the four test plates had thermocouples attached using a capacitance discharge method. The thermocouples were protected from the furnace radiant heat using fire putty to ensure the actual material temperature was being measured. The temperature of the test pieces was recorded on a chart recorder.

3.5.3 Extended Heat Treatment:

The conditions for the extended heat treatment were designed to give a level of diffusion equivalent to that anticipated in a conventional coal fired power station operating for a nominal period of 100,000hrs.

Coal fired power stations operate at a normal temperature of 565°C. It was necessary to calculate a temperature so that the treatment would be finished within a reasonable time. The conditions were derived using the Larson Miller parameter[31], the actual conditions used and the method of calculation are described **Appendix B**.

Temperature - 638°C to 645°C
Time - 884hrs

The heat treatment was carried out in a small furnace under an Argon atmosphere. Thermocouples were attached to each specimen as before.

3.5.4 Heat Treatment Condition

The heat treatment condition of samples was identified as follows;

AW - As welded
PWHT - Post weld heat treated (PWHT)
AGED - PWHT and artificially aged

3.6 METALLURGICAL INVESTIGATIONS:

3.6.1 Macroscopic Examinations:

Macroscopic Examination was carried out on sections removed from each of the test pieces. The sections were ground to a 400 grit finish and etched in 10% Nital and Acidified Ferric Chloride in the case of the 9Cr sample. This enabled the weld run sequence to be identified and qualitative assessment to be made of the degree of grain refinement achieved.

3.6.2 Microscopic Examination

i) Microscopic Examination of a macro etched section removed from each of the test piece was carried out by first hot mounting the section, polishing to a 3μm finish and then etching in 5% Nital. The surface was examined using an optical microscope.

The proportion of refinement down the fusion boundary of each sample was identified by the use of the vernier scale on the microscope stage. The cumulative length of grain refined and coarser grained microstructural regions was measured along the fusion boundary. Grain refined regions were defined as areas with a grain size of 3-10μm. Coarser grained regions were identified as areas with a grain size between 10μm and 40μm. The parent material grain size was also recorded.

ii) Microscopic examination was carried out on a further section from each of the test pieces in each heat treatment condition. The sections were polished to a 1μm

finish and etched in 2% Nital. The sections were used for metallurgical analysis and micro hardness testing.

ii) A third section from each test block in each heat treatment condition was mounted in conductive mounting material. The sections were prepared by polishing to a 1μm finish and lightly etched, just sufficiently to identify the fusion boundary, and sent to Harwell for nuclear microprobe analysis.

3.6.3 Micro-hardness Measurement

Micro-hardness measurements were taken using a Leitz micro hardness testing machine with a load of 500g. The spacing between hardness indentations was at least 3x the size of an indentation.

Micro-hardness measurements were taken across the full width of HAZ of the 2CrMo samples in each heat treatment condition.

Micro-hardness readings either side of the fusion boundary were measured for all the samples.

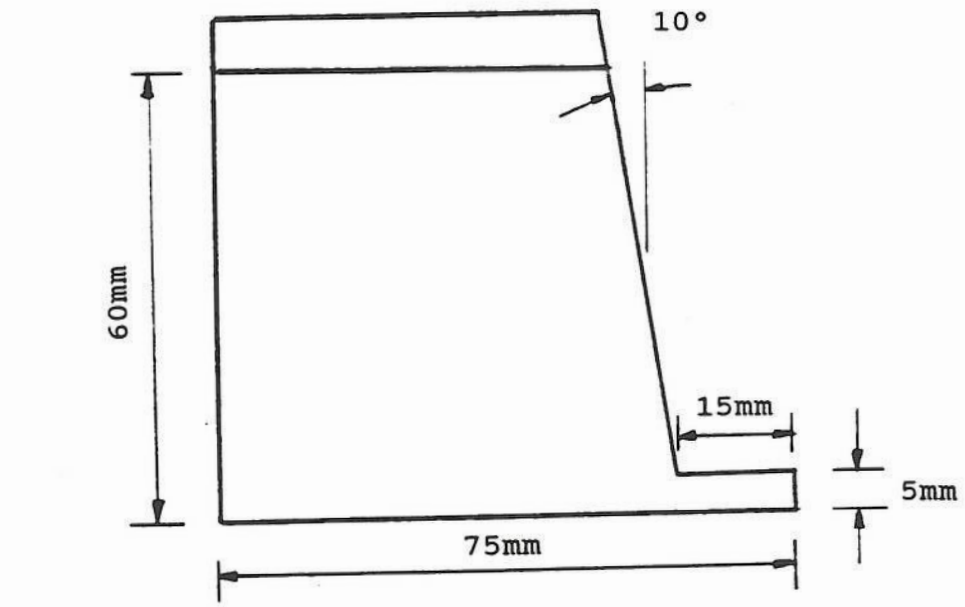

SIDE VIEW

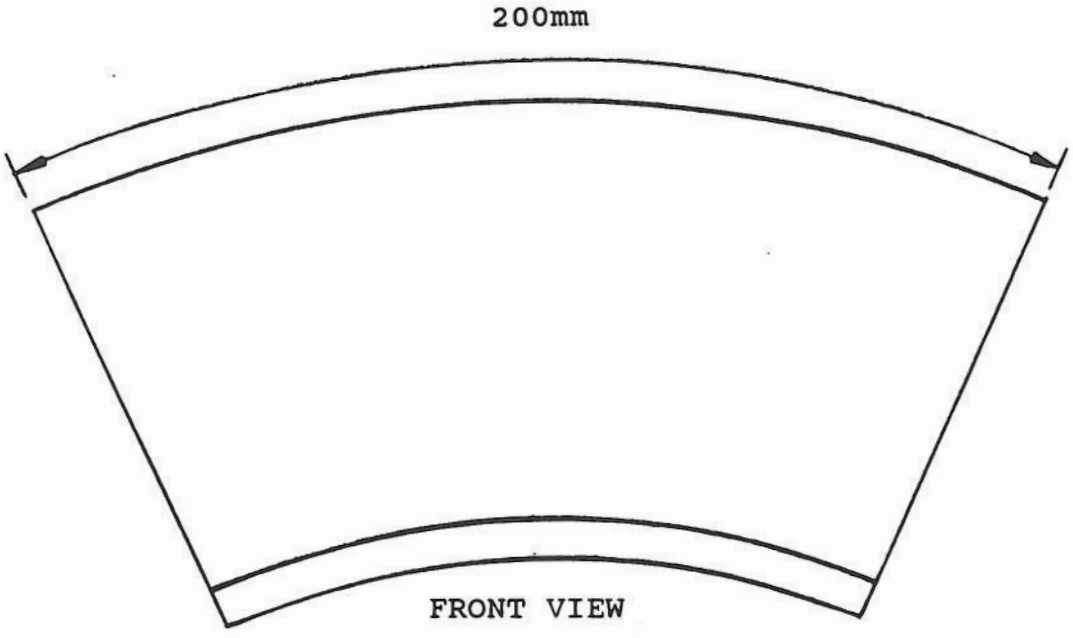

FRONT VIEW

FIG 3.1

Weld Test Piece Dimensions

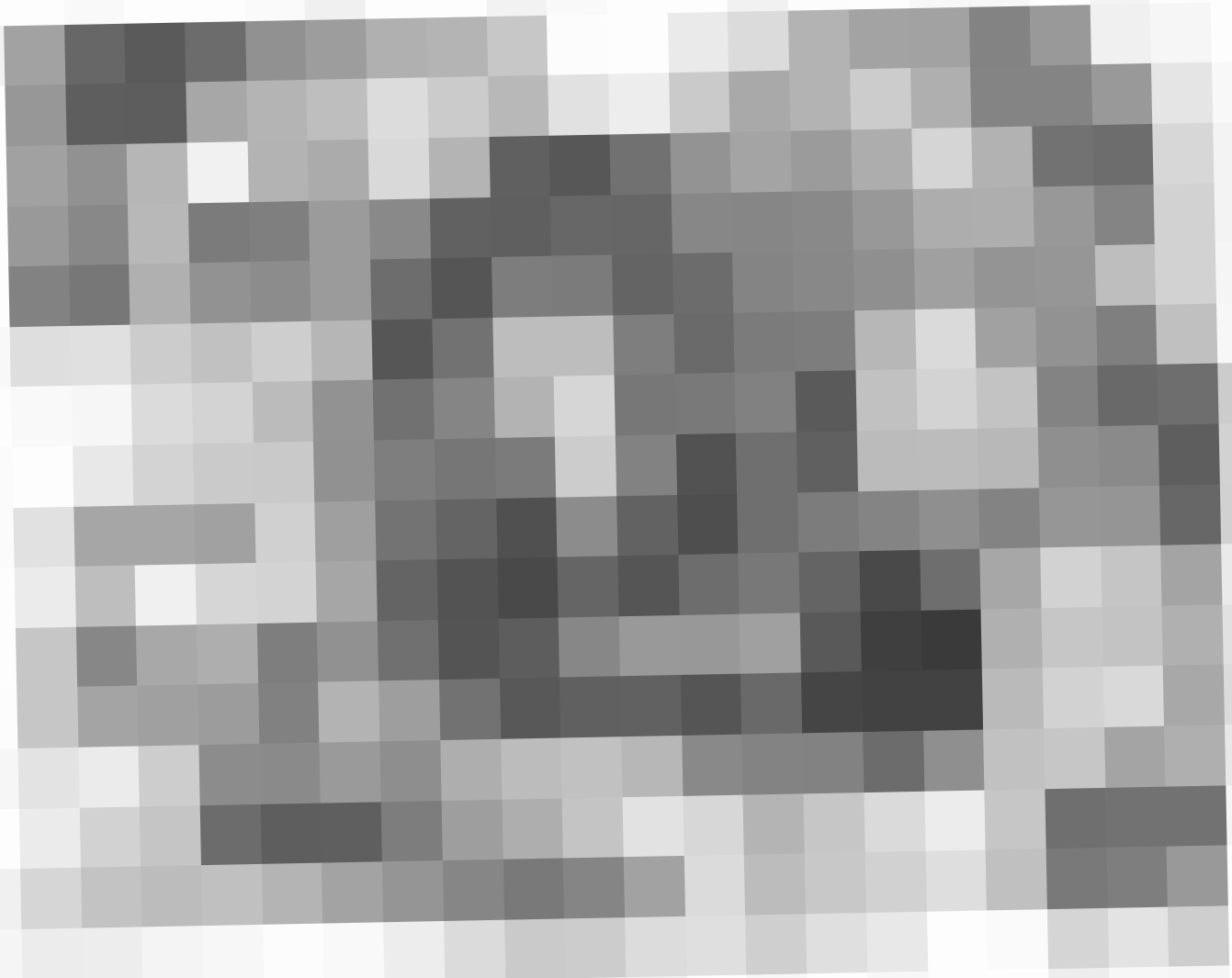

FIG 3.3

Test Piece during Production

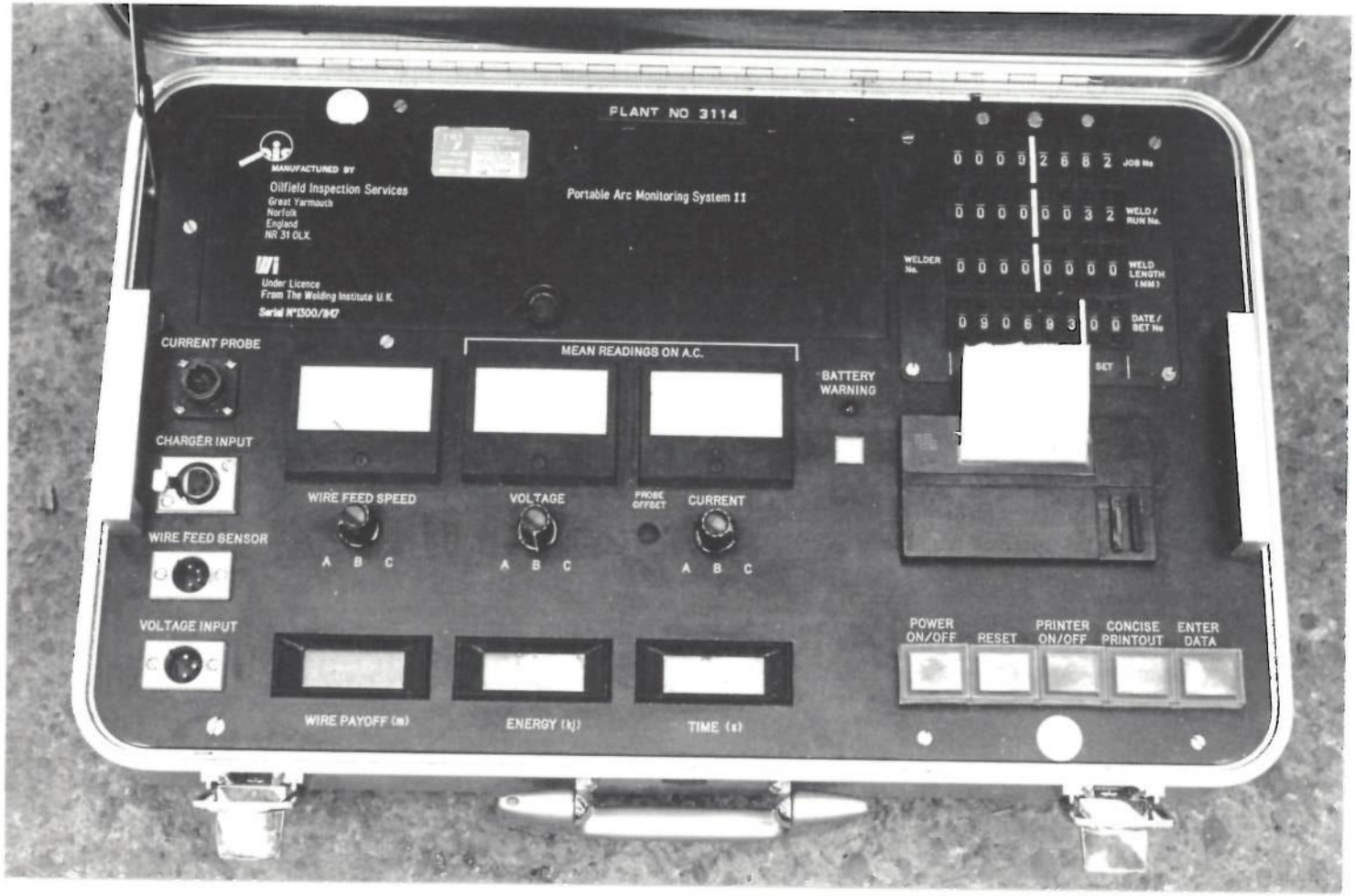

FIG 3.4

Welding Monitor used to record Welding Variables

Composition (%)										
C	Si	Mn	P	S	Cr	Mo	Ni	Cu	Nb	V
0.13	0.19	0.51	0.021	0.033	0.39	0.53	0.12	0.16	<.01	0.26

Table 3.1

Composition of CMV Parent Material

Electrode Type	Size (mm)	Composition (%)										
		C	Si	Mn	P	S	Cr	Mo	Ni	Cu	Nb	V
Suprex F (CMV)	3.2	0.033	0.26	0.52	0.021	0.016	0.57	0.48	0.03	0.04	<.005	0.19
	4.0	0.054	0.22	0.53	0.021	0.012	0.47	0.42	0.03	0.04	<.005	0.17
E5156B (MS)	3.2	0.053	0.30	1.27	0.016	0.005	0.03	0.17	0.02			<0.02
	4.0	0.047	0.33	1.39	0.015	0.006	0.04	0.16	0.02			<0.02
2CrMoB (2Cr)	3.2	0.06	0.35	1.03	0.012	0.006	2.0	0.95				
	4.0	0.06	0.40	1.03	0.013	0.008	2.30	0.94	0.04	0.04		
9CrMoB (9Cr)	3.2	0.061	0.34	0.73	0.013	0.009	8.72	1.01	0.05	0.05	0.01	
	4.0	0.057	0.39	0.73	0.013	0.012	8.39	0.96	0.11	0.05	0.01	

Table 3.2

MMA Electrode Chemical Analysis

4.0 **RESULTS**

4.1 HAZ GRAIN REFINEMENT

Visual examination of micro's etched with 5% Nital enabled weld bead overlap and its effect on HAZ grain refinement to be observed, **Fig 4.1**. Two distinct areas of grain size can be seen, the darker etched areas being finer grained. Examination of these areas at a higher magnification enabled the grain sizes in these two regions to be identified. The darker etched regions had a grain size of between 3μm and 10μm, **Fig 4.2**. The more lightly etched HAZ region was identified as having a grain size between 10μm and 40μm, **Fig 4.3**. The parent material was also examined and had a typical grain size of around 50μm, **Fig 4.4**.

The HAZ microstructure of the specimens examined consisted of alternate bands of grain refined and coarser grained regions, as defined in the experimental procedure. The percentage of fine grained region in a sample removed from each of the weldments is shown in **Table 4.1** below. A photomicrograph identifying regions of fine grained and coarser grained microstructure is shown in **FIG 4.5**. The actual position of transition between fine grained and coarse grained regions was made using observations at a magnification of x200.

SAMPLE	LENGTH OF FUSION BOUNDARY (mm)	CUMULATIVE LENGTH AND PERCENTAGE			
		FINE GRAINED		U FINE GRAINED	
		L (mm)	%	L(mm)	%
C	10.25	4.1	40	6.15	60
CMV	11.20	4.2	37.5	7.0	62.5
2Cr	12.30	4.4	36	7.9	64
9Cr	11.50	3.5	30	8.0	70

Table 4.1

4.2 CARBON PROFILES

All the carbon and Chromium profiles produced are contained in **Appendix C**. In some cases the fusion boundary region was missed during scanning, the profiles are therefore of little value however, they have been included for completeness. The Carbon and Chromium profiles of particular interest and which form part of the discussion are presented in **Figs 4.6 to 4.18**. The following identification system has been used.

MS - Mild Steel weld metal
CMV - CMV weld metal
2Cr - 2CrMo weld metal
9Cr - 9CrMo weld metal

AW - As welded
PWHT - Post Weld Heat Treated
AGED - Post Weld Heat Treated and Aged

C - Coarse scanning sensitivity, 250μm between readings.
M - Medium scanning sensitivity, 40μm between readings.
F - Fine scanning sensitivity, 5μm between readings.

For example an identifier CMV.C.AGED denotes that a CMV weld metal was used, the sample had been post weld heat treated and aged, and that the carbon profile was generated on a coarse scanning sensitivity.

The initial carbon content of the weld (ICCW) and parent (ICCP) materials is indicated on the profiles in **Figs 4.6 to 4.18**.

The carbon contents have only been recorded to two decimal places as opposed to three which would have been desirable. Although, this is considered to detract from the appearance of the recorded profiles, it does not significantly affect interpretation.

The fusion boundary location has not been specifically identified on the graphs, however the difference in chromium content between weld and parent metal generally allows clear identification of the fusion boundary position. This is not the case with the CMV weld metal to CMV parent samples, with these samples the fusion boundary can be identified by the initially lower carbon content in the weld material and the slightly higher chromium content in the weld metal.

The results of the carbon profiling work are summarised in **Table 4.2**. The following notes apply to the table:

a) Initial Carbon and Chromium values are those taken from the chemical analysis certificates for the electrodes.

b) Maximum Carbon and Location are the peak carbon content recorded on the trace and its location. It should be appreciated that as the weld metal in all cases had considerably lower initial carbon content than the parent material. The location does not necessarily identify the direction of carbon migration.

c) Minimum Carbon content and Location, the minimum carbon content identified on the trace at a particular scanning sensitivity i.e coarse, medium or fine and its location.

d) Width of Carbon Loss, the width of carbon loss has only been recorded for the 2Cr and 9Cr weld samples and has been defined as areas with a carbon content <0.1%.

e) The letter 'M' used in the table identifies cases in which the fusion boundary had been missed.

4.3 MICRO HARDNESS MEASUREMENTS

The results of micro hardness tests on the welds made using 2CrMo weld metal are shown in **Table 4.3**. The results are also shown in graph form **Fig 4.19**.

The results of hardness tests taken adjacent to the fusion boundary in the parent HAZ and weld metal of all the weld samples are shown in **Table 4.4** The table also shows the hardness difference either side of the fusion boundary.

4.4 MACROSCOPIC EXAMINATION

Macroscopic examination of sections through each of the test welds, **Figs 4.20 to 4.23**, show a fairly uniform bead deposition sequence along the fusion boundary and high overlap between weld passes.

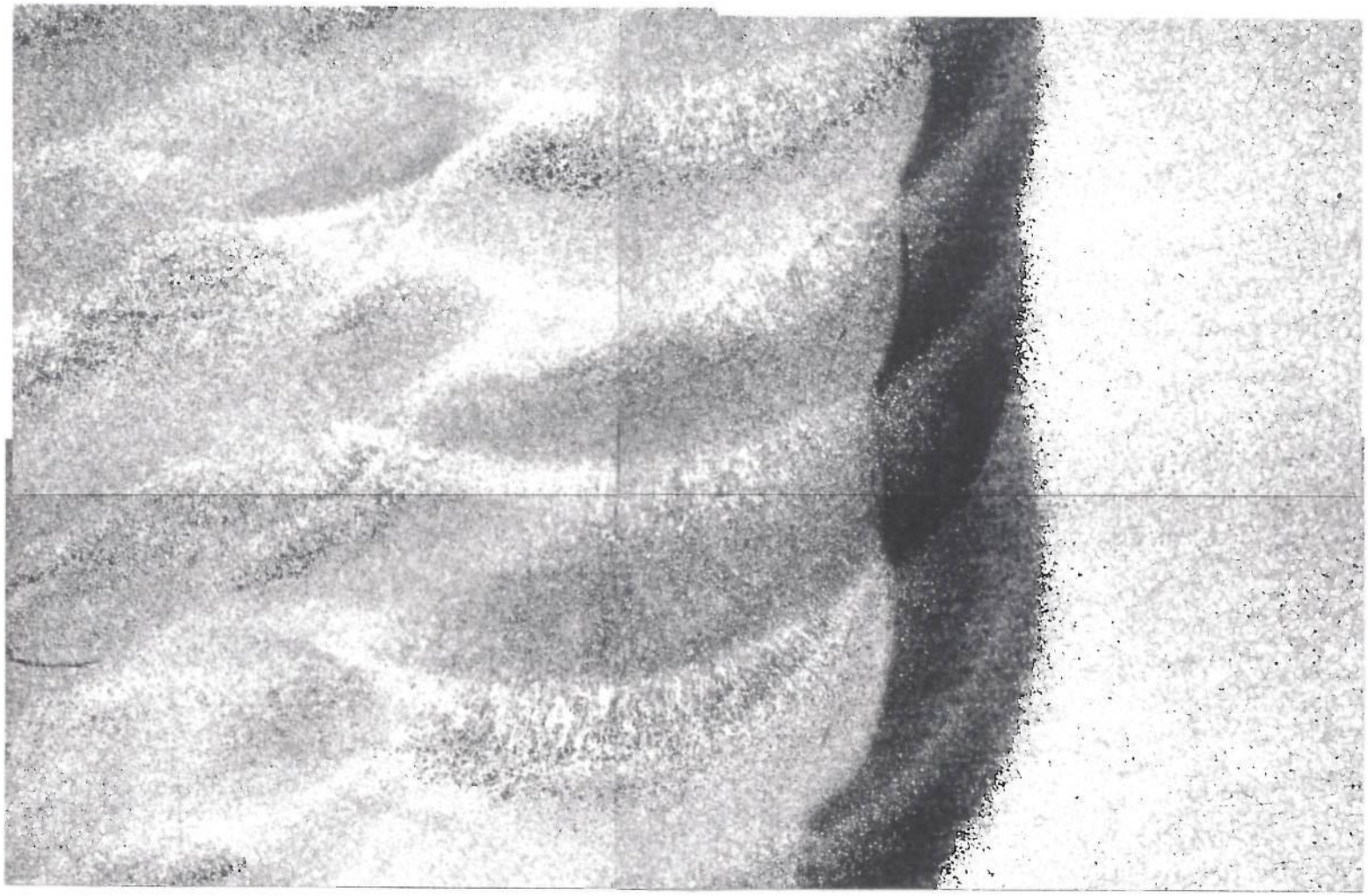

FIG 4.1

CMV Sample after Aging showing Weld Bead Overlap and HAZ Refinement (x13)

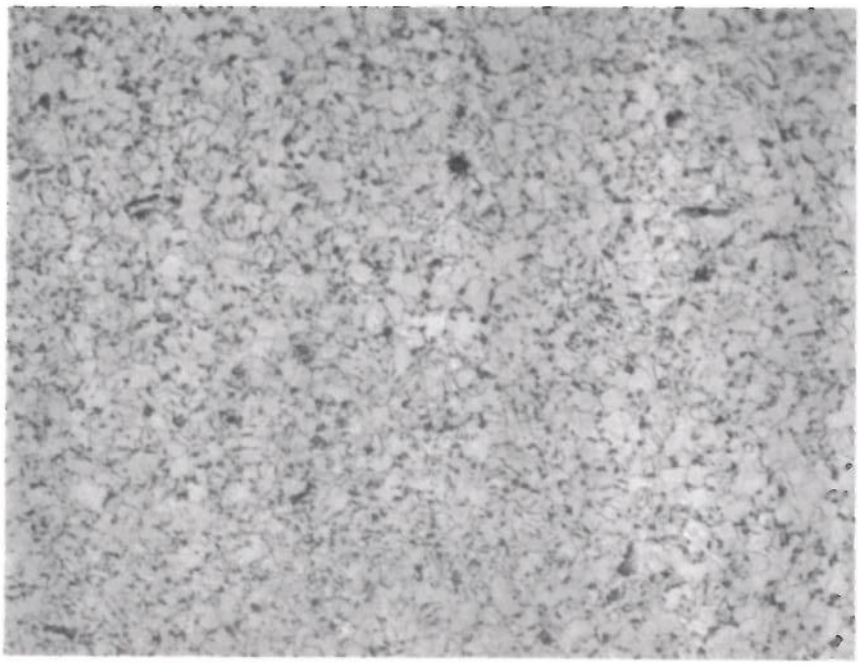

FIG 4.2

Fine Grained HAZ region in CMV Parent, As Welded (x500)

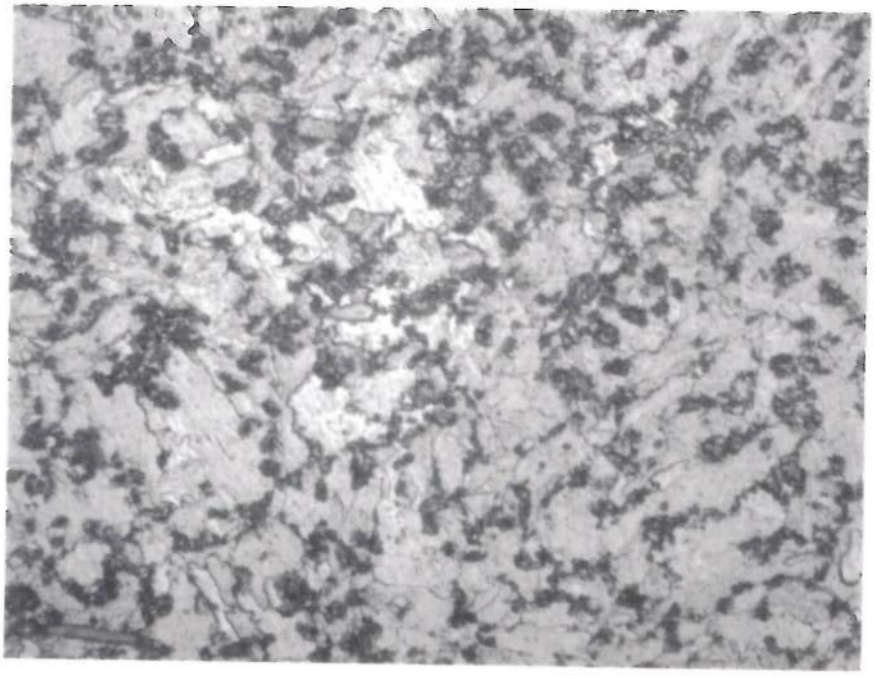

FIG 4.3

Coarser Grained HAZ region in CMV Parent, As Welded (x500)

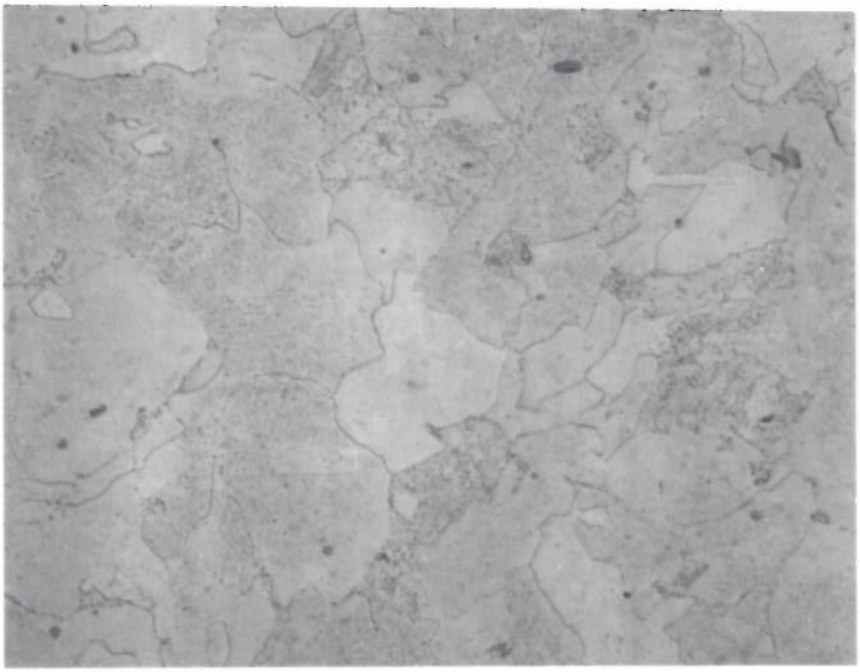

FIG 4.4

CMV Parent Material (x500)

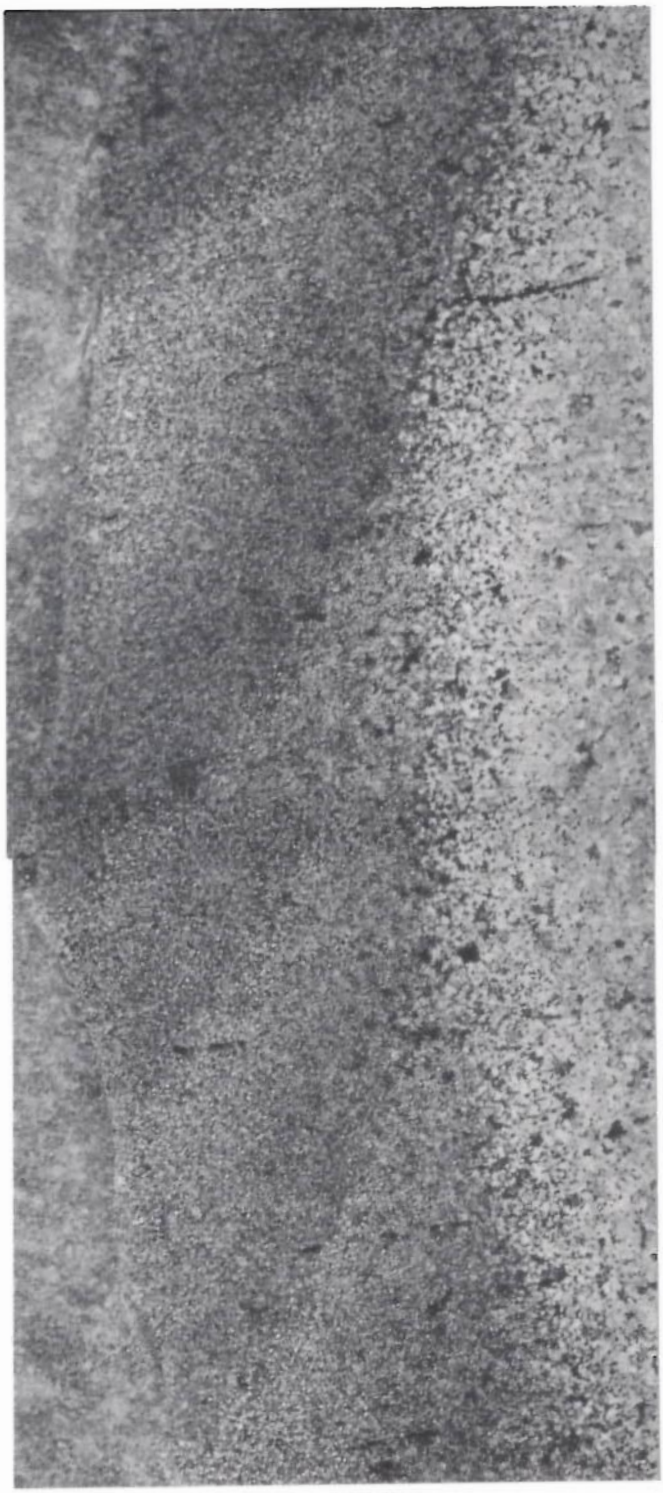

Fig 4.5

Fusion Boundary Grain Refined and Coarser Grained Regions

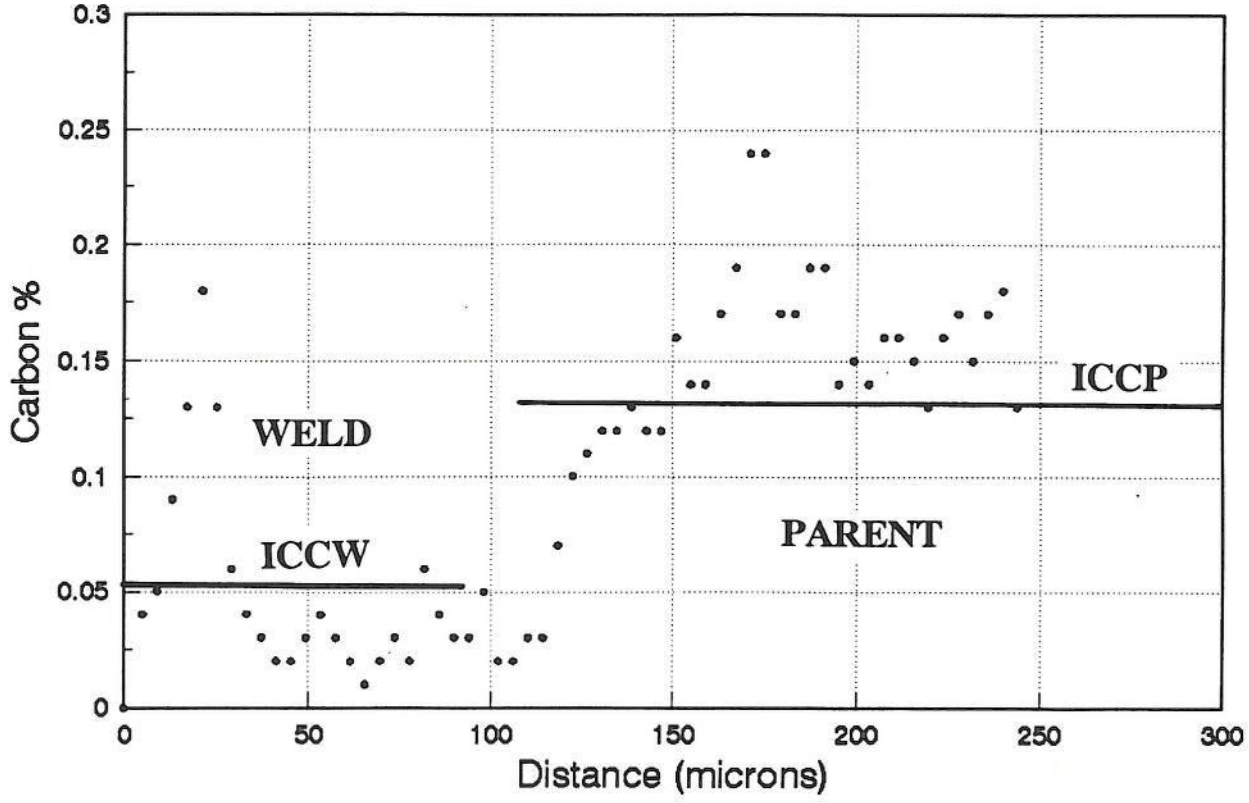

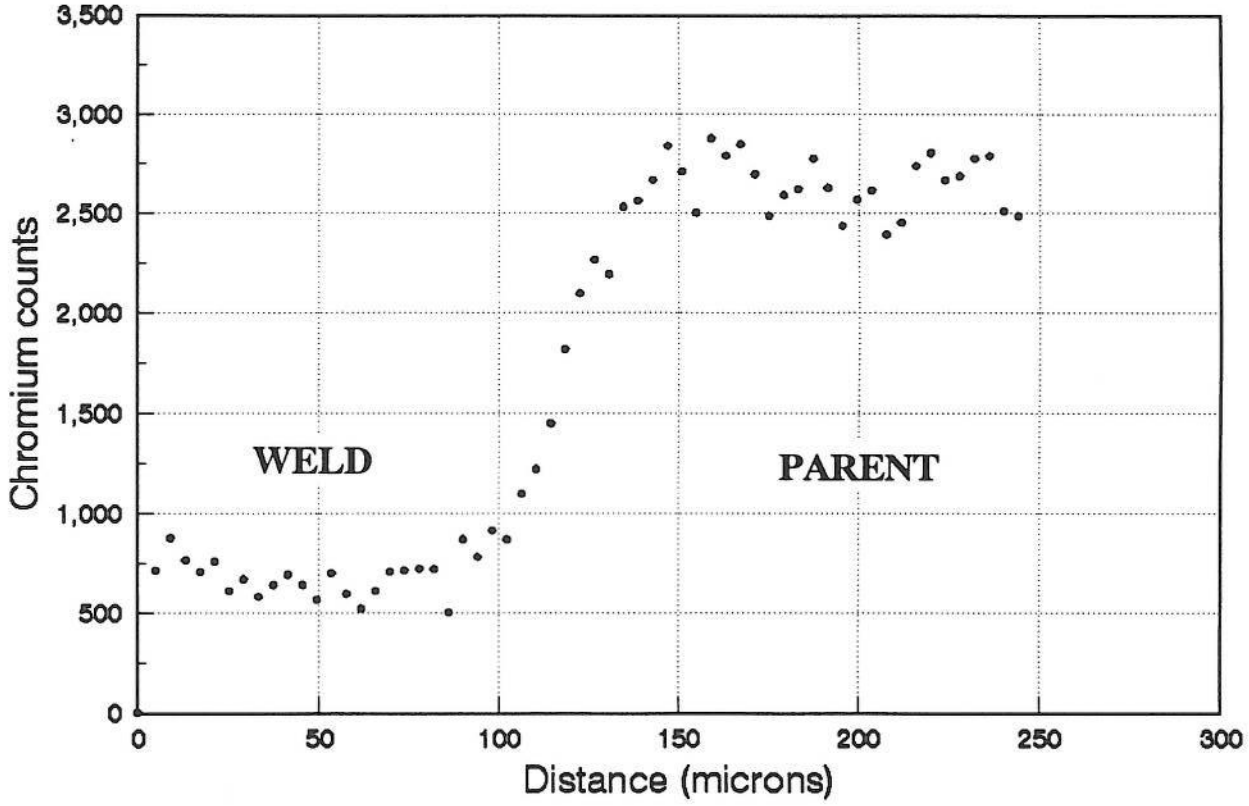

FIG 4.6

Carbon and Chromium Profiles Sample MS.F.AGED

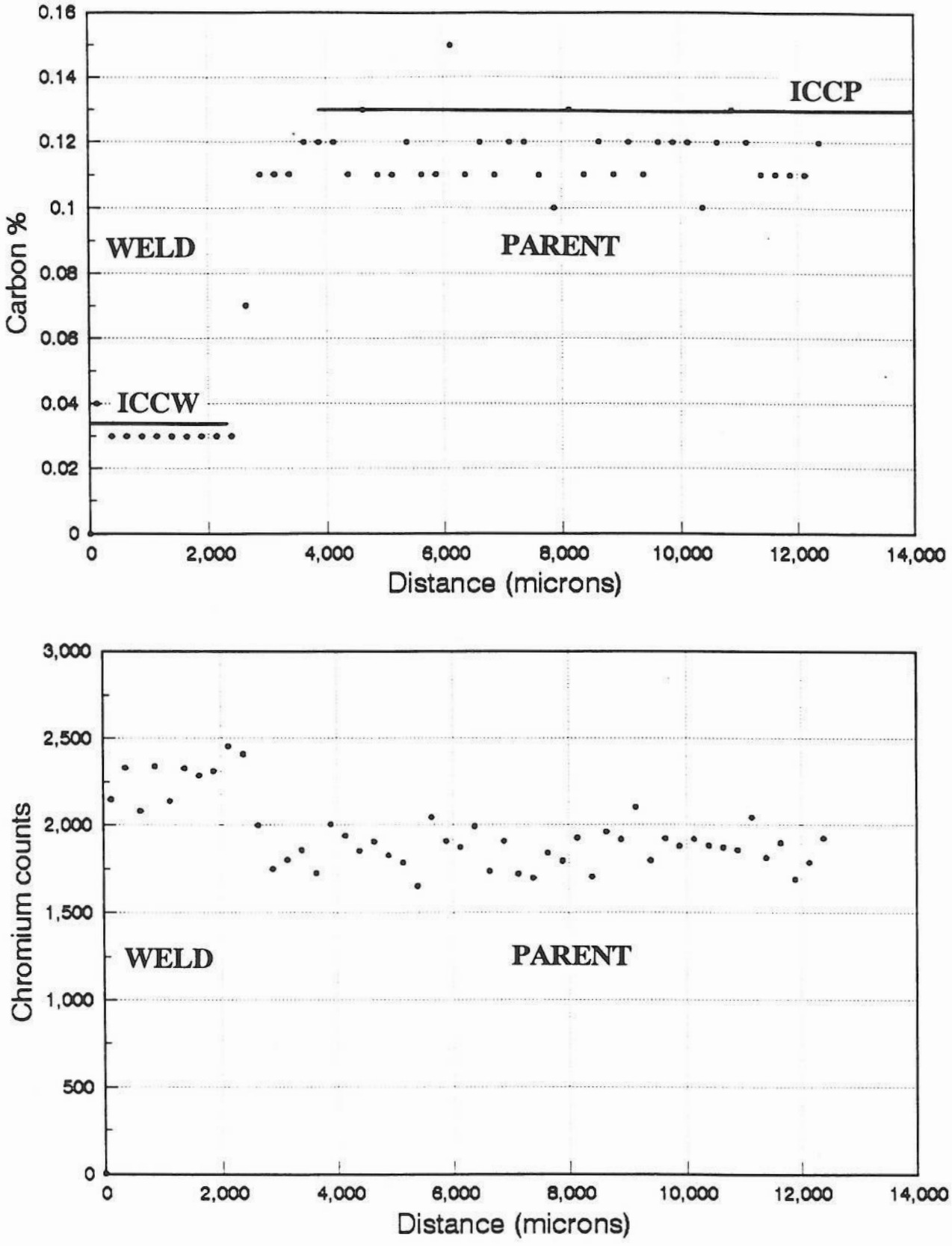

FIG 4.7

Carbon and Chromium Profiles Sample CMV.C.AW

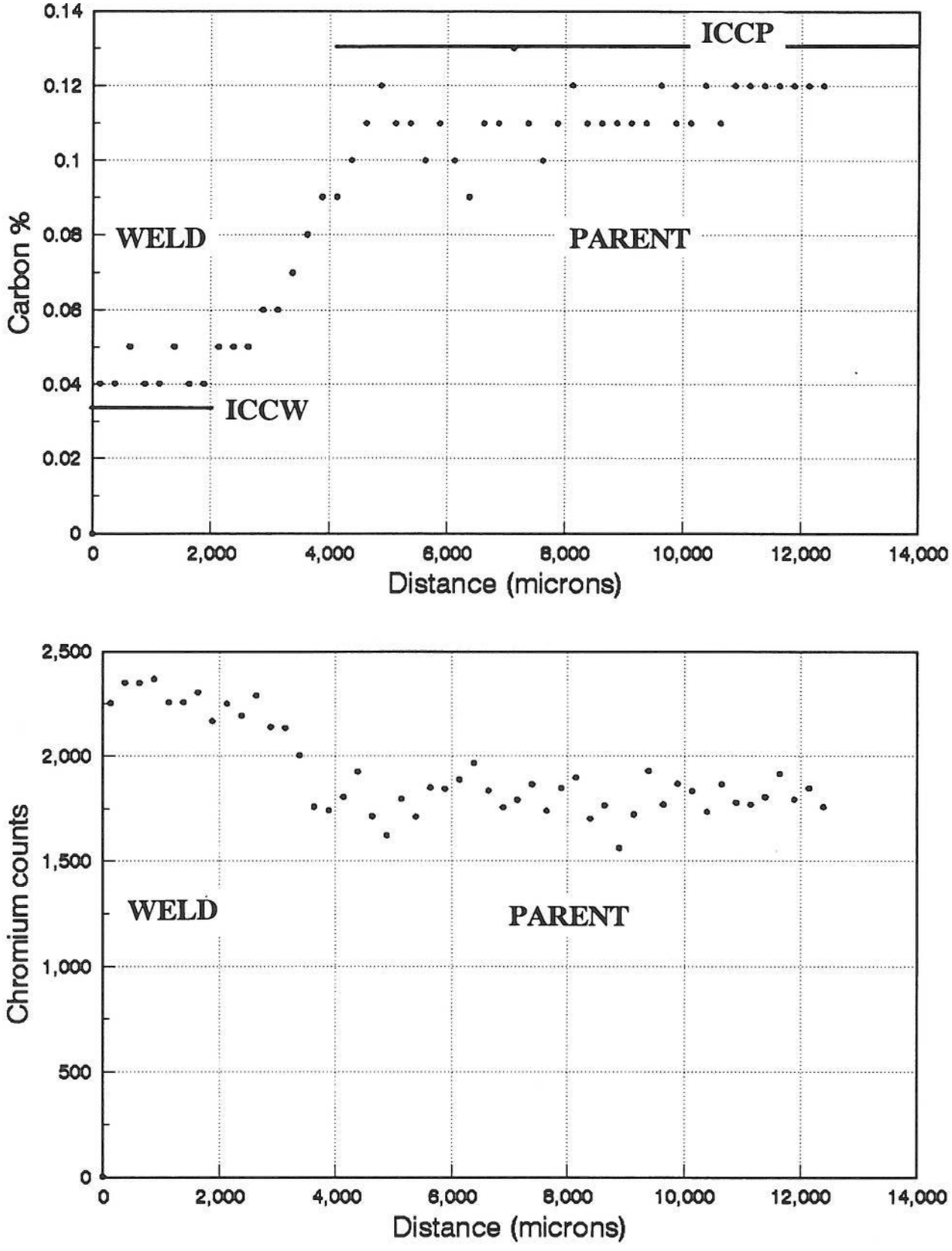

FIG 4.8

Carbon and Chromium Profiles Sample CMV.C.AGED

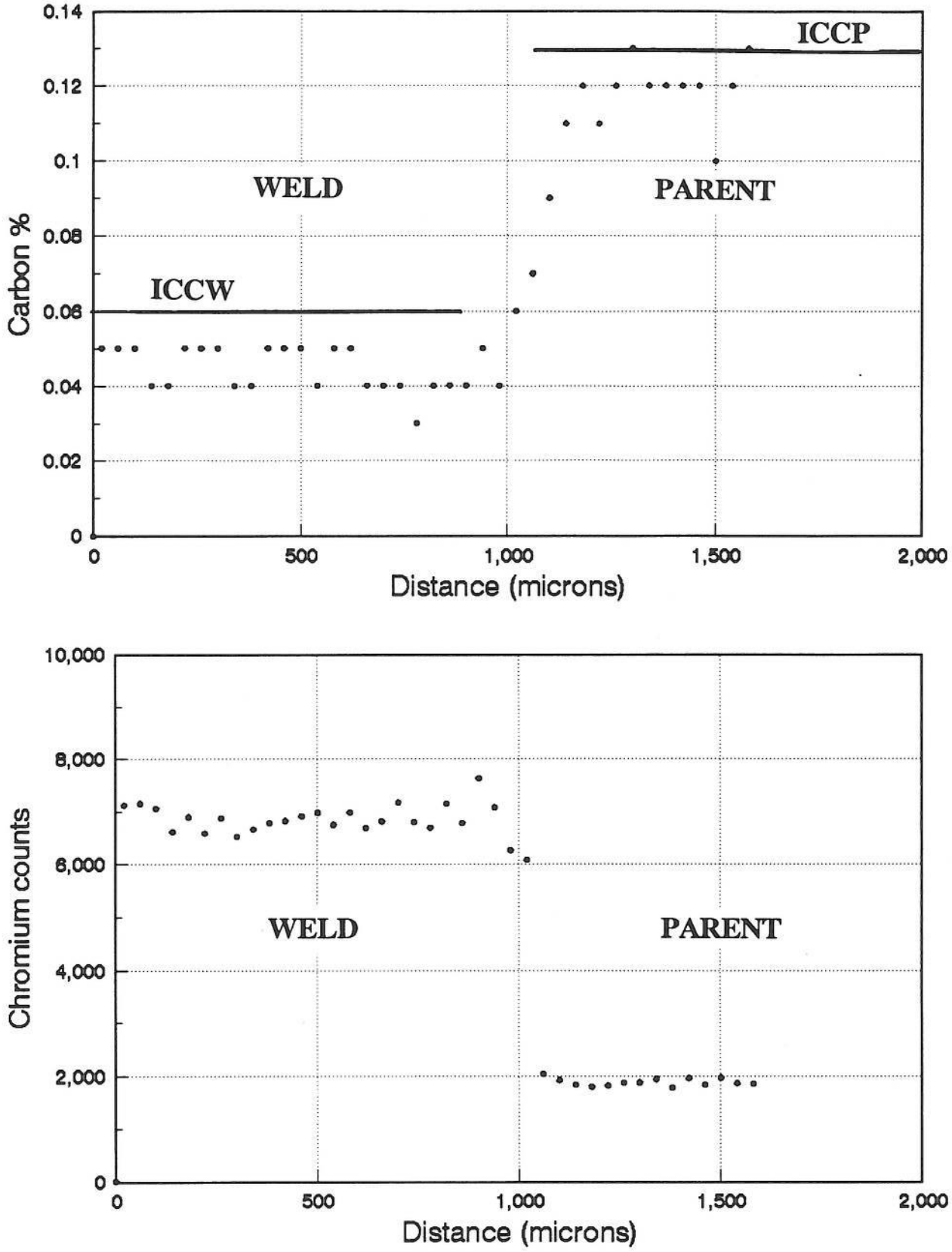

FIG 4.9

Carbon and Chromium Profiles Sample 2Cr.M.AW

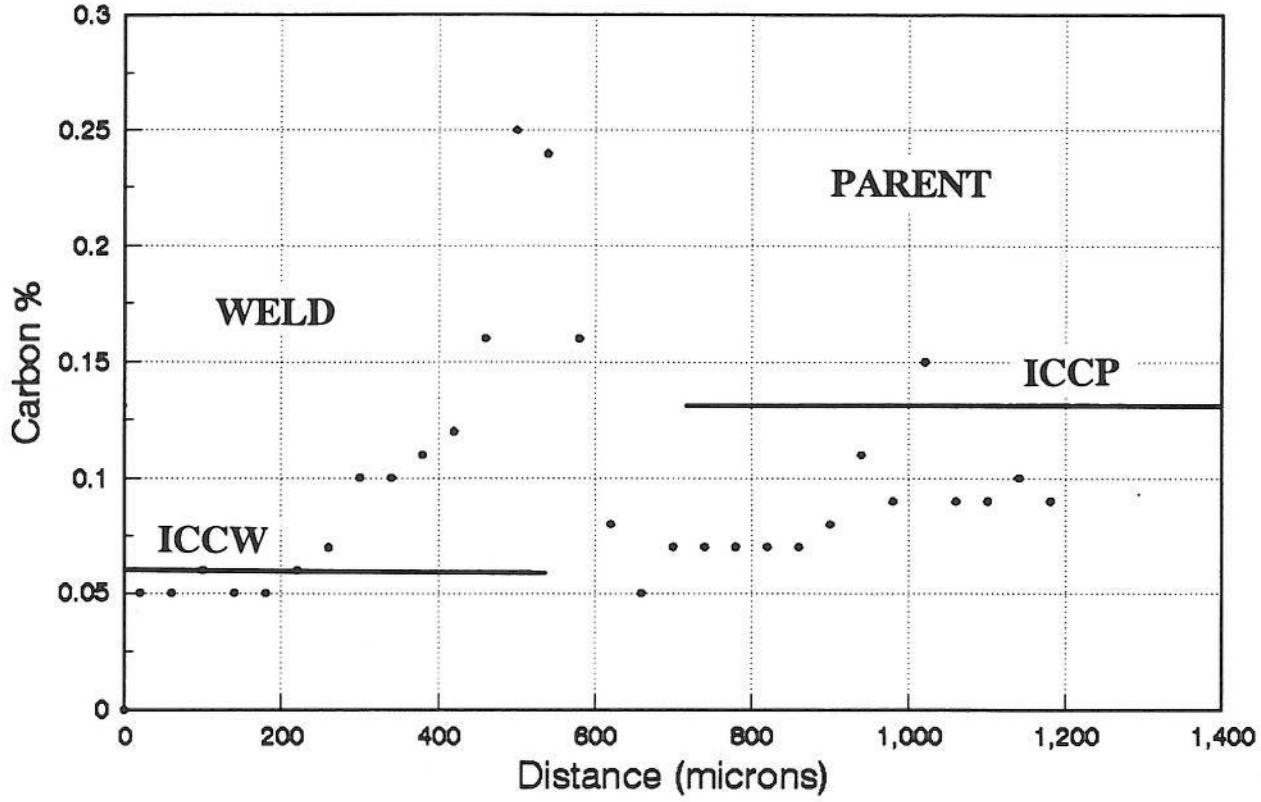

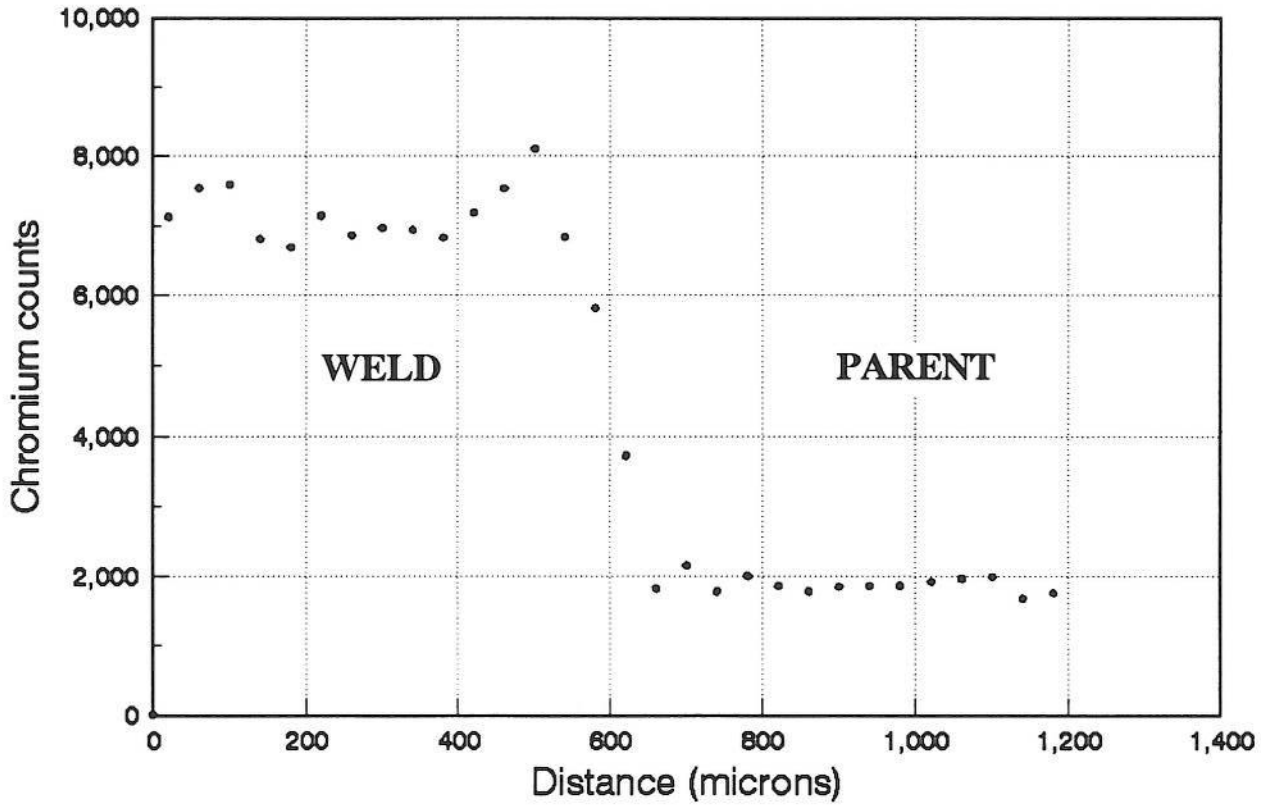

FIG 4.10

Carbon and Chromium Profiles Sample 2Cr.M.PWHT

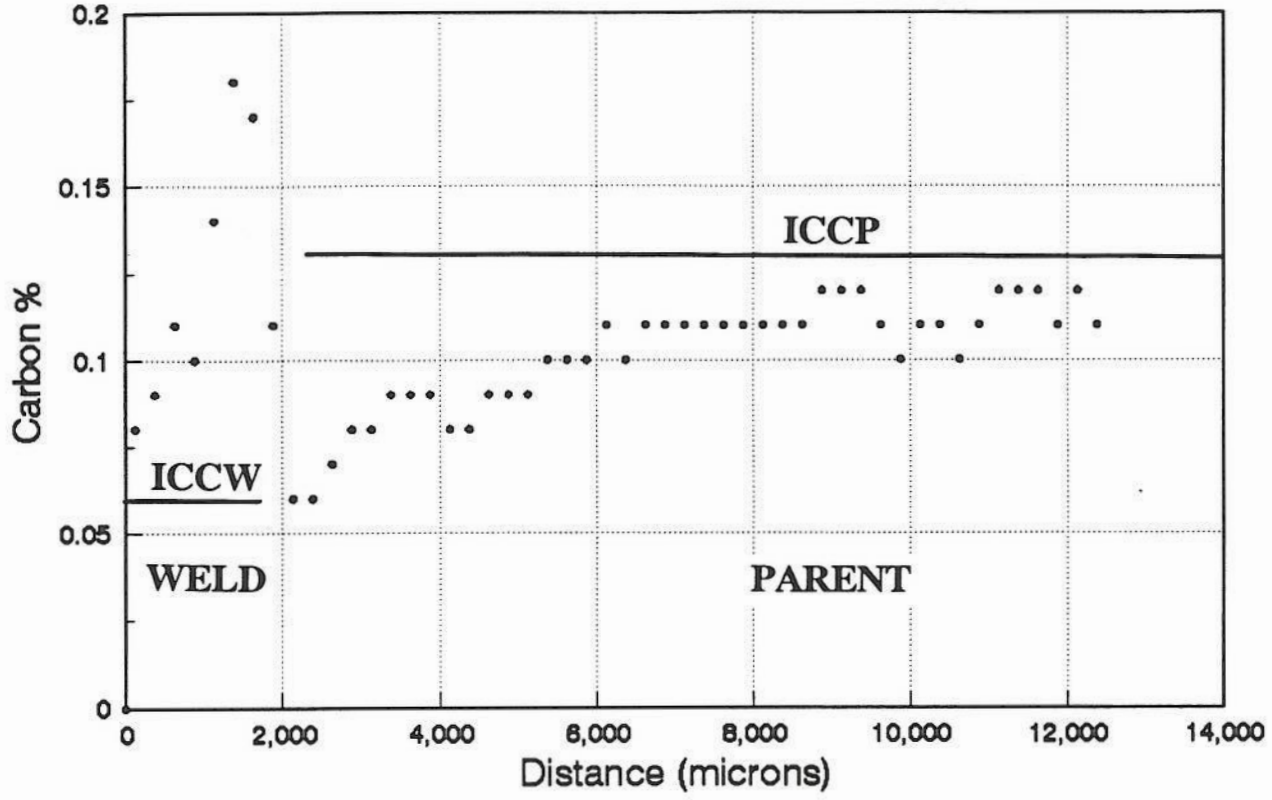

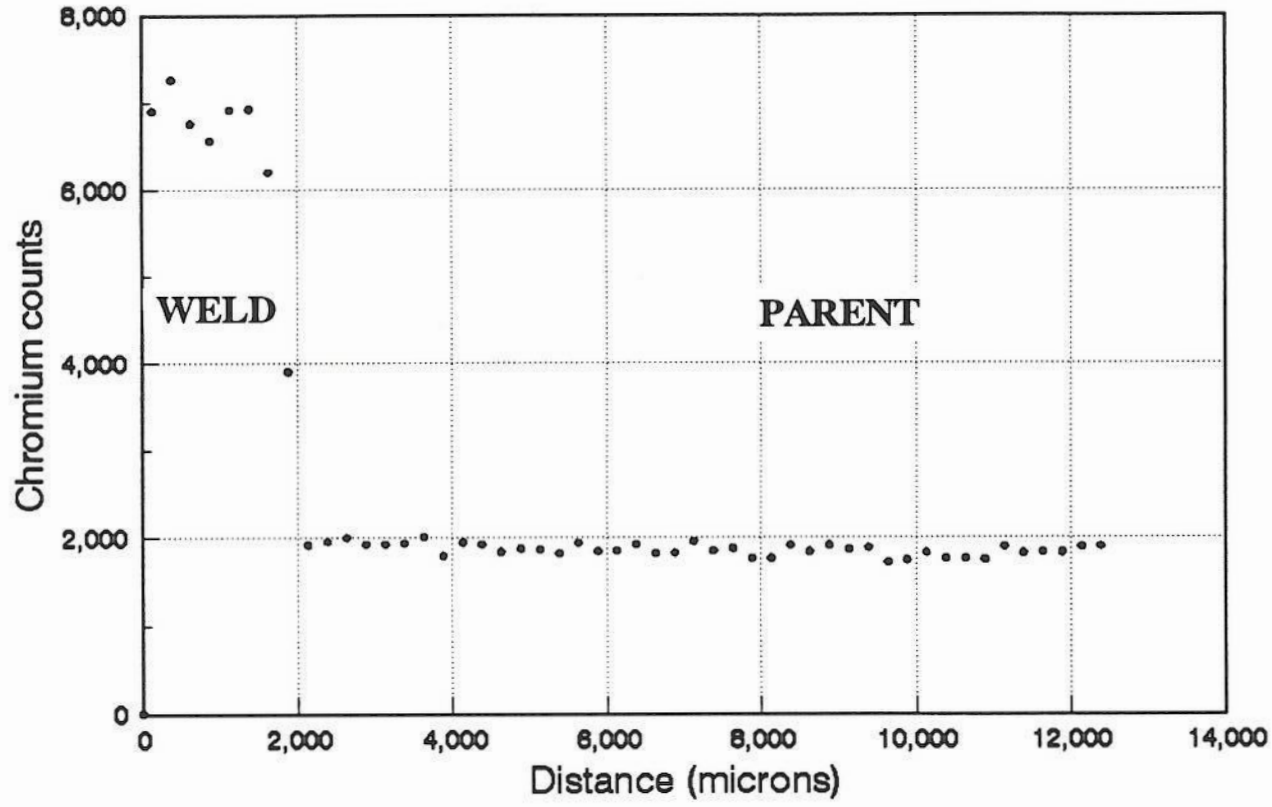

FIG 4.11

Carbon and Chromium Profiles Sample 2Cr.C.AGED

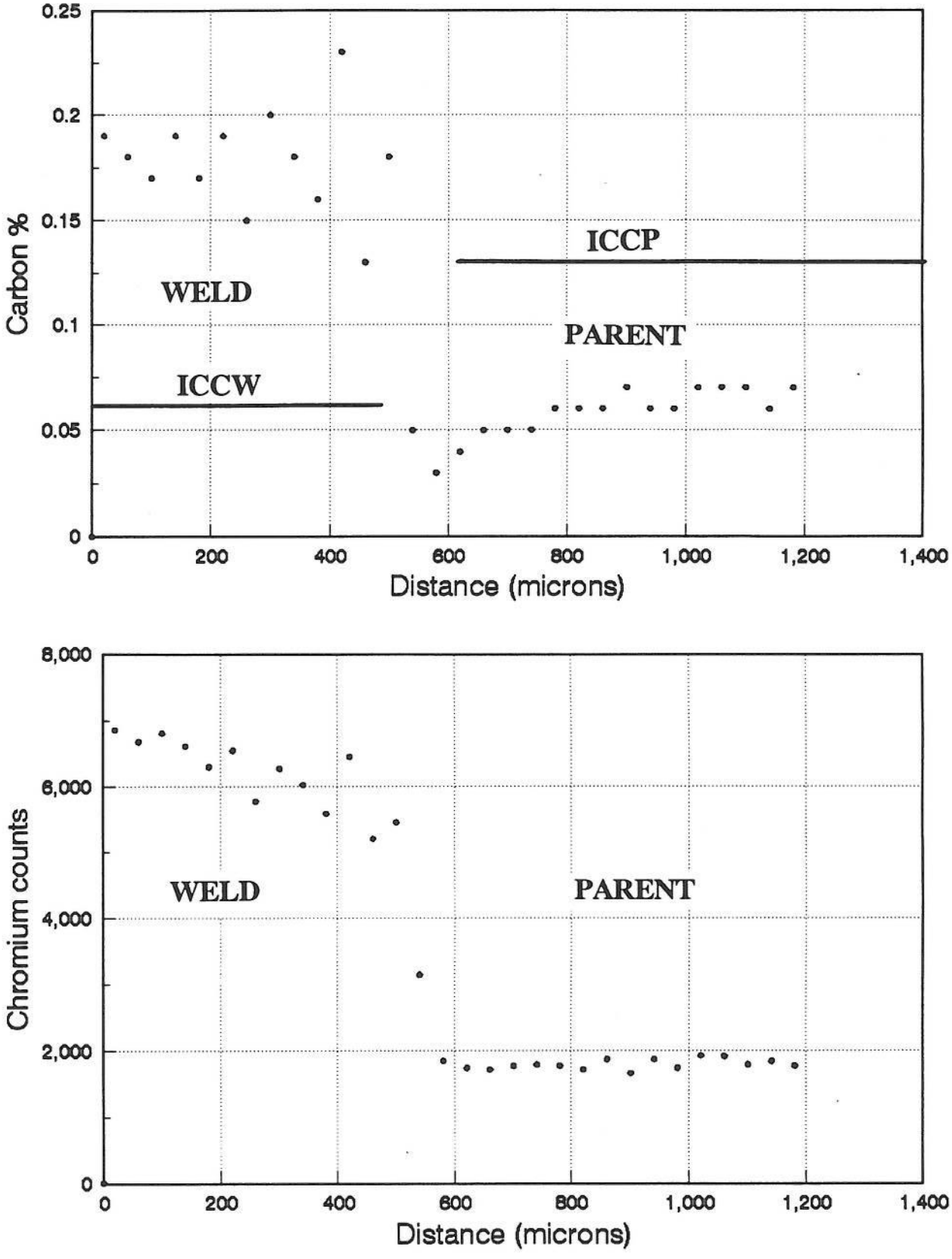

FIG 4.12

Carbon and Chromium Profiles Sample 2Cr.M.AGED

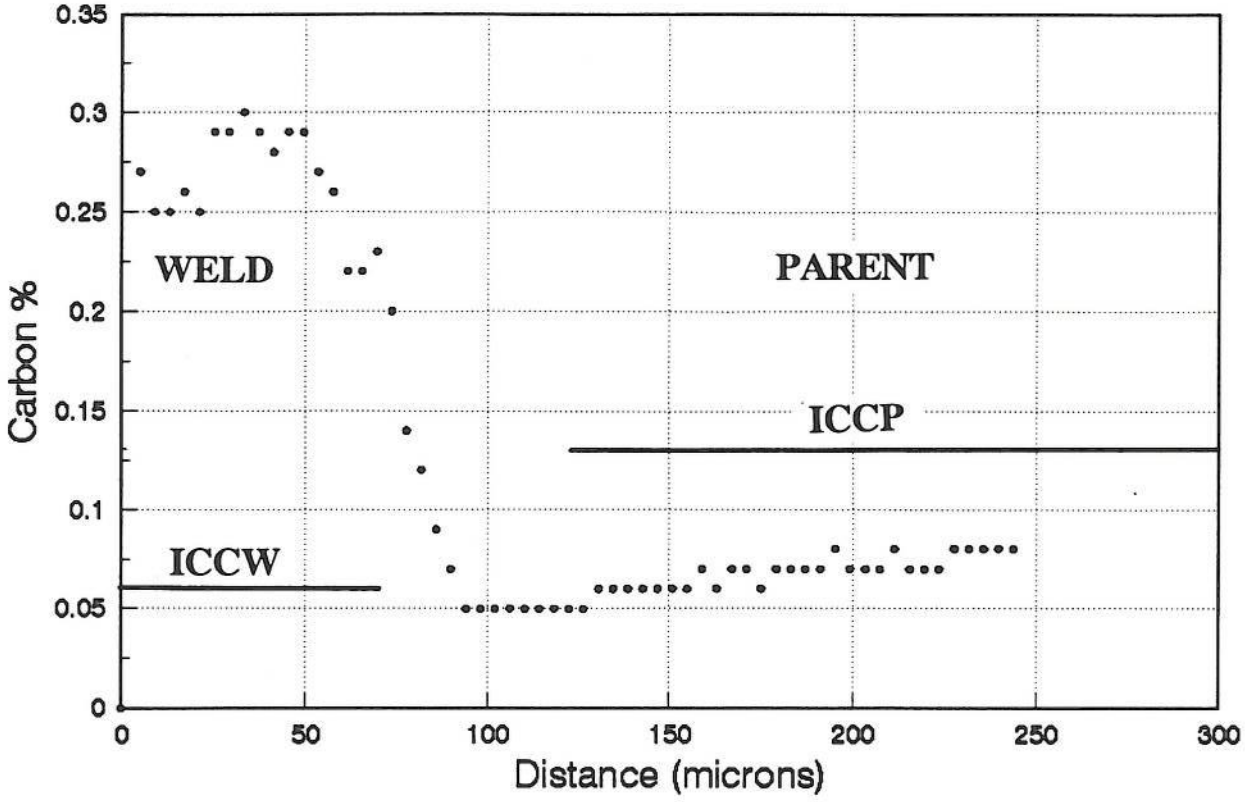

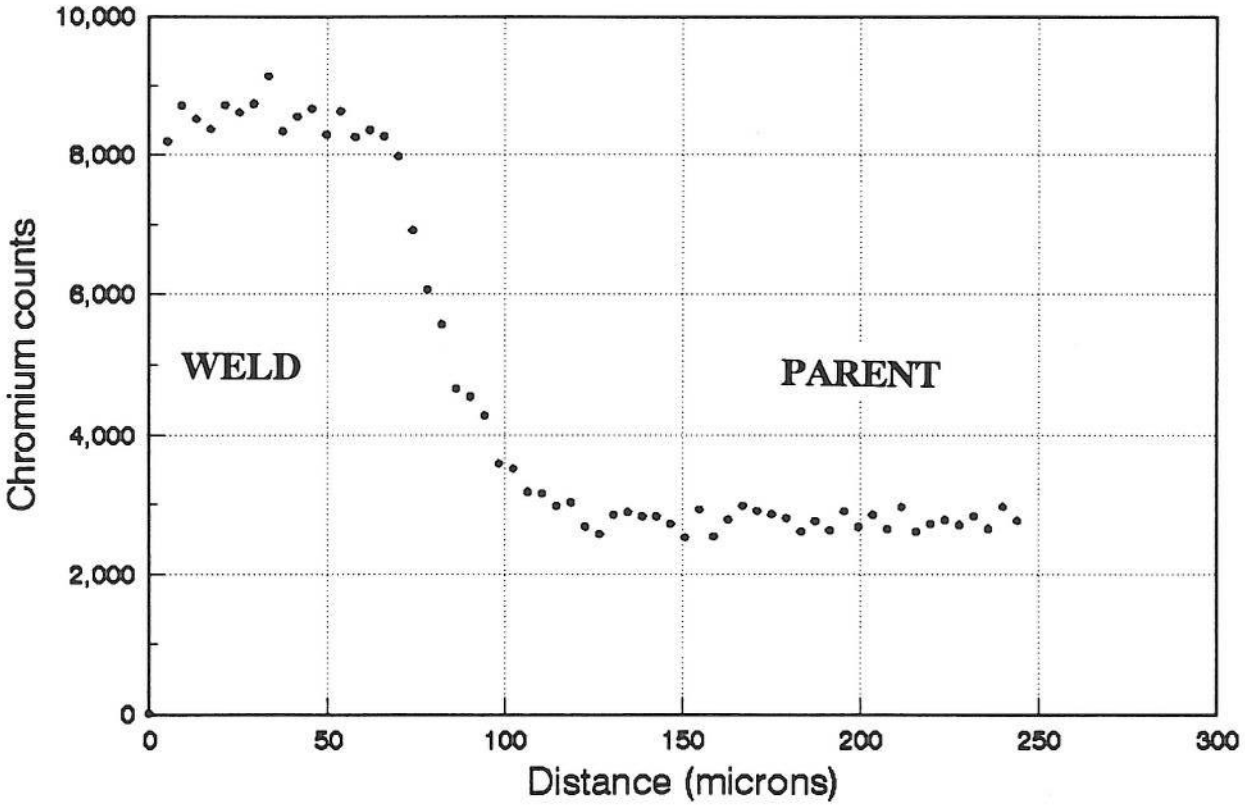

FIG 4.13

Carbon and Chromium Profiles Sample 2Cr.F.AGED

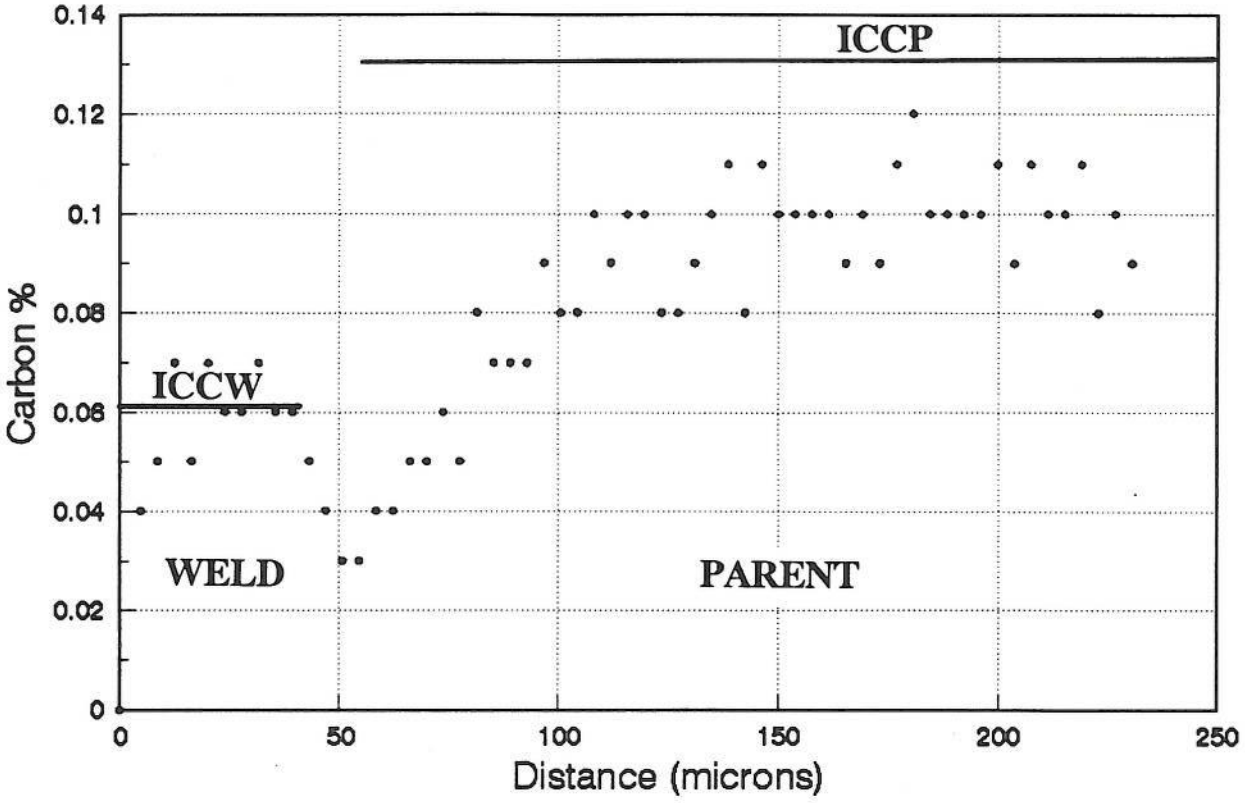

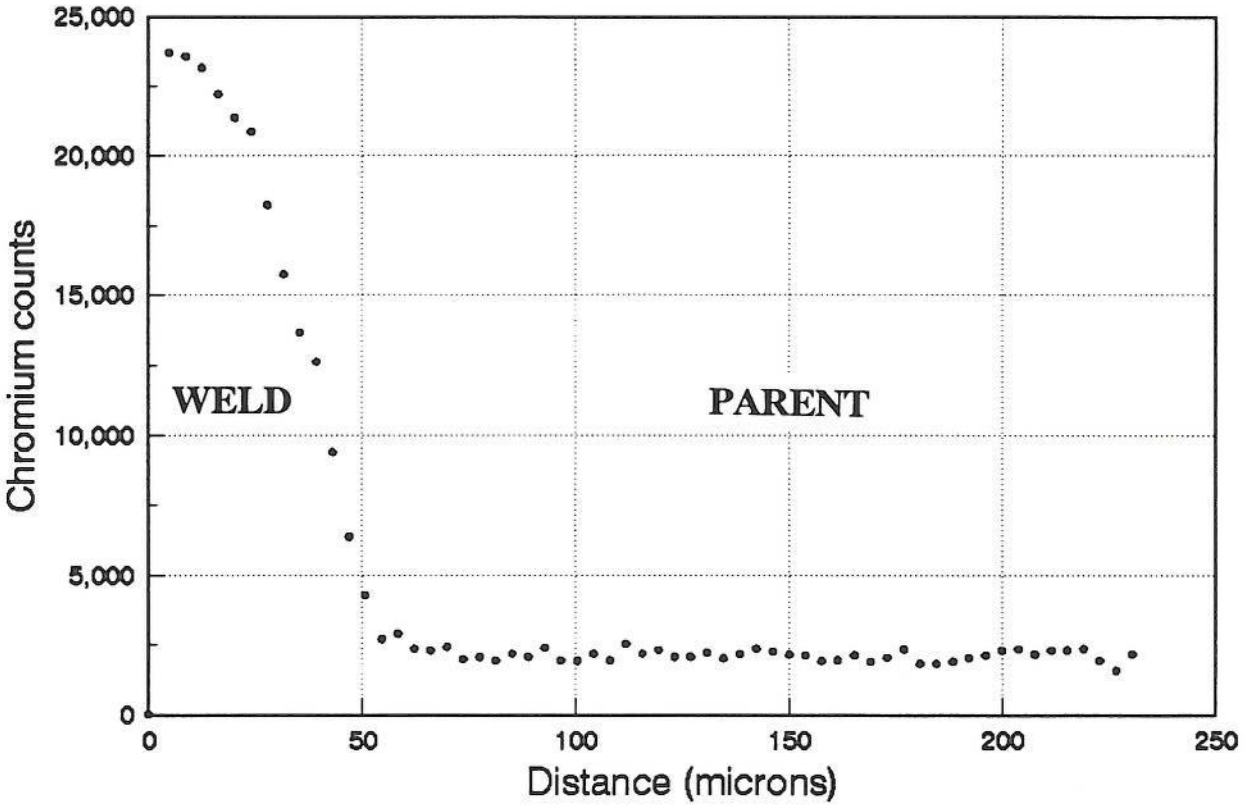

FIG 4.14

Carbon and Chromium Profiles Sample 9Cr.F.AW

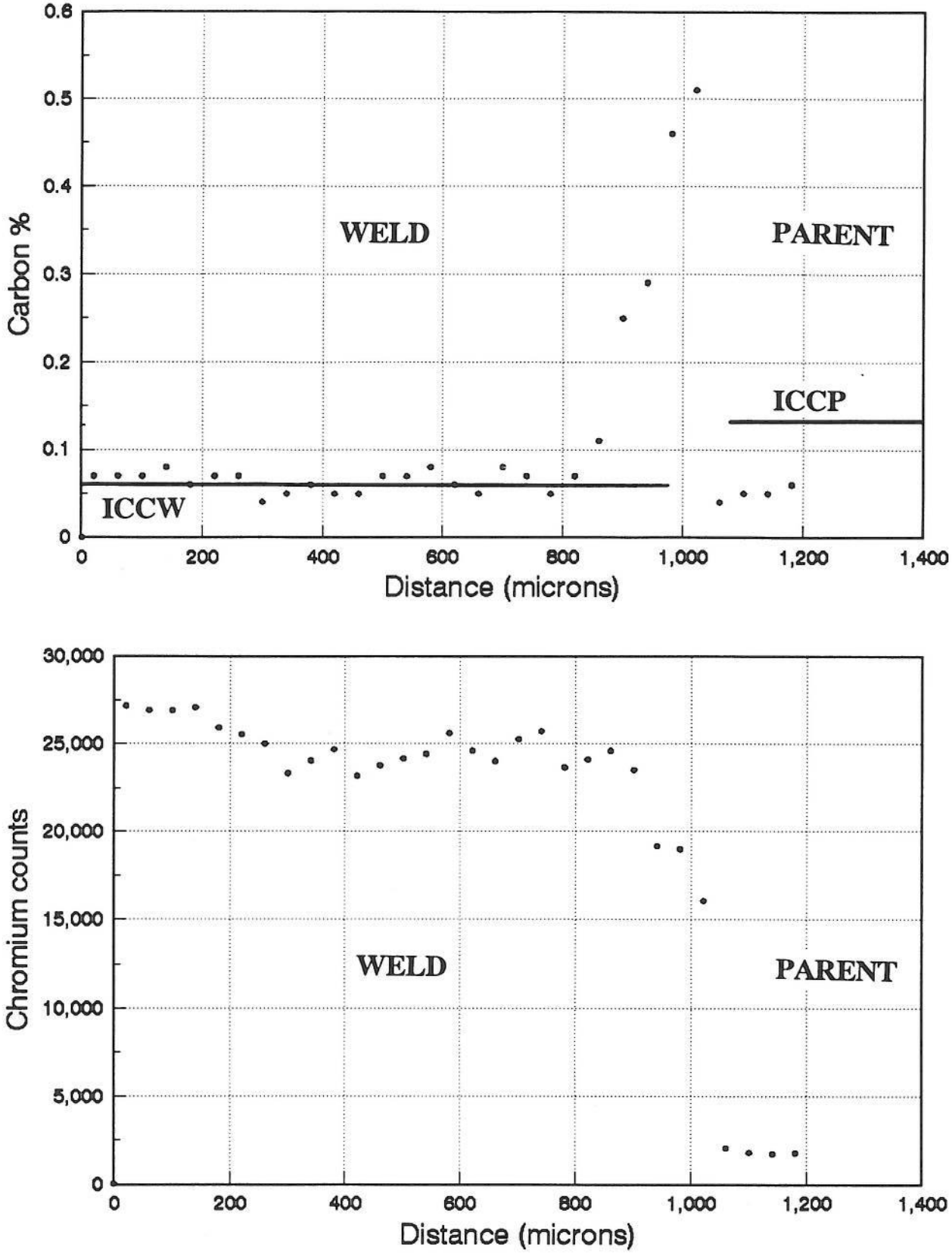

FIG 4.15

Carbon and Chromium Profiles Sample 9Cr.C.PWHT

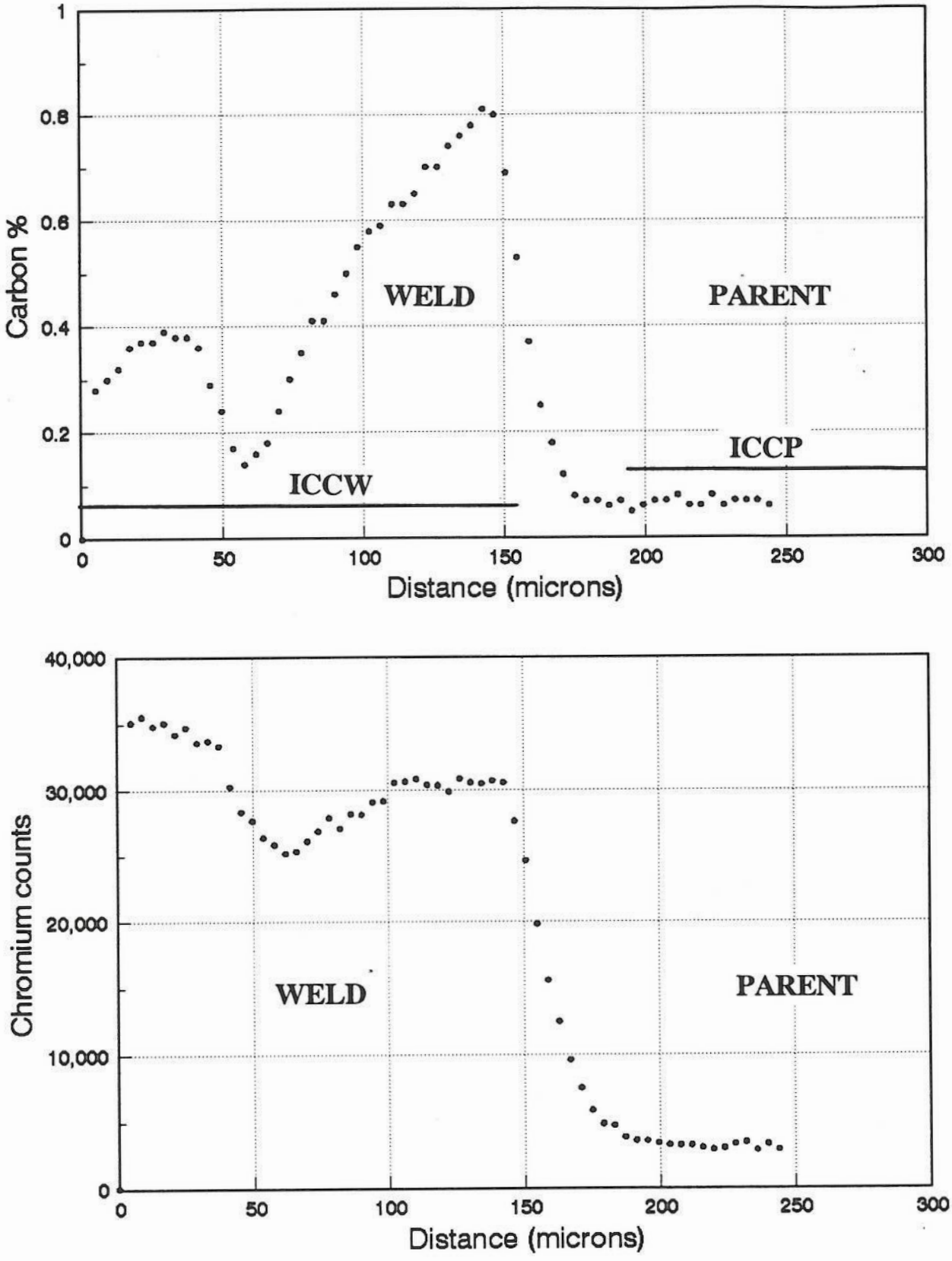

FIG 4.16

Carbon and Chromium Profiles Sample 9Cr.F.PWHT

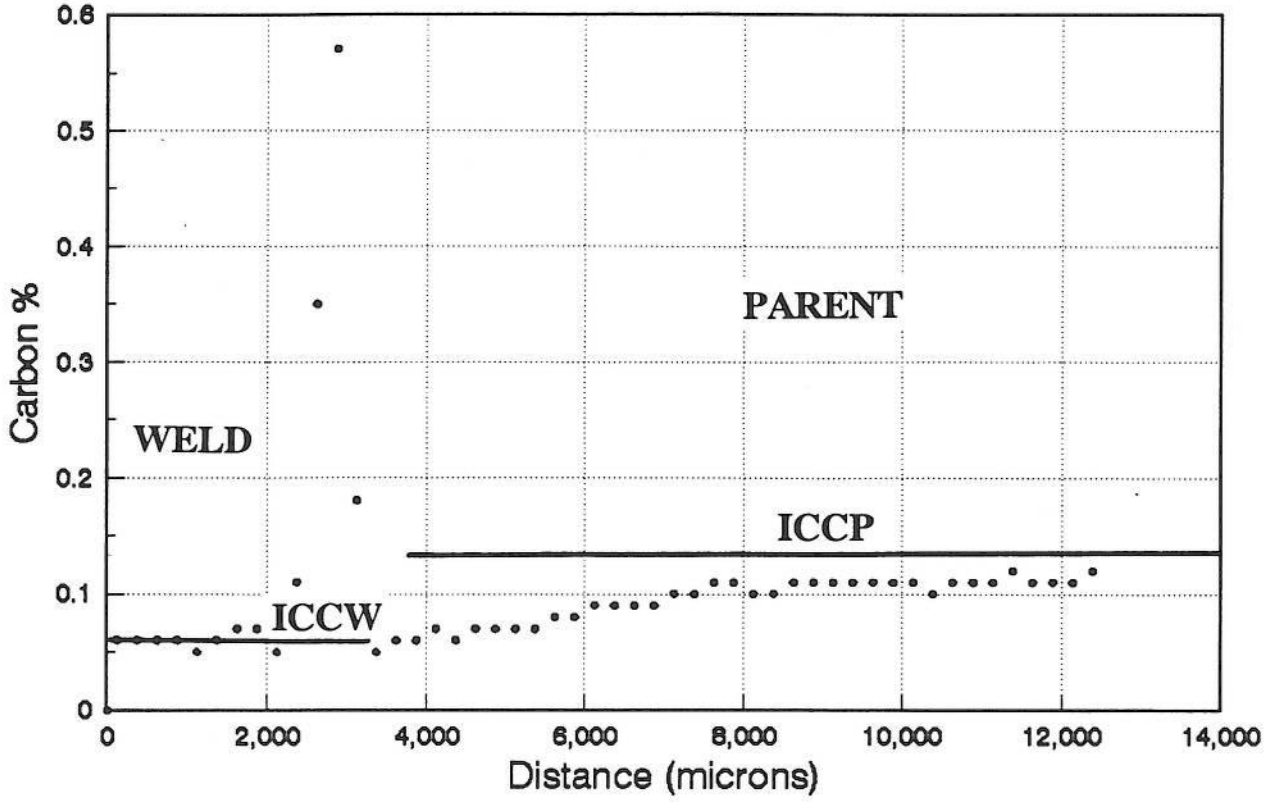

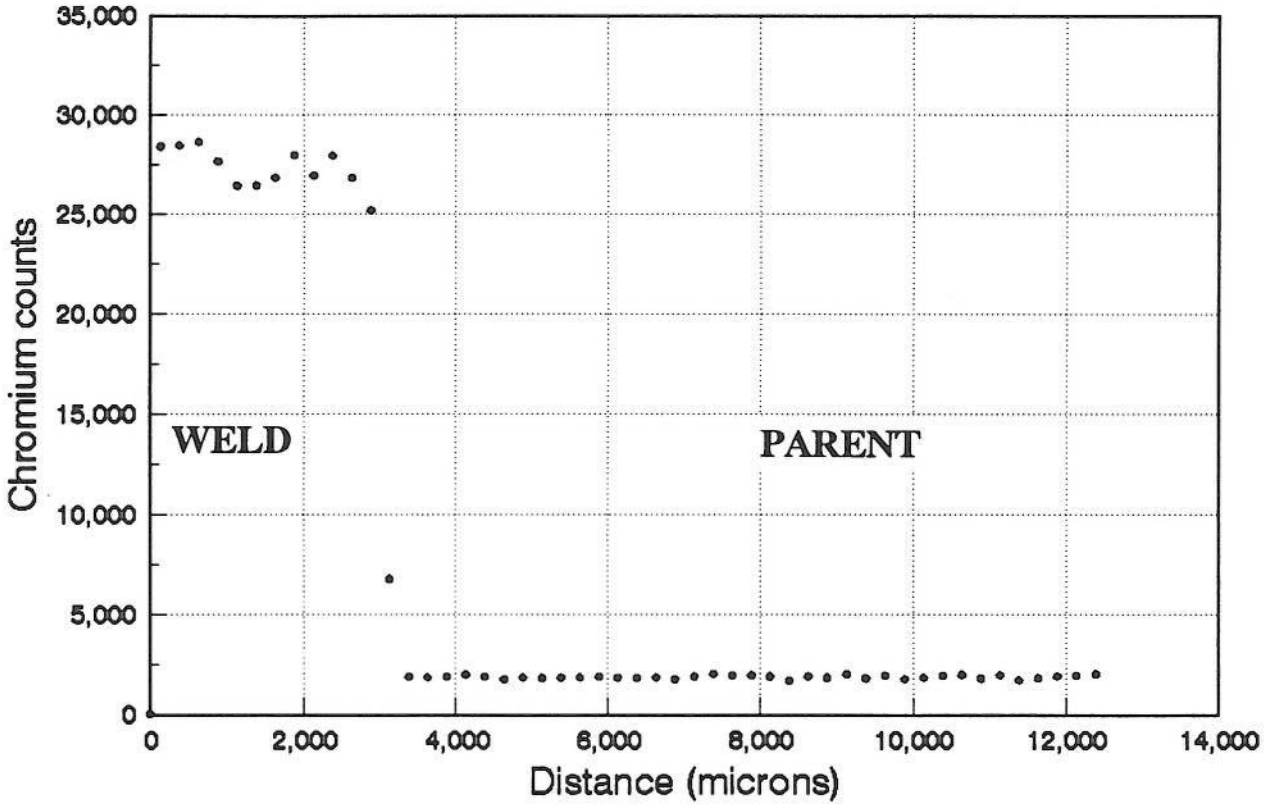

FIG 4.17

Carbon and Chromium Profiles Sample 9Cr.C.AGED

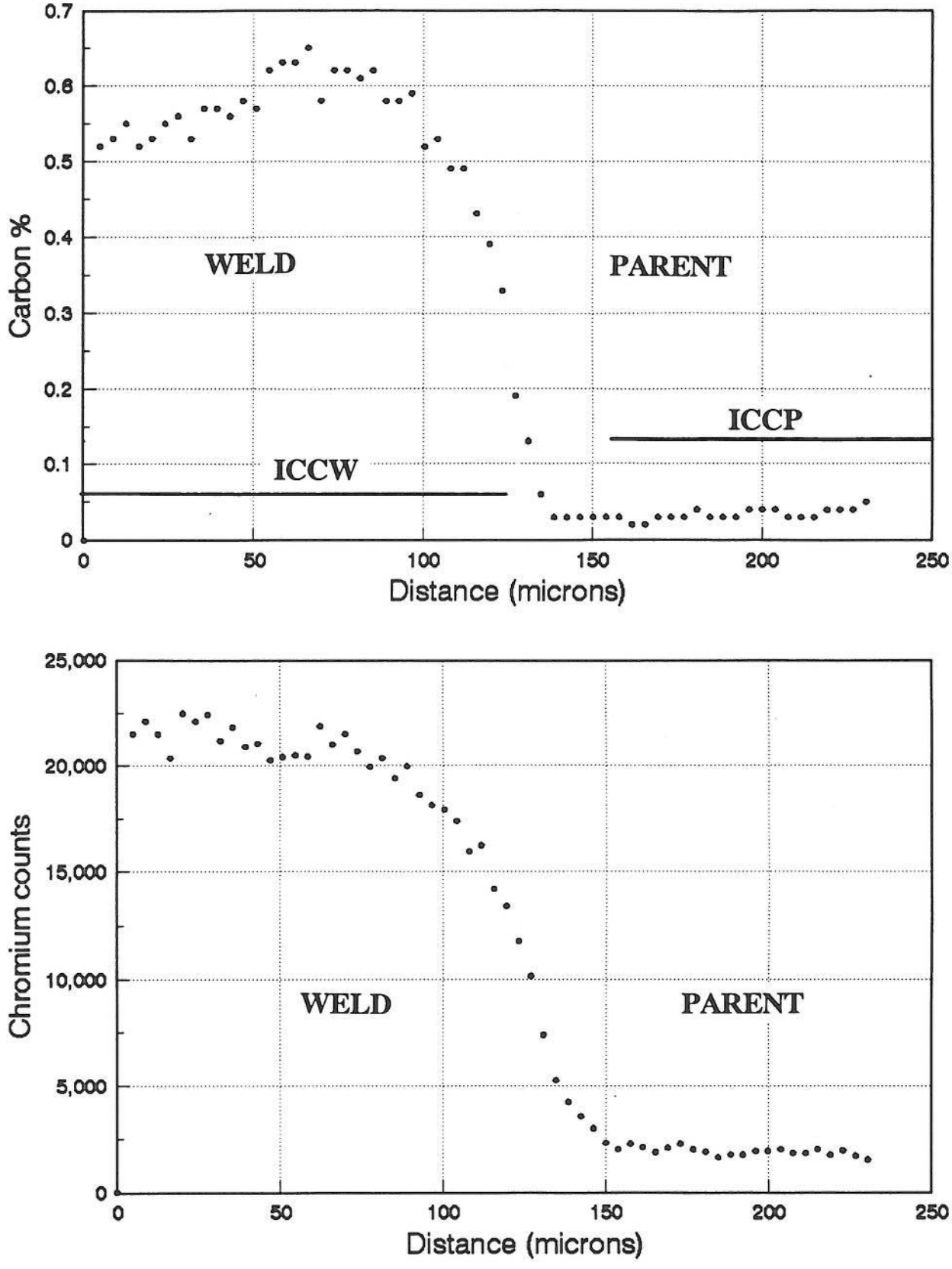

FIG 4.18

Carbon and Chromium Profiles Sample 9Cr.F.AGED

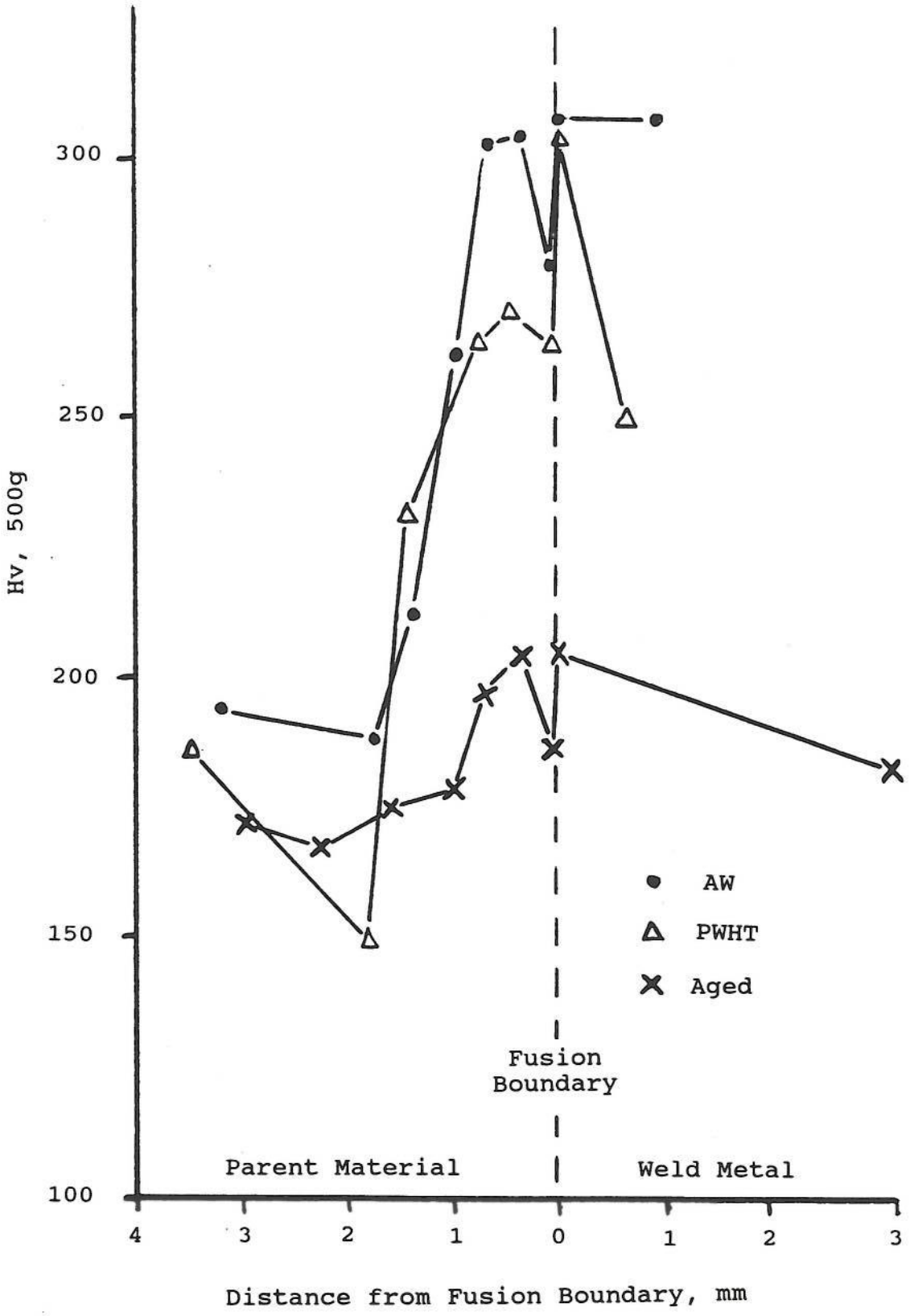

FIG 4.19

Microhardness Profile across the Fusion Boundary of 2CrMo Weldments in the AW, PWHT and Aged Conditions

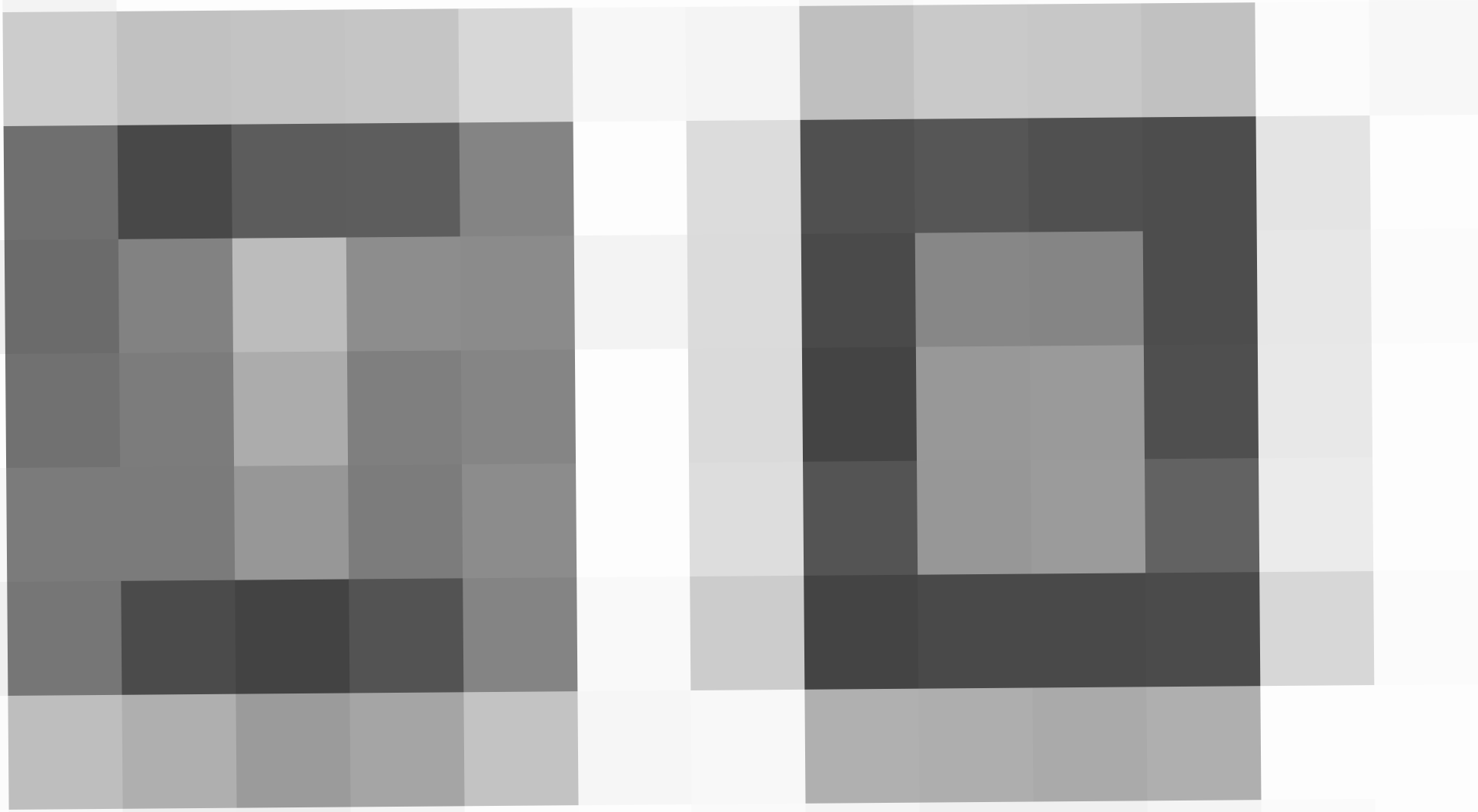

5.0 **DISCUSSION**

5.1 HAZ GRAIN REFINEMENT

The welding sequence employed in the production of the weld test pieces has produced between 60-70% grain refinement along the fusion boundary, **Table 4.1**. It had been anticipated that between 80-90% refinement would have been achieved.

Examination of the macro etched sections through the weld samples **Figs 4.20 to 4.23** show a generally uniform bead deposition sequence. The fusion boundary in all cases is generally planar rather than cusped indicating a high degree of overlap[2]. However there are isolated instances of a more cusped appearance, indicating that overlap had been reduced. The most likely reason for this is considered to be an increase in electrode angle. A cusp being formed as the energy of the arc is directed more toward the parent material.

If the welding speeds recorded during test piece production, **Appendix A**, are reviewed, it is clear that in many cases the actual welding speed for each weld pass in the first layer is outside the range originally specified. The specified travel speed range was 2.5-2.9mm/s. Those recorded for passes in the first layer of weld metal are generally in excess of 3.0mm/s with values as high as 3.72mm/s. Although the generally higher travel speeds will reduce the volume of weld metal per unit length it will also reduce the heat input, see equation section 3.3[29]. It would appear that heat input is the more significant variable in terms of level of grain refinement achieved. This assertion is supported by work[32] showing that the distance of any HAZ isotherm from the fusion boundary is approximately proportional to the square root of the heat input for practical welding conditions.

The occasional reduction in overlap and the generally lower than anticipated heat inputs probably explain the level of refinement being 60-70% rather than the anticipated 80-90%.

In spite the lower than anticipated level of refinement, the 60%-70% achieved in the samples is still considered representative of the sort of HAZ microstructures in which Type IIIa cracking has been observed. An example of such a failure[14] was reported as having between 60-80% refinement around the circumference of the weld.

5.2 GRAIN SIZE AND MICROSTRUCTURE

The refined microstructural regions adjacent to the fusion boundary have a grain size of between 3μm and 10μm, **Fig 4.2.** This is consistent with reports of Type IIIa cracking being associated with areas of exceptionally fine grain size, typically of 5μm[14], often referred to as ultra-fine grained.

The microstructure of the ultra-fine grained region cannot be determined satisfactorily using an optical microscope. However, work on simulated CMV HAZ microstructures reports the structure of such regions as being one of bainite[30]. Another author has identified it as a mixture of bainite and ferrite[14]. Both observations could be correct as the transformation kinetics of the particular phases will be influenced by alloy content.

The coarser grained regions between the fine grained regions have a grain size of between 10μm and 40μm. Reference to these areas as being coarse grained has been avoided in the text as the grain size is considerably smaller than that normally associated with the coarse grained region of CMV welds deposited conventionally. Indeed other authors have identified fusion boundary microstructures with grain sizes <50μm as being fine grained[33]. Typical coarse grain sizes in CMV weldments have been observed by the author to be between 50μm and 150μm. The smaller grain size produced in the weld samples is almost certainly the result of the bead deposition sequence used. Because the energy of the arc is being directed toward the proceeding bead rather than at the fusion boundary, the peak temperature reached adjacent to the fusion boundary will be lower than normal. Consequently, as the prior austenite grain size to a first approximation[30] is dictated by the peak temperature reached, the grain size will be smaller. The critical factor being the temperature and time of the region above the dynamic dissolution temperature of the alloy carbides. It would be anticipated that the lower peak temperature at the fusion boundary would result in an overall narrower HAZ width. This is confirmed by measurements of the HAZ width in this study at between 1.2mm and 1.7mm. The width of the HAZ associated with conventionally deposited welds in material of comparable thickness have been measured by the author as being typically between 2mm and 2.5mm.

Although these coarser grained regions have a grain size that is smaller than is usual in conventionally deposited welds, it is considered that this will only have a small influence on the levels of carbon diffusion observed. Although diffusion along grain boundaries is quicker

because of the increased lattice irregularity than bulk diffusion through the grain interiors[34]. The dominant mechanism of diffusion even in the ultra-fine grained areas is likely to be by bulk diffusion, as there is a much greater area of grain interior than grain boundary. These points are discussed more fully later.

The coarser grained areas are clearly generally of a bainitic microstructure **Fig 4.3**. However, the larger bainitic grains are decorated with very fine grained material. Microscopically it was not possible to determine the microstructure of the fine grained areas. Nonetheless this fine grained decoration has previously been identified as very fine grained bainite[31]. The phase was observed following simulated MMA heating cycles with a peak temperatures of 800 and 900°C. This is consistent with these areas being heated to temperatures below the general grain refinement temperature but above the A1 temperature in this exercise.

It is considered that the weld samples produced for this exercise have a fusion boundary microstructure that matches closely that found associated with Type IIIa cracking.

5.3 AGEING HEAT TREATMENT

The Larson Miller parameter was used to identify a time and temperature for the aging heat treatment in order to produce an equivalent level of carbon diffusion to that occurring in weldments operating at 565°C for around 100,000hrs.

As shown in **Appendix B** the Larson Miller parameter is based on the Arrenhius rate equation which includes the process dependant variables Q, activation energy, and A, a process related constant sometimes referred to as the 'frequency factor'[35]. The constant 'C' in the Larson Miller parameter is related to both Q and A and as such should also be related the process, in this case carbon diffusion. However, as far as the author is aware values of 'C' for carbon diffusion in bainite do not exist. The value for 'C' of 20 used in this exercise has been found to give good agreement with experimental results for the diffusion driven processes creep and tempering in low alloy steels[31]. The question we need to address is whether this value will also hold for carbon diffusion.

The author was unable to obtain values of Q and A for carbon diffusion in low alloy steel bainitic microstructures. It was therefore decided to take an

empirical approach. The carbon profile for the aged CMV to 2Cr weldment generated in this exercise, **Fig 4.11** (2Cr.C.AGED), was compared with a carbon profile produced from a service exposed weld that had failed by Type IIIa cracking in service[15]. The carbon profile for the failed weld, identified by the abbreviation SEF, is shown in **Fig 5.1.** A comparison of the two plots shows the profiles to be similar in shape. There are however a number of differences in the plot, particularly in the area under the curve delineating the carbon peak in the weld metal. It is suggested that the area under the curve should give an indication to the volume of carbon diffusion. Measurement of these areas using a planimeter show that the area under the SEF curve is just over 3 times greater than under the curve following aging. The operating hours of the SEF weldment were just under 90,000hrs at the time of failure, whereas the simulated operating time at 565°C for the aged sample was 113,000hrs, **Appendix B.** Although the approach is not very rigorous, in that alloying differences and initial carbon content in the two cases may have had an effect on the volume of carbon diffusion. it would appear that the ageing times and temperatures used to simulate service exposure are not as high as the they should have been. This probably suggests that Q values for carbon diffusion are lower than those for creep and tempering. The process could be said to be more time dependant and less temperature dependant than creep. This would be analogous with what is observed with oxidation during creep testing, where oxidation is not normally a problem with short term creep tests carried out at relatively high temperatures because the Q value for oxidation is lower than it is for creep.

Comparison of the test results with just one service exposed sample cannot be considered to be conclusive in deciding whether the Larson Miller parameter with a value of 'C' of 20 was a reasonable approach. However it appears that longer times and/or higher temperatures should have been used. Nevertheless, the differences in the volume of observed carbon diffusion are not considered to be sufficiently great to affect the significance of the observed levels of carbon diffusion. Indeed as mentioned above, the profiles are of quite similar shape.

5.4 CARBON PROFILES

The carbon profiles produced across the fusion boundary of weldments made with a common ½Cr½Mo¼V (CMV) parent material and a range of ferritic weld metals are discussed below. A full set of carbon and chromium profiles are contained in **Appendix C**. It is apparent, particularly on the fine scans, that there is significant scatter between some of the points making up the carbon profiles. It should be appreciated that on the fine scan an area of approximately 5μm diameter is being sampled. This corresponds to size of a typical fine grain. The observed scatter may therefore represent differences in carbon content between adjacent grains. An explanation for this is considered to relate to when particular grains are formed from austenite during cooling through the A1 and A3 temperatures. The grains of higher carbon content would be expected to be the last to form. However, it might also be expected that there would be general homogenisation of the local carbon content with time at temperature. Local diffusion of carbon between adjacent grains must occur, but as there is also likely to be local differences in alloy content between adjacent grains, this effect is considered unlikely to result in uniformity of carbon content.

Another source of scatter in the readings could be experimental errors. As seen in section 2.4 these errors can be high particularly when using a fine scanning sensitivity and when the carbon concentration is low. The carbon concentration for the majority of the readings was in excess of 0.03% C, errors are therefore unlikely to be greater than 5%. Errors will be much lower for the higher carbon regions particularly where either the coarse or medium scanning sensitivities were used as the deposited charge is higher.

5.4.1 Mild Steel Weld Metal

The carbon profile produced using a mild steel weld metal after ageing shows clearly that there has been carbon diffusion from the weld metal to the parent material, **Fig 4.6** (MS.F.AGED). The peak carbon content in the parent material rises to a peak of 0.24%C well above the original carbon content of the parent material at 0.13%C. A corresponding drop in carbon content is evident in the weld metal adjacent to the fusion boundary, with the carbon content falling to below 0.025% from an initial 0.053%C. This shows that observations of uphill diffusion made by Darken[18] in austenite also occur in ferrite.

On the carbon trace in **Fig 4.6** (MS.F.AGED) there is also a pronounced carbon peak in the weld metal away from the fusion boundary. An explanation for this is not immediately apparent, however it is considered too big to be a carbide particle. There is no corresponding chromium peak that would have indicated an area of undiluted parent material that had been swept into the weld metal, this effect has previously been observed by the author in ferritic weldments. A possible explanation is that there was some contamination on the surface of the sample during scanning.

5.4.2 CMV Weld Metal

The carbon and chromium profiles for the as welded CMV weldment, **Fig 4.7** (CMV.C.AW), shows a pronounced difference in carbon content and only a slight difference in chromium content, reflecting the original alloy contents of the materials. After ageing **Fig 4.8** (CMV.C.AGED) the small but sharp change in chromium content at the fusion boundary is still apparent. However there is a more gradual change in carbon content across the fusion boundary over a distance of about 3mm, with carbon migrating to the weld metal which has slightly higher chromium and lower carbon content. A slight increase in the background carbon content of the weld metal is also apparent. The carbon profile across the fusion boundary is more representative of that predicted by Fick's second law **Fig 2.5**, there being no sharp discontinuity at the fusion boundary. It would appear that with an almost matching alloy content carbon is diffusing downhill primarily due to the difference in carbon concentration across the fusion boundary.

5.4.3 2CrMo Weld Metal

The carbon profiles for the 2CrMo weldment are of particular interest as it is in these weldments that Type IIIa cracking has been observed.

The carbon profile produced in the as welded condition at a medium scanning sensitivity, **Fig 4.9** (2Cr.M.AW) clearly shows that carbon diffusion has occurred during welding, the carbon content having dropped to between 0.06% and 0.07% from an initial value of between 0.12 and 0.13%. However, there is no corresponding peak in weld metal carbon content. This observation suggests that the majority of the carbon diffusion is occurring when the material is in the austenite phase. Carbon diffusion occurring when the material is ferritic generally results

in the formation in stable carbides which would be anticipated to create a local carbon peak in the weld metal. This is observed in profiles after post weld heat treatment and aging. This is also consistent with results of diffusion measurements in austenite which show that the frequency factor A[35], which has a major influence on the rate of the diffusion process, is 16 times higher for carbon diffusion in austenite than it is for diffusion in ferrite.

After Post weld heat treatment **Fig 4.10** (2Cr.M.PWHT) a local trough in carbon concentration is apparent at the fusion boundary, where the carbon content has fallen to 0.05% C. The general background carbon concentration within 0.5mm of the fusion boundary also appears to have fallen below 0.1%C although there are a couple of points indicating higher carbon content, these are considered to be spurious results as they do not follow the overall trend. There is also a very marked peak in carbon concentration of 0.25%C formed in the weld metal. The peak is apparent over a distance of 0.2mm, the carbon content then falls back to the original carbon content of the weld metal. It would appear that stable carbides have been formed.

After ageing **Fig 4.11** (2Cr.C.AGED) carbon diffusion is apparent over a distance of approximately 6mm, with the carbon content below 0.8%C throughout the HAZ. **Fig 4.12** (2Cr.M.AGED) shows an apparent trough in carbon content at the fusion boundary where the carbon content has fallen to 0.025%C. However this is not confirmed at the fine scanning sensitivity, **Fig 4.13** (2Cr.F.AGED), which shows no apparent trough and a minimum carbon content adjacent to the fusion boundary of 0.05%C. This difference in results suggests that there may some variability in the level of carbon diffusion along the fusion boundary.

The width of the carbon peak in the weld metal after aging is approximately 2mm wide, **Fig 4.11** (2Cr.C.AGED). This is much wider than the peak observed after post weld heat treatment which was only 0.2mm wide. However the peak carbon level does not appear to have changed significantly. There is however substantial variation between the three traces after ageing Figs. F,G & H, the peak carbon content in the weld metal varying between 0.18% and 0.3% carbon. This may again suggest local variations in carbon concentration along the fusion boundary.

5.4.4 9Cr Weld Metal

In the as welded condition using the fine scanning sensitivity, **Fig 4.14** (9Cr.F.AW) there is clear evidence of carbon diffusion resulting from the weld thermal cycles. A similar observation was made with the 2Cr sample. However, the effect is more pronounced in the 9Cr sample. Interestingly again there is no evidence of a peak in carbon content in the weld metal above the initial 0.061%C, suggesting that the majority of carbon migration took place with the material in the austenite phase. The lack of a carbon rich region is confirmed by metallography, **Fig 5.2**. Surprisingly the carbon denuded region in the parent material adjacent to the fusion boundary extends into the weld metal. This can probably be explained by looking at the associated chromium trace. It is apparent that there is a local dilution effect at the fusion boundary resulting in a gradual rise to the peak chromium concentration over a distance of 0.04mm. The lack of a clearly defined fusion boundary in terms of chromium content has therefore resulted in the carbon trough formed during welding, extending into the weld metal.

After post weld heat treatment the coarse scan, **Fig 4.15** (9Cr.C.PWHT) shows a sharp rise in the carbon concentration in the weld metal adjacent to the fusion boundary. The width of this area is approximately 0.1mm wide. This sample was given the same post weld heat treatment as the 2Cr sample. However, the peak width is narrower 0.1mm against 0.2mm, but the peak carbon content is approximately 0.5%, twice as high as the peak observed in the 2Cr sample. The explanation for this must be the difference in chromium content of the weld materials. The higher chromium content in the 9Cr material results in more carbides being formed. This formation of a larger population of carbides appears to have shortened the range of carbon migration, i.e. there is less carbon to diffuse further as it has been moped up in the formation of stable carbides.

Interestingly the width of the carbon peak above 0.4%C on the fine scan, **Fig 4.16** (9Cr.F.PWHT) is identical to the width of the dark etching phase on a section removed from the same sample **Fig 5.2**. This suggests that the carbide rich layer observed on the section after etching in Nital has a carbon content in excess of 0.4%C. **Fig.4.16** also shows a secondary carbon peak. The peak ties in well with the associated chromium trace below. The pronounced secondary peak suggests that carbon concentration is very sensitive to local alloy content. It is also apparent in **Fig 4.16** that the carbon concentration at the fusion boundary has fallen to approximately 0.3% carbon. There is

however no evidence of a local trough. Interestingly the minimum carbon concentration seen at the fusion boundary in the as welded sample Fig.G was also at 0.3%C. There is no apparent increase in the minimum carbon concentration following post weld heat treatment.

After ageing **Fig 4.17** (9Cr.C.AGED) the carbon peak has not increased in height, however its width has increased to approximately 1mm from 0.1mm after PWHT. This is comparable with the increase in width seen in the 2Cr samples. The width of the carbon peak at 0.4%C is about 0.4mm, which again ties in well with the observed width of the carbide band on the aged sample **Fig 5.2**. The width of the decarburised region extends for at least 9mm into the parent material. The whole of the heat affected zone having a carbon content of below 0.7%C.

The fine scan after aging **Fig 4.18** (9Cr.F.AGED) shows the minimum carbon content at the fusion boundary to be about 0.3%C. Again there has been no further reduction from the minimum carbon content observed after welding and post weld heat treatment.

5.4.5 Summary of Carbon Profiles

The results produced in the form carbon profiles are considered to be very interesting. The key information determined from the carbon profiles can be summarised as follows.

1. Uphill diffusion, where carbon migrates from an area of lower carbon concentration to an area of higher carbon concentration under the influence of higher alloy content has been identified.

2. The level of carbon diffusion observed in weldments of nominally matching alloy content is reduced and it appears that diffusion is largely driven by differences in carbon concentration.

3. The weldments between CMV material and the more highly alloyed 2Cr and 9Cr weld metals have revealed:

a) Carbon diffusion does occur as a result of the weld heating cycle. A pronounced reduction in carbon concentration is apparent in the HAZ adjacent to the fusion boundary. A rise in the carbon concentration in the more highly alloyed weld metal is not apparent.

b) After post weld heat treatment a pronounced peak in carbon concentration is formed in the weld metal adjacent

to the fusion boundary. The marked reduction in carbon concentration in the heat affected zone adjacent to the fusion boundary is still apparent and increases in the 2Cr sample. The width of the carbon denuded area also increases.

c) After aging the width of the carbon peak in the weld metal increases significantly. The minimum carbon content is still apparent in the HAZ adjacent to the fusion boundary, but the actual carbon concentration does not change significantly. The width of the carbon denuded band increases markedly with the whole of the HAZ lying in an area of significantly reduced carbon concentration.

d) The photomicrographs. **Fig 5.2** suggest that the width of carbon diffusion is generally uniform down the fusion boundary. The results from carbon profiling suggest that although the overall pattern of carbon diffusion is uniform there may be some local differences in carbon concentration. The significance of this is unclear.

e) The width of the carburised band in the 9Cr samples corresponds to a carbon content of around 0.4% measured on the carbon profiles.

The carbon profile produced on a medium scanning sensitivity from the 2Cr weldment after aging suggests there is a small local trough in carbon concentration adjacent to the fusion boundary. This is not confirmed by the fine scanning sensitivity or by the carbon profiles produced from the 9Cr weldment. It is considered that there is no continuous trough in carbon concentration along the fusion boundary, although the minimum carbon content always occurs at the fusion boundary. However, there may be local areas where a small trough occurs, it is considered that as the trough is localised it is probably of little significance in terms of Type IIIa cracking.

As anticipated the majority of carbon diffusion occurs during post weld heat treatment and particularly aging. However it would appear that there is little change in the minimum carbon concentration at the fusion boundary following post weld heat treatment. The main effect being a significant increase in the width of the carbon denuded band and an increase in the width of the carbon peak formed in the weld metal. This effect has been shown schematically in **Fig 5.3.**

5.5 CARBON DIFFUSION MECHANISM

The mechanism of carbon diffusion in ferritic weldments is often described in terms of carbon activity gradient[18][19]. Where carbon is described as having a lower energy on the high alloy side of the joint. The tendency is then for carbon to migrate to areas of lower energy or lower activity.

Before discussing a suggested carbon diffusion mechanism based on the carbon profiles generated in this study it is considered useful to review the description of the mechanism put forward by another author[19]. The mechanism was proposed following observations made from metallographic studies and is shown schematically in **Fig 5.4**. The description of the mechanism is reproduced below.

1. Carbon in solution crosses the fusion line from the low alloy material to the high alloy material. The prime driving force which causes the carbon to migrate is the alloy difference between the two steels which results in a lower energy for carbon in the high-alloy steel at a higher-carbon concentration than in the low alloy steel at a lower concentration. A measure of the magnitude of this driving force is the difference in carbon concentration of the high-alloy and low-alloy sides of the fusion line (C_E-C_D).

2. The addition of carbon to the high alloy side increases the carbon concentration on this side of the joint and may result in the precipitation of some carbides if the carbon concentration is above the solubility limit. The added carbon will result in a carbon concentration gradient and carbon will tend to migrate away from the fusion line under the influence of this gradient (C_E-C_A).

3. The carbon which has crossed the fusion line reduces the concentration of the carbon in solution in the low alloy material. This results in a carbon concentration gradient in the low-alloy material (C_C-C_D). The carbon diffuses to the fusion line in the low-alloy material under the action of the concentration gradient.

4. When the carbon concentration in the low alloy material has dropped below the solubility value by virtue of the migration across the fusion line, some of the total carbon which is the form of carbide breaks up and goes into solution (carbon can only migrate when in solution -not as a carbide) to bring the carbon level in solution back up to its solubility value at this point.

The final point in the description is used to describe the

sharp transition between C_B and C_C which was proposed following the observation of a sharp transition in etching response. The apparent sharp transition suggested in the description is not apparent on the carbon profiles produced in this exercise. From the profiles it would appear that a dynamic equilibrium exists between the proportion of carbon in the form of carbides and carbon in the matrix (in solution). The dissolution of carbides is therefore occurring to maintain this equilibrium and no sharp transition is observed.

In the description, para.2., it is proposed that carbon reaches a peak at the fusion boundary with a gradual reduction in carbon concentration away from the fusion boundary due to the influence of the concentration gradient. This observation is confirmed by the results in this exercise. However, it is also apparent that the carbon peak at the fusion boundary does not rise indefinitely. It would appear that the matrix becomes saturated in carbon such that a plateau in carbon concentration is formed. This was apparent with both the 2Cr and 9Cr samples.

It is therefore proposed that the schematic representation of the observed carbon profiles should be modified to include these observed features. **Fig 5.3** shows a modified schematic representation of carbon profiles formed after PWHT, and Aging.

The term activity gradient used in many of the mechanistic descriptions only reflects the average activity of carbon within the particular alloy system. It seems likely that carbon in the form of carbides will have a very low activity but carbon in the matrix will have a much higher activity. It may therefore be that the activity of carbon in the matrix is the same in both the high alloy and low alloy materials. The overall activity of carbon on the high alloy side being lower as more carbon is present in the form of carbides. This suggestion is supported by the fact that after a certain period of time the minimum carbon content at the fusion boundary appears to remain fairly constant with further aging. It is suggested that the reason for this may be that the matrix carbon content either side of the fusion boundary is the same. However, it would be hard to prove as it is difficult to distinguish accurately between carbon in the form of carbides and carbon in the matrix.

It had been suggested that the mechanism of carbon diffusion changes between 700°C and 565°C[21]. There is no indication from this exercise that there is a significant change in mechanism between the post weld heat treatment

temperature of 690 to 720°C and the ageing temperature of around 640°C. There is also very little difference between the shape of the carbon profile for a service exposed sample, **Fig 5.1.** and one aged at 640°C, **Fig 4.11.** It is considered therefore that there is no major change in mechanism apparent from this exercise over the investigated temperature range. However, it appears that there is a difference between carbon diffusion in ferrite and carbon diffusion in Austenite. It is not possible to say from this study whether a carbon gradient produced by service exposure would be removed by an austenitising heat treatment as reported by some authors[21]. This would however be relatively simple to investigate.

5.6 MICRO HARDNESS MEASUREMENTS

Insufficient micro hardness testing has been carried out for a detailed study. However, it was the intension of this limited study to identify significant trends in hardness which could be related to the observed carbon profiles.

5.6.1 2Cr Weldments

Micro-hardness traverses were carried out from the parent material through the HAZ, and into the weld metal of the 2CrMo weld samples in each heat treatment condition. The results shown in **Table 4.3** and **Fig 4.19** are discussed below.

1. The hardness of the parent material drops as you move toward the visible HAZ this is consistent with the area being tempered as part of the weld heating cycle.

2. The hardness then increases to a value above the parent material hardness in the intercritical region.

3. Readings 4, 5 and 6 were all taken in fine grain regions which had seen two heating cycles. The trend is for the hardness to increase as you move toward the fusion boundary. This is probably due to the fact that the material at the fusion boundary was transformed from coarser grained material, whereas the regions further away will have been fine grained after the first heating cycle, only to be given a second lower temperature refining treatment and hence are softer.

4. The hardness of the microstructure adjacent to the fusion boundary was consistently lower than that in the fine grained regions. This observation may be due to carbon diffusion but could also be the result of a tempering effect of subsequent weld passes.

6. Hardness readings taken in the weld metal adjacent to the fusion boundary are consistently higher than readings in the HAZ adjacent to the fusion boundary.

7. The hardness away from the fusion boundary in the weld material after post weld heat treatment and aging shows a lower hardness than the weld material adjacent to the fusion boundary. These results confirm observations from the carbon profiles that carbon has concentrated in the weld metal adjacent to the fusion boundary.

The results of this hardness survey suggest that there

could be a significant step change in properties either side of the weld interface. With the HAZ side showing consistently lower strength through out the life of the weldment. This in turn probably suggests a significant difference in creep properties.

5.6.2 Fusion Boundary Measurements

A study was carried out of the micro-hardness differences either side of the fusion boundary of each weldment, in each heat treatment condition, **Table 4.4.**

The results from this study for the 2Cr weldment after post weld heat treatment show the weld metal having a hardness lower than the HAZ adjacent to the fusion boundary. This is not consistent with the trend identified above. It is not easy to explain this difference in the results, however it could be associated with the effect of heat input during welding. The other hardness differences are as anticipated with the more highly alloyed weld metals being stronger and the matching and mild steel weld materials being weaker than the CMV parent material.

In is noticeable that the hardness of the CMV weld metal in the as welded condition is very low, it is in fact lower than that of the mild steel. The explanation for this is probably the very low carbon content of the 3.25mm CMV welding electrodes.

The micro-hardness measurements taken in the HAZ adjacent to the fusion boundary clearly show the effects of carbon diffusion. If the hardness results for the CMV sample are compared with the hardness values identified for the 2Cr and 9Cr weld samples, the CMV results are consistently higher after aging. The CMV results are 23Hv higher than for the 2Cr weldment and 41Hv higher than the 9Cr weldment. These results are in spite of the CMV sample being given a significantly longer aging treatment, **Appendix B,** than either the 2Cr or 9Cr samples. This is considered clear evidence that carbon diffusion is having a significant effect on the strength and therefore almost certainly the creep properties of fusion boundary material.

5.7 IMPLICATIONS FOR TYPE IIIA CRACKING

The carbon profiles have clearly identified significant carbon loss in the HAZ adjacent to the fusion boundary of the 2Cr weldments following PWHT and aging. Micro hardness measurements have also shown that after aging there is a significant reduction in hardness of this region compared with a weldment in which little carbon diffusion has occurred. As the presence of carbides in these alloy materials is essential for creep strength. These two factors strongly suggest that this fusion boundary region will be weaker in creep as a result of carbon diffusion. The observed carbon diffusion might therefore explain why the Type IIIa region is weaker in creep than the Type IV region which as discussed in section 2.1.2 had until recently been considered to be the weakest region of the HAZ.

The carbon profiles did not however identify a consistent trough in carbon content at the fusion boundary which might have explained the very local nature of cavitation normally found associated with Type IIIa cracks. Instead a gradual carbon gradient was observed on moving away from the fusion boundary.

However, the sharp discontinuity in carbon content across the fusion boundary might create a metallurgical notch effect. The carbon enriched weld metal possibly having greater creep strength and lower ductility than the weaker and more ductile HAZ region. Recent work[36] has shown that deviations in creep properties between the weld metal and HAZ can lead to substantial life reductions. The work also refers to cross-weld strain measurements that have demonstrated very high creep strains in locally creep weak HAZ regions. It is considered that this local mismatch in properties between the weld and HAZ might be responsible for enhanced creep strains adjacent to the fusion boundary which in turn would explain the very localised cavitation within a few grain widths of the fusion boundary.

This being the case the problem of Type IIIa cracking is likely to get worse with time. Further carbon diffusion will increase the width of the carburised band in the weld metal and exacerbate the mismatch in properties.

It is interesting to consider that if a matching CMV weld metal had been used instead of 2CrMo weld metal Type IIIa cracks would probably not have occurred. The majority of other countries with CMV pipework systems use a matching CMV welding consumable. The author is not aware of Type IIIa cracking problems being reported in these systems. Changing to a matching weld metal is therefore likely to

be one solution to the problem. However, it would be uneconomic to replace all the welds in power station steam pipework systems. Nevertheless, repairs could be carried out using a matching filler material at no extra cost.

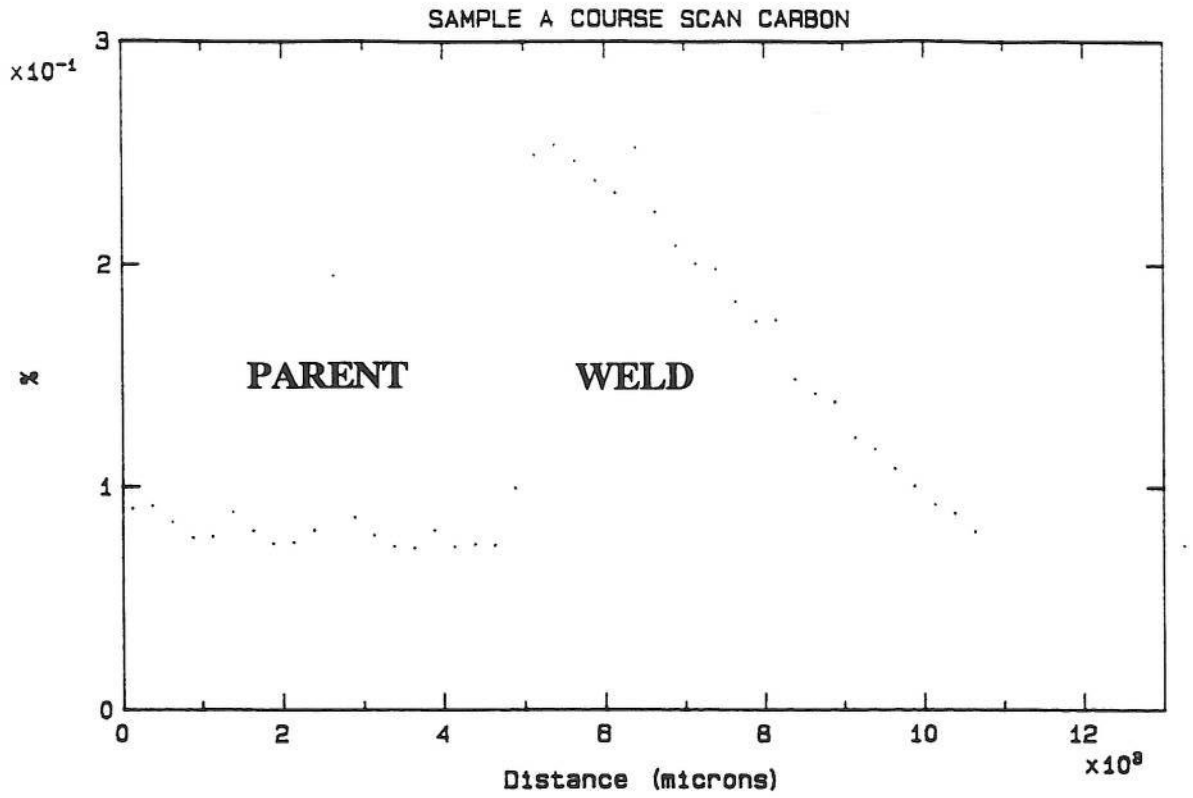

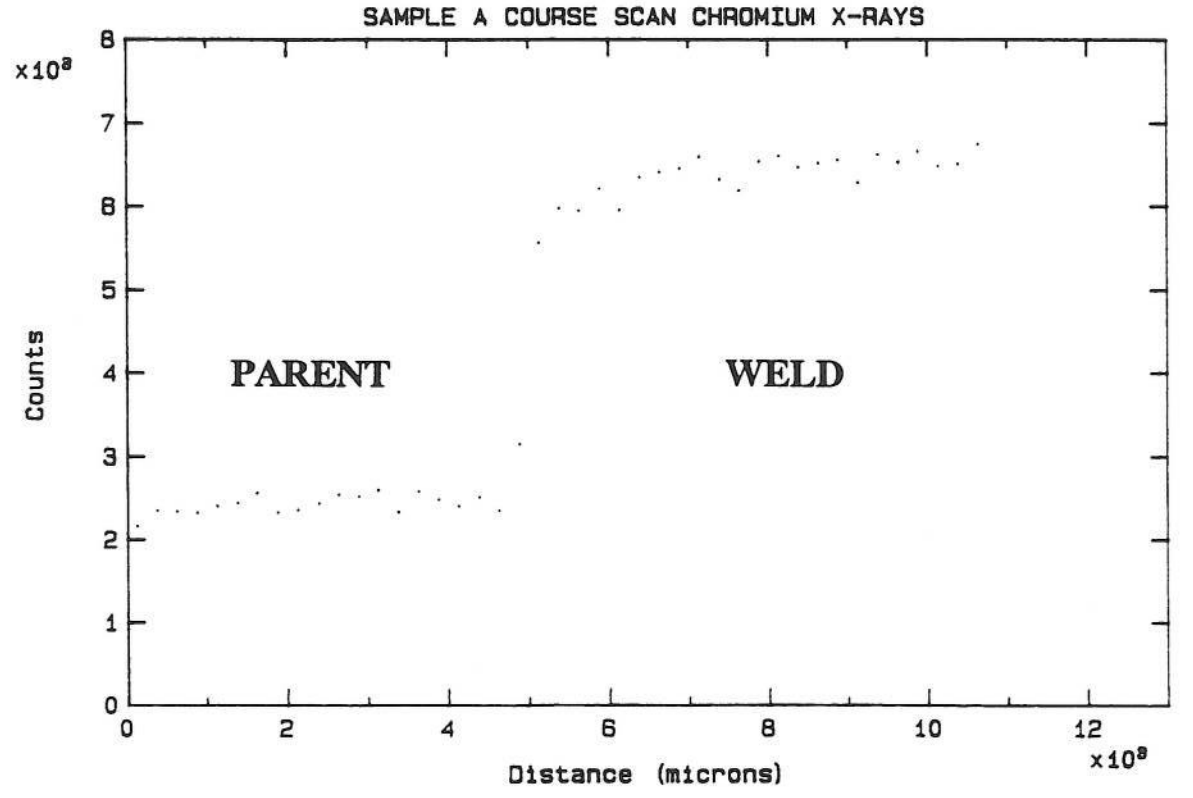

FIG 5.1

Carbon and Chromium Profiles from Service Exposed Sample SEF

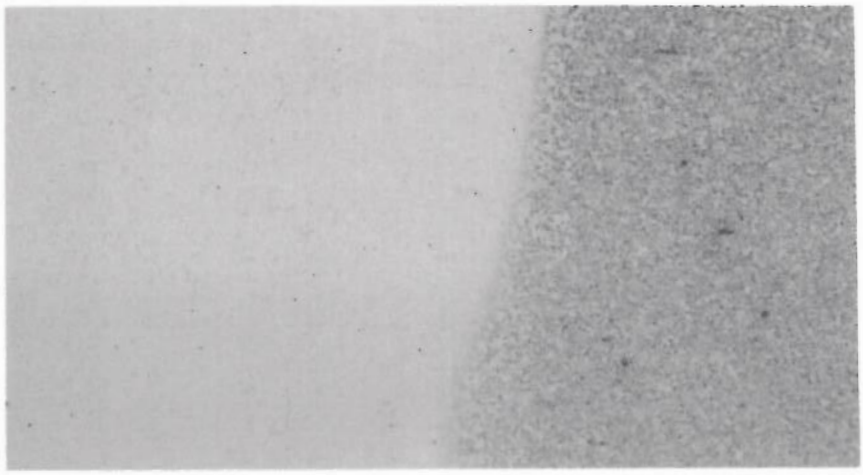

1.

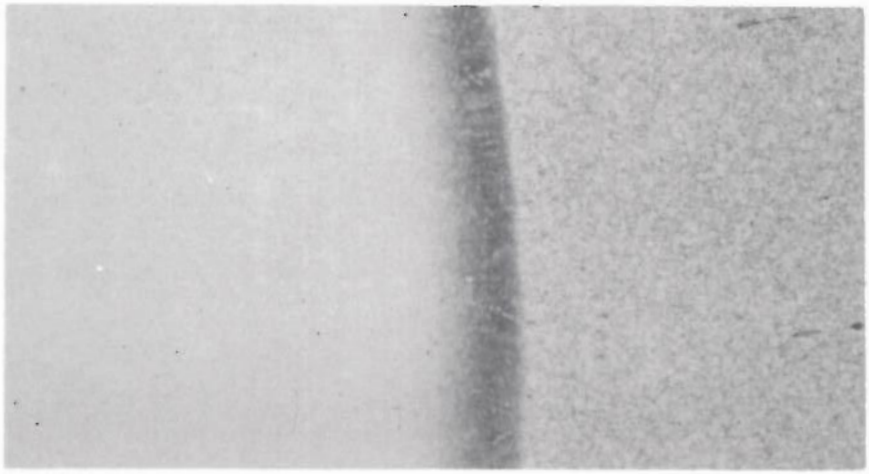

2.

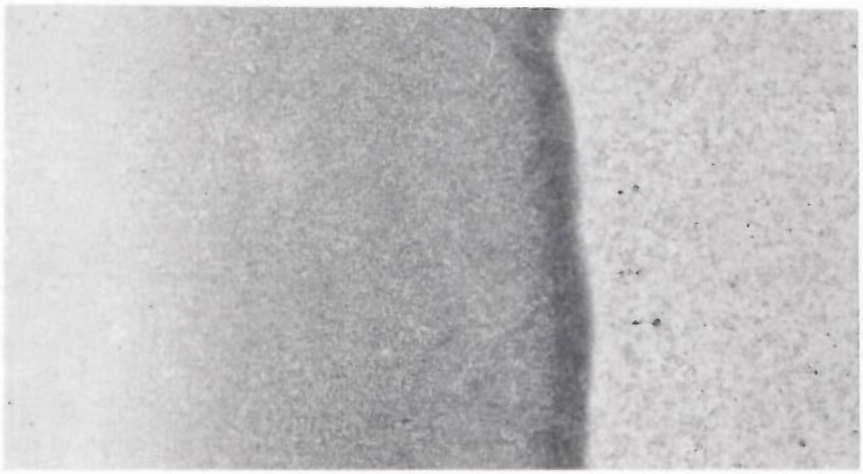

3.

FIG 5.2

Change in Width of the Carbon Enriched Band in the 9Cr Weld Metal Adjacent to the Fusion Boundary, (1) As Welded, (2) After PWHT and (3) After PWHT and Aging - Etchant 2% Nital (x150).

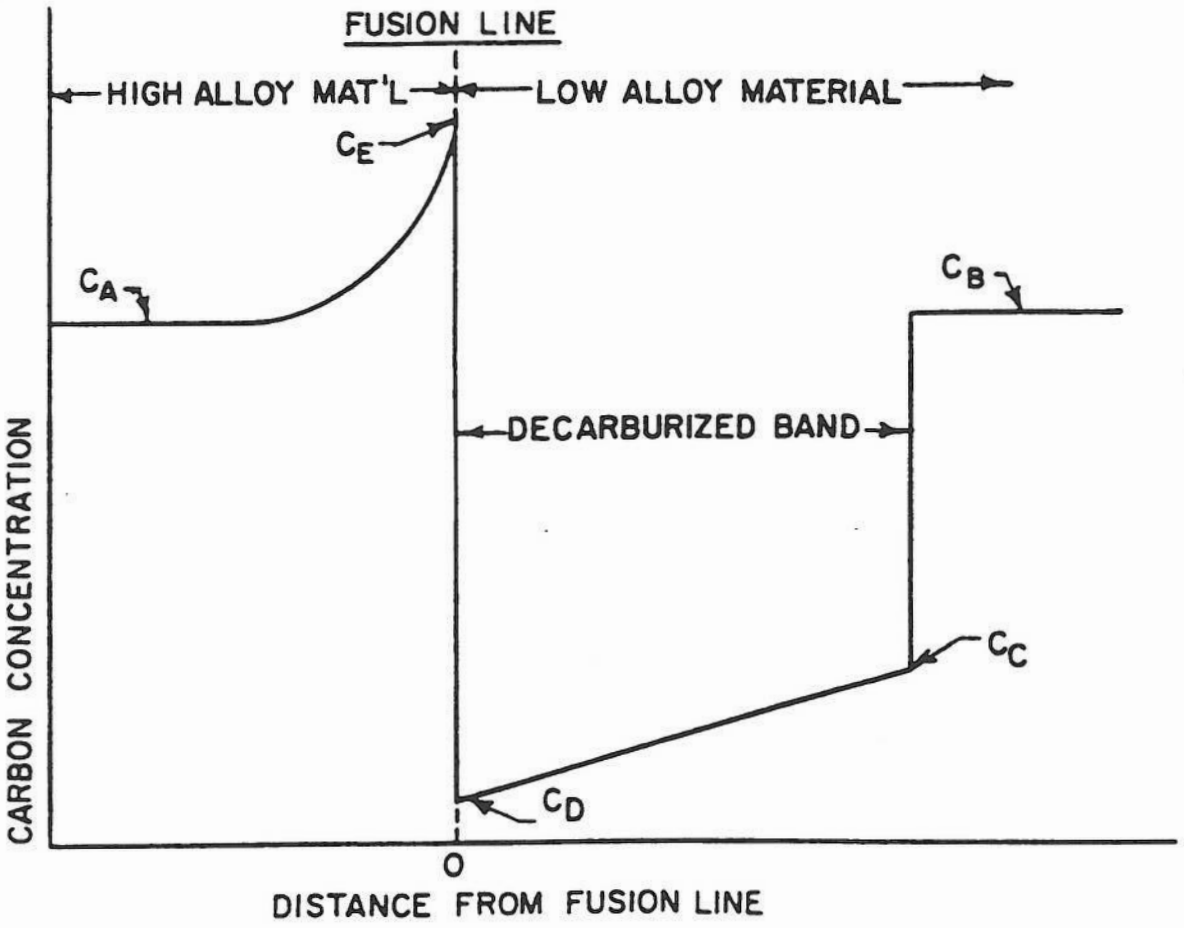

C_A = ORIGINAL TOTAL CARBON CONTENT IN HIGH ALLOY MATERIAL

C_B = ORIGINAL TOTAL CARBON CONTENT IN LOW ALLOY MATERIAL

C_C = CARBON SOLUBILITY CONCENTRATION IN LOW ALLOY MATERIAL

C_D = CARBON CONTENT IN LOW ALLOY MATERIAL AT THE FUSION LINE

C_E = CARBON CONTENT IN HIGH ALLOY MATERIAL AT THE FUSION LINE

FIG 5.4

Schematic diagram of carbon distribution in a composite weldment after exposure for some time interval at an elevated temperature[20]

6.0 **CONCLUSIONS**

1. The welding sequence adopted in test piece production has successfully produced a fusion boundary microstructure similar to that found associated with Type IIIa cracking.

2. The use of the Larson Miller parameter T(C+logt) with a value for C of 20 underestimated the time and temperature required to simulate carbon diffusion occurring during service exposure.

3. The phenomenon of uphill diffusion, where carbon migrates from an area of lower carbon concentration to an area of higher carbon concentration under the influence of higher alloy content has been identified.

4. Carbon migration in weldments between materials of nominally matching alloy content is largely driven by differences in carbon concentration.

5. Carbon diffusion in weldments of different alloy content does occur during welding.

6. In weldments of different alloy content significant carbon diffusion occurs during post weld heat treatment. However, at operating temperatures of 565°C the majority of carbon diffusion occurs during service.

7. In dissimilar alloy weldments carbon migration to the more highly alloyed weld material results in a sharp increase in carbon concentration adjacent to the fusion boundary. The width of this carbon enhanced region increases with time at temperature.

8. In dissimilar alloy weldments the width of the carburised band in the more highly alloyed material adjacent to the fusion boundary is relatively uniform along the fusion boundary. However local differences in carbon concentration do occur.

9. In dissimilar alloy weldments the minimum carbon concentration occurs at the fusion boundary in the lower alloy material following post weld heat treatment and aging. However, no sharp trough in carbon concentration was consistently identified in the HAZ adjacent to the fusion boundary.

10. In dissimilar alloy weldments carbon diffusion results in a reduction in hardness at the low alloy side of the joint and an increase in hardness on the higher alloy side of the joint.

11. In dissimilar alloy weldments carbon migration probably results in a reduction in creep strength on the low alloy side of the joint.

12. In dissimilar alloy weldments carbon migration results in a sharp discontinuity in carbon concentration either side of the fusion boundary which is likely to effect creep properties . This local mismatch in properties may explain why creep cavitation found associated with Type IIIa cracks is very localised, within a few grain widths of the fusion boundary.

13. In dissimilar alloy weldments the combination of a predominantly fine grained HAZ microstructure, carbon diffusion and the resultant mismatch in creep properties either side of the fusion boundary probably result in the Type IIIa region being weaker in creep than the Type IV region.

14. The problem of Type IIIa cracking is likely to get worse with time.

15. Type IIIa cracking is unlikely to occur in weldments of matching alloy content.

7.0 FURTHER WORK

1. A cross weld creep rupture testing programme is suggested to investigate the relative strengths of the Type IV and Type IIIa regions in CMV/2CrMo weldments. The programme would need to use a common parent material in which welding creates; (a) a predominantly fine grained HAZ microstructure at the fusion boundary in one set of specimens and (b) a conventional HAZ microstructure adjacent to the fusion boundary consisting of predominantly coarse grains in the other specimens. Testing should then generate Type IIIa failures in the fine grained specimens and Type IV failures in the coarse grained specimens. In this way the rupture lives of the regions can be compared.

2. A comparison of the creep properties of the local HAZ and weld metal regions adjacent to the fusion boundary after aging may be possible using the recently developed indentation creep testing techniques[37]. This should confirm a difference in creep properties between the two regions.

3. Carbon extraction replicas could be used to compare the carbide distribution either side of the fusion boundary. This information should increase our understanding of the carbon diffusion mechanism.

4. Finite element modelling of the fusion boundary area in CMV/2Cr weldments will allow the effects of differential fusion boundary creep properties to be investigated. This may enable the life of such weldments to be calculated, provided accurate creep data was available.

5. Carbon profiling on dissimilar weldments that have been renormalised following service exposure, or simulated aging, would allow reports that renormalisation can remove the carbon profile local to the fusion boundary to be investigated.

REFERENCES

1. BS806: 1993 Specification for the Design and Construction of Ferrous Piping Installations for and in Connection with Land Boilers, British Standards Institution London.

2. King B L, Middleton C J and Townsend R D, Prevention of Heat Affected Zone and Weld Metal Cracking through Control of Microstructure in CrMoV - 2¼CrMo Weldments, CERL Report RD/L/R1919, 1975.

3. King B L, Intergranular Embrittlement in CrMoV Steels: An Assessment of the Effects of Residual Impurity Elements on High Temperature Ductility and Crack Growth, Phil. Trans. R. Soc. London, A295, P235, 1980.

4. Myers J, Influence of Alloy and Impurity Content on Stress Relief Cracking in CrMoV Welds, Metals Technology,5, P391, 1978.

5. Alberry P J, Myers J and Chew B, An Improved Welding Technique for Heat Affected Zone Refinement, Welding and Metal Fabrication, 45, P549, 1977.

6. Gooch D J and King B L, High Temperature Crack Propagation in 2¼Cr-1Mo Manual Metal Arc Weld Metals, Conf. on Weldments, Physical Metallurgy and Failure Phenomena, General Electric Co., Schenectady, P393, 1979.

7. BS2633: 1973, Class 1 Arc Welding of Ferritic Steel Pipework for Carrying Fluids, British Standards Institution London.

8. BS2633: 1987, Class 1 Arc Welding of Ferritic Steel Pipework for Carrying Fluids, British Standards Institution London.

9. Fidler R, Hepworth J k, 1984, Residual stresses in CrMoV-2CrMo welds, Metal Construction, Sept '94, P540-545.

10. Schuller, Hagn and Woistcheck, Cracking in the Weld Region of Shaped Components in Hot Steam Pipe Lines - Material Investigations, Der Machinenschaden, 47, P1, 1974.

11. Brett S J, Cracking Experience in Steam Pipework Welds in National Power, Proceedings, VGB Conference "Materials and Welding Technology in Power Plants", Paper 8, 1994.

12. Gooch D J, Kimmins S T, A study of Type IV cracking in ½Cr½Mo¼V Weldments, CEGB report RD/L/3383/R88, 1988.

13. Brett S J, Type IV cracking in Steam Line Components, CEGB Report SWR/SSD/0727/N/86, 1986.

14. Kimmins S T and Longley E L, The Metallurgical Investigation of Weld BW14, NP Report PPIS/R/002, 1991.

15. Pilous V, Stransky K and Bursa M, Redistribution of Carbon in Welded Joints in Steels and its Effect on the Structure and Mechanical Properties of Welded Joints, Zvaranie 1989, 38, (6), P161-167, 1989.

16. Lunden C D, Dissimilar Metal Welds - Transition Joints Literature Review, Welding Research Supplement, P58s - P63s, 1982.

17. Smallman R E, Modern Physical Metallurgy, Fourth Edition, P142-145 Butterworths, 1985.

18. Darken L S, Diffusion of Carbon in Austenite with a Discontinuity in Composition, TRANS. AIME, P430-438, 1948.

19. Christoffel R J and Curran R M, Carbon Migration in Welded Joints at Elevated Temperatures, Welding Research Supplement, P457s-P468s, Sept. 1956.

20. Bhadeshia H K D H, The Redistribution of Carbon in Dissimilar Metal Joints, CERL Report No. TRPD/L/3236/R87, 1987.

21. Kimmins S T and Gooch D J, Microstructural Features of Renormalised and Tempered ½Cr½Mo¼V/2½Cr1Mo Weldments, CEGB Report RD/L/3529/R89, 1989.

22. Clarke J N and Lambert J A, Controlled All-Position Butter Temper Bead Welding Technique for Nuclear Repairs, Welding Journal, P42-P47, Feb 1986.

23. Easterling, Introduction to the Physical Metallurgy of Welding, Second Edition, Butterworth Heinemann, 1992.

24. McMillan J W, Nuclear Microprobe Measurement of the Spatial Distribution of Non-Metals in Metals; Analysis of Non Metals, Walter de Gruyter & Co., Berlin - New York, P174-P191, 1981.

25. McMillan J W, Nuclear Microprobe Applications in Material Science, Nuclear Instruments and Methods in Physics Research, B30, P474-479, 1988.

26. McMillan J W, Pummery F C W and P M Pollard, Experience in the use of the Harwell Nuclear Microprobe, Nuclear Instruments and Methods, 197, P171-177, 1982.

27. J W McMillan, The Determination of High Resolution Carbon Profiles in Weld Specimens, Letter, Ref. FSH-CB/A-Tech 14, Nov. 1993.

28. BS3604: Part 1: 1990, Steel Pipes and Tubes for Pressure Purposes: Ferritic Alloy Steel with Specified Elevated Temperature Properties. Part 1, Specification for Seamless and Electric Resistance Welded Tubes, British Standards Institution London.

29. BS5135: 1984, Process of Arc Welding of Carbon and Carbon Manganese Steels, British Standards Institution London.

30. Alberry P J and Jones W K C, The Structure and Hardness of ½Cr½Mo¼V and 2CrMo Simulated Heat Affected Zones, CEGB Report R/M/R241, 1976.

31. Larson R F and Miller J, A Time Temperature Relationship for Rupture and Creep Stresses, Trans. ASME, 51, P765-775, 1952.

32. Clark J N, Manual Metal Arc Weld Modelling Part 1: Dependence of Weld Bead and Heat Affected Zone Dimensions on Process Parameters, CEGB Report TPRD/M/1300/R83, 1983.

33. Brett S J, Private Communication.

34. Smallman R E, Modern Physical Metallurgy, Fourth Edition, P148 Butterworths, 1985.

35. Brandes E A, Smithells Metals Reference Book, 6th Edition, Chapter 13, P7-P17, 1983.

36. Samelson A, Life Reduction in High Temperature Structures due to Mis-Match of Weld and Parent Material Creep Properties, SA/FoU-Report 93/05, 1993.

APPENDIX A

Welding Conditions for Test Weld Production

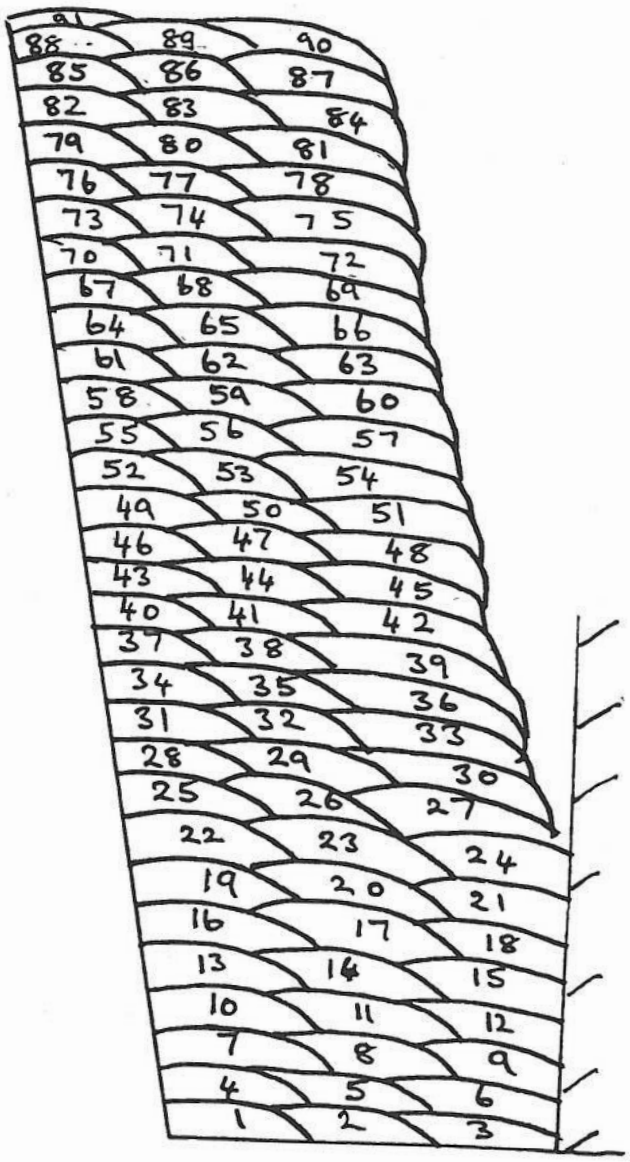

SUPREX F AND A2.

(CMV) (MS)

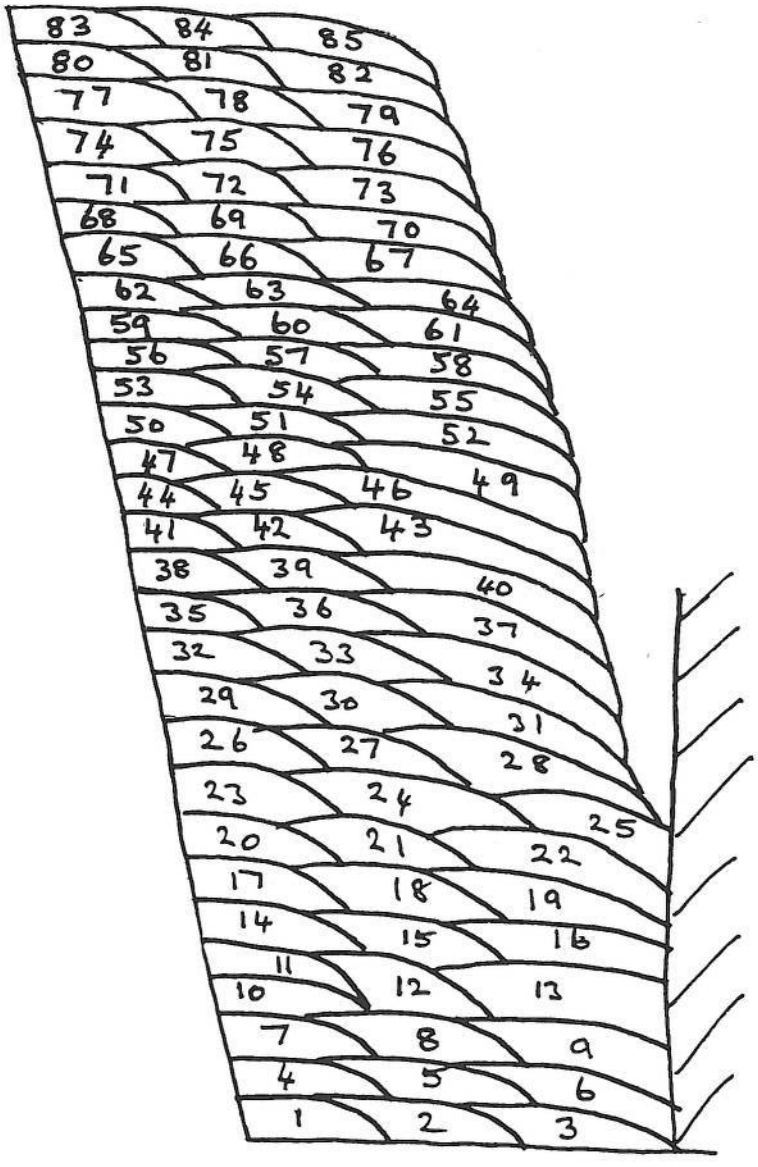

9Cr Mo B. and 76.28.

(9Cr) (2Cr)

A2 (1) (MS)

Run No.	ELECTRODE DIAMETER	SPEED mm/sec	SPEED inches/minute	HEAT INPUT KJ/mm	ROL mm.
1	3·25	3·5	8·29	0·80	200
2	4·0	4·08	9·64	0·75	200
3	4·0	3·72	8·91	0·82	200
4	3·25	3·22	7·62	0·84	200
5	4·0	3·92	9·26	0·82	200
6	4·0	3·45	8·15	0·96	200
7	3·25	3·45	8·15	0·89	200
8	4·0	3·7	8·74	0·96	200
9	4·0	4·0	9·44	0·89	200
10	3·25	3·0	7·08	0·96	210
11	4·0	3·89	9·18	0·89	210
12	4·0	3·5	8·29	0·99	210
13	3·25	2·8	6·61	1·03	210
16	3·25	2·96	6·98	0·97	210
19	3·25	2·89	6·84	0·99	220
20	4·0	4·4	10·39	0·79	220
21	4·0	3·93	9·28	0·89	220
22	3·25	3·05	7·22	0·94	220
25	3·25	3·14	7·42	0·93	220
28	3·25	3·19	7·53	0·90	220
31	3·25	2·97	7·02	0·98	220
34	3·25	2·85	6·73	1·03	225
385	4·0	4·09	9·66	0·85	225
37	3·25	2·64	6·25	1·11	225
40	3·25	2·71	6·39	1·11	230
43	3·25	2·76	6·53	1·06	235
44	4·0	3·92	9·25	0·94	235
46	3·25	2·53	5·97	1·16	240
49	3·25	2·37	5·60	1·21	230
50	4·0	3·93	9·28	0·87	220
51	4·0	4·15	9·81	0·82	220.
52.	3·25	2·55	6·03	1·13	250.

A2 (2) (MS)

Run No.	ELECTRODE DIAMETER	SPEED mm/sec	SPEED inches/minute	HEAT INPUT KJ/mm	ROL mm.
55	3·25	2·65	6·27	1·09	260
58	3·25	2·7	6·37	1·05	275
61	3·25	2·98	7·04	0·96	275
62	4·0	4·82	11·13	0·71	270
64	3·25	2·45	5·8	1·14	280
67	3·25	2·53	5·96	1·14	280
70	325	2·57	6·06	1·12	290
71	4·0	4·46	10·54	0·76	250
72	4·0	3·91	9·23	0·87	250
73	3·25	2·46	5·81	1·19	295
76	3·25	2·63	6·22	1·13	295
79	3·25	2·61	6·16	1·08	305
82	3·25	2·84	6·71	1·02	310
83	4·0	5·36	12·66	0·68	300
85	3·25	3·05	7·21	0·96	290
86	4·0	4·28	10·1	0·78	295
88	3·25	2·74	6·48	1·08	310
91	3·25	3·01	7·11	0·96	310.

SUPREX ~~AF~~ ① (CMV)

Run No.	ELECTRODE DIAMETER	SPEED mm/sec	SPEED inches/minute	HEAT INPUT KJ/mm	ROL mm.
1	3·25	3·25	7·68	0·96	205
2	4·0	3·75	8·86	0·92	210
3	4·0	3·63	8·6	0·99	200
4	3·25	3·41	8·06	0·91	215
5	4·0	3·84	9·07	0·89	215
6	4·0	3·58	8·46	1·0	215
7	3·25	3·1	7·32	0·98	220
8	4·0	3·93	9·28	0·83	220
9	4·0	4·07	9·62	0·86	215
10	3·25	3·03	7·15	0·97	215
11	4·0	4·13	9·77	0·88	215
12	4·0	3·58	8·46	1·02	215
13	3·25	3·19	7·53	0·94	220
16	3·25	3·1	7·32	0·97	220
19	3·25	2·94	6·96	1·02	215
20	4·0	3·71	8·76	0·96	215
21	4·0	3·58	8·46	0·99	215
22	3·25	3·14	7·42	0·99	220
25	3·25	3·19	7·53	0·94	220
26	4·0	4·07	9·62	0·86	220
27	4·0	3·67	8·66	0·94	220
28	3·25	3·33	7·88	0·90	220
31	3·25	2·81	6·64	1·02	225
34	3·25	2·56	6·04	1·22	230
37	3·25	2·67	6·31	1·13	235
40	3·25	2·53	5·97	1·19	240
43	3·25	2·63	6·22	1·08	245
44	4·0	4·38	10·33	0·9	245
46	3·25	2·63	6·22	1·16	245
47	4·0	3·83	9·06	0·91	230
48	4·0	3·90	9·21	0·91	230
49	3·25	2·5	5·91	1·15	260

SUPREX 8F (2) (CMV)

Run No.	ELECTRODE DIAMETER	SPEED mm/sec	SPEED inches/minute	HEAT INPUT KJ/mm	ROL mm.
52	3·25	2·45	5·79	1·28	245
53	4·0	3·97	9·37	0·9	230
54	4·0	4·18	9·88	0·85	230
55	3·25	2·71	6·4	1·08	260
58	3·25	2·67	6·31	1·04	270
61	3·25	2·73	6·44	1·04	270
62	4·0	4·64	10·97	0·77	260
64	3·25	2·5	5·91	1·28	270
67	3·25	2·59	6·12	1·18	280
70	3·25	2·54	6·01	1·20	285
71	4·0	4·42	10·43	0·81	265
73	3·25	2·48	5·86	1·21	285
76	3·25	2·93	6·92	1·05	290
79	3·25	2·56	6·06	1·15	300
82	3·25	3·12	7·37	1·06	290
83	4·0	4·92	11·6	0·76	290
85	3·25	3·14	7·41	0·99	295
86	4·0	4·84	11·42	0·76	295
88	3·25	2·9	6·85	1·01	290
91	3·25	3·54	8·35	0·86	290

76·28 (1) (2Cr)

Run No.	ELECTRODE DIAMETER	SPEED mm/sec	SPEED inches/minute	HEAT INPUT KJ/mm	ROL mm.
1	3·25	3·1	7·5	0·77	205
2	4·0	3·94	9·3	0·8	205
3	4·0	3·01	7·12	1·04	205
4	3·25	2·77	6·54	0·98	205
6	4·0	3·1	7·34	1·01	205
7	3·25	3·1	7·34	0·91	205
8	4·0	3·66	8·65	1·24	205
9	4·0	3·1	7·34	1·04	205
10	3·25	2·8	6·6	1·0	215
11	3·25	2·62	6·19	1·04	215
12	4·0	3·16	7·47	0·97	215
14	3·25	2·75	6·50	1·02	220
17	3·25	3·05	7·2	0·92.	220
20	3·25	2·89	6·83	1·0	240
23	3·25	2·88	6·79	0·93	230
26	3·25	2·61	6·17	0·96	230
27	4·0	4·18	9·88	0·76	230
28	4·0	3·21	7·59	1·04	225
29	3·25	3·05	7·20	0·99	250
32	3·25	2·84	6·70	0·95	230
33	4·0	4·04	9·53	0·77	230
35	3·25	3·26	7·71	0·94	235
38	3·25	3·01	7·12	0·97	250
41	3·25	3·13	7·39	0·92	250
44	3·25	3·09	7·30	0·98	250
47	3·25	2·93	6·92	0·97	240
50	3·25	2·98	7·04	0·99	250
53	3·25	2·66	6·28	1·10	250
56	3·25	2·77	6·54	1·11	260
59	3·25	2·52	5·95	1·22	265
60	4·0	3·79	8·95	0·79	265
62	3·25	2·6	6·14	1·13	260.

76.28 (2) (2Cr)

Run No.	ELECTRODE DIAMETER	SPEED mm/sec	SPEED inches/minute	HEAT INPUT KJ/mm	ROL mm.
65	3·25	2·62	6·19	1·13	270
68	3·25	2·6	6·14	1·16	270
71	3·25	2·86	6·76	1·01	280
74	3·25	2·88	6·79	1·03	280
77	3·25	2·87	6·78	1·03	280
78	4·0	4·08	9·64	0·85	290
80	3·25	3·37	7·96	0·88	280
83	3·25	3·33	7·87	0·87	290
84	4·0	3·98	9·4	0·89	290.

9Cr Mo B. (1) (9Cr)

Run No.	ELECTRODE DIAMETER	SPEED mm/sec	SPEED inches/minute	HEAT INPUT KJ/mm	ROL mm.
1	3·25	3·72	8·8	0·76	205
2	4·0	4·66	11·0	0·73	205
3	4·0	3·2	7·57	1·02	205
4	3·25	3·42	8·07	0·84	205
5	4·0	3·66	8·65	0·87	205
6	4·0	3·10	7·34	0·98	205
7	3·25	2·69	6·36	1·02	210
8	4·0	4·2	9·92	0·76	210
9	4·0	2·84	6·7	1·22	210
10	3·25	2·18	5·15	1·26	220
11	3·25	2·42	5·72	1·14	220
14	3·25	2·5	5·91	1·12	220
17	3·25	2·34	5·52	1·28	220
18	4·0	3·24	7·64	1·04	220
20	3·25	2·16	5·1	1·33	220
23	3·25	2·97	7·02	0·93	220
26	3·25	2·87	6·79	1·03	250
27	4·0	3·97	9·37	0·92	250
29	3·25	2·87	6·79	1·04	250
32	3·25	2·77	6·55	1·07	230
35	3·25	3·18	7·51	0·95	245
38	3·25	2·85	6·73	1·04	245
39	4·0	3·82	9·04	0·98	245
41	3·25	2·61	6·17	1·18	235
44	3·25	2·86	6·76	1·01	240
47	3·25	2·76	6·52	1·10	240
50	3·25	2·72	6·43	1·10	245
53	3·25	2·66	6·28	1·10	250
56	3·25	2·72	6·43	1·09	245
59	3·25	2·72	6·43	1·11	250
60	4·0	3·57	8·43	1·08	250
62	3·25	2·78	6·57	1·11	250

9Cr Mo B (2) (9Cr)

Run No.	ELECTRODE DIAMETER	SPEED mm/sec	SPEED inches/minute	HEAT INPUT KJ/mm	ROL mm.
65	3·25	2·48	5·86	1·12	255
68	3·25	2·84	6·71	1·06	250
71	3·25	2·83	6·69	1·06	255
74	3·25	2·83	6·71	1·03	260
77	3·25	2·77	6·55	1·05	260
80	3·25	2·77	6·55	1·06	260
83	3·25	2·91	6·87	1·05	260

APPENDIX B

Larson Miller Parameter and Aging Heat Treatment Conditions

LARSON MILLER PARAMETER

The Larson Miller Parameter[30] is a relationship between time and temperature appropriate to diffusion driven processes such as tempering and creep. The parameter is derived from the Arrhenius rate equation which states that the rate of a certain process is related to temperature by the following equation.

$$r = Ae^{-Q/RT}$$

where

r = rate
A = constant
Q = activation energy for the process
R = gas constant
T = absolute temperature

If the rate of a process is constant it will be inversely proportional to time, so the equation can be rewritten as;

$$1/t = Be^{-Q/RT}$$

By taking logs of both sides the equation can written in the form, which is the Larson Miller Parameter;

$$T(C + \log t) = Q/2.3R = \text{const}$$

where $C = \log B$

It was found empirically[Ref 30] that a value for C of 20 gave good agreement with a wide range of materials including low alloy steels for creep and tempering processes.

In this investigation the author has used the relationship to establish a time and temperature for an aging heat treatment that will produce an equivalent level of carbon diffusion to service exposure for 100,000hrs at 565°C. It is not immediately apparent whether this approach is technically valid, this point has been addressed in the discussion.

AGEING HEAT TREATMENT

To establish a suitable time and temperature for the aging treatment, the Larson Miller Parameter was used in the form;

$T_1(20 + \log t_1) = T_2(20 + \log t_2)$

Service Conditions;

t_1 = 100,000hrs
T_1 = 565 + 273 = 838K

Ageing Conditions;

t_2 - chosen as 884hrs
T_2 - calculated from the above equation to be 913k (640°C)

An acceptable deviation from the 640°C was specified by the author as -2 to +5°C. Entering these values in the equation above, the possible time of simulated service exposure will vary between 88,000 to 137,000hrs. This range was considered to still reflect acceptable periods of service exposure.

During the heat treatment it was not possible to control the temperature of each of the specimens to within the required temperature range. The table below summarises the heat treatments given and the equivalent service hours at 565°C calculated using the Larson Miller parameter.

WELDMENT	HEAT TREATMENT		ADDITIONAL HEAT TREATMENT		EQUIVALENT SERVICE HOURS
	MEAN TEMP °C	TIME Hrs	MEAN TEMP	TIME Hrs	
9Cr	635	884	642	156	90,000
2Cr	642	884	-	-	113,000
C	645	884	-	-	137,000
CMV	648	884	-	-	165,000

APPENDIX C

Carbon and Chromium Profiles

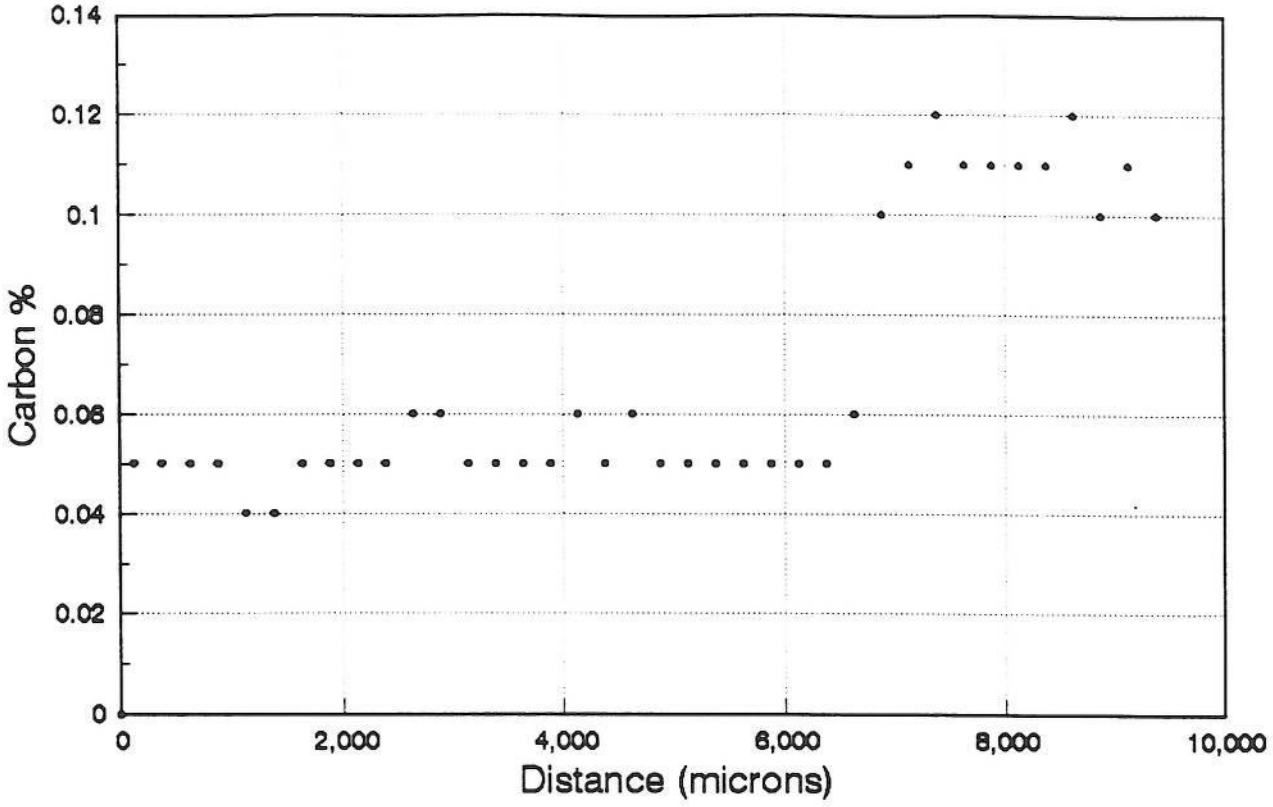
0.14
0.12
0.1
0.08
0.06
0.04
0.02
0
Carbon %
0
2,000
4,000
6,000
8,000
10,000
Distance (microns)

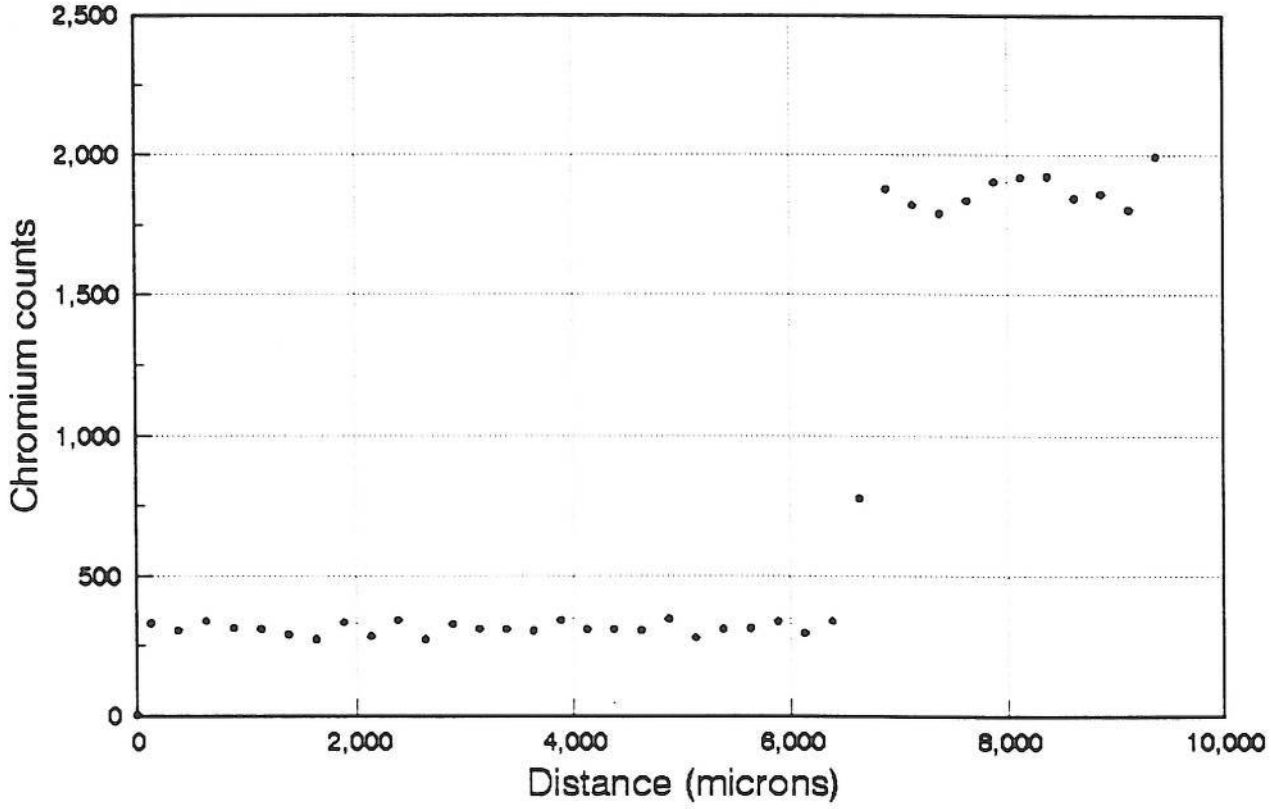
2,500
2,000
1,500
1,000
500
0
Chromium counts
0
2,000
4,000
6,000
8,000
10,000
Distance (microns)

MS.C.AW

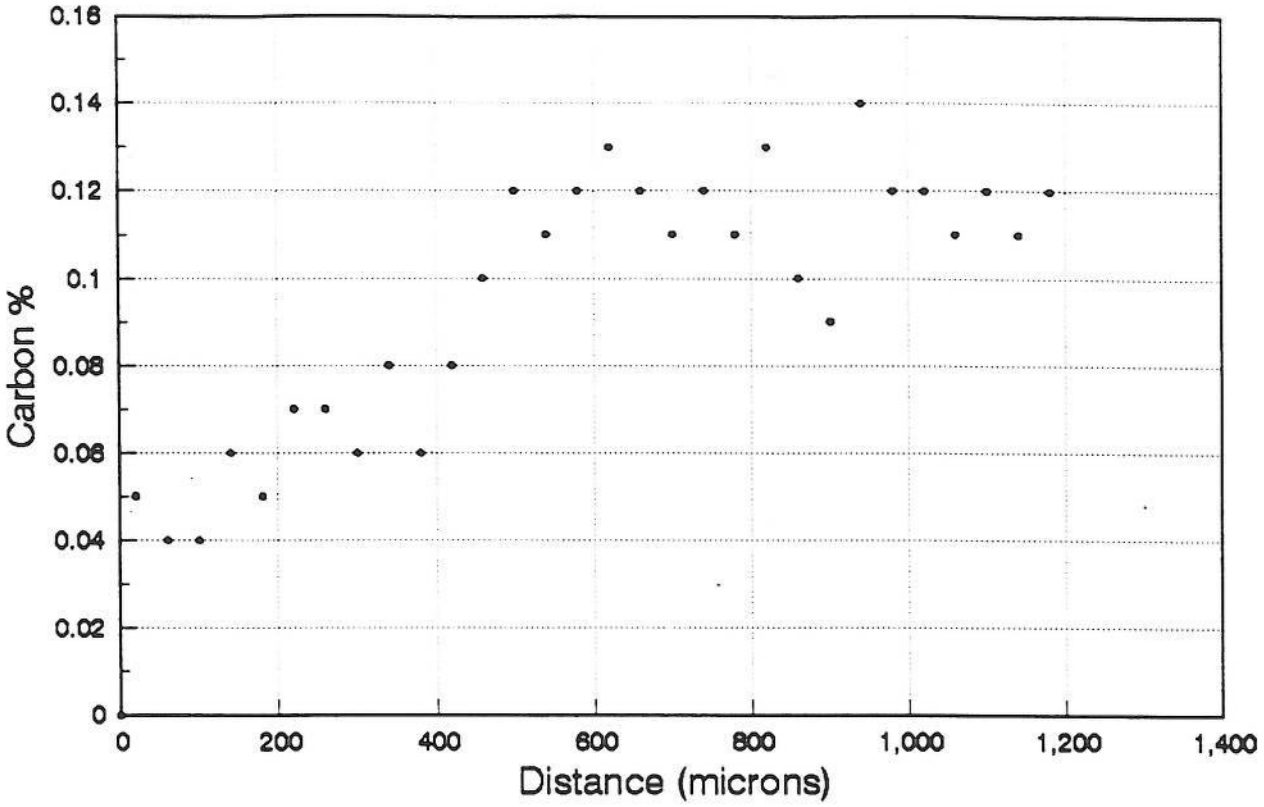
Carbon %
0.16
0.14
0.12
0.1
0.08
0.06
0.04
0.02
0
0
200
400
600
800
1,000
1,200
1,400
Distance (microns)

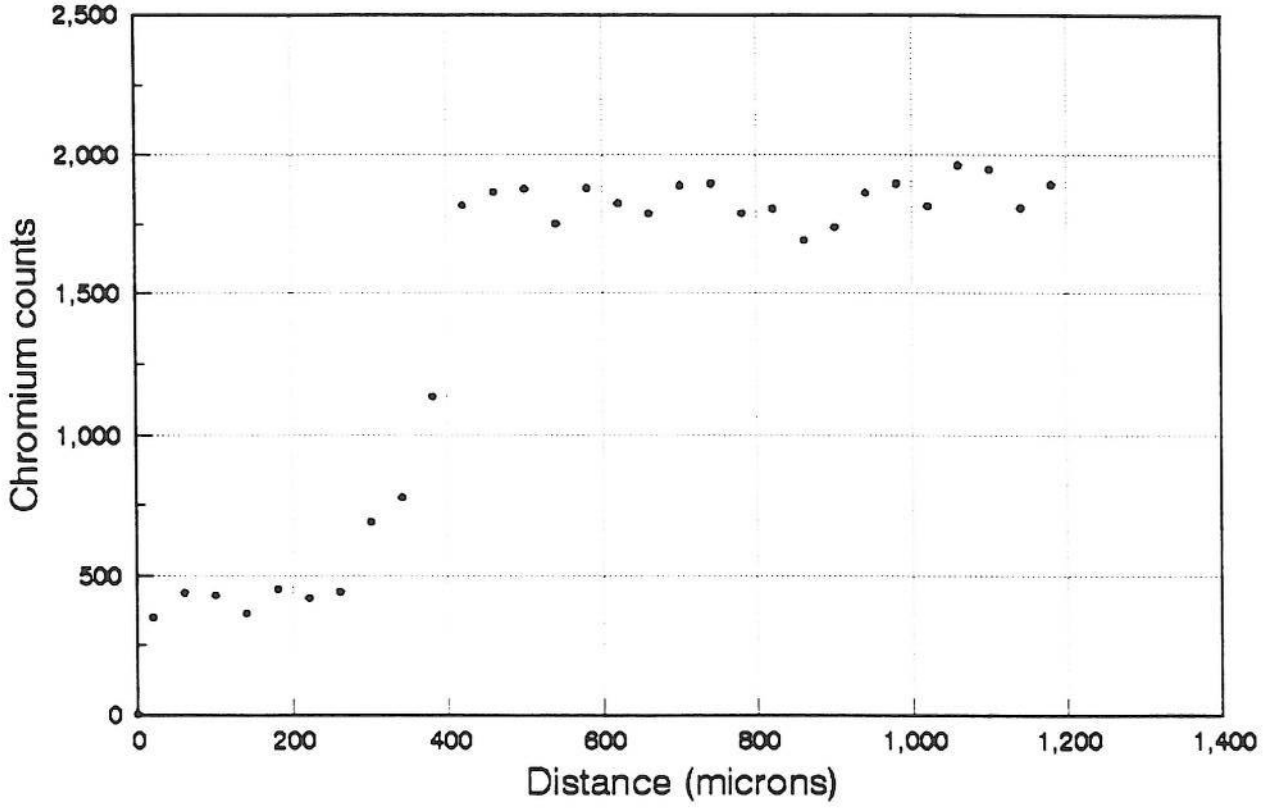
Chromium counts
2,500
2,000
1,500
1,000
500
0
0
200
400
600
800
1,000
1,200
1,400
Distance (microns)

MS.M.AW

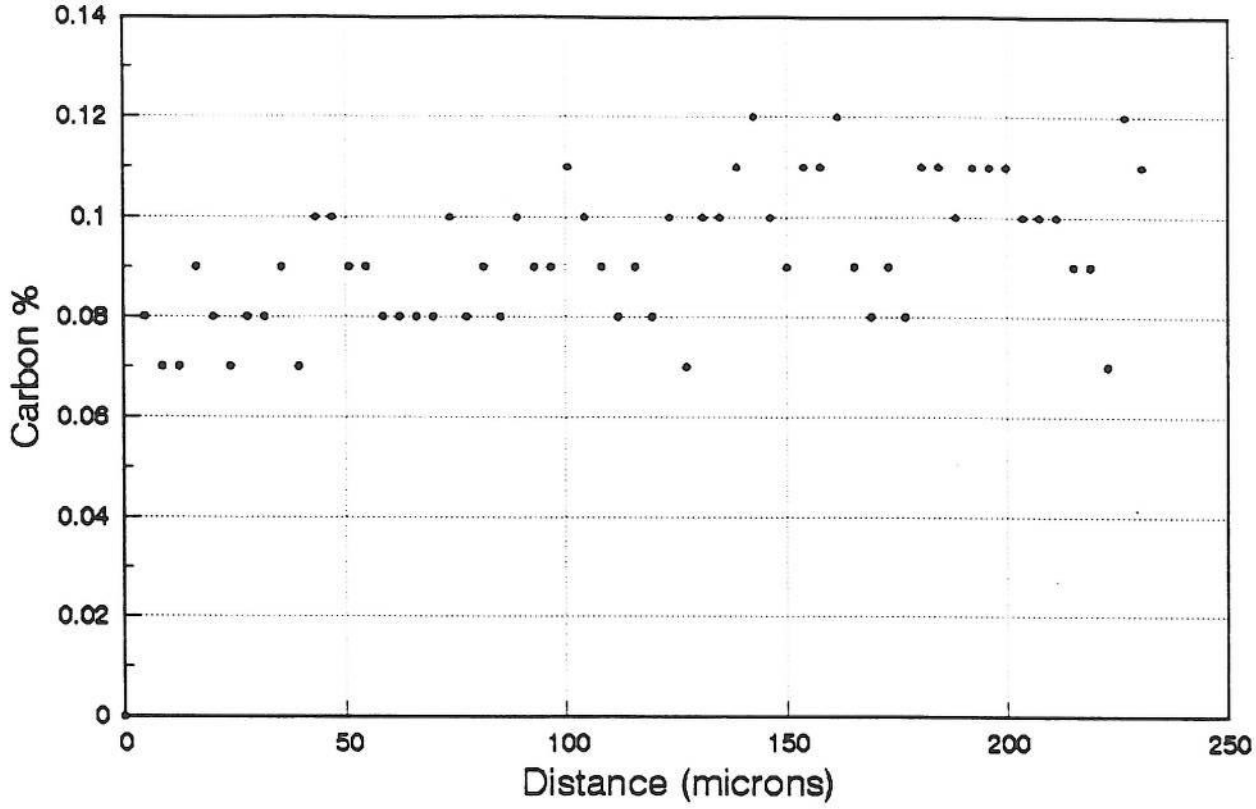
0.14
0.12
0.1
0.08
0.06
0.04
0.02
0
Carbon %
0
50
100
150
200
250
Distance (microns)

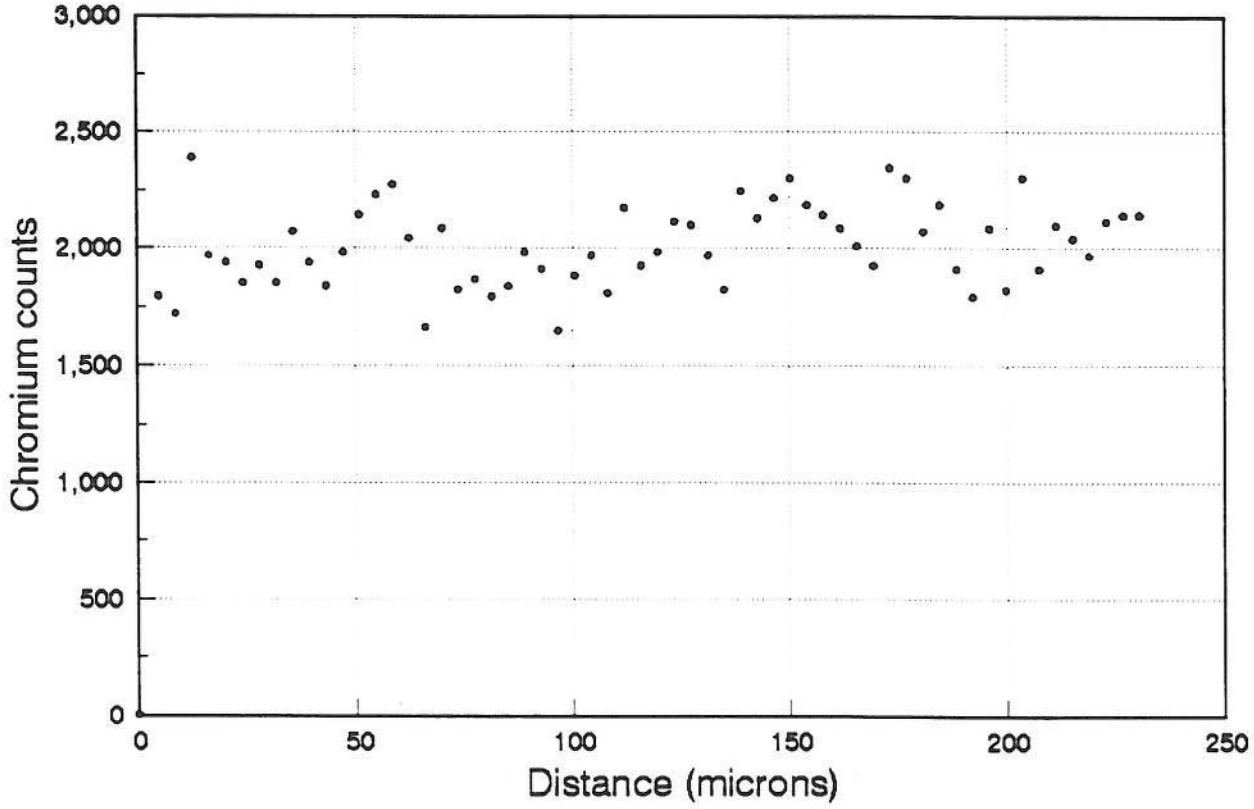
3,000
2,500
2,000
1,500
1,000
500
0
Chromium counts
0
50
100
150
200
250
Distance (microns)

MS.F.AW

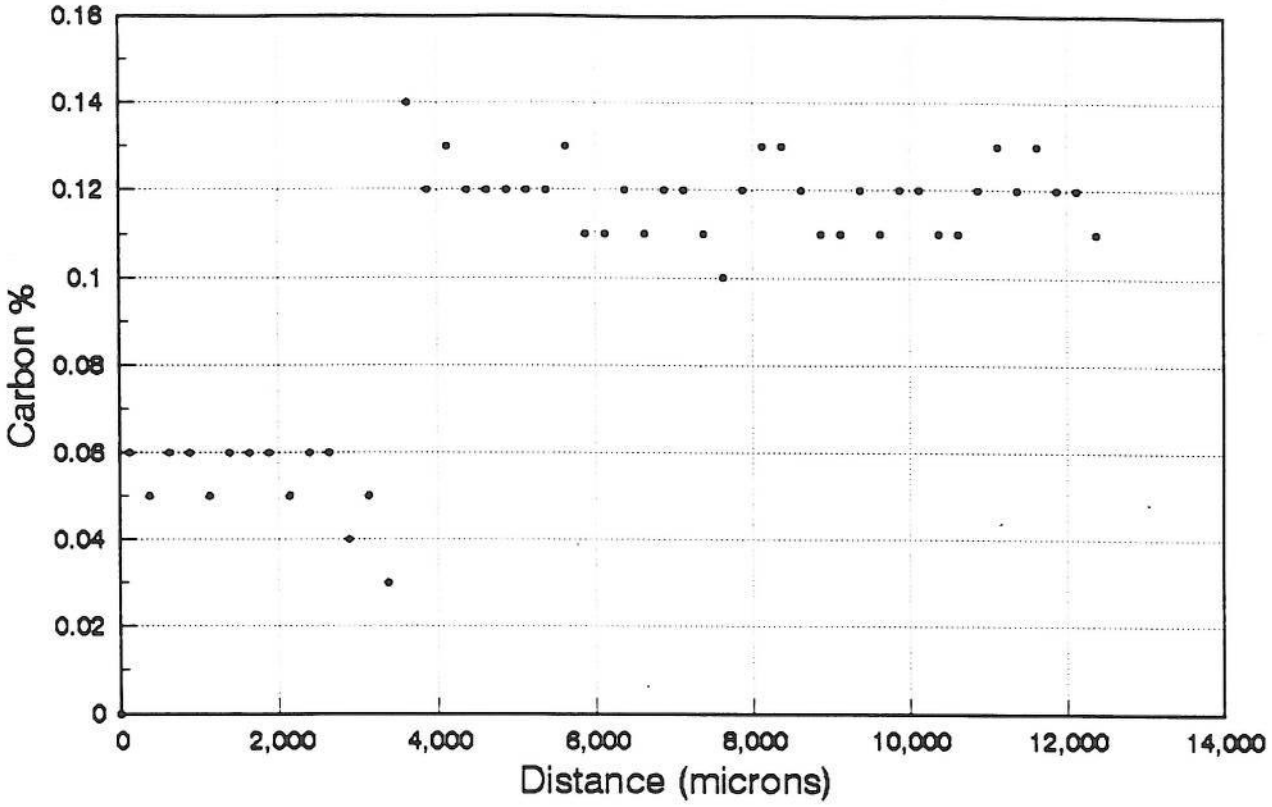
0.16
0.14
0.12
0.1
0.08
0.06
0.04
0.02
0
Carbon %
0
2,000
4,000
6,000
8,000
10,000
12,000
14,000
Distance (microns)

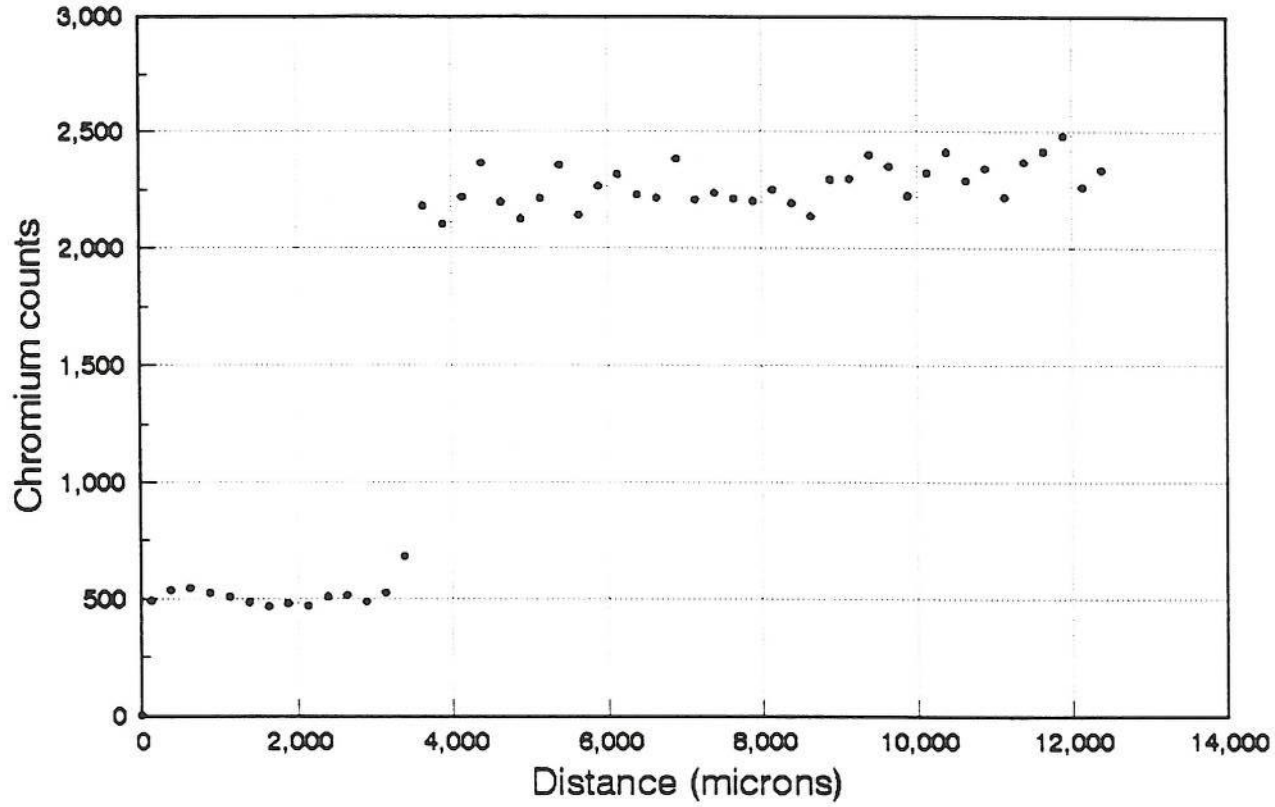
3,000
2,500
2,000
1,500
1,000
500
0
Chromium counts
0
2,000
4,000
6,000
8,000
10,000
12,000
14,000
Distance (microns)

MS.C.PWHT

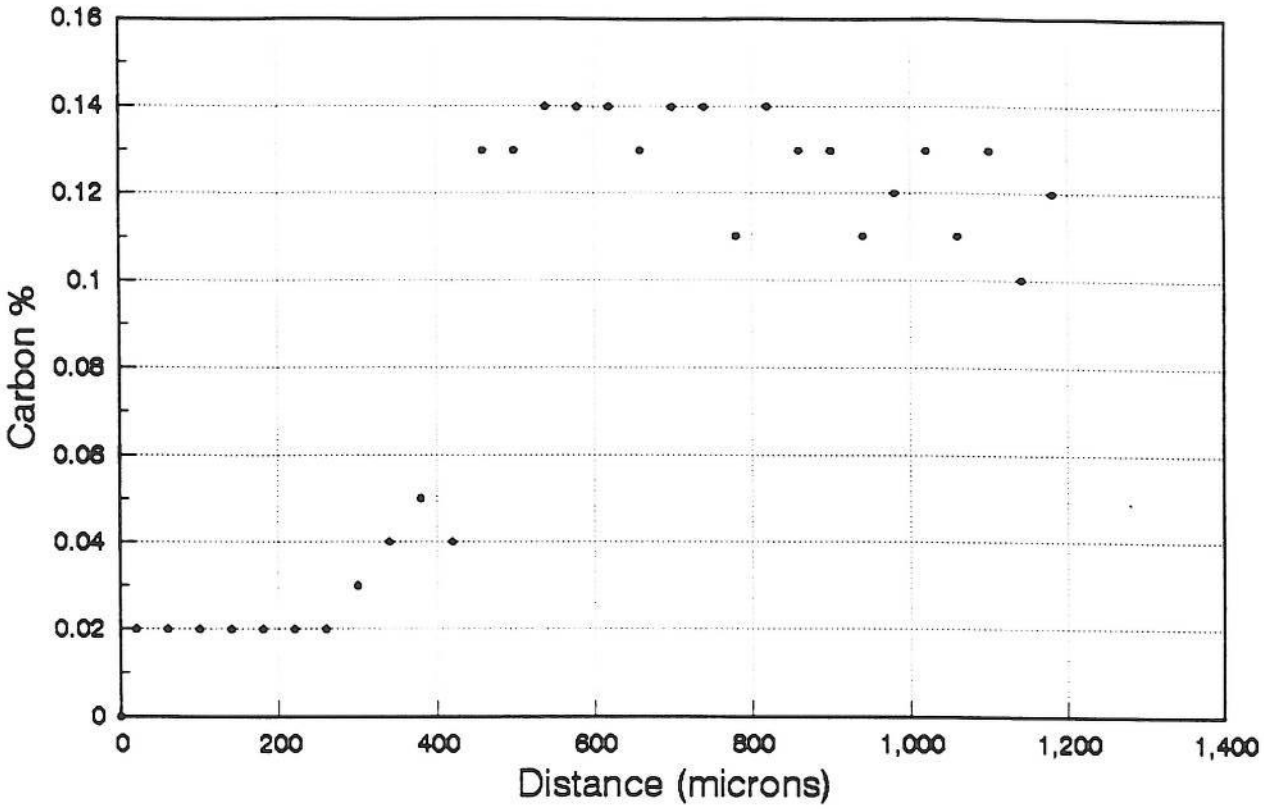
0.16
0.14
0.12
0.1
0.08
0.06
0.04
0.02
0
Carbon %
0
200
400
600
800
1,000
1,200
1,400
Distance (microns)

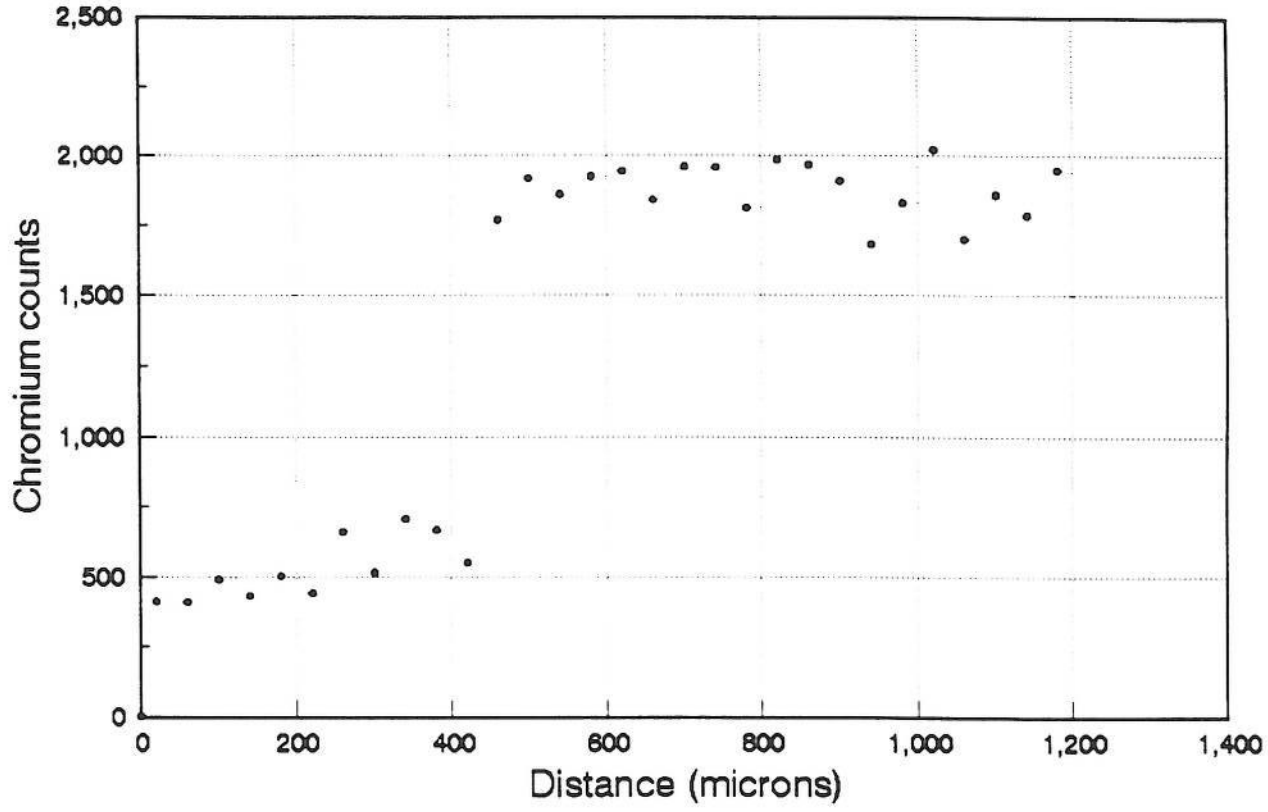
2,500
2,000
1,500
1,000
500
0
Chromium counts
0
200
400
600
800
1,000
1,200
1,400
Distance (microns)

MS.M.PWHT

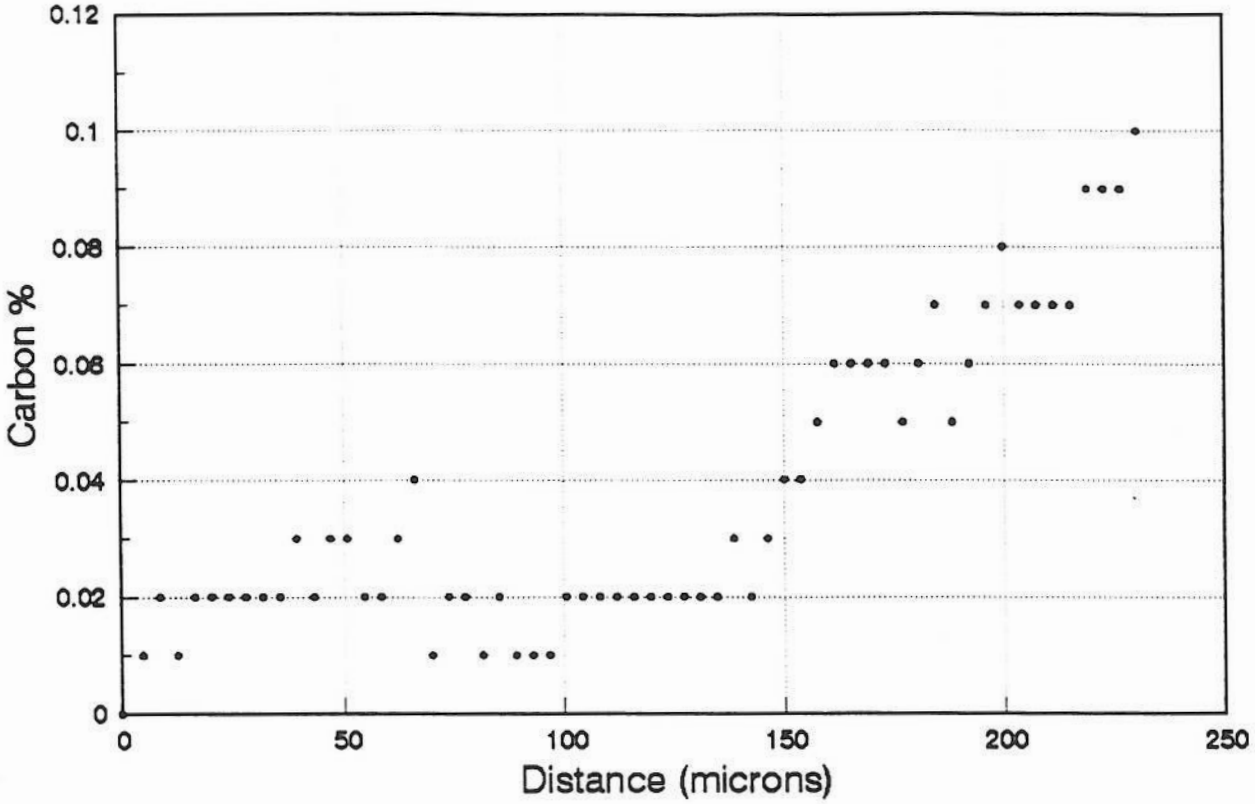
0.12
0.1
0.08
0.06
0.04
0.02
0
Carbon %
0
50
100
150
200
250
Distance (microns)

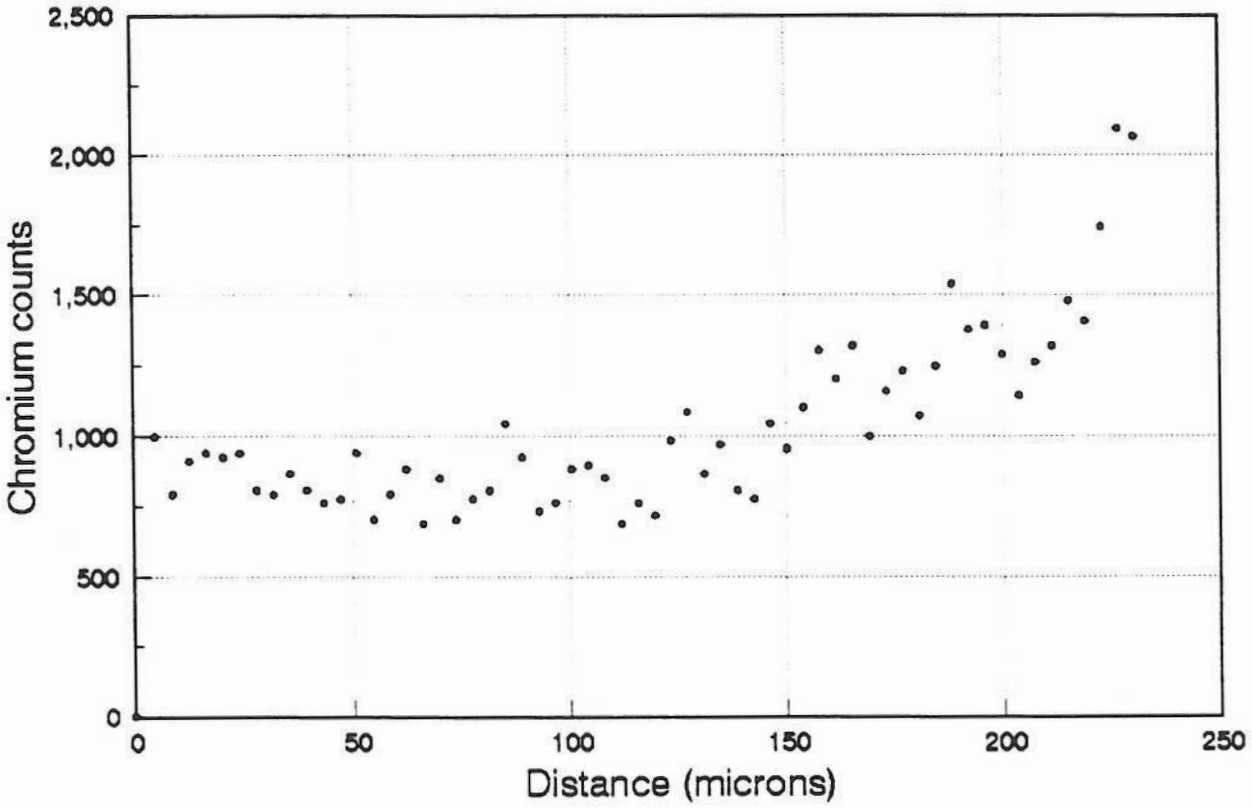
2,500
2,000
1,500
1,000
500
0
Chromium counts
0
50
100
150
200
250
Distance (microns)

MS.F.PWHT

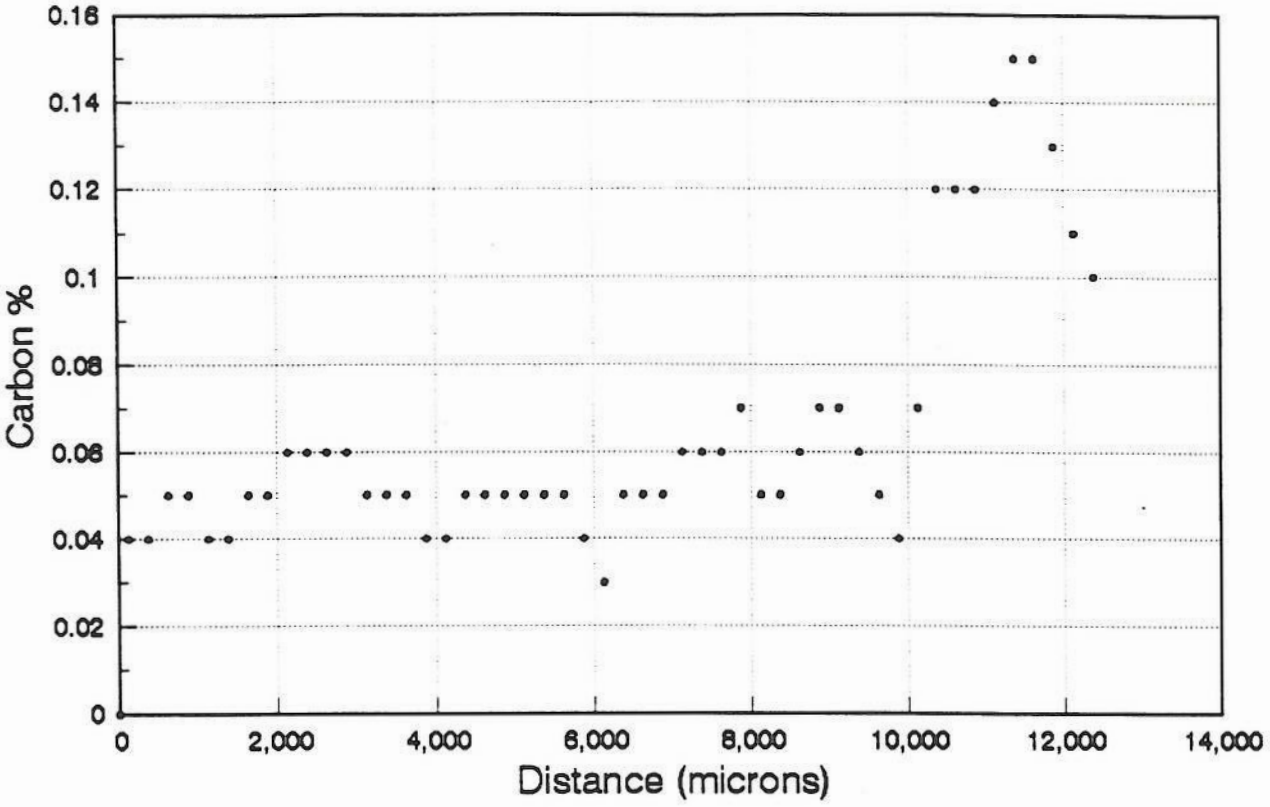
0.16
0.14
0.12
0.1
0.08
0.06
0.04
0.02
0
Carbon %
0
2,000
4,000
6,000
8,000
10,000
12,000
14,000
Distance (microns)

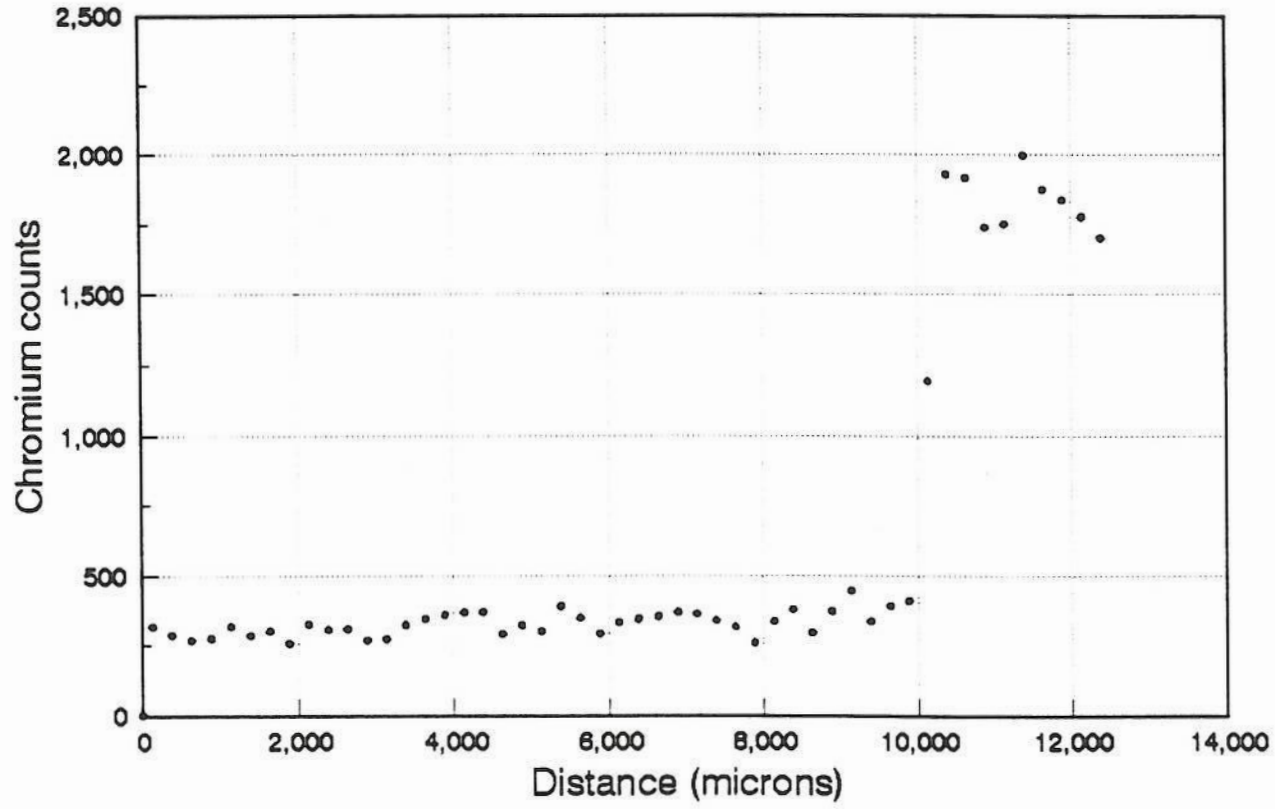
2,500
2,000
1,500
1,000
500
0
Chromium counts
0
2,000
4,000
6,000
8,000
10,000
12,000
14,000
Distance (microns)

MS.C.AGED

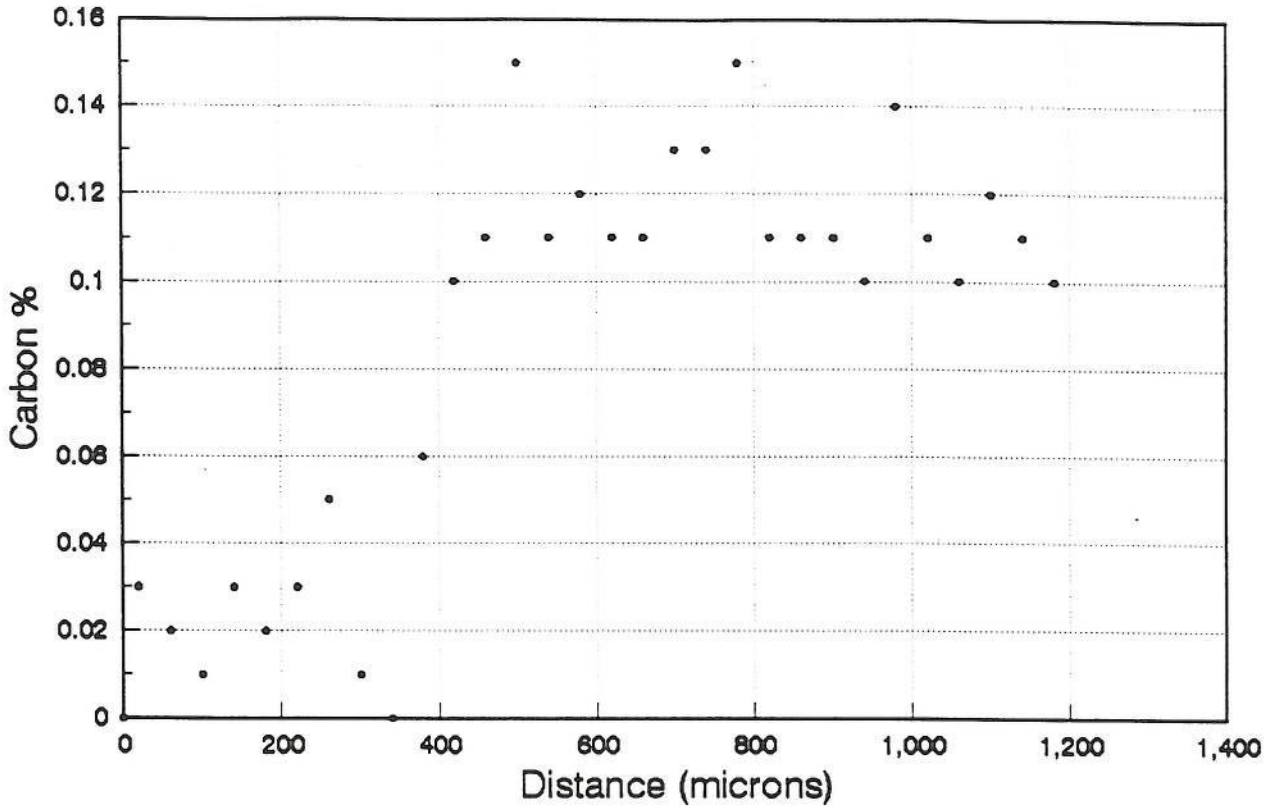
0.16
0.14
0.12
0.1
0.08
0.06
0.04
0.02
0
Carbon %
0
200
400
600
800
1,000
1,200
1,400
Distance (microns)

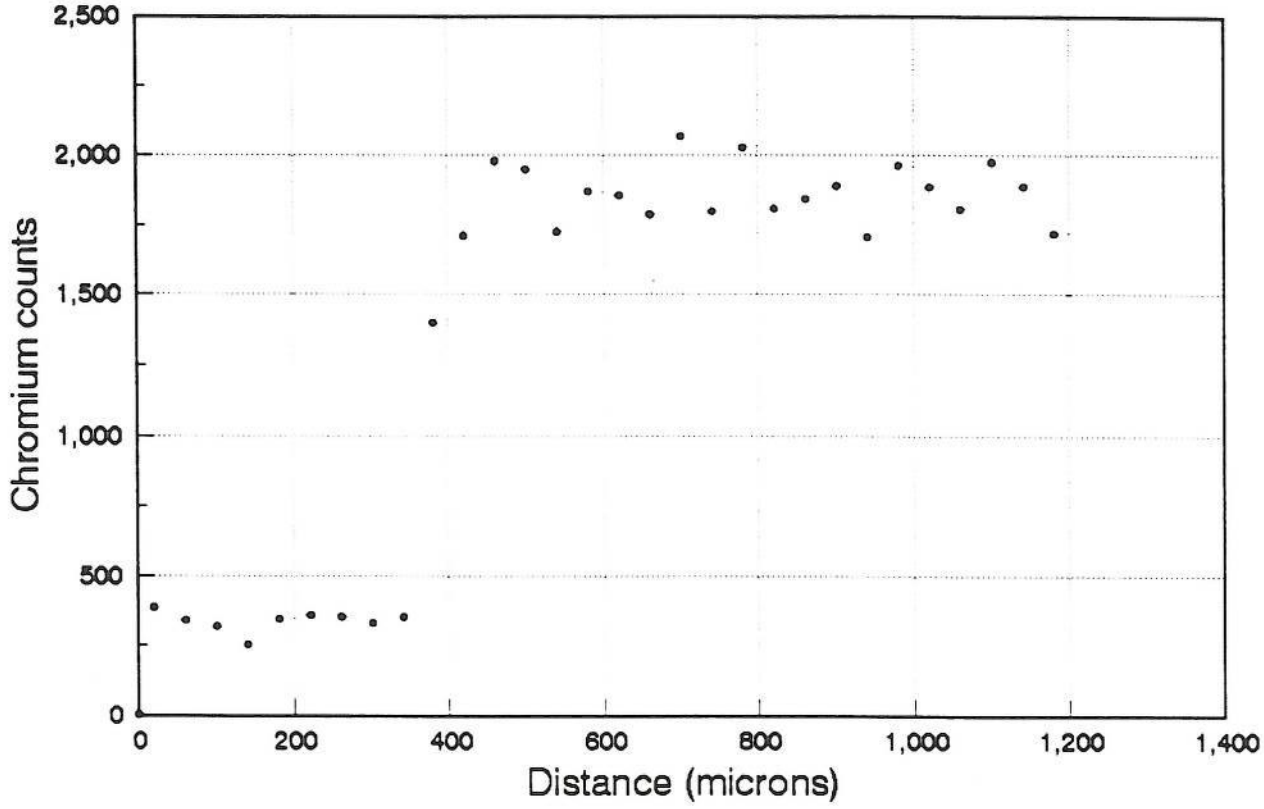
2,500
2,000
1,500
1,000
500
0
Chromium counts
0
200
400
600
800
1,000
1,200
1,400
Distance (microns)

MS.M.AGED

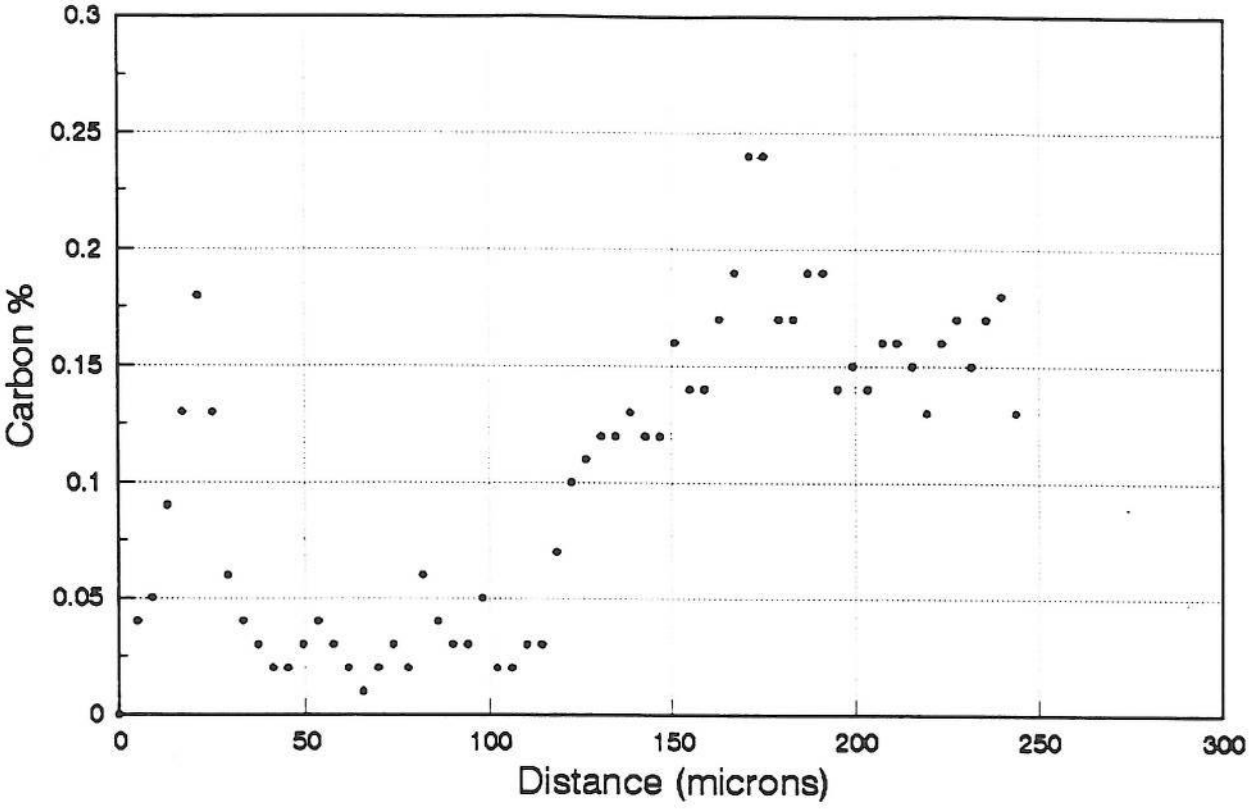
Carbon %
0.3
0.25
0.2
0.15
0.1
0.05
0
0
50
100
150
200
250
300
Distance (microns)

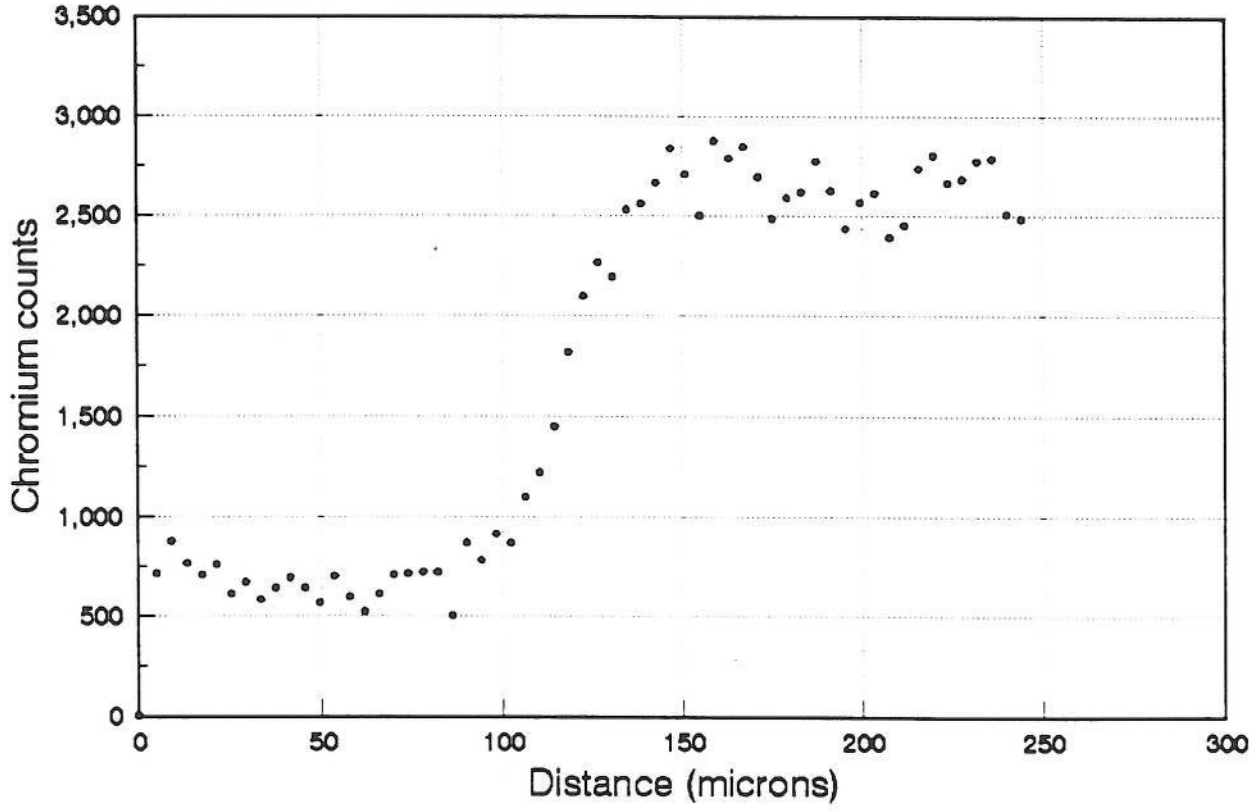
Chromium counts
3,500
3,000
2,500
2,000
1,500
1,000
500
0
0
50
100
150
200
250
300
Distance (microns)

MS.F.AGED

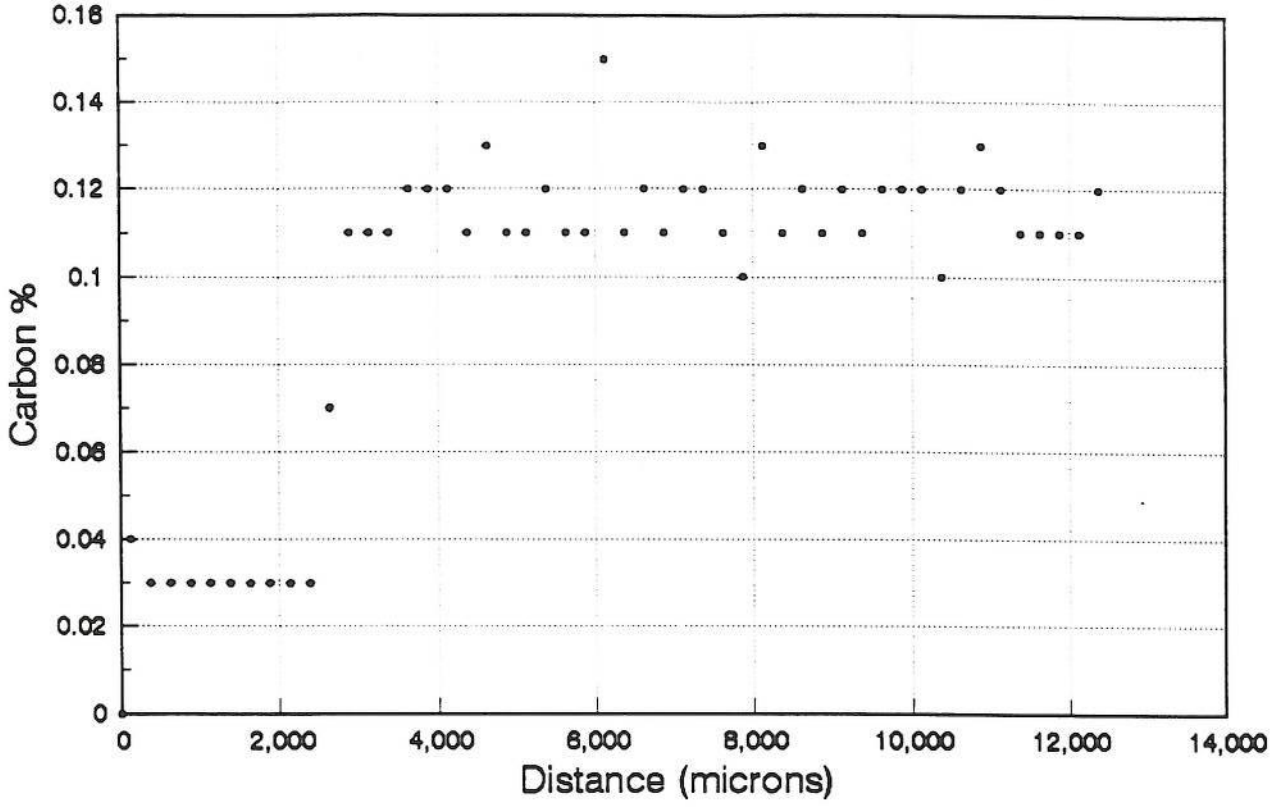
0.16
0.14
0.12
0.1
0.08
0.06
0.04
0.02
0
Carbon %
0
2,000
4,000
6,000
8,000
10,000
12,000
14,000
Distance (microns)

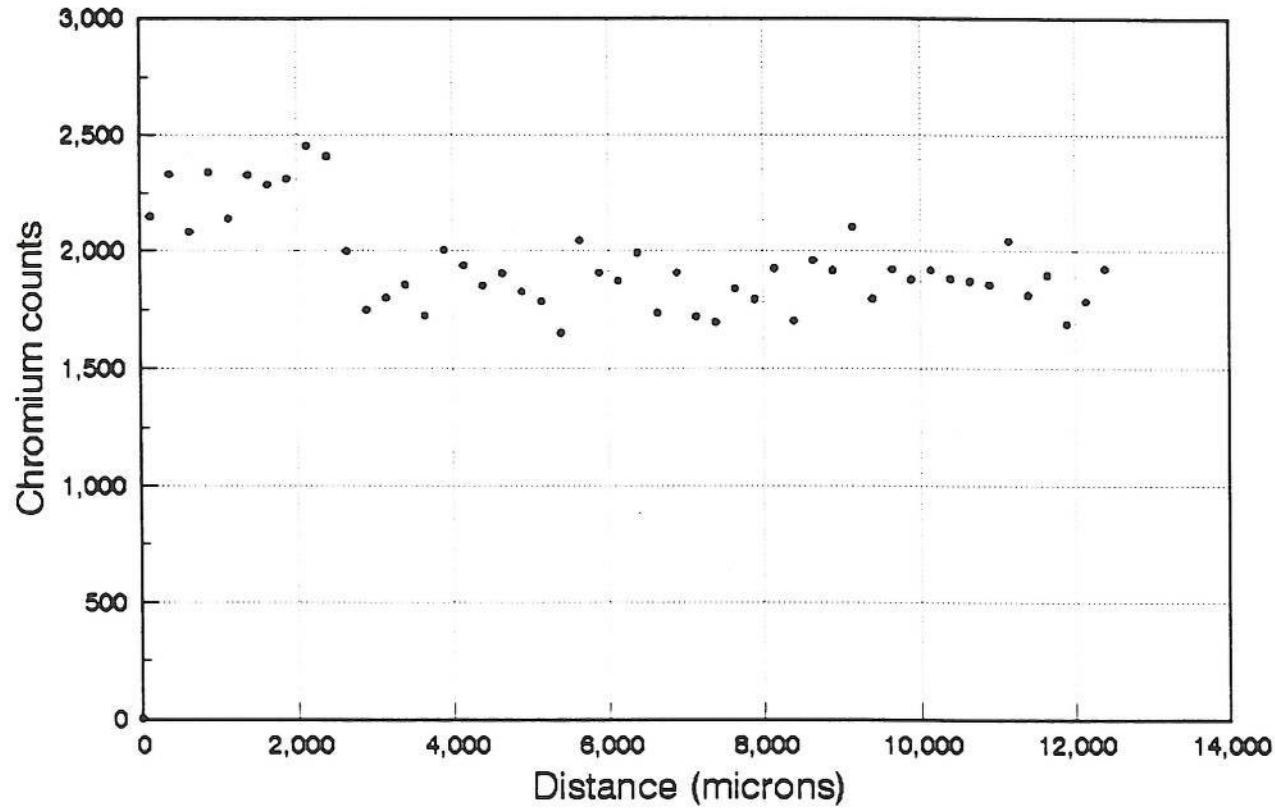
3,000
2,500
2,000
1,500
1,000
500
0
Chromium counts
0
2,000
4,000
6,000
8,000
10,000
12,000
14,000
Distance (microns)

CMV.C.AW

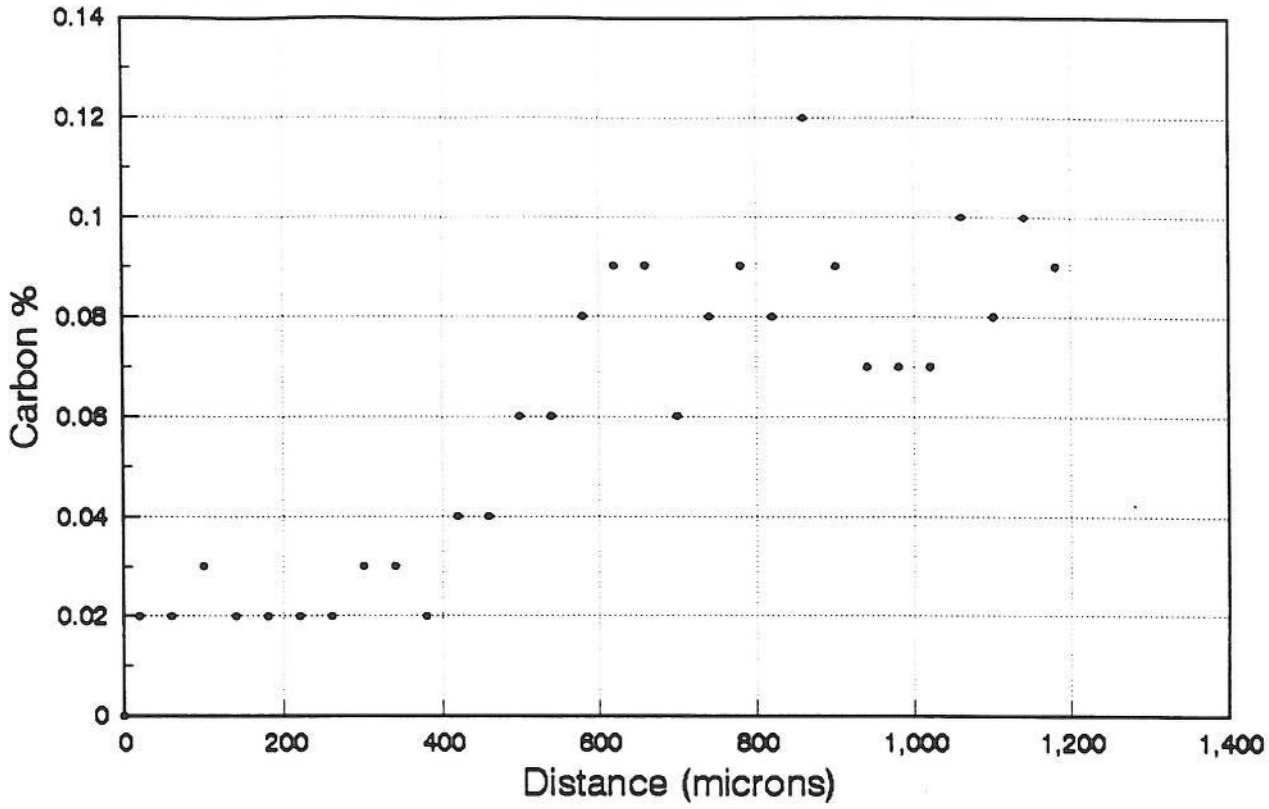
0.14
0.12
0.1
0.08
0.06
0.04
0.02
0
Carbon %
0
200
400
600
800
1,000
1,200
1,400
Distance (microns)

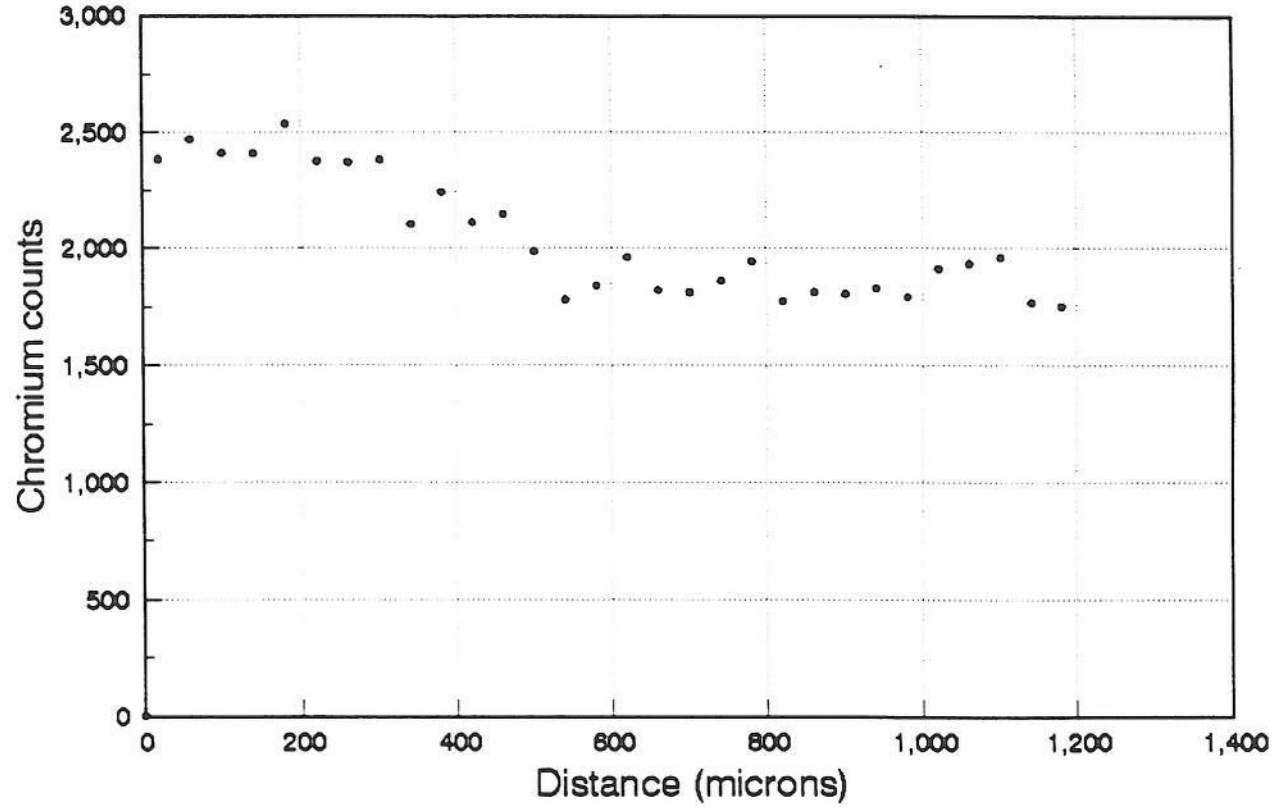
3,000
2,500
2,000
1,500
1,000
500
0
Chromium counts
0
200
400
600
800
1,000
1,200
1,400
Distance (microns)

CMV.M.AW

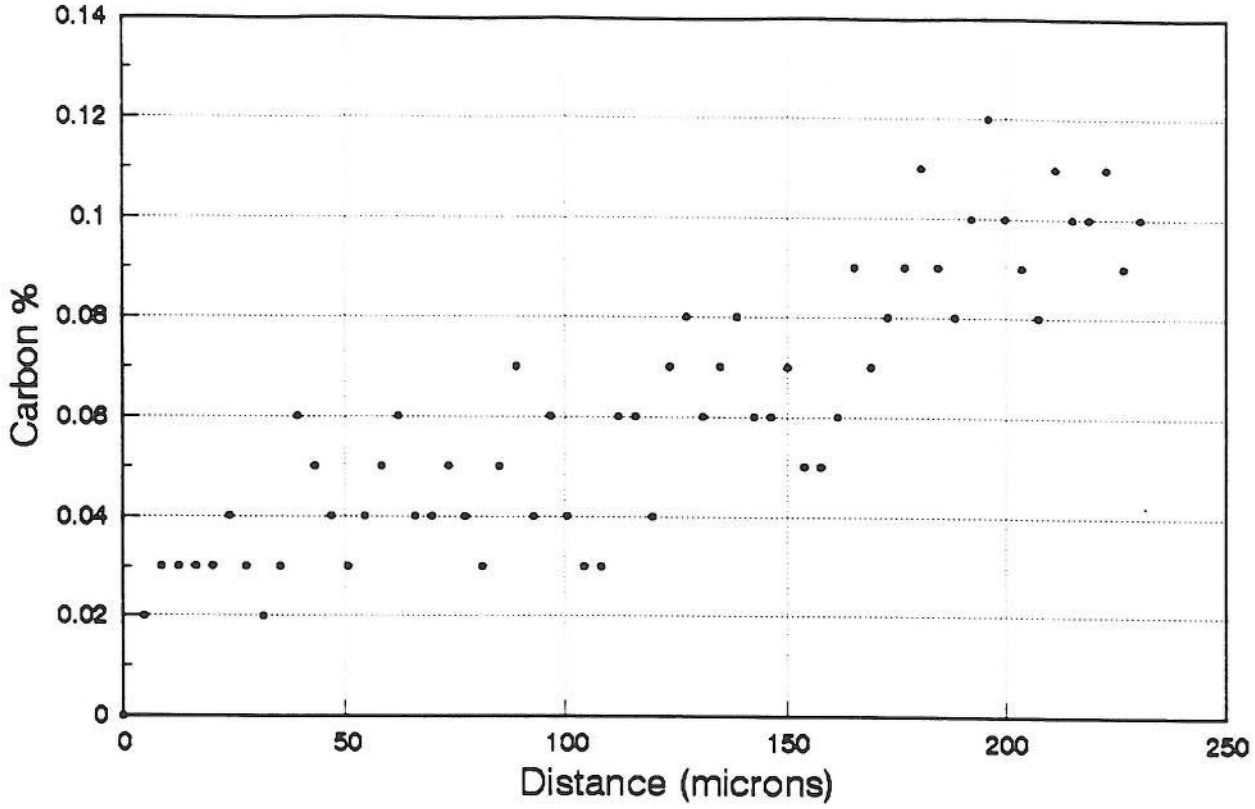
0.14
0.12
0.1
0.08
0.06
0.04
0.02
0
Carbon %
0
50
100
150
200
250
Distance (microns)

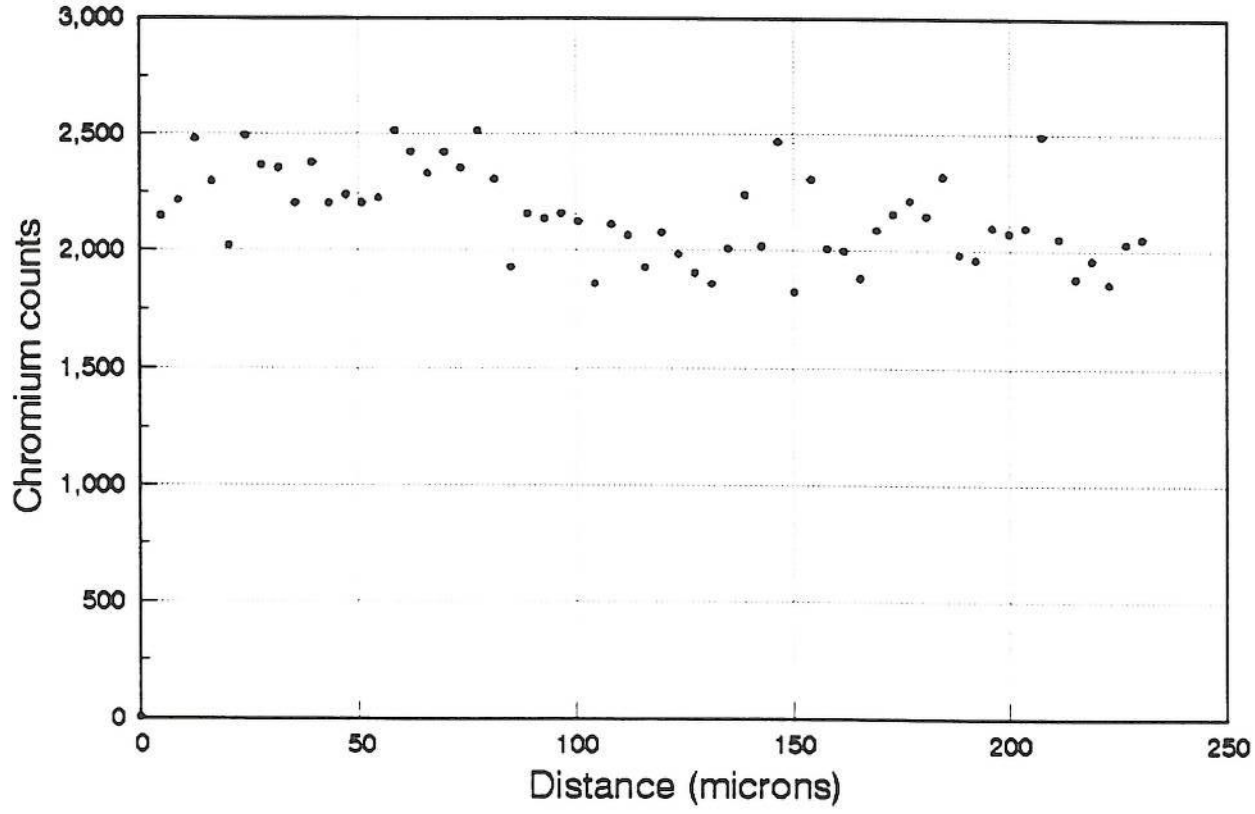
3,000
2,500
2,000
1,500
1,000
500
0
Chromium counts
0
50
100
150
200
250
Distance (microns)

CMV.F.AW

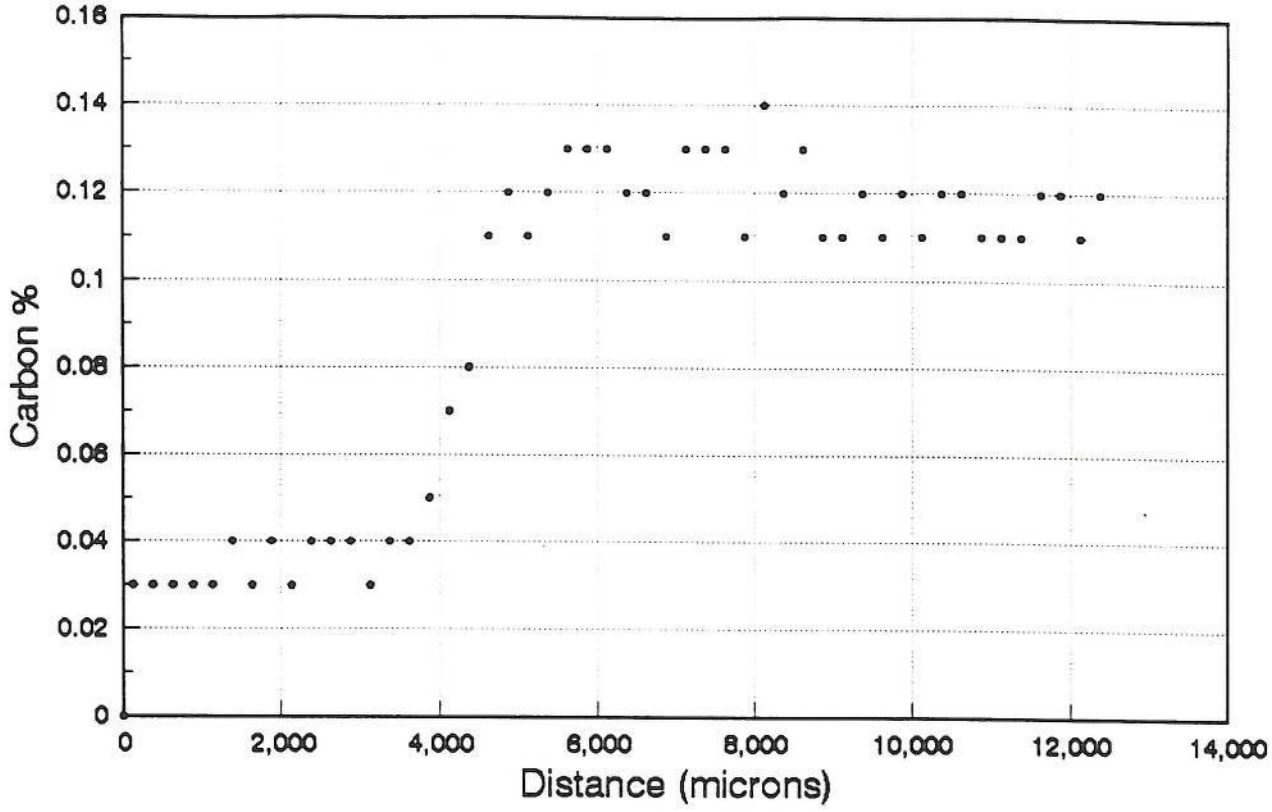
0.16
0.14
0.12
0.1
0.08
0.06
0.04
0.02
0
Carbon %
0
2,000
4,000
6,000
8,000
10,000
12,000
14,000
Distance (microns)

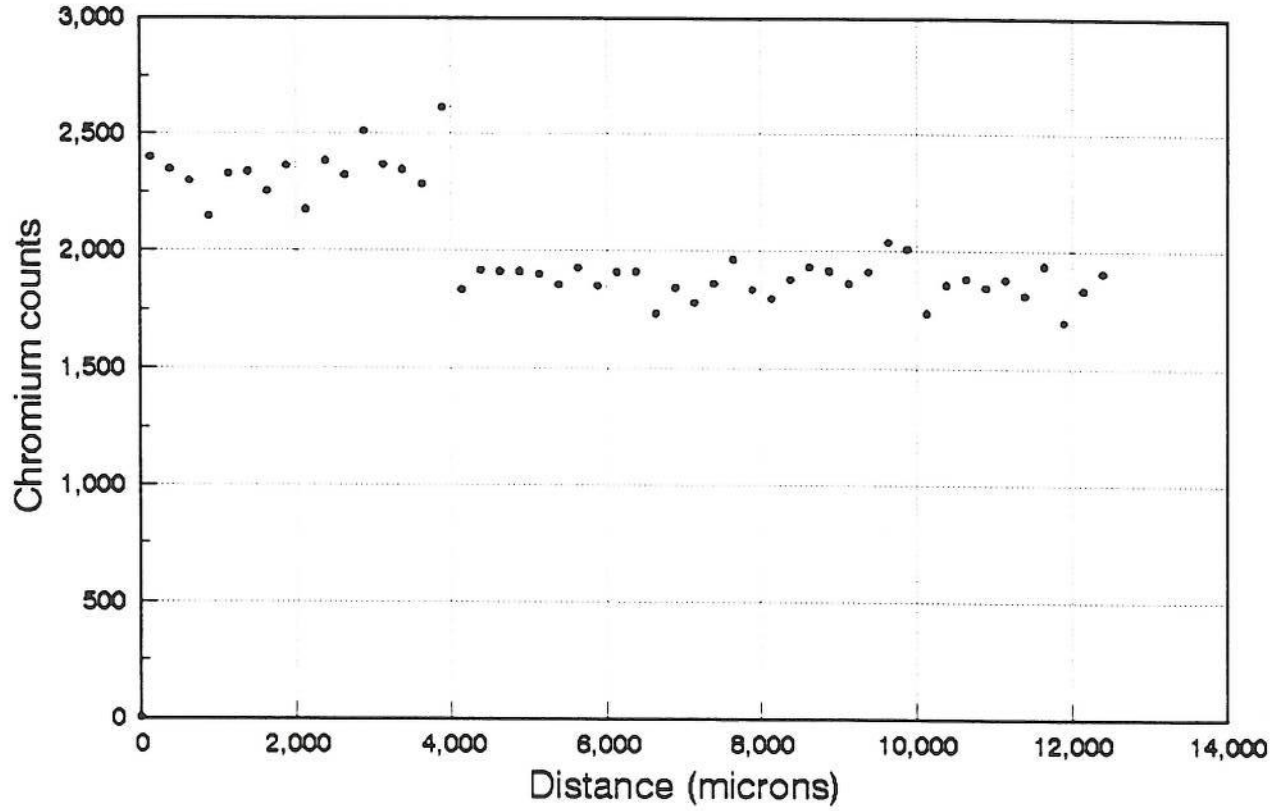
3,000
2,500
2,000
1,500
1,000
500
0
Chromium counts
0
2,000
4,000
6,000
8,000
10,000
12,000
14,000
Distance (microns)

CMV.C.PWHT

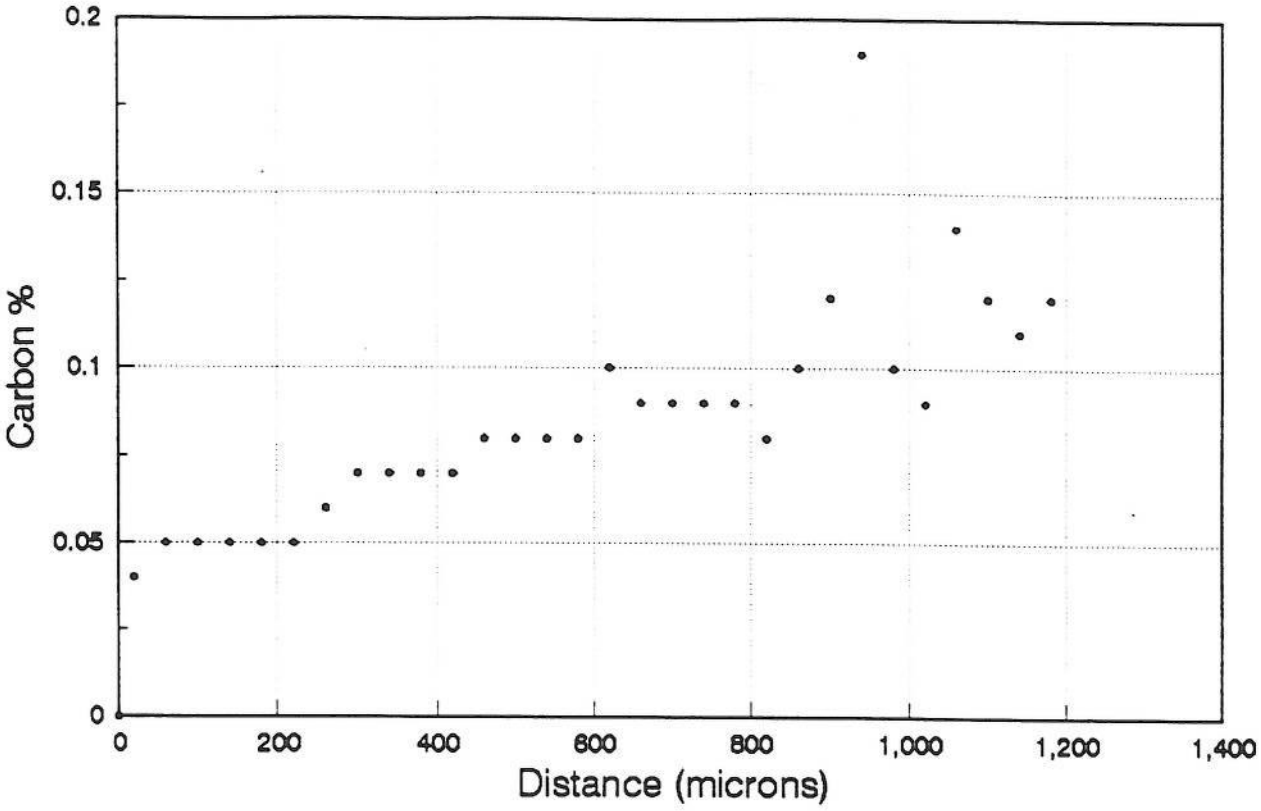
0.2
0.15
0.1
0.05
0
Carbon %
0
200
400
600
800
1,000
1,200
1,400
Distance (microns)

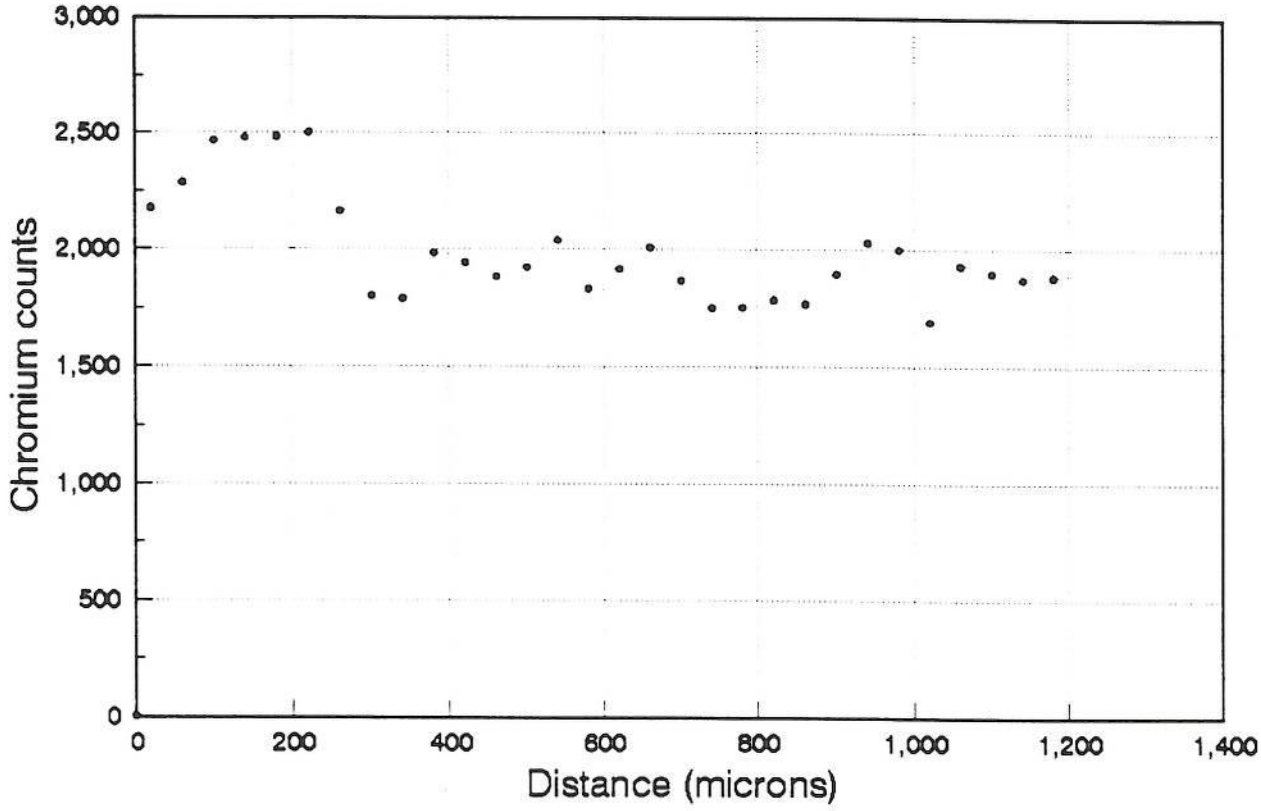
3,000
2,500
2,000
1,500
1,000
500
0
Chromium counts
0
200
400
600
800
1,000
1,200
1,400
Distance (microns)

CMV.M.PWHT

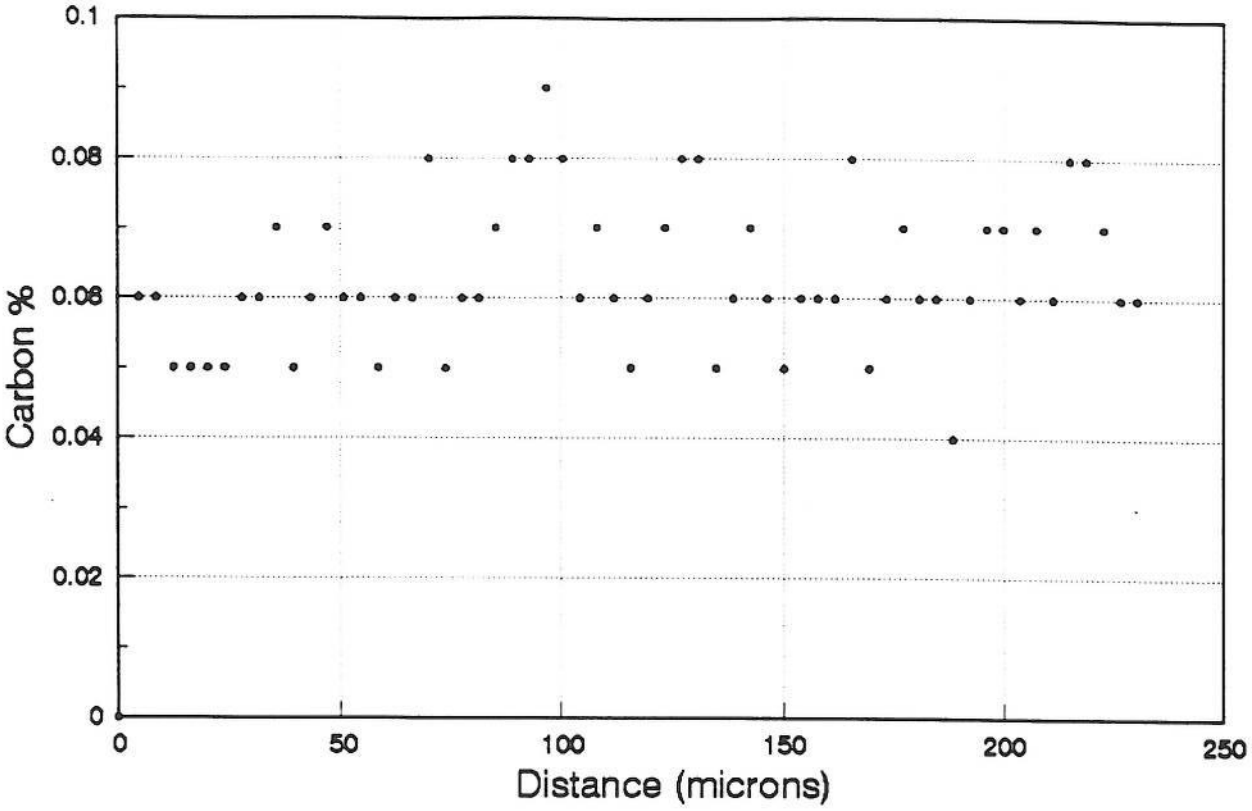
0.1
0.08
0.06
0.04
0.02
0
Carbon %
0
50
100
150
200
250
Distance (microns)

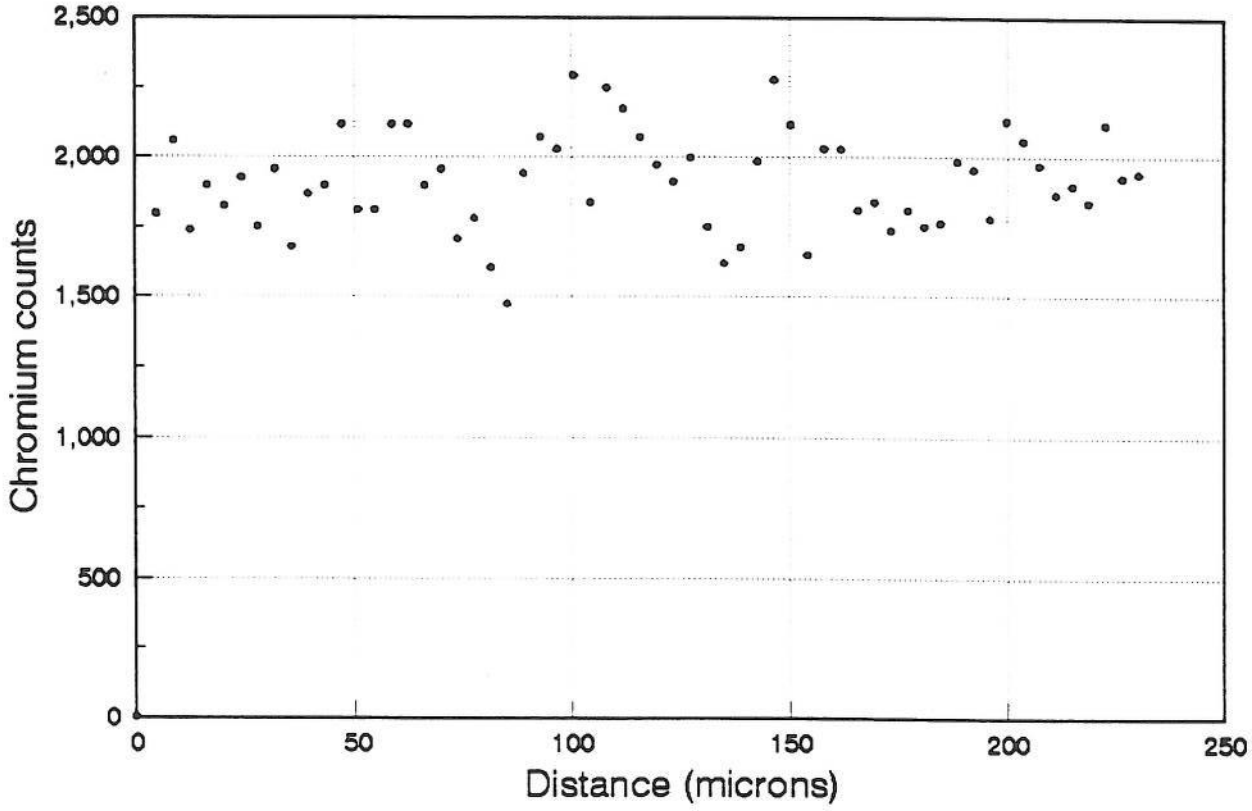
2,500
2,000
1,500
1,000
500
0
Chromium counts
0
50
100
150
200
250
Distance (microns)

CMV.F.PWHT

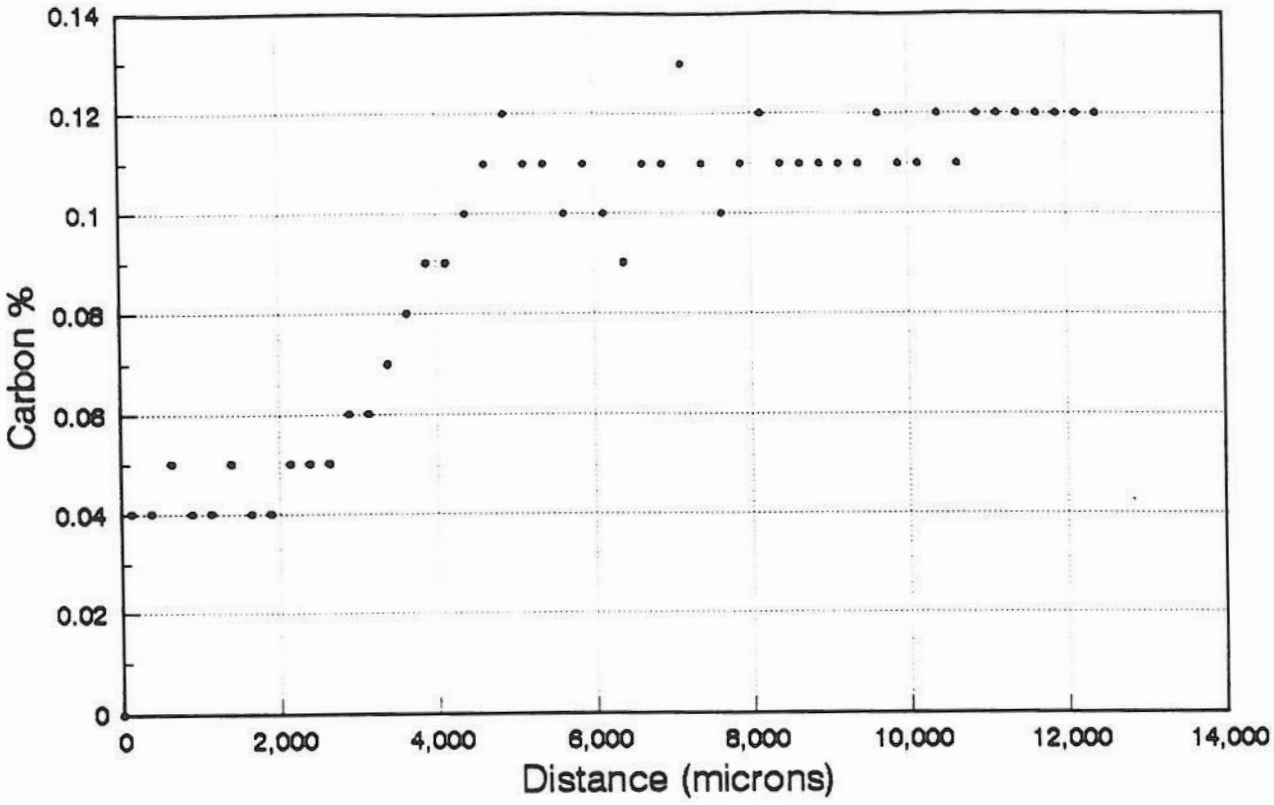
0.14
0.12
0.1
0.08
0.06
0.04
0.02
0
Carbon %
0
2,000
4,000
6,000
8,000
10,000
12,000
14,000
Distance (microns)

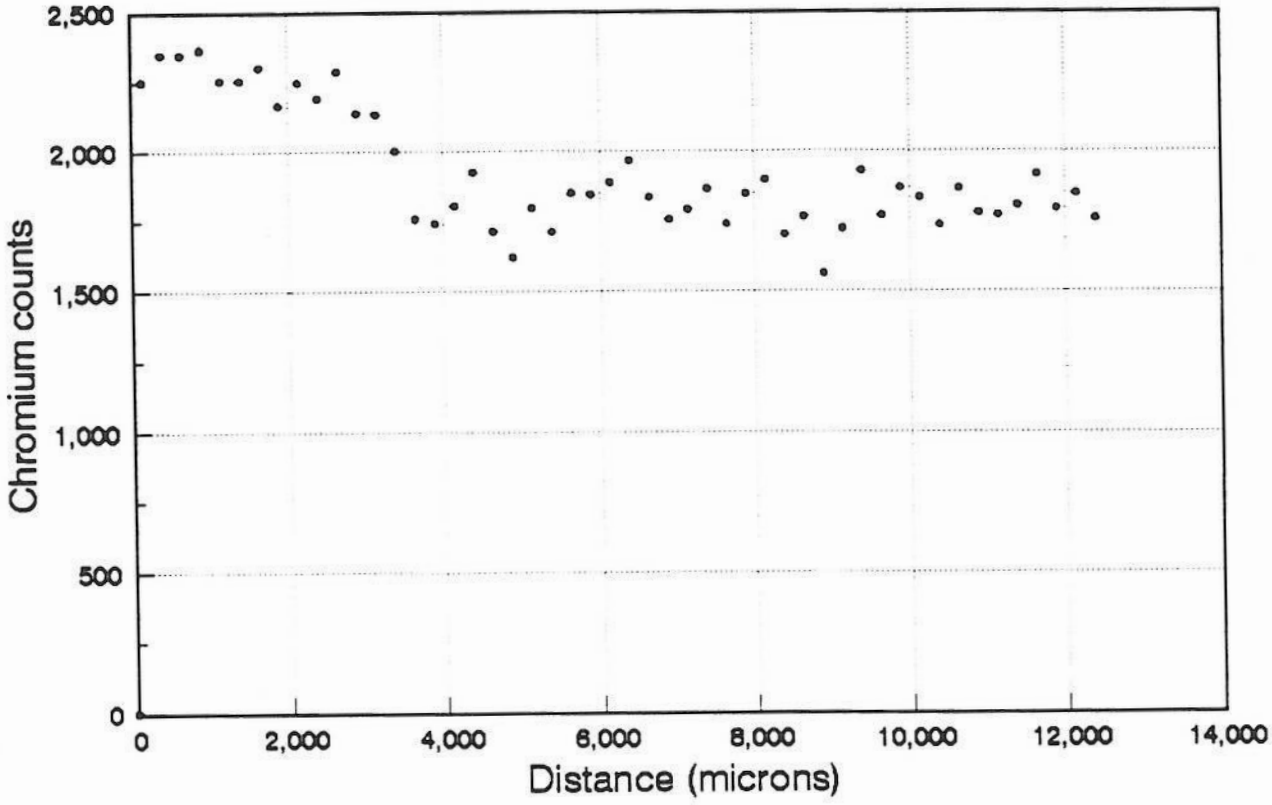
2,500
2,000
1,500
1,000
500
0
Chromium counts
0
2,000
4,000
6,000
8,000
10,000
12,000
14,000
Distance (microns)

CMV.C.AGED

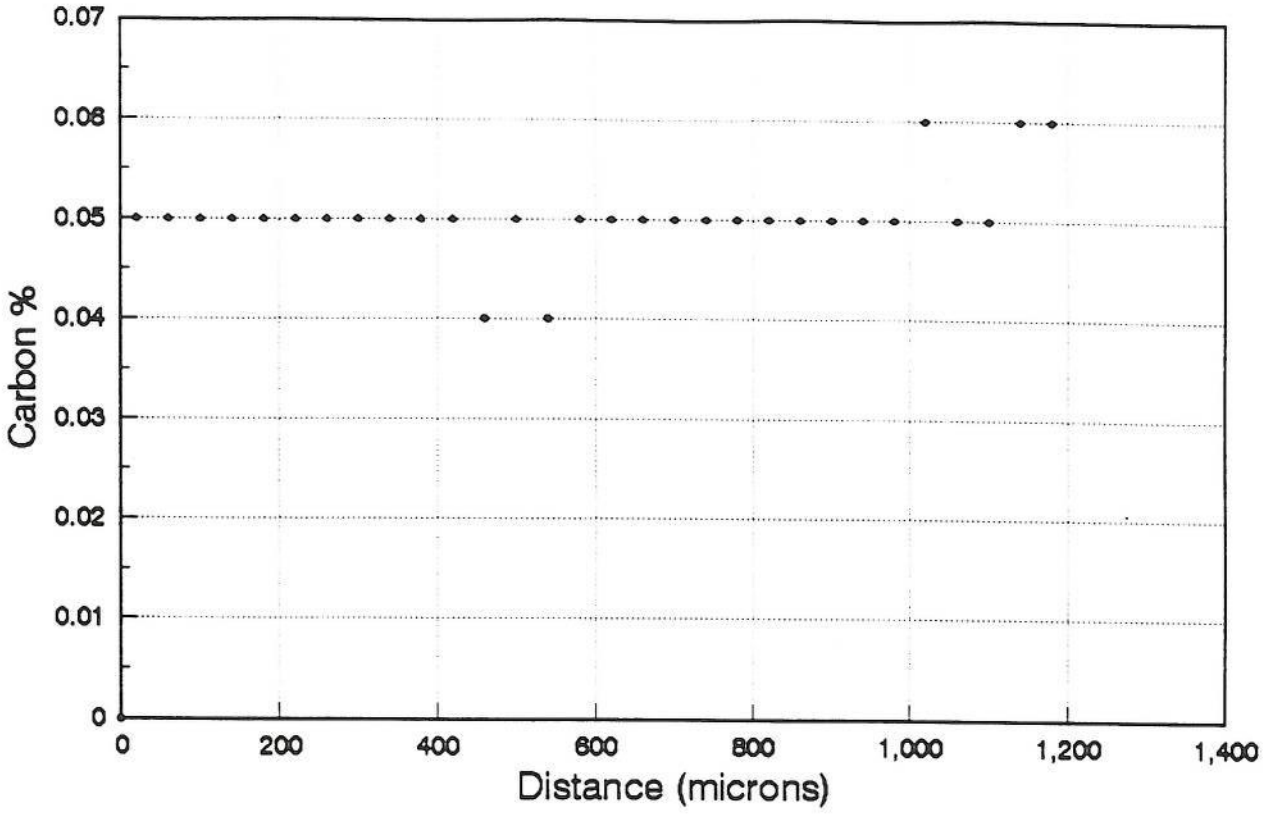
0.07
0.06
0.05
0.04
0.03
0.02
0.01
0
Carbon %
0
200
400
600
800
1,000
1,200
1,400
Distance (microns)

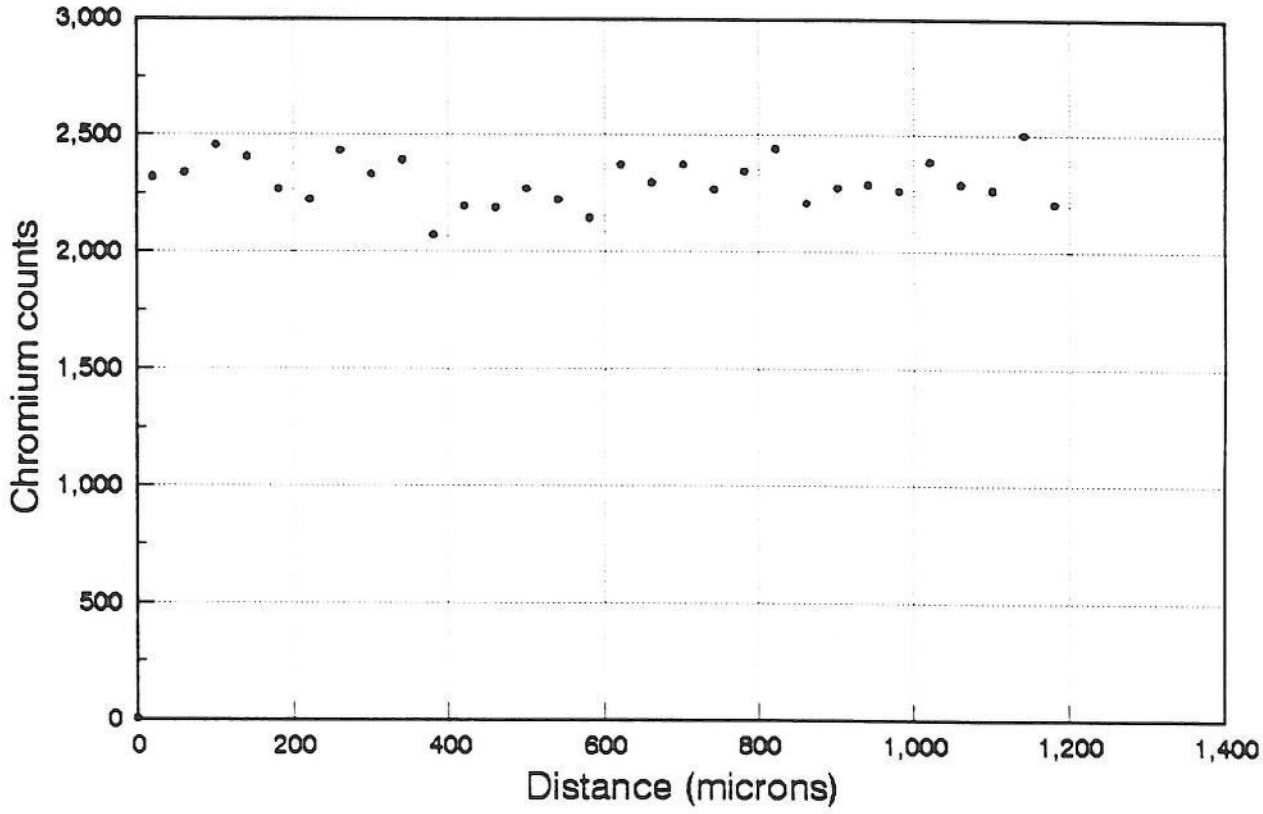
3,000
2,500
2,000
1,500
1,000
500
0
Chromium counts
0
200
400
600
800
1,000
1,200
1,400
Distance (microns)

CMV.M.AGED

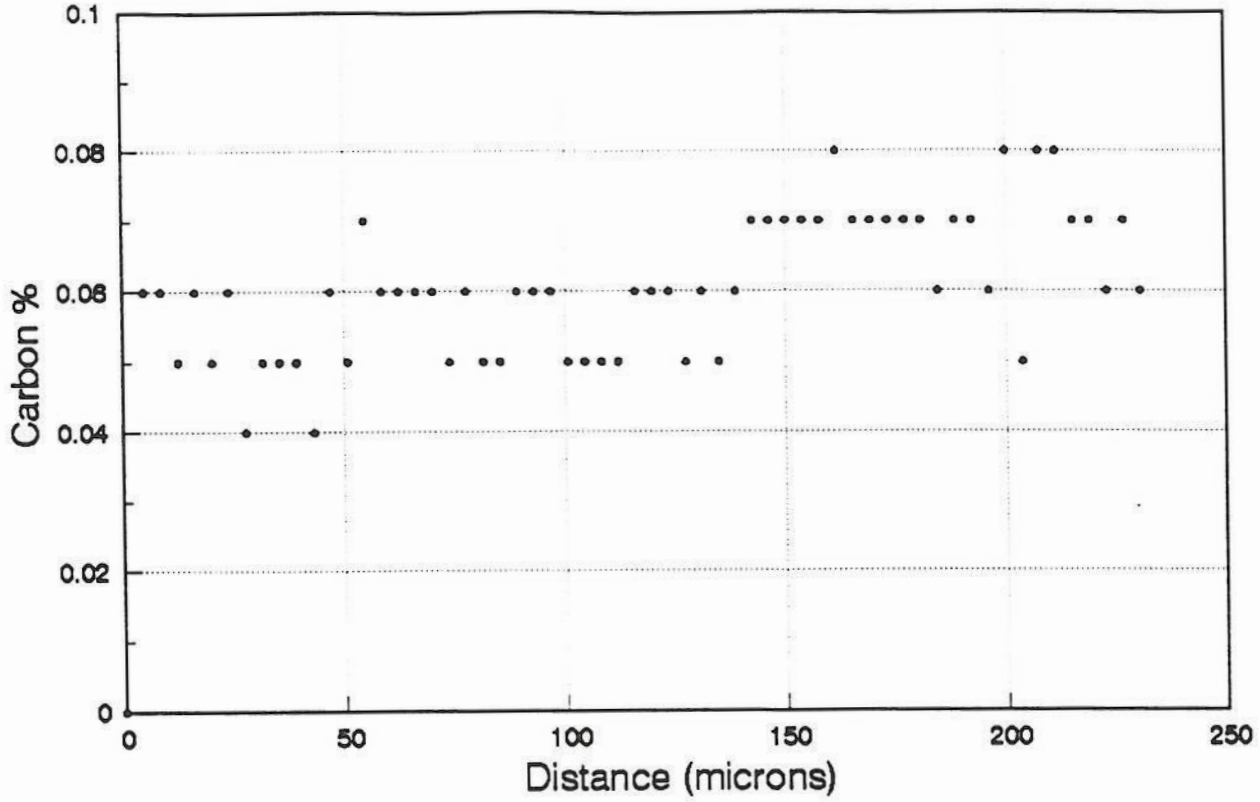
0.1
0.08
0.06
0.04
0.02
0
Carbon %
0
50
100
150
200
250
Distance (microns)

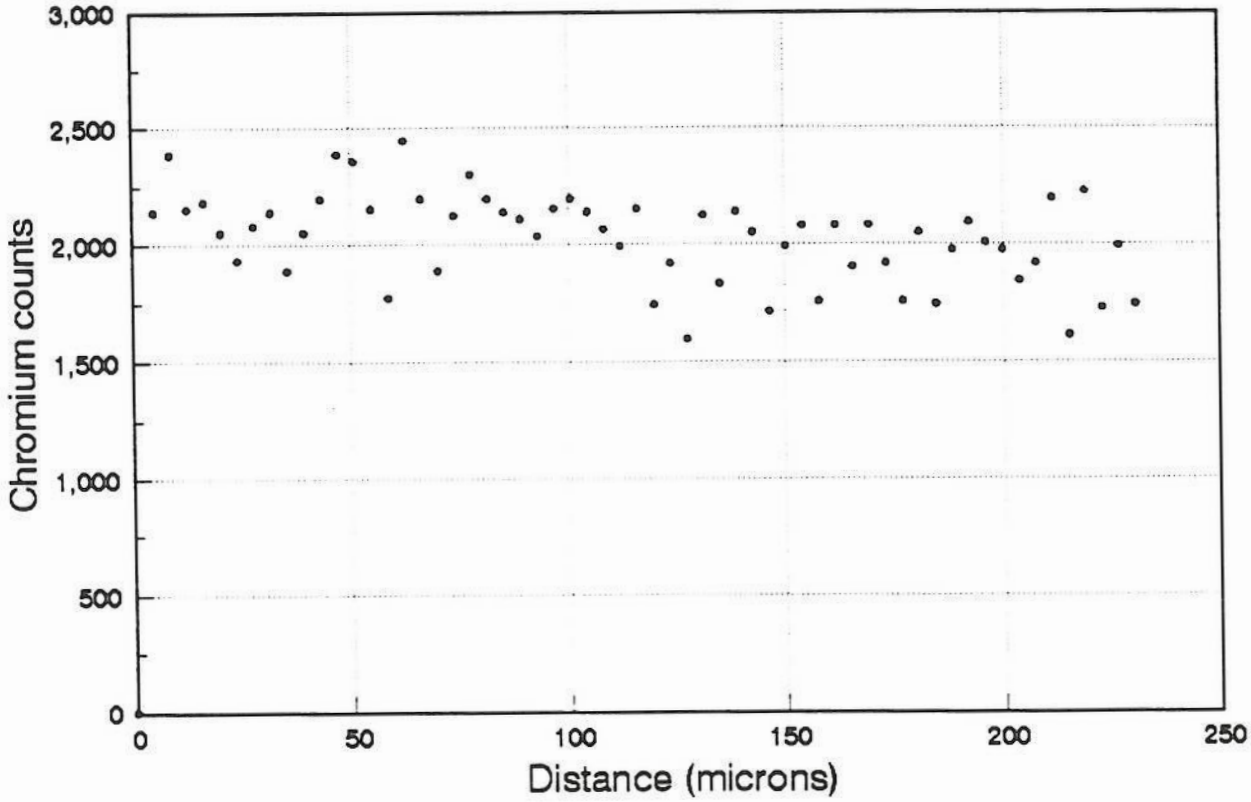
3,000
2,500
2,000
1,500
1,000
500
0
Chromium counts
0
50
100
150
200
250
Distance (microns)

CMV.F.AGED

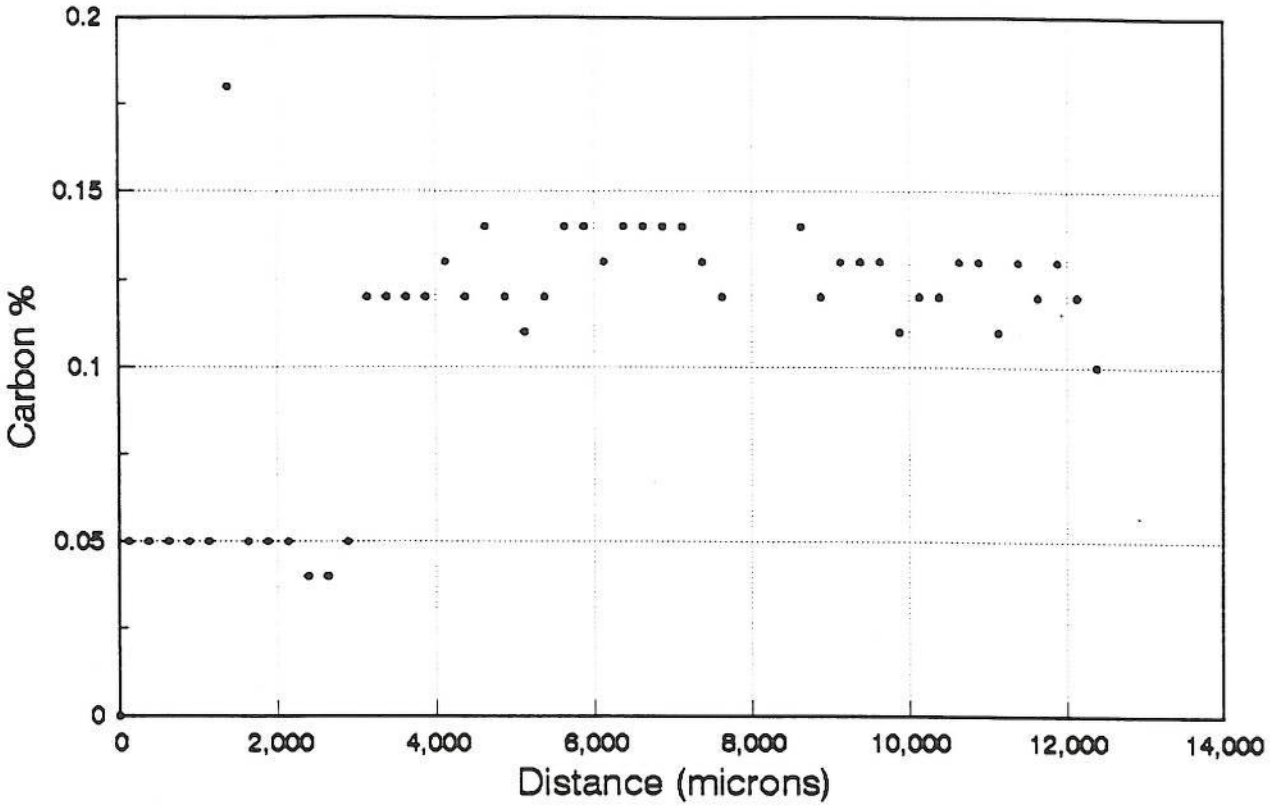
0.2
0.15
0.1
0.05
0
Carbon %
0
2,000
4,000
6,000
8,000
10,000
12,000
14,000
Distance (microns)

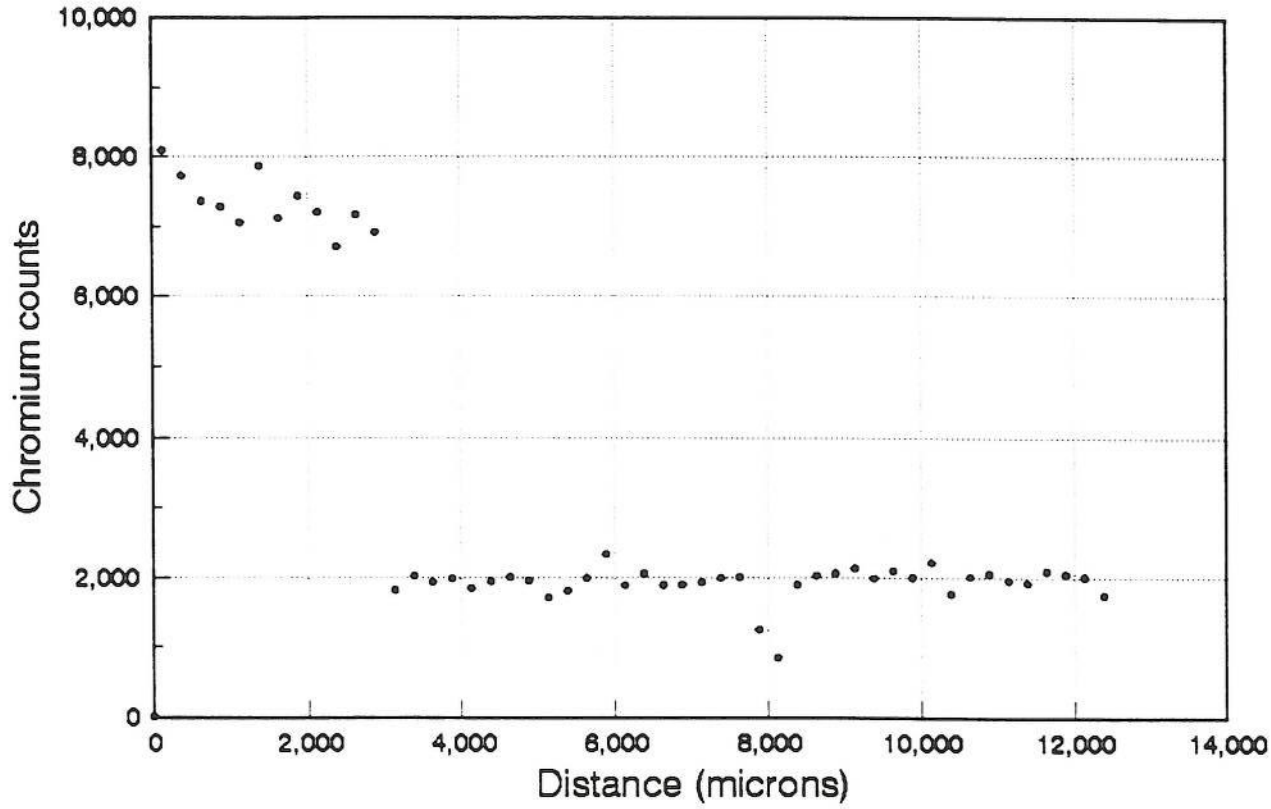
10,000
8,000
6,000
4,000
2,000
0
Chromium counts
0
2,000
4,000
6,000
8,000
10,000
12,000
14,000
Distance (microns)

2Cr.C.AW

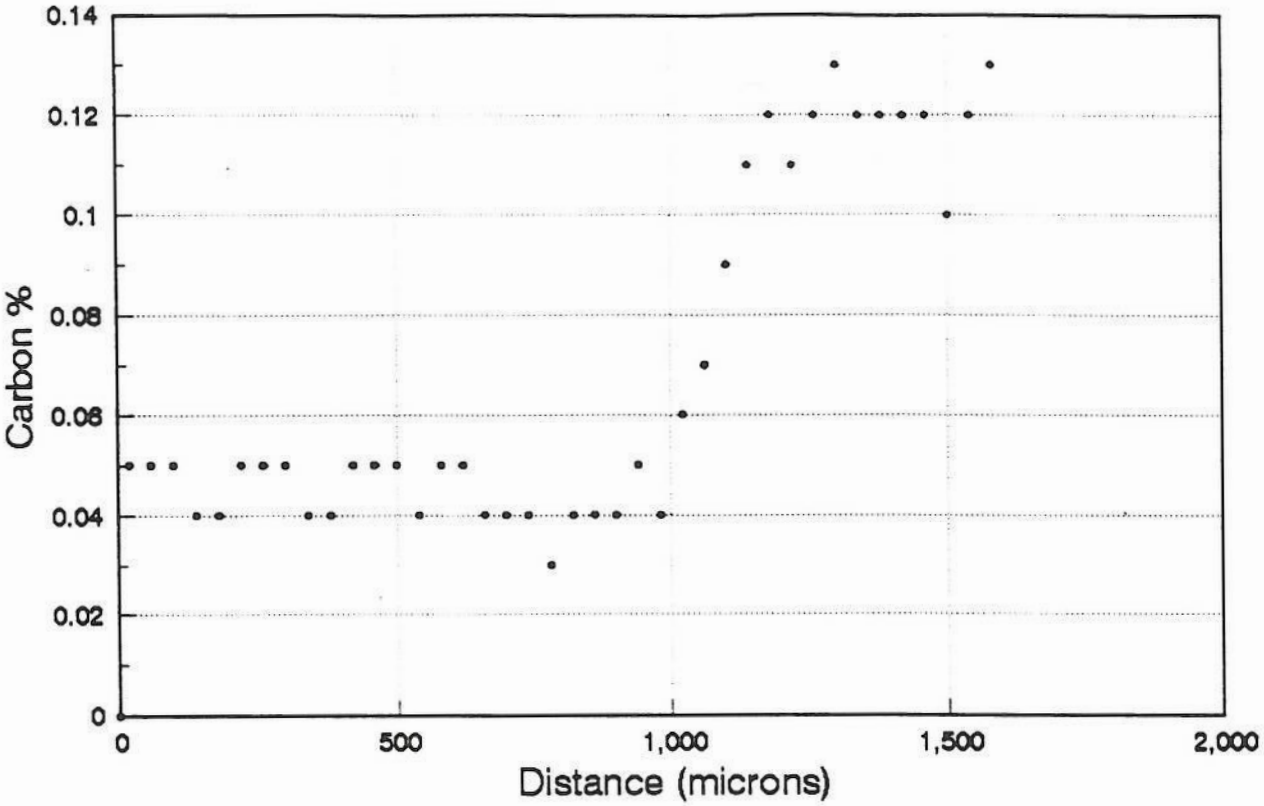
0.14
0.12
0.1
0.08
0.06
0.04
0.02
0
Carbon %
0
500
1,000
1,500
2,000
Distance (microns)

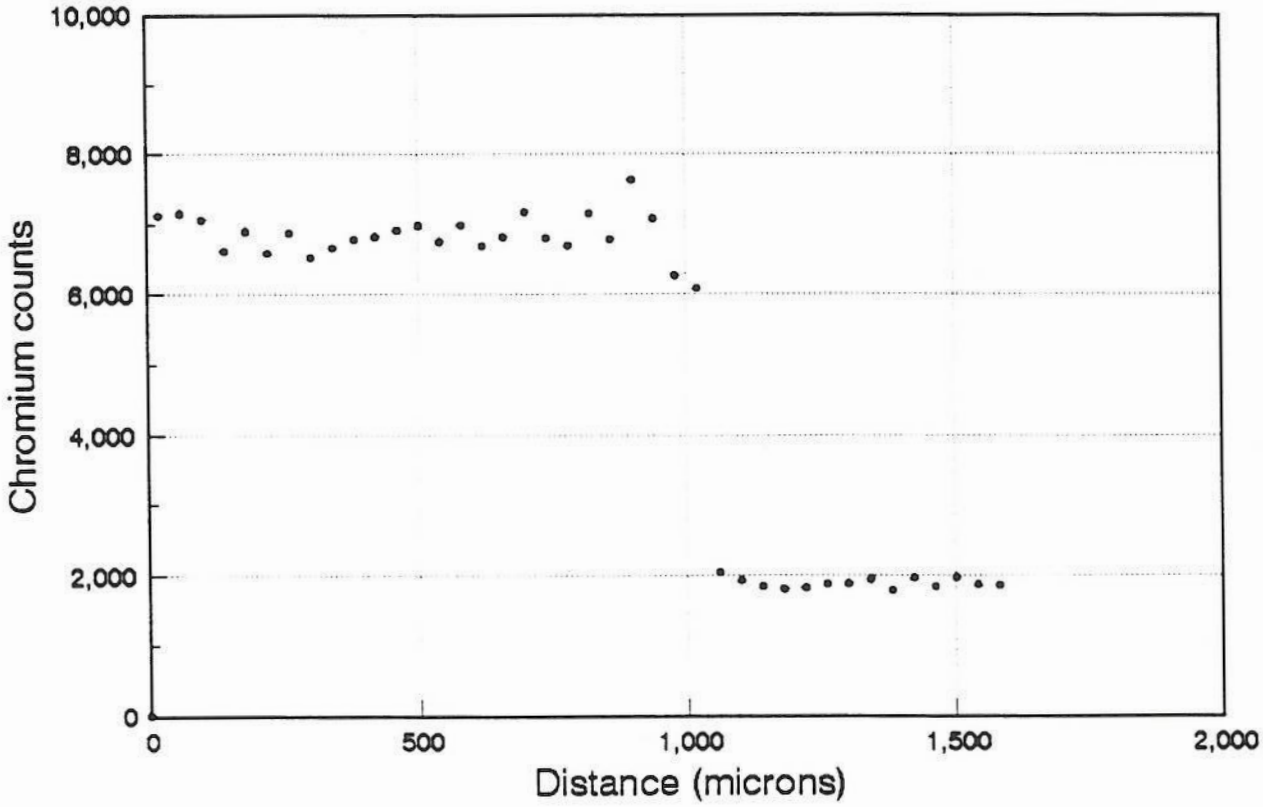
10,000
8,000
6,000
4,000
2,000
0
Chromium counts
0
500
1,000
1,500
2,000
Distance (microns)

2Cr.M.AW

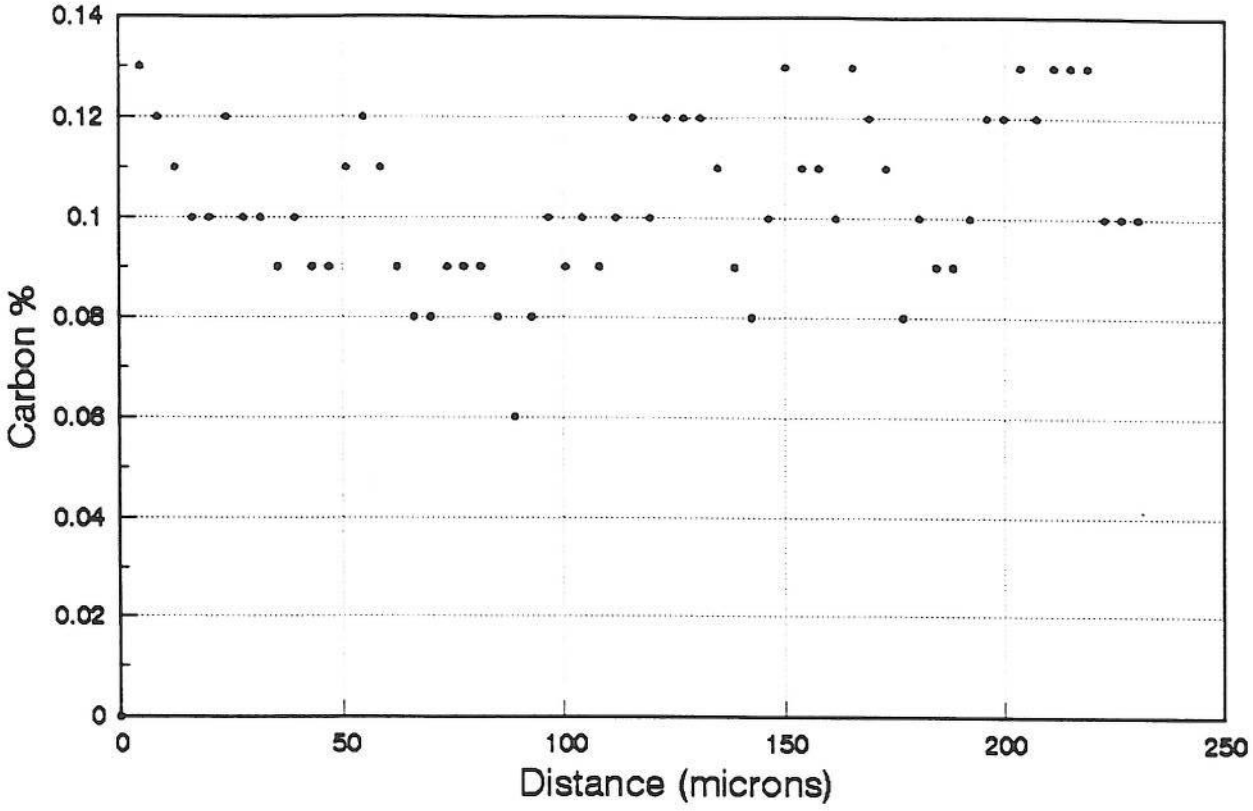
0.14
0.12
0.1
0.08
0.06
0.04
0.02
0
Carbon %
0
50
100
150
200
250
Distance (microns)

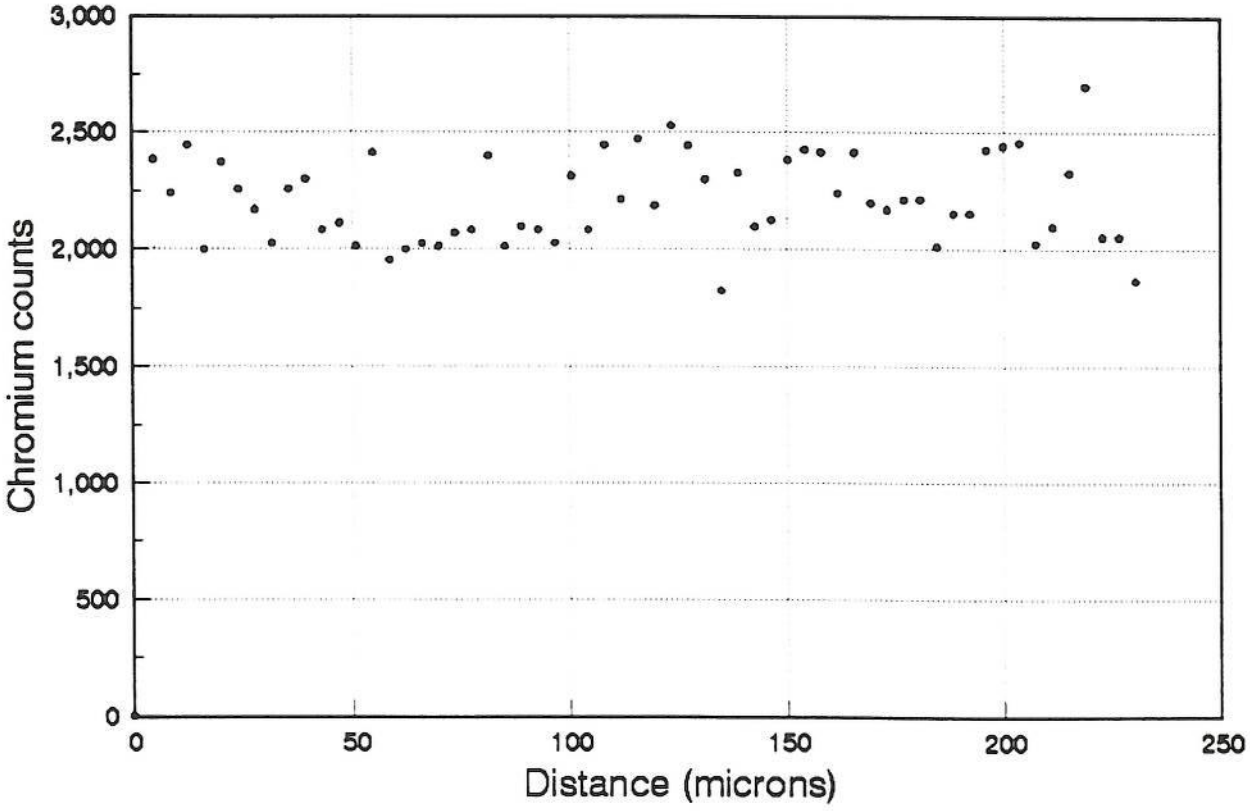
3,000
2,500
2,000
1,500
1,000
500
0
Chromium counts
0
50
100
150
200
250
Distance (microns)

2Cr.F.AW

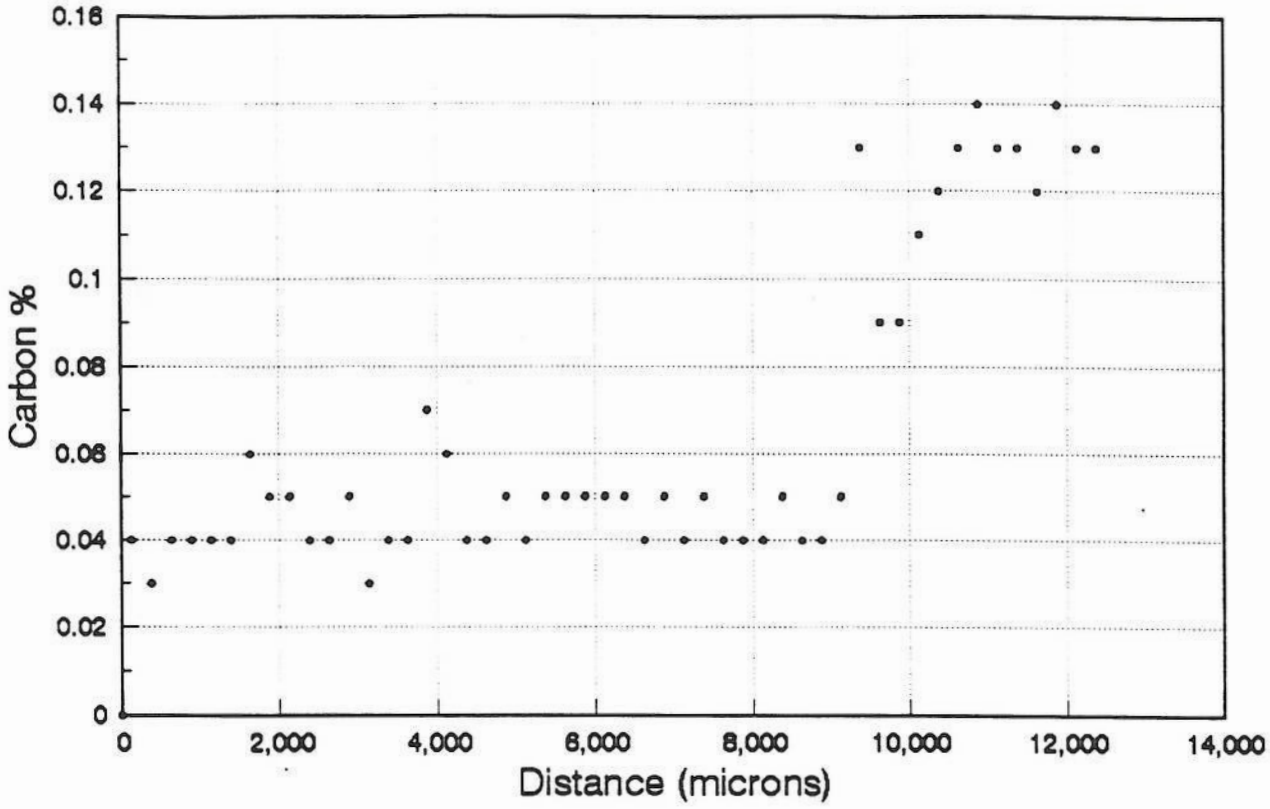
0.16
0.14
0.12
0.1
0.08
0.06
0.04
0.02
0
Carbon %
0
2,000
4,000
6,000
8,000
10,000
12,000
14,000
Distance (microns)

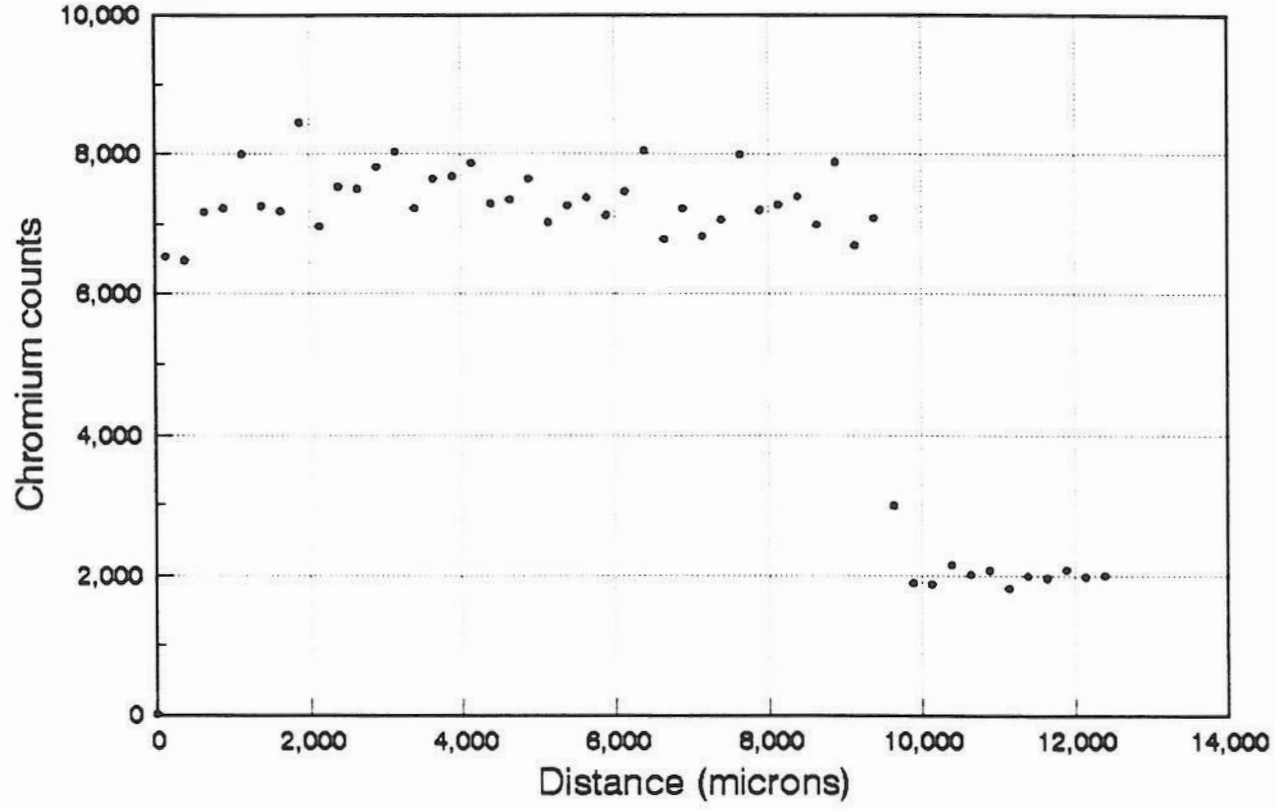
10,000
8,000
6,000
4,000
2,000
0
Chromium counts
0
2,000
4,000
6,000
8,000
10,000
12,000
14,000
Distance (microns)

2Cr.C.PWHT

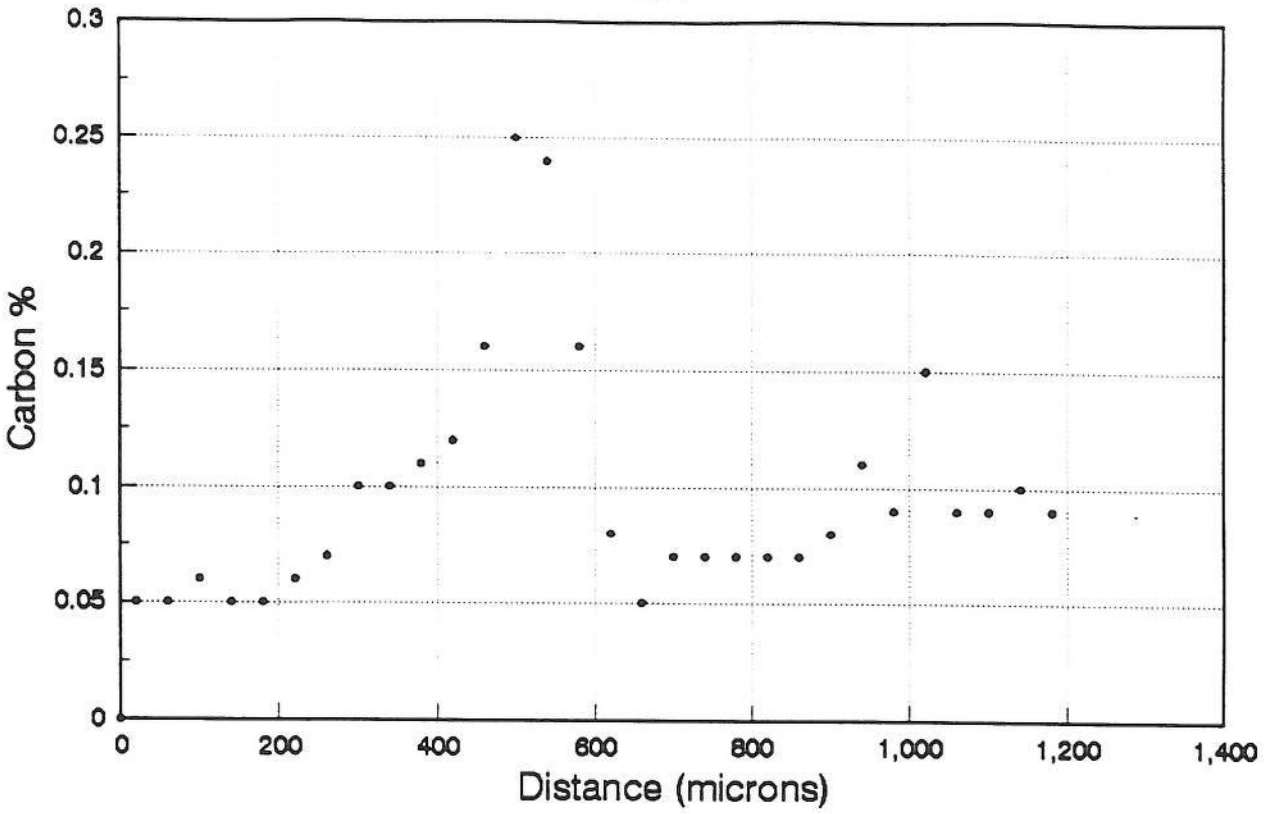
0.3
0.25
0.2
0.15
0.1
0.05
0
Carbon %
0
200
400
600
800
1,000
1,200
1,400
Distance (microns)

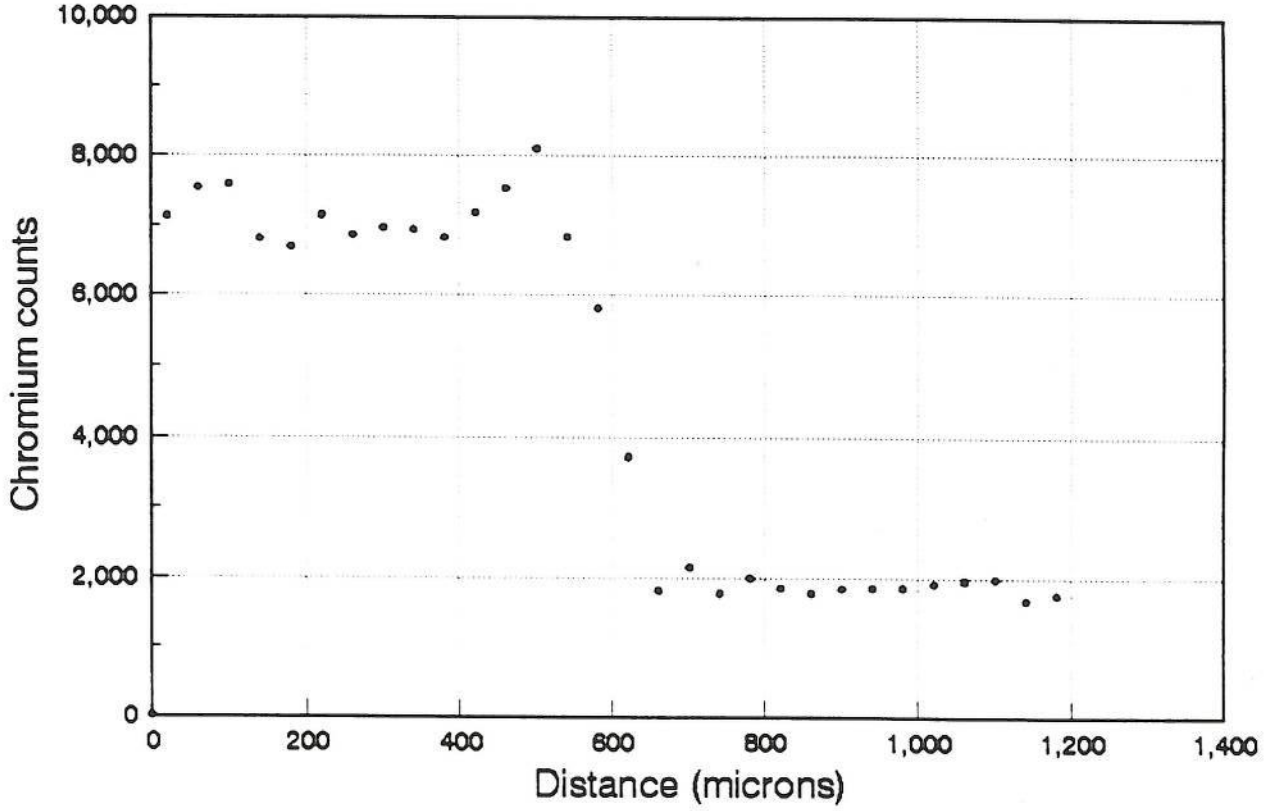
10,000
8,000
6,000
4,000
2,000
0
Chromium counts
0
200
400
600
800
1,000
1,200
1,400
Distance (microns)

2Cr.M.PWHT

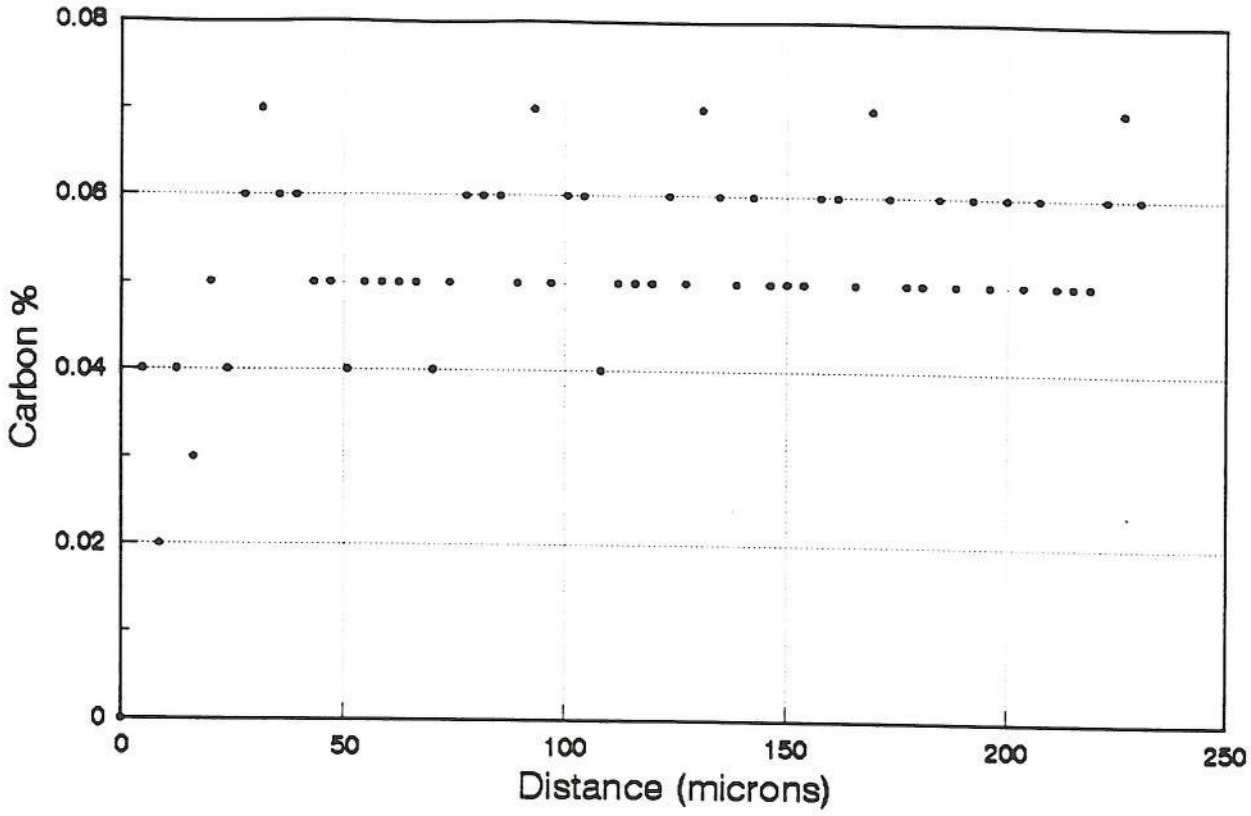
0.08
0.06
0.04
0.02
0
Carbon %
0
50
100
150
200
250
Distance (microns)

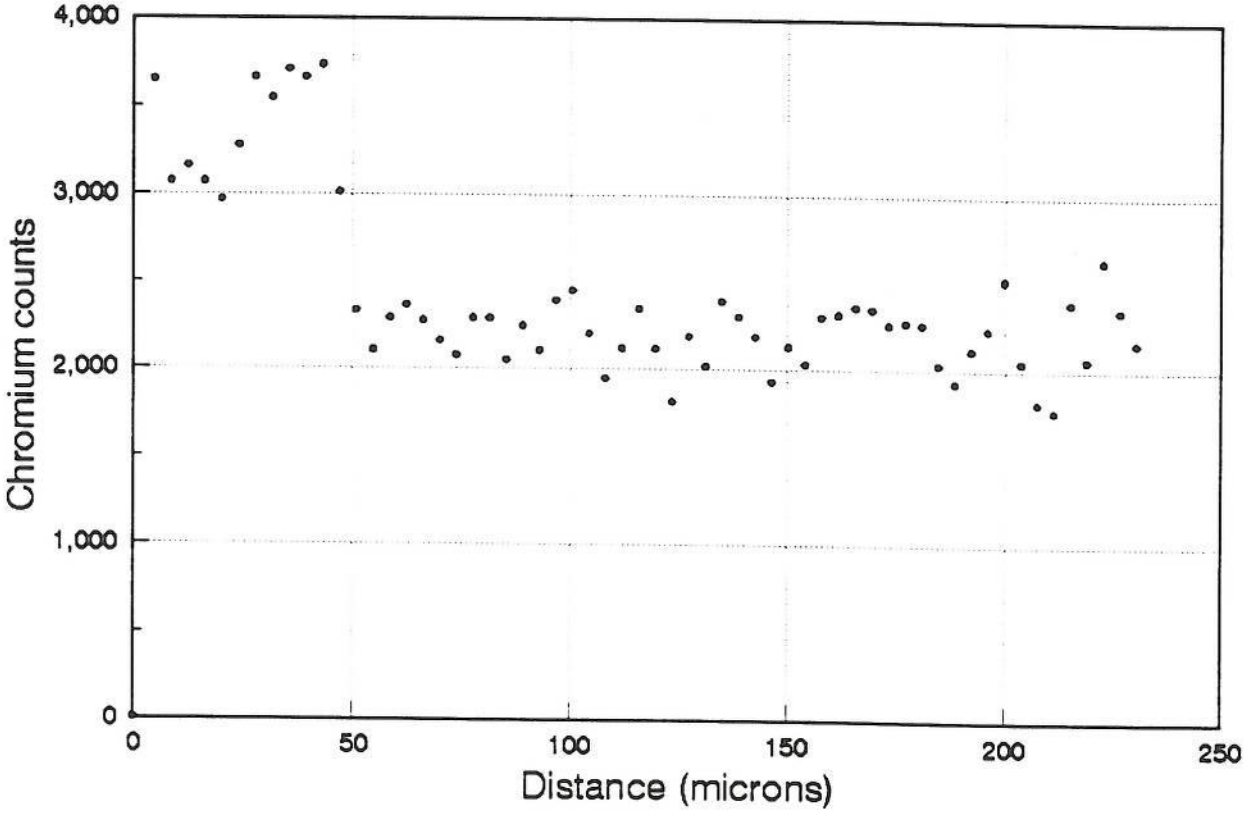
4,000
3,000
2,000
1,000
0
Chromium counts
0
50
100
150
200
250
Distance (microns)

2Cr.F.PWHT

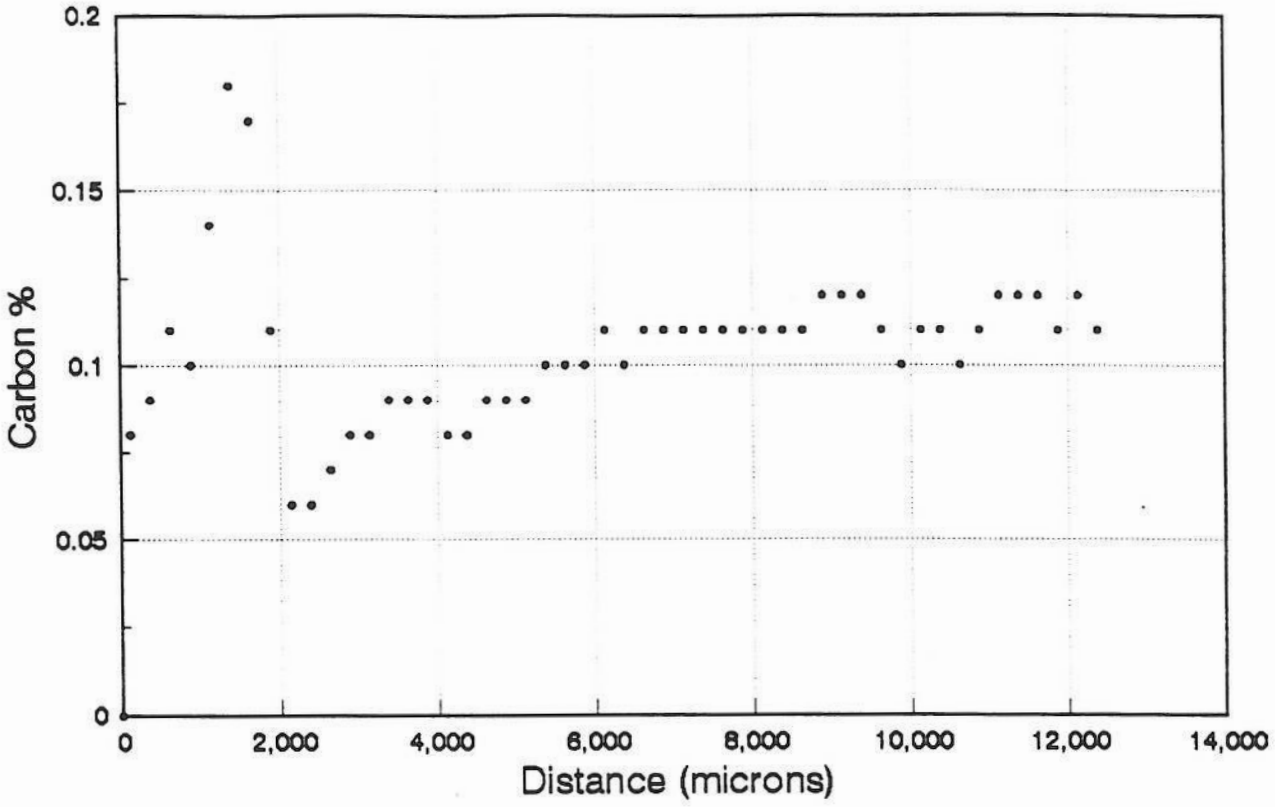
0.2
0.15
0.1
0.05
0
Carbon %
0
2,000
4,000
6,000
8,000
10,000
12,000
14,000
Distance (microns)

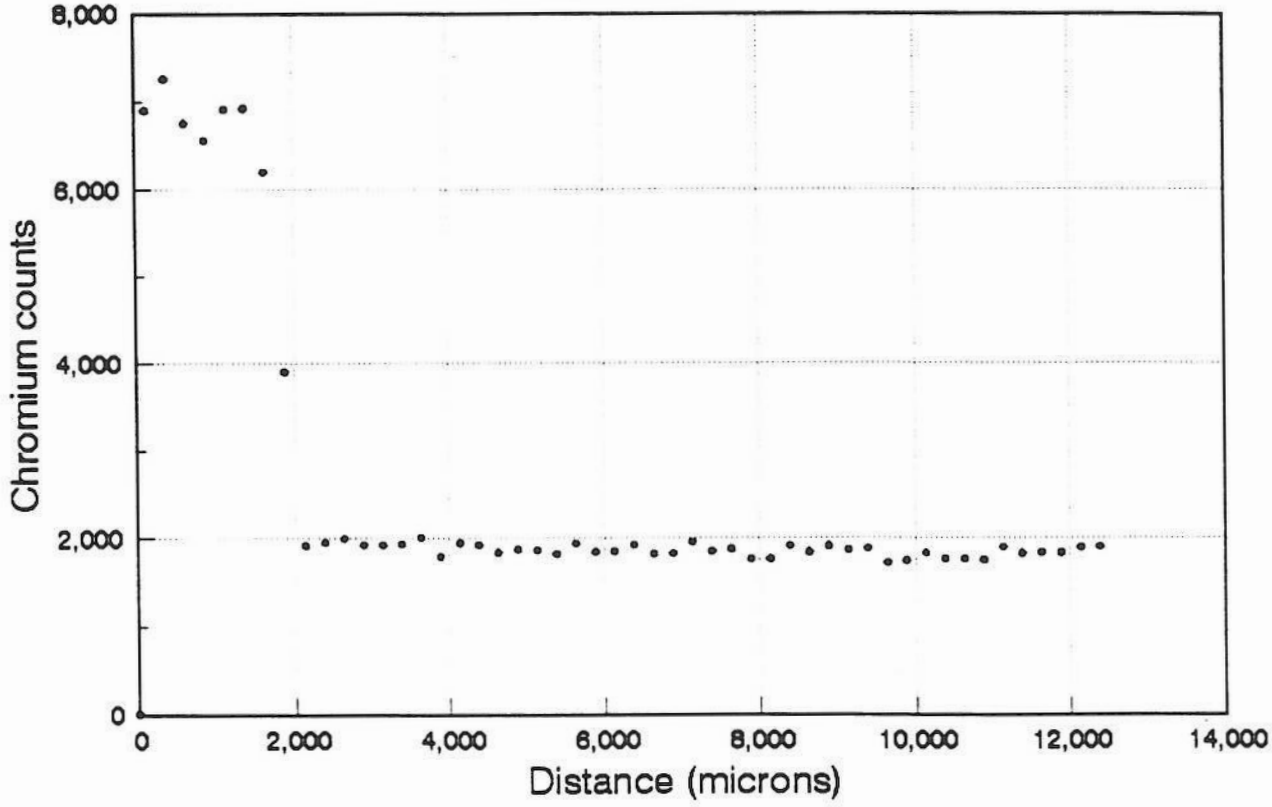
8,000
6,000
4,000
2,000
0
Chromium counts
0
2,000
4,000
6,000
8,000
10,000
12,000
14,000
Distance (microns)

2Cr.C.AGED

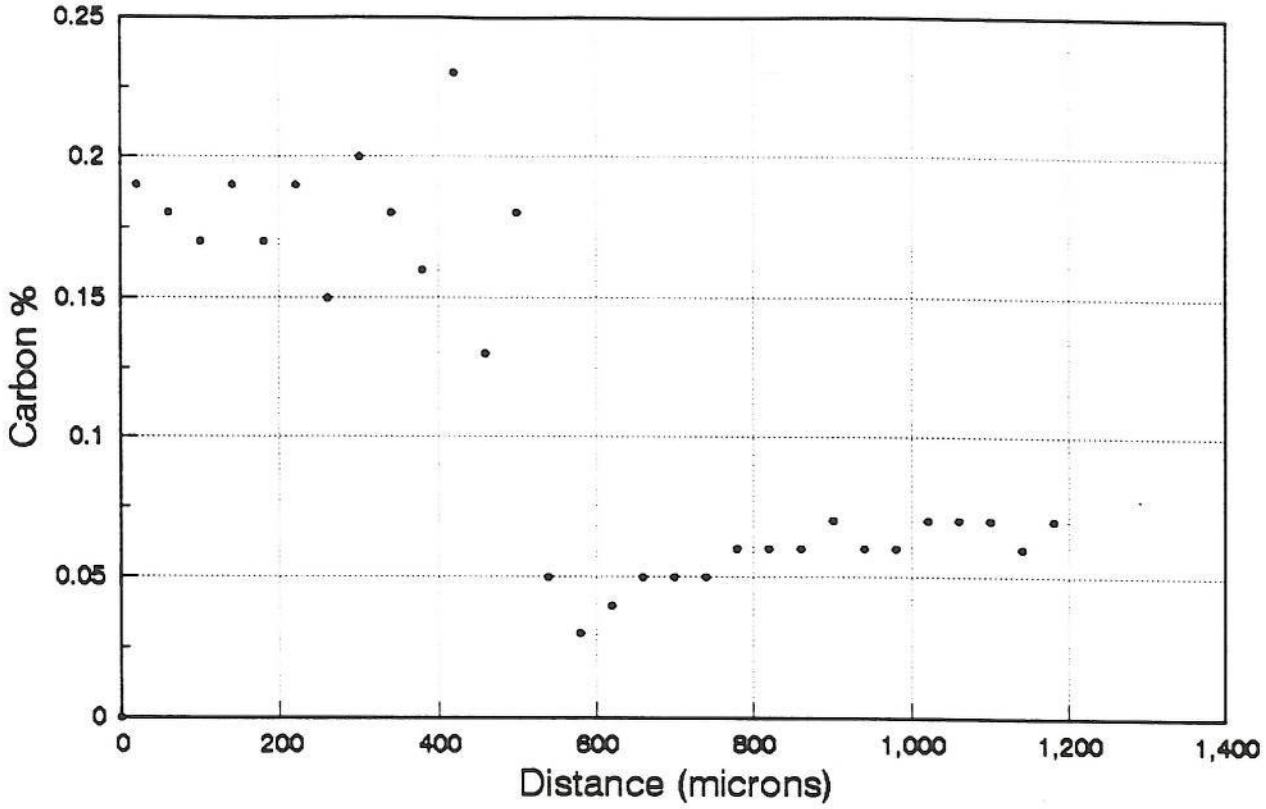
0.25
0.2
0.15
0.1
0.05
0
Carbon %
0
200
400
600
800
1,000
1,200
1,400
Distance (microns)

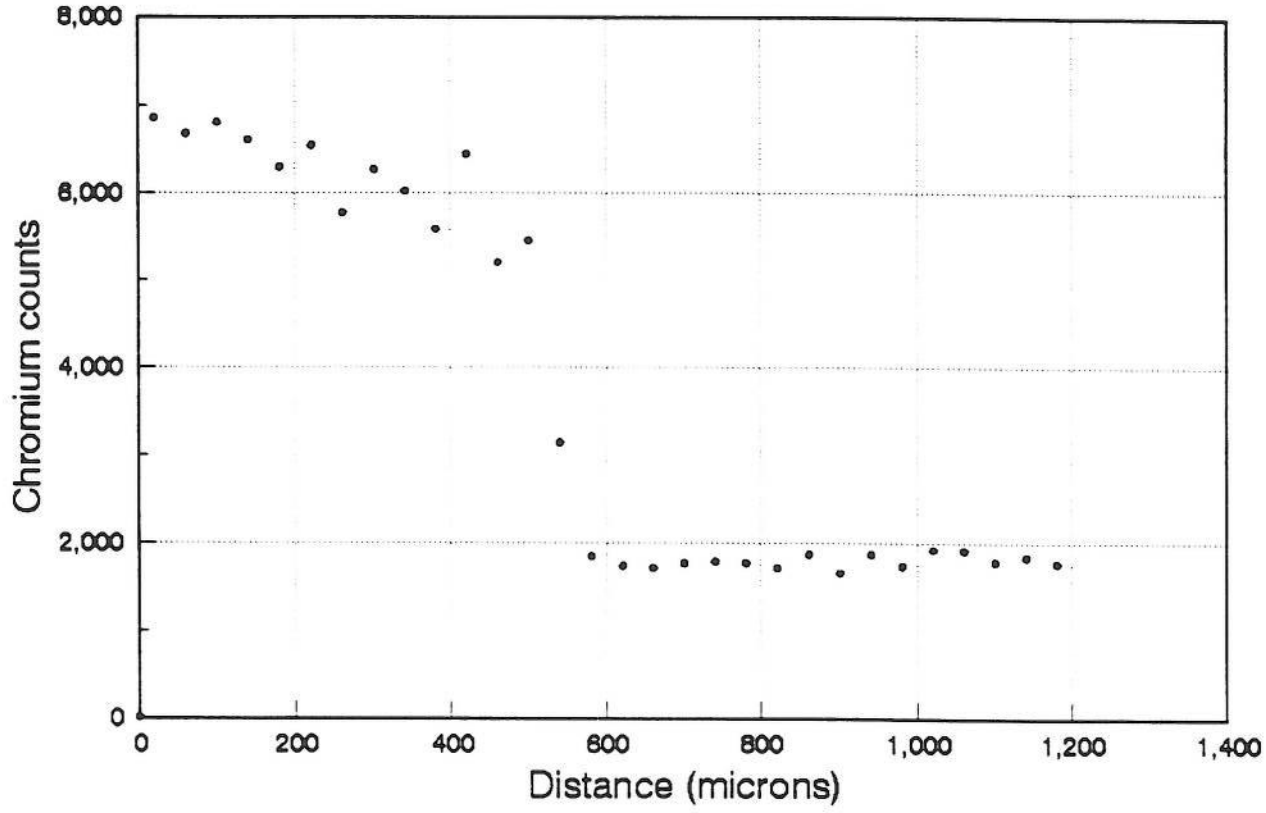
8,000
6,000
4,000
2,000
0
Chromium counts
0
200
400
600
800
1,000
1,200
1,400
Distance (microns)

2Cr.M.AGED

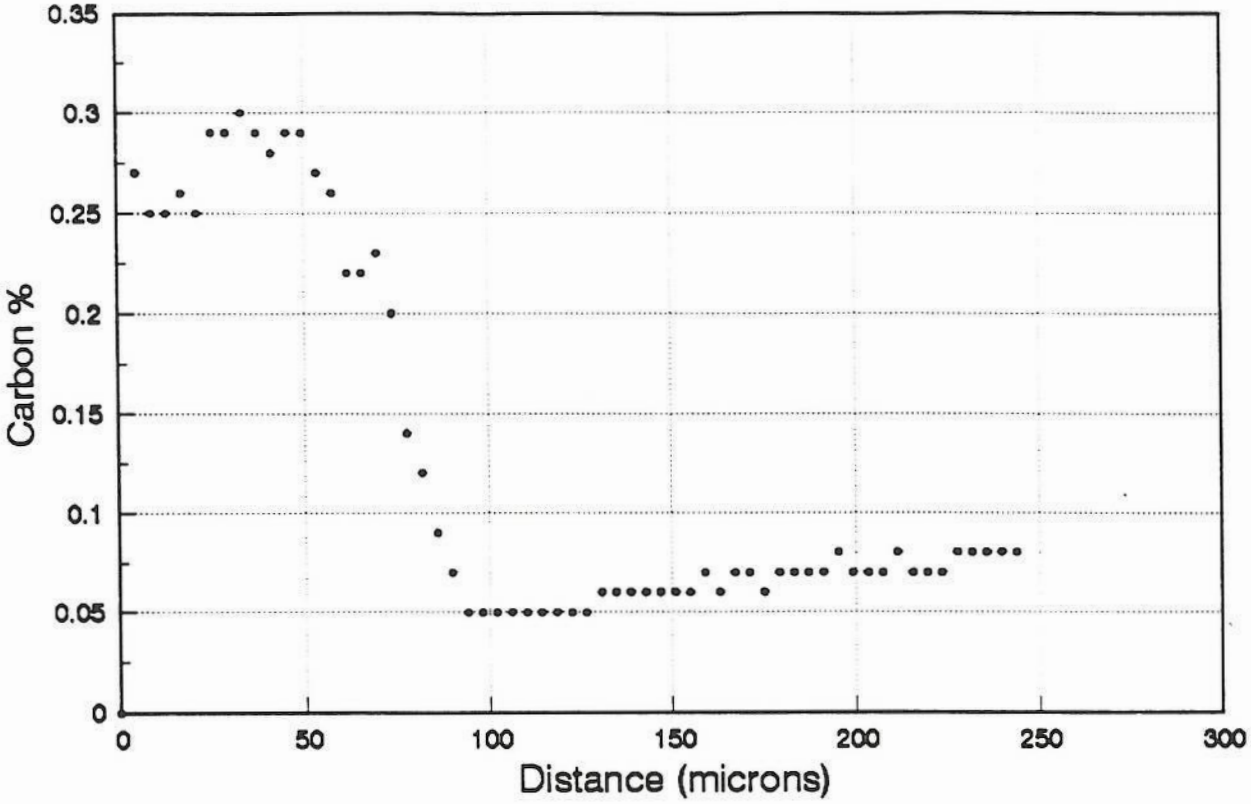
0.35
0.3
0.25
0.2
0.15
0.1
0.05
0
Carbon %
0
50
100
150
200
250
300
Distance (microns)

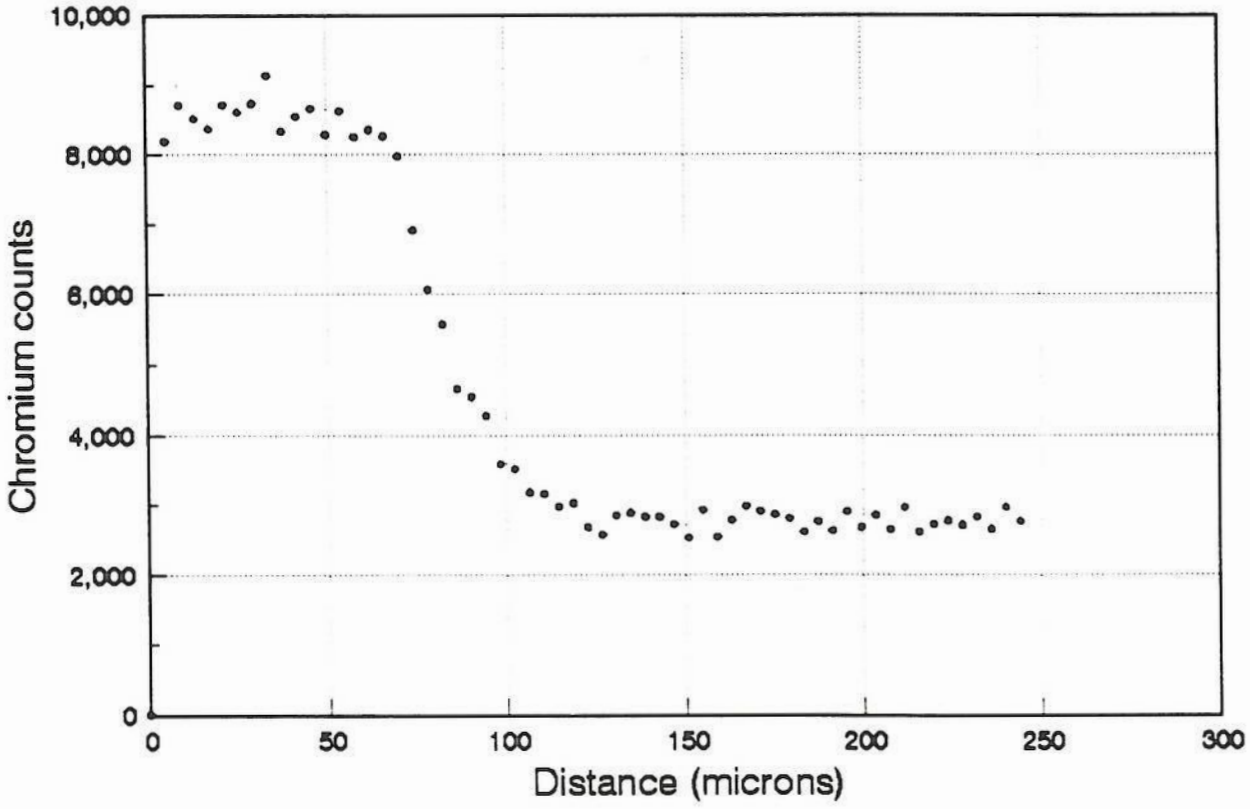
10,000
8,000
6,000
4,000
2,000
0
Chromium counts
0
50
100
150
200
250
300
Distance (microns)

2Cr.F.AGED

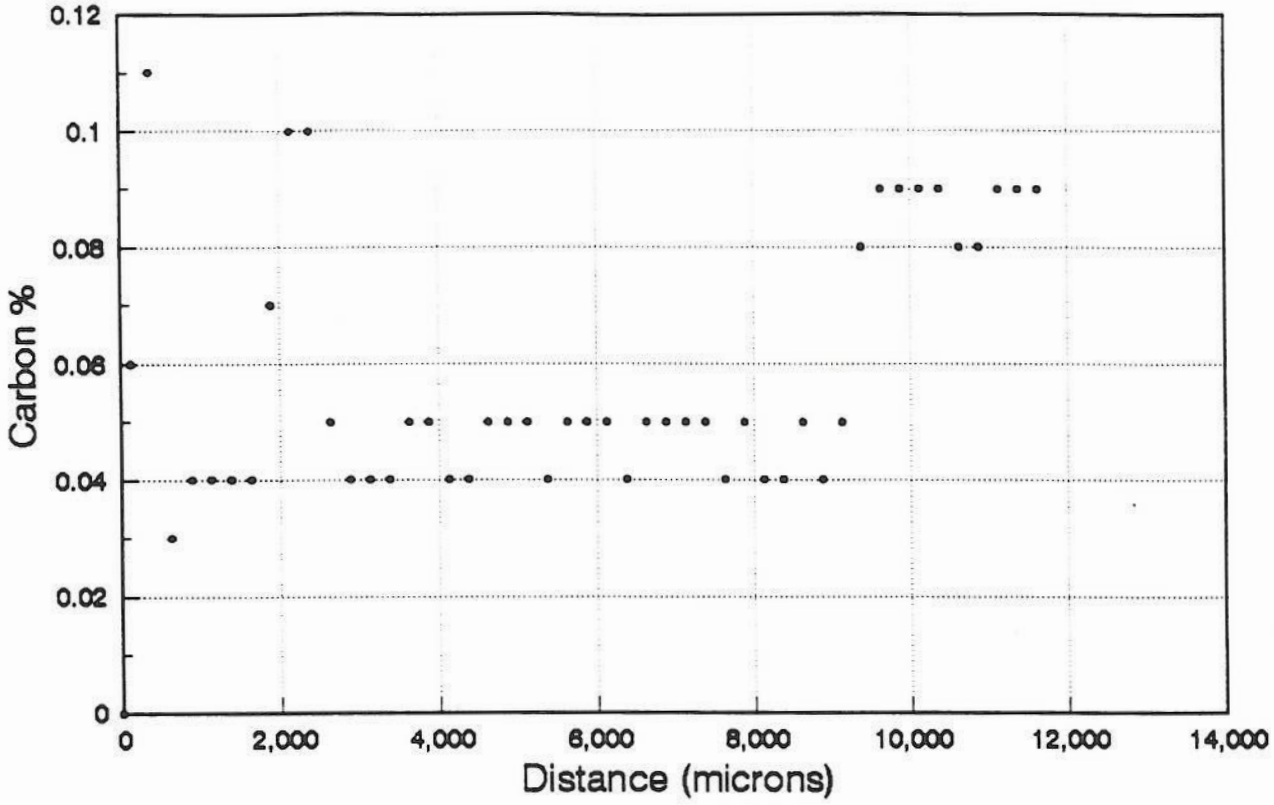
0.12
0.1
0.08
0.06
0.04
0.02
0
Carbon %
0
2,000
4,000
6,000
8,000
10,000
12,000
14,000
Distance (microns)

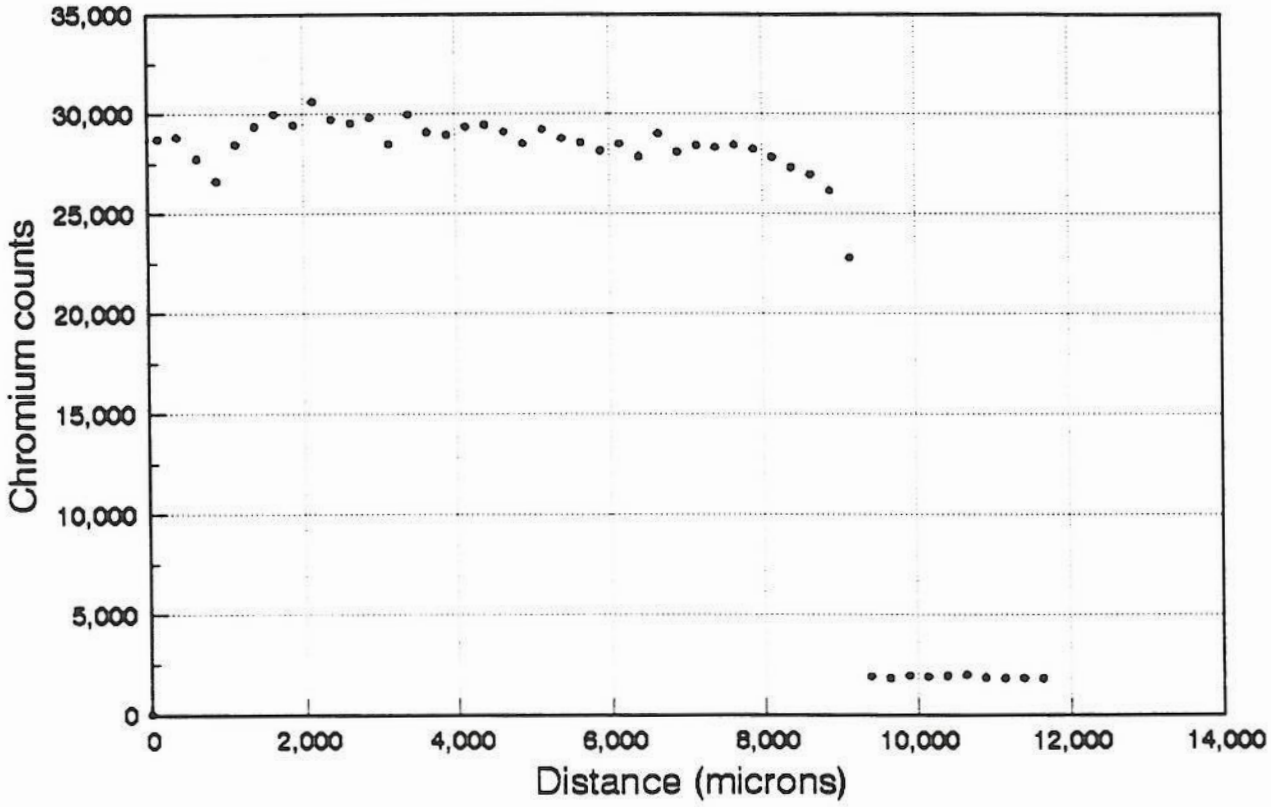
35,000
30,000
25,000
20,000
15,000
10,000
5,000
0
Chromium counts
0
2,000
4,000
6,000
8,000
10,000
12,000
14,000
Distance (microns)

9Cr.C.AW

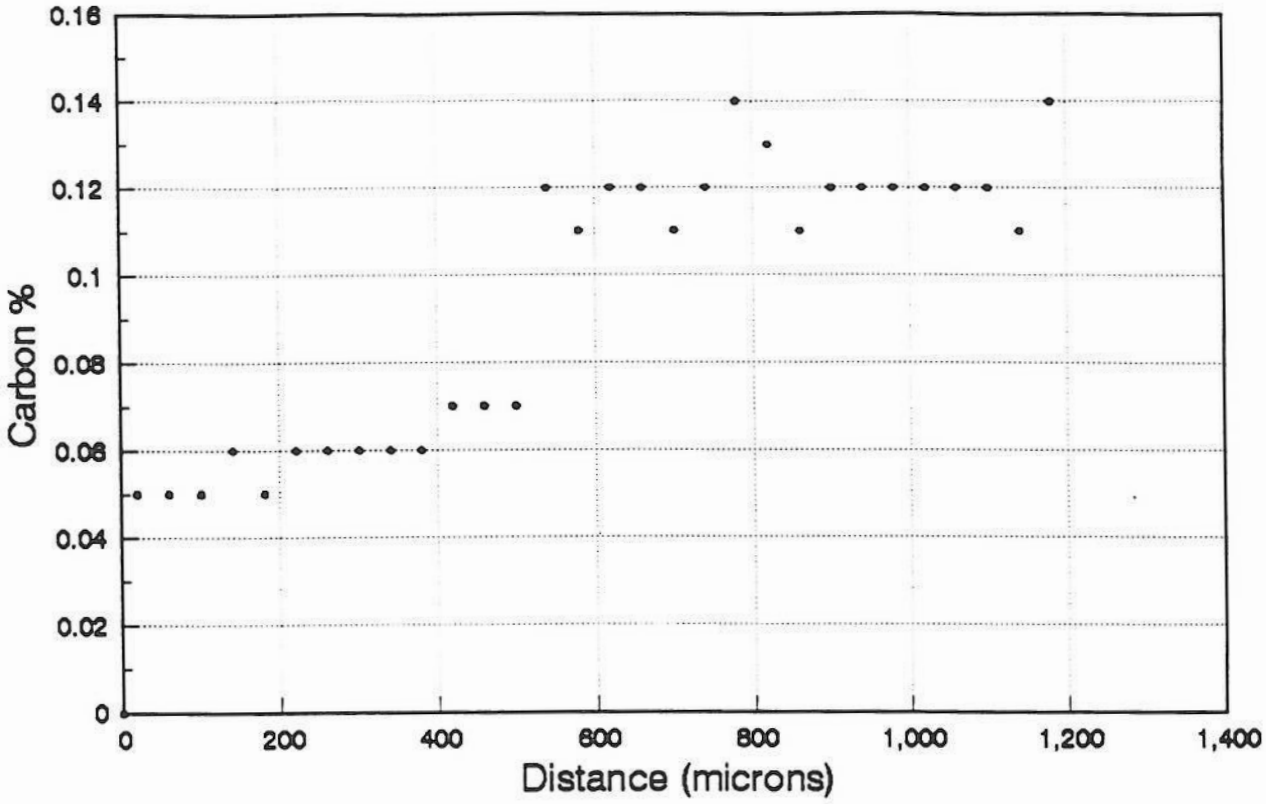
0.16
0.14
0.12
0.1
0.08
0.06
0.04
0.02
0
Carbon %
0
200
400
600
800
1,000
1,200
1,400
Distance (microns)

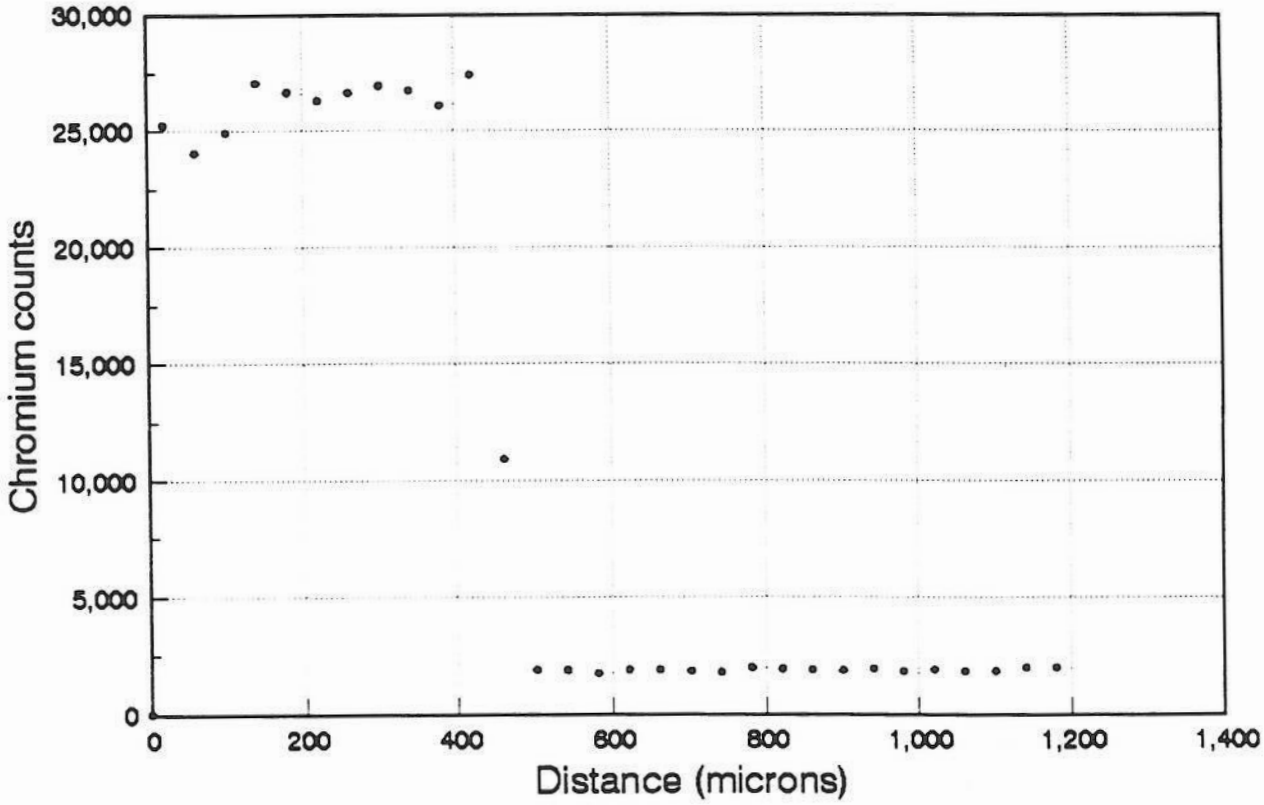
30,000
25,000
20,000
15,000
10,000
5,000
0
Chromium counts
0
200
400
600
800
1,000
1,200
1,400
Distance (microns)

9Cr.M.AW

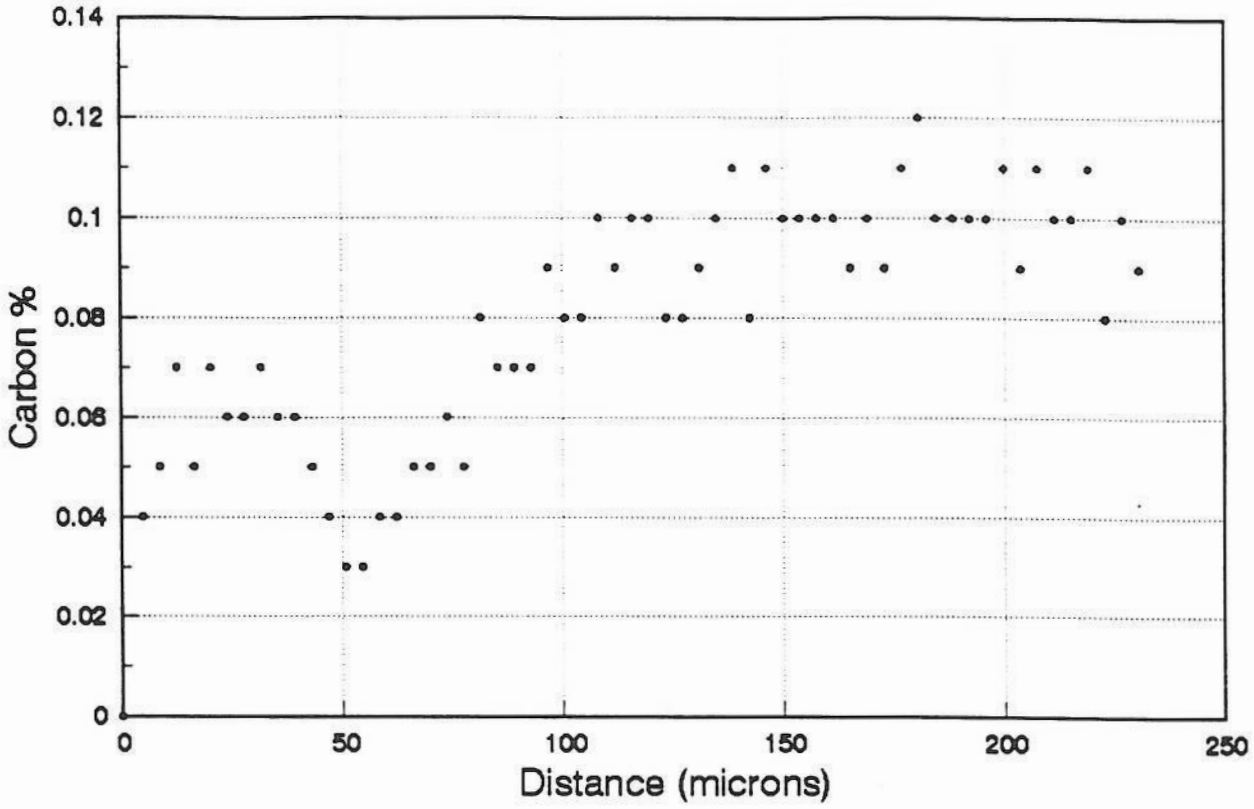
0.14
0.12
0.1
0.08
0.06
0.04
0.02
0
Carbon %
0
50
100
150
200
250
Distance (microns)

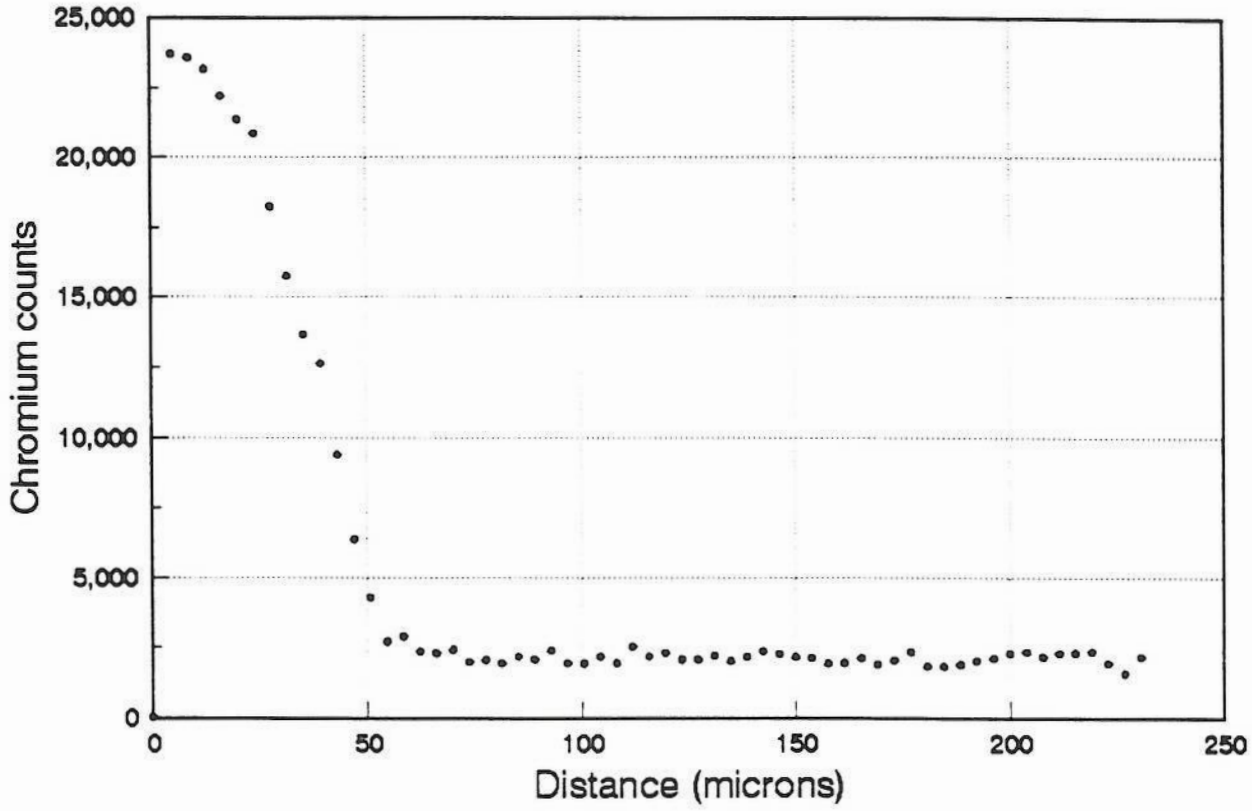
25,000
20,000
15,000
10,000
5,000
0
Chromium counts
0
50
100
150
200
250
Distance (microns)

9Cr.F.AW

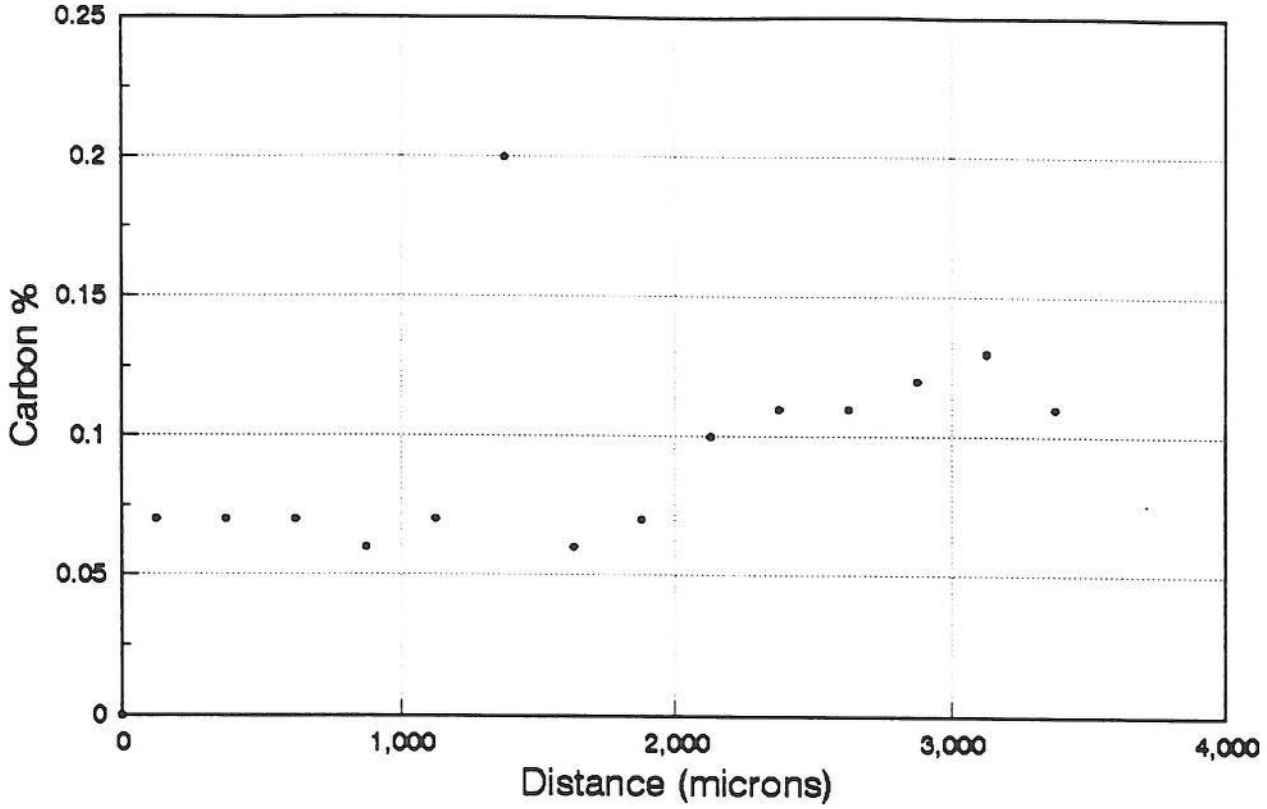
0.25
0.2
0.15
0.1
0.05
0
Carbon %
0
1,000
2,000
3,000
4,000
Distance (microns)

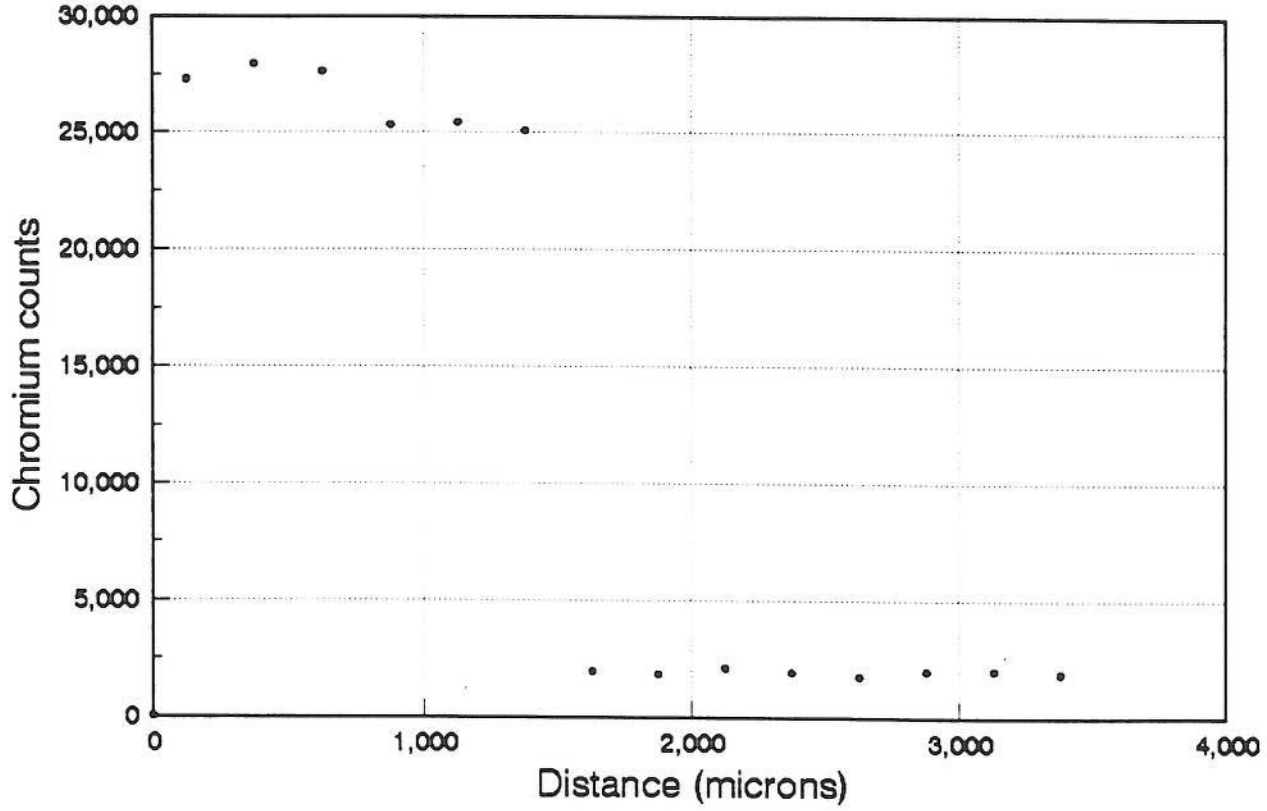
30,000
25,000
20,000
15,000
10,000
5,000
0
Chromium counts
0
1,000
2,000
3,000
4,000
Distance (microns)

9Cr.C.PWHT

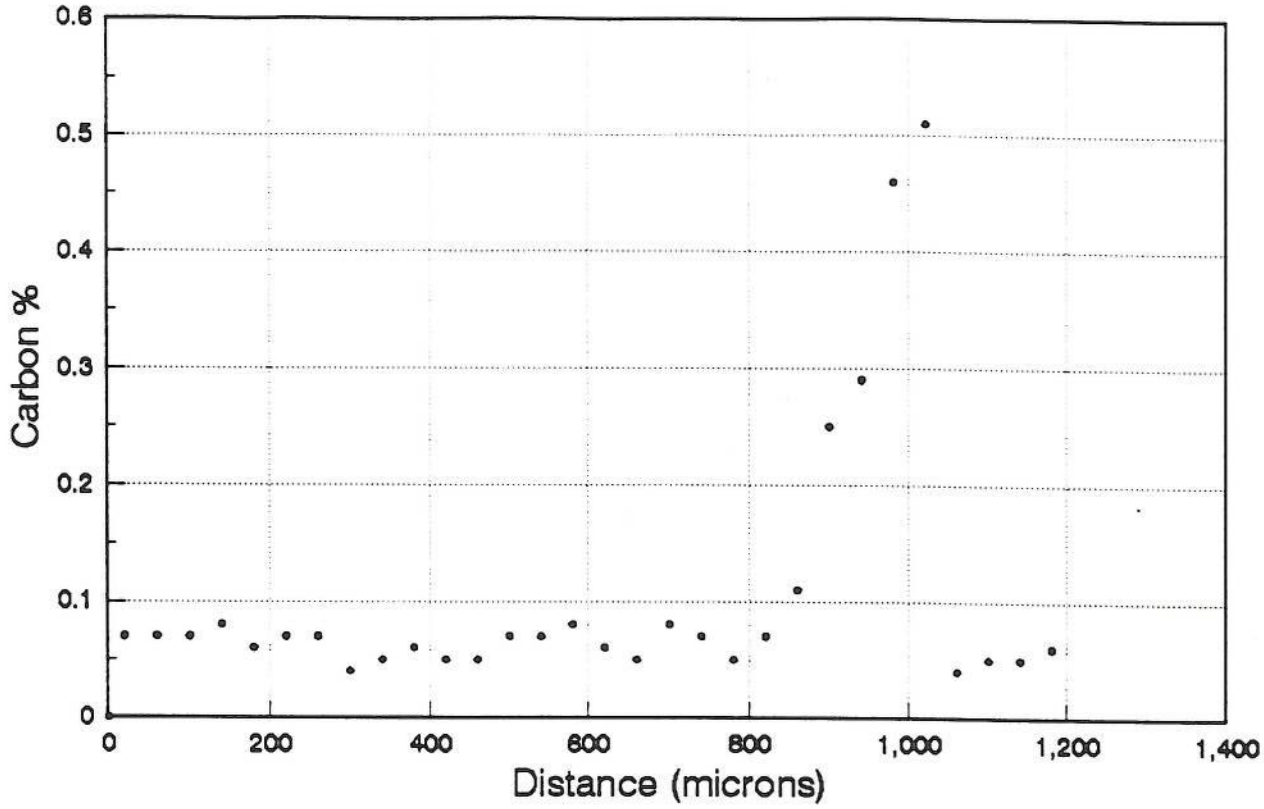
0.6
0.5
0.4
0.3
0.2
0.1
0
Carbon %
0
200
400
600
800
1,000
1,200
1,400
Distance (microns)

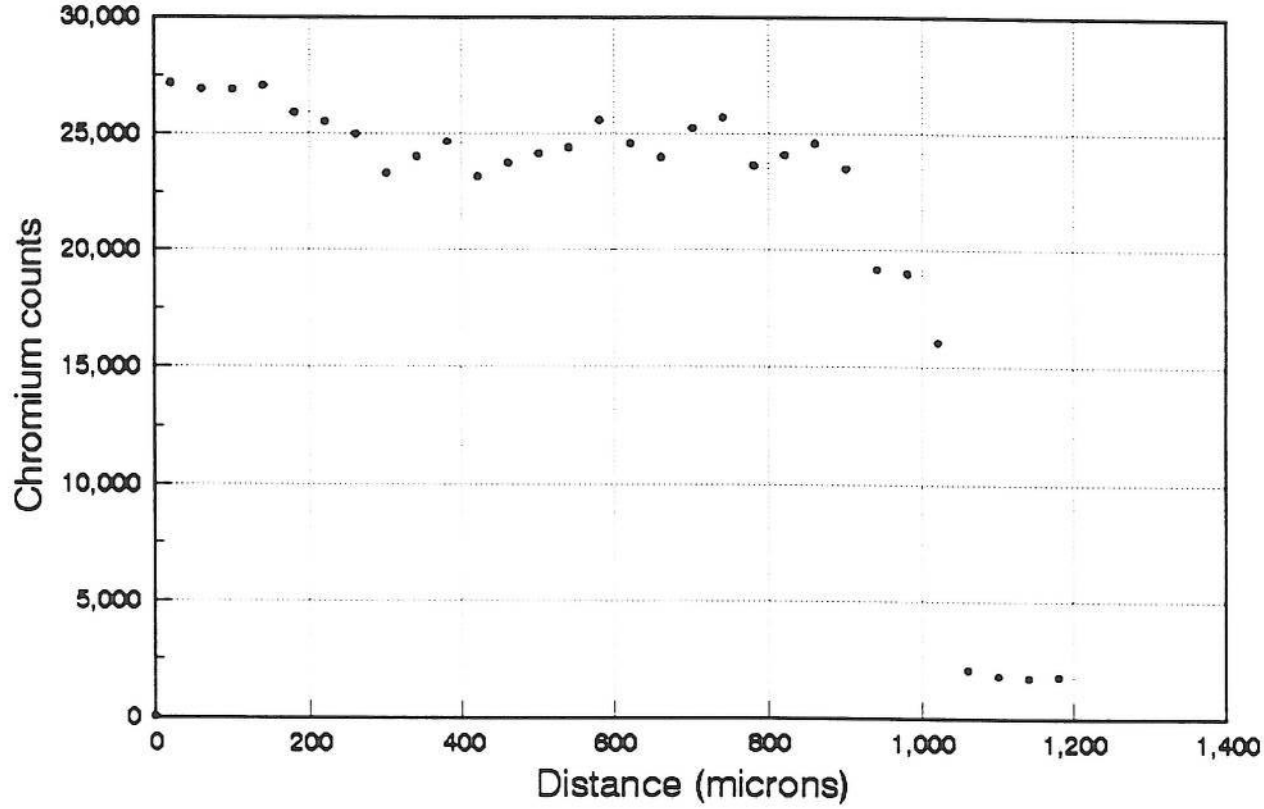
30,000
25,000
20,000
15,000
10,000
5,000
0
Chromium counts
0
200
400
600
800
1,000
1,200
1,400
Distance (microns)

9Cr.M.PWHT

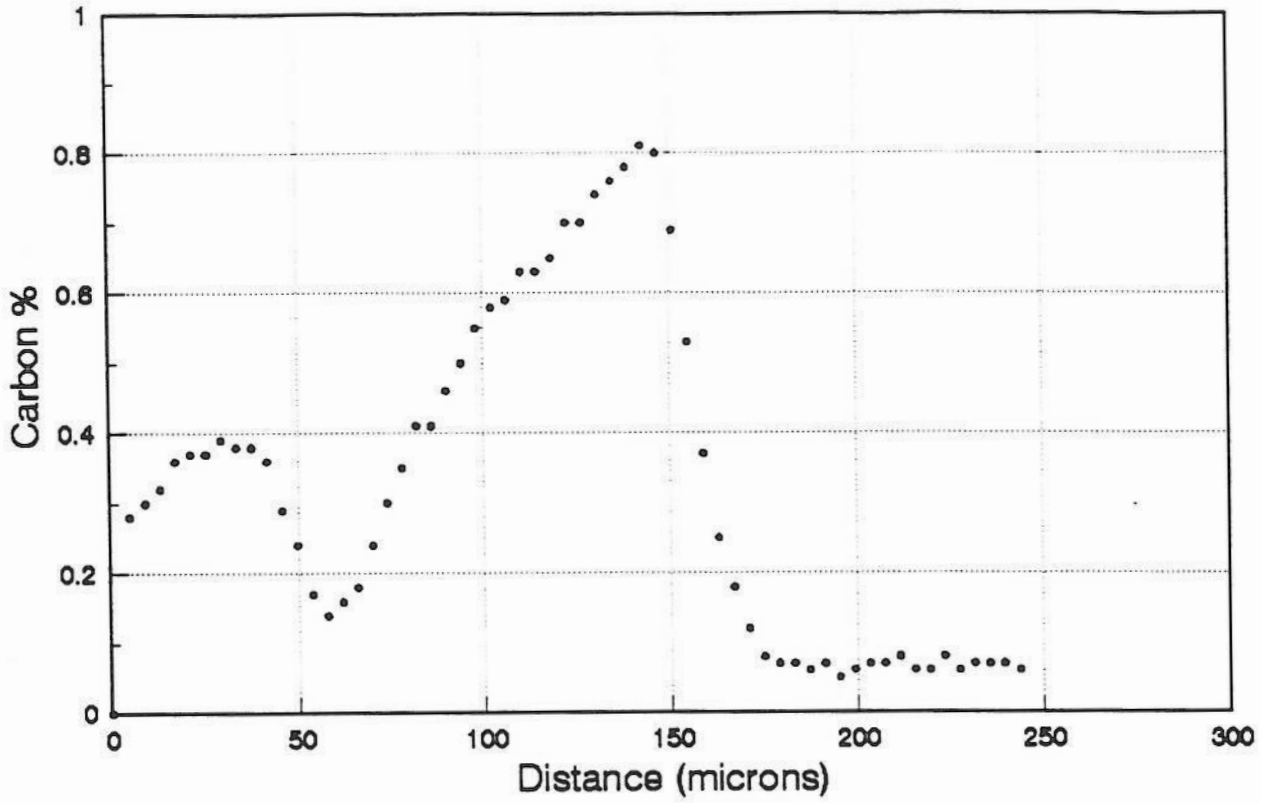
Carbon %
1
0.8
0.6
0.4
0.2
0
0
50
100
150
200
250
300
Distance (microns)

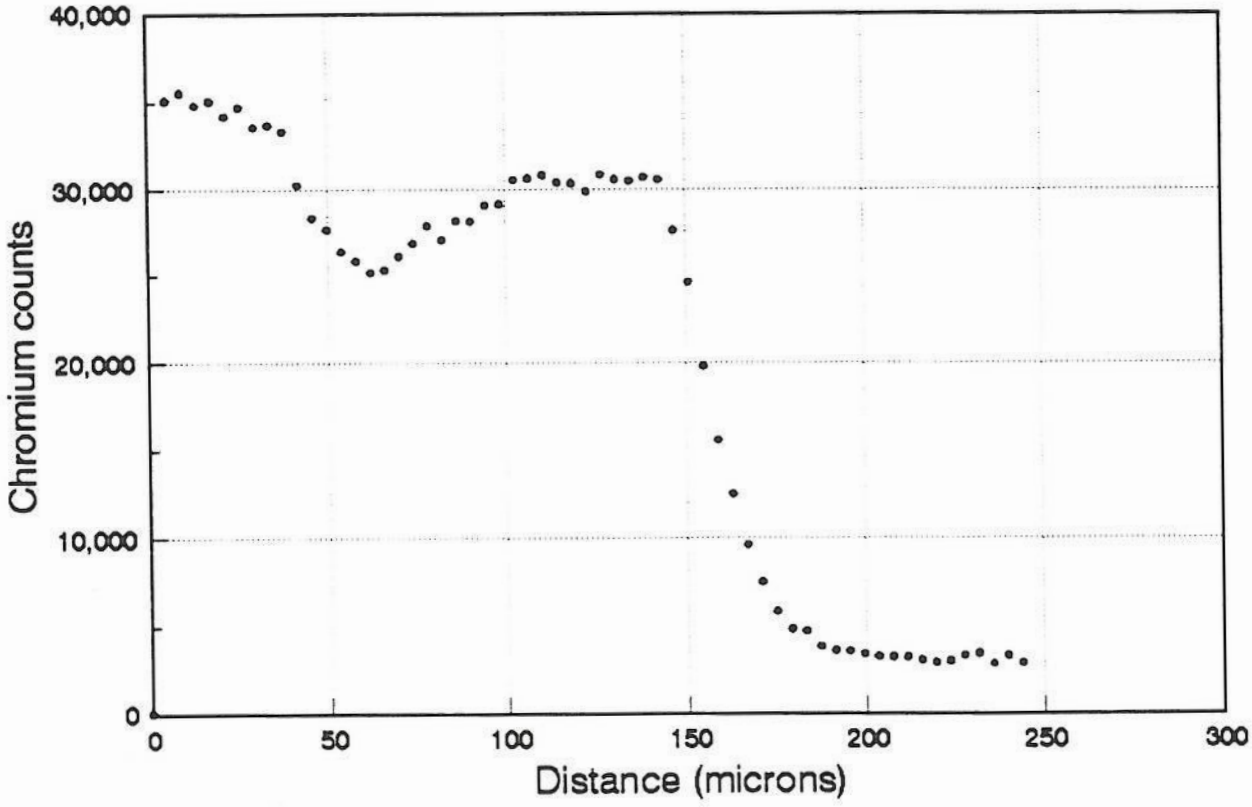
Chromium counts
40,000
30,000
20,000
10,000
0
0
50
100
150
200
250
300
Distance (microns)

9Cr.F.PWHT

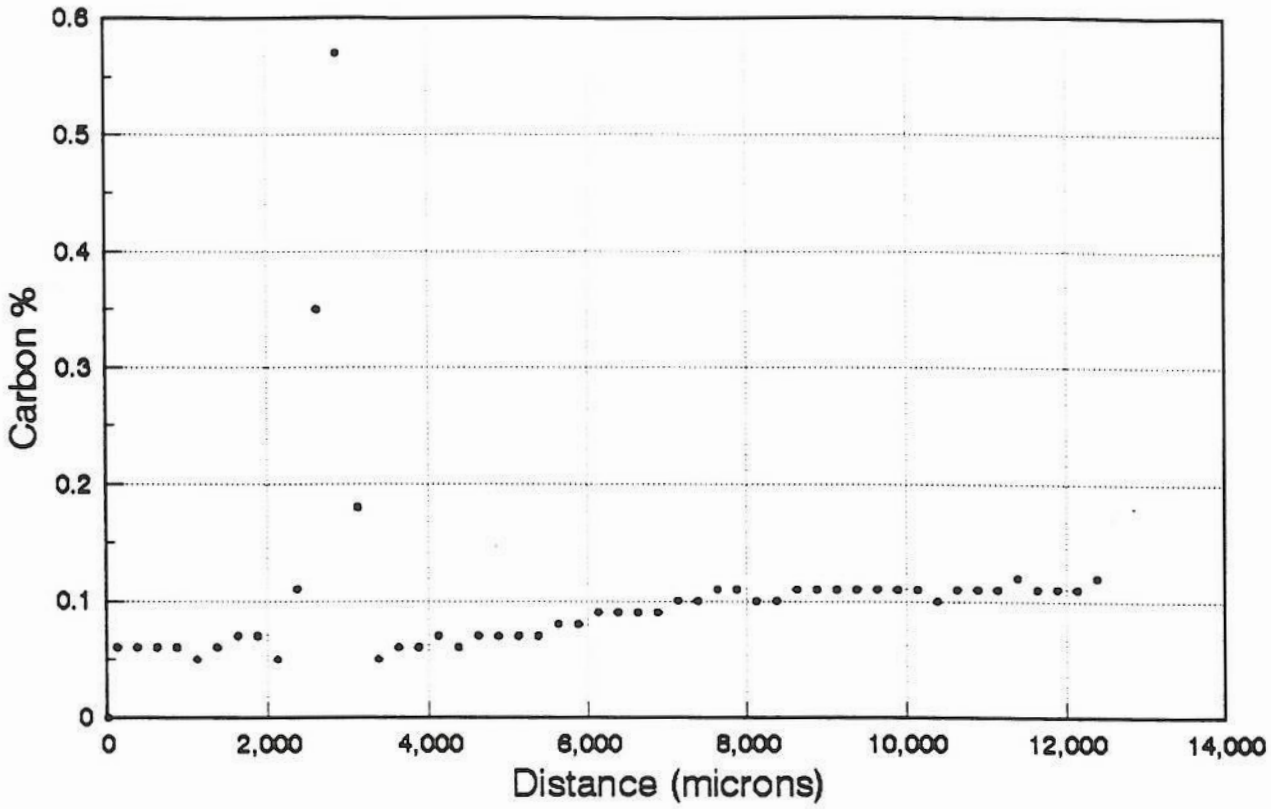
0.6
0.5
0.4
0.3
0.2
0.1
0
Carbon %
0
2,000
4,000
6,000
8,000
10,000
12,000
14,000
Distance (microns)

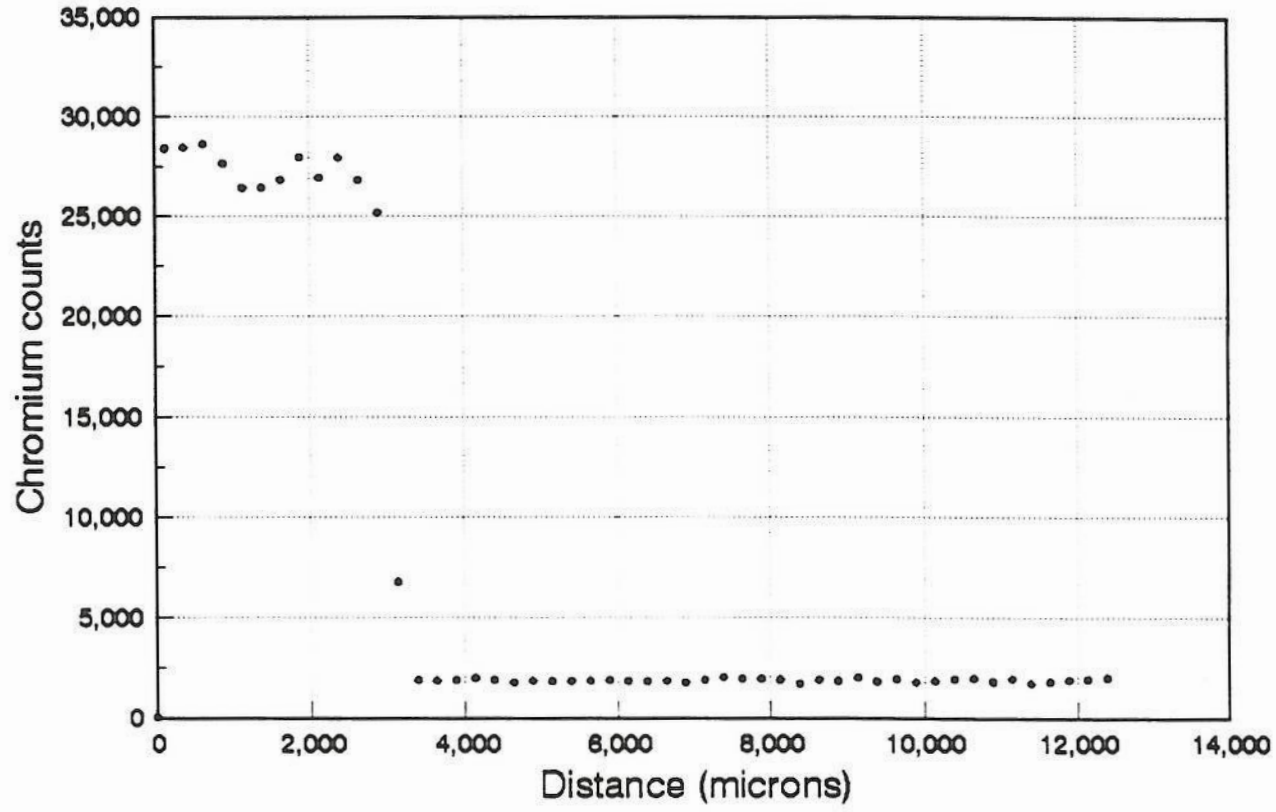
35,000
30,000
25,000
20,000
15,000
10,000
5,000
0
Chromium counts
0
2,000
4,000
6,000
8,000
10,000
12,000
14,000
Distance (microns)

9Cr.C.AGED

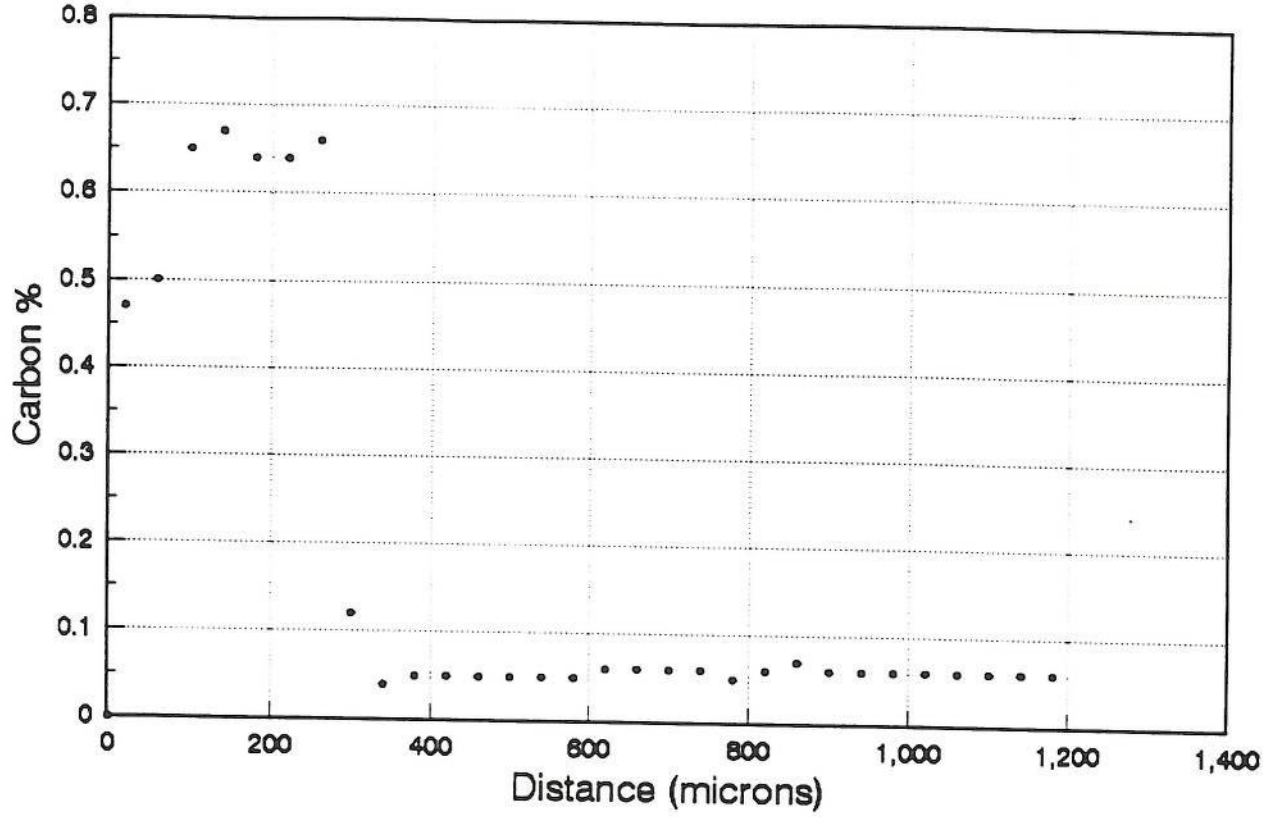
0.8
0.7
0.6
0.5
0.4
0.3
0.2
0.1
0
Carbon %
0
200
400
600
800
1,000
1,200
1,400
Distance (microns)

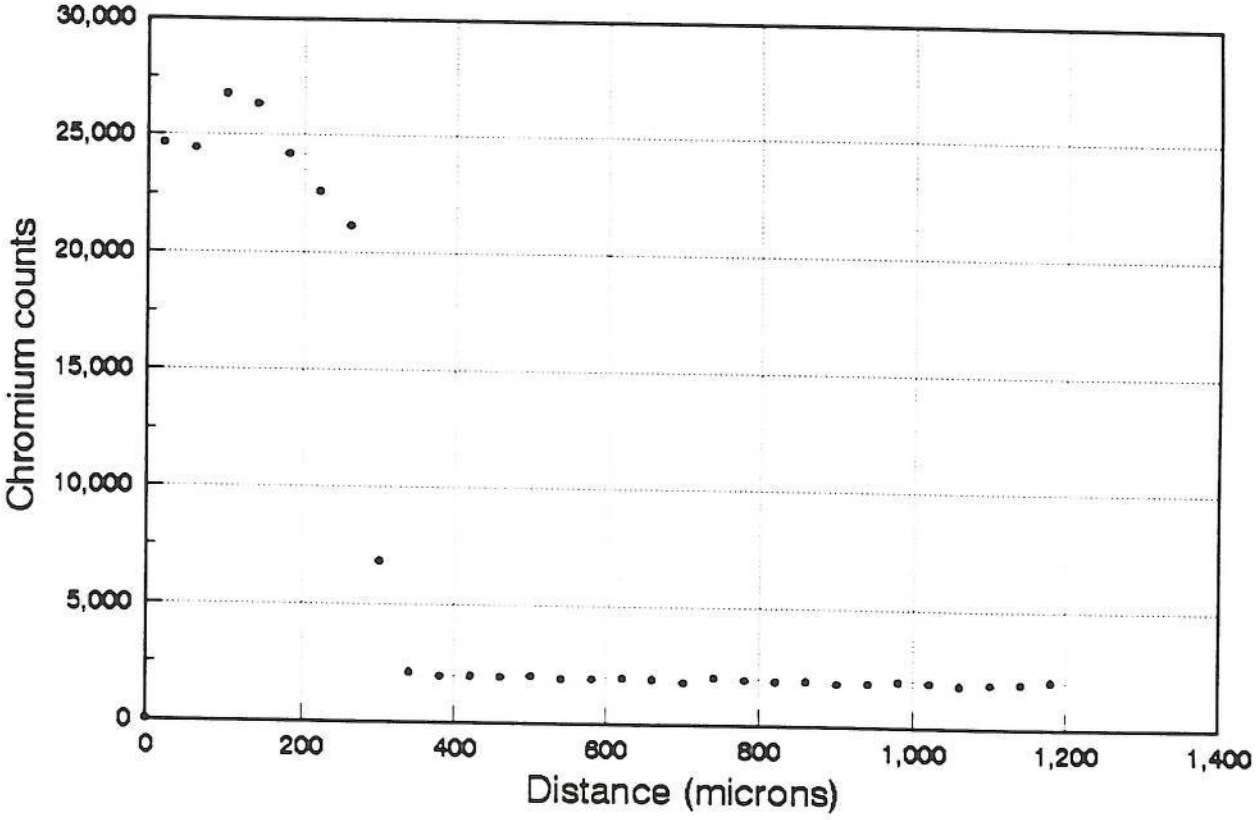
30,000
25,000
20,000
15,000
10,000
5,000
0
Chromium counts
0
200
400
600
800
1,000
1,200
1,400
Distance (microns)

9Cr.M.AGED

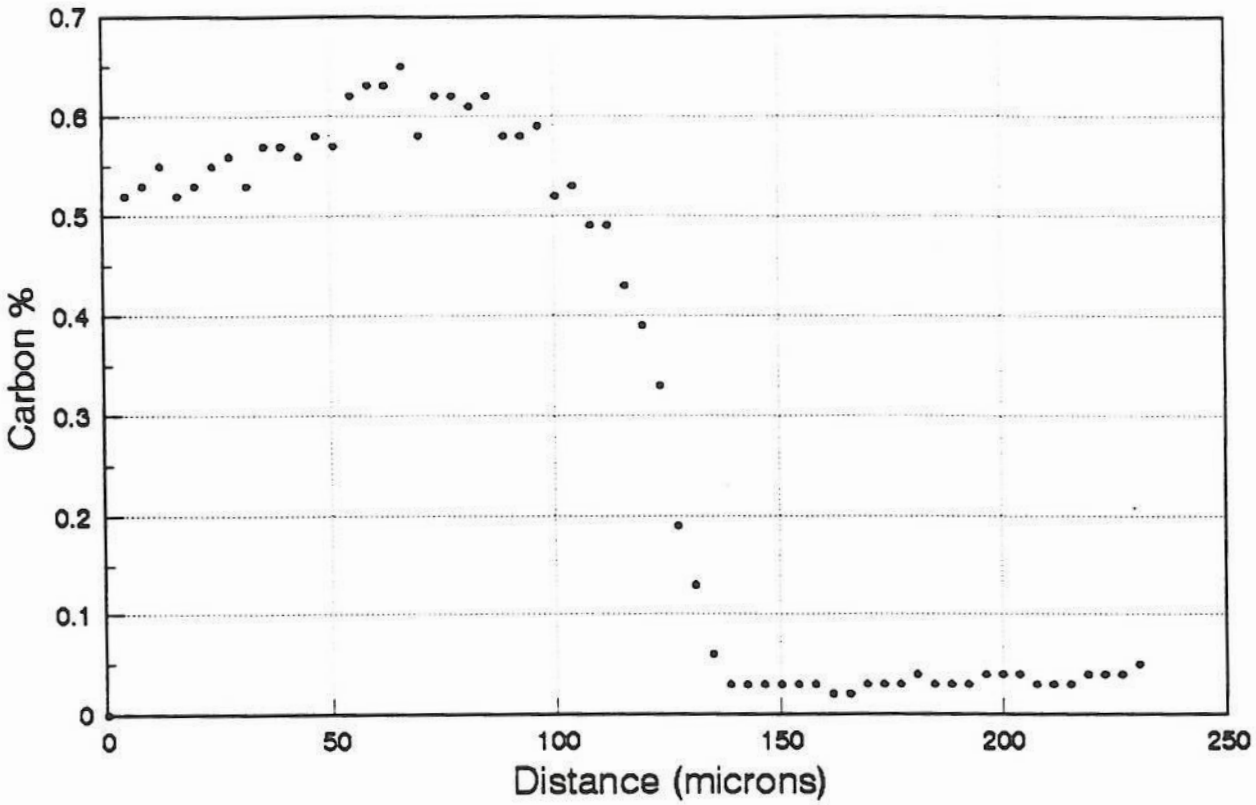
0.7
0.6
0.5
0.4
0.3
0.2
0.1
0
Carbon %
0
50
100
150
200
250
Distance (microns)

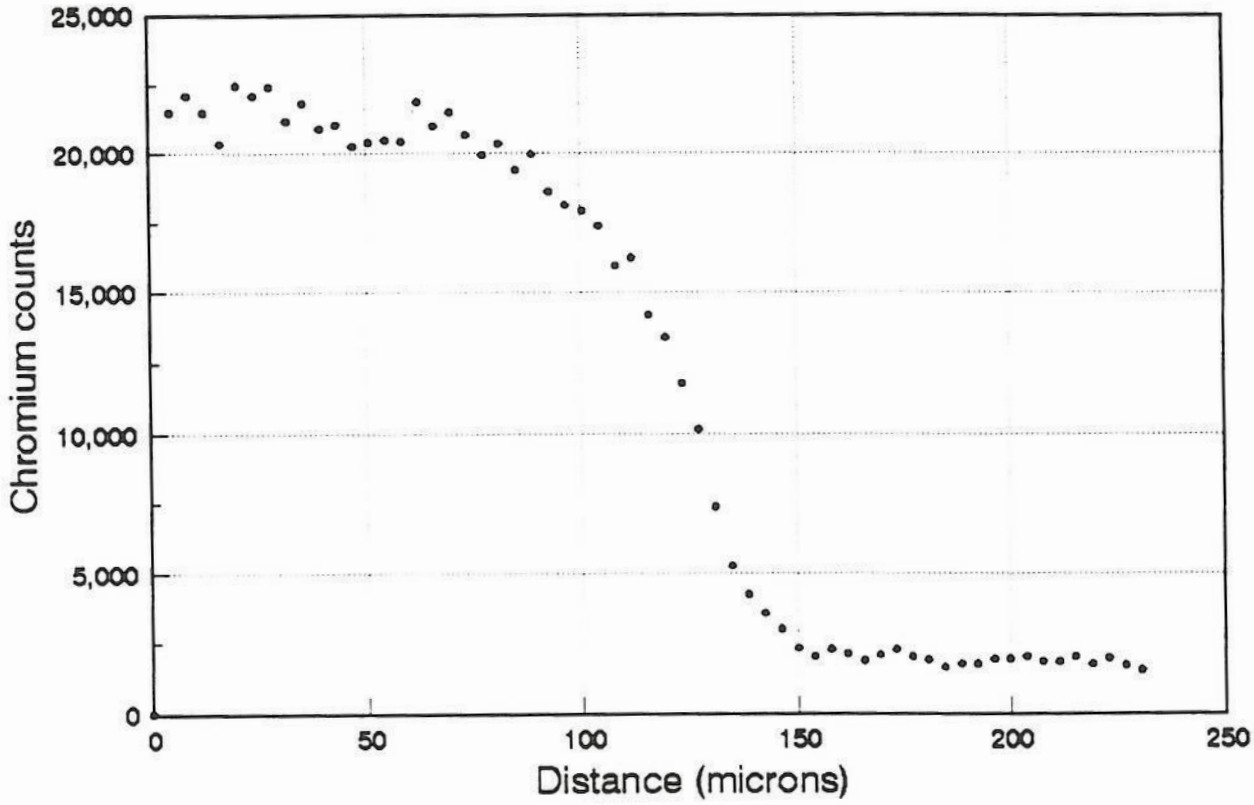
25,000
20,000
15,000
10,000
5,000
0
Chromium counts
0
50
100
150
200
250
Distance (microns)

9Cr.F.AGED